Identification and structure activity relationship of small molecule antagonists of the human P2X$_4$ receptor.

Izzuddin Bin Ahmad

A Thesis Presented for the Degree of Doctor of Philosophy to the University of East Anglia

Faculty of Science, School of Biological Science

University of East Anglia

Handy note

Declaration

I hereby declare that the thesis is my original work except for quotations and citations which have been duly acknowledged. I also declare that it has not been previously, and is not concurrently submitted for any other degree at University of East Anglia or at any other institution. This thesis contains 55217 words including appendices.

Abstract

$P2X_4$ is a purinergic receptor distributed all over the body with various roles. Among them, it was reportedly overexpressed in several neuronal and immune cell types following peripheral nerve injury and its activation leads to neuropathic pain. Several compounds were found to block $P2X_4$ but none has gone into a clinical stage, probably due to insufficient information about the compound itself and $P2X_4$ in general. One of such compounds, 5-(3-Bromophenyl)-1,3-dihydro-2H-Benzofuro[3,2-e]-1,4-diazepin-2-one (5-BDBD) is known to be widely used in $P2X_4$-related studies despite its limited information. Therefore, this study aimed to (i) find a novel compound that can block the activation of $P2X_4$ through high throughput screening and characterise it, and (ii) study structural-activity relationship between 5-BDBD and $P2X_4$. Human $P2X_4$ receptor was stably expressed in human 1321N1 astrocytoma cells and 1710 compounds from National Cancer Institute were screened for their activity at $P2X_4$. Extensive tests led to identifying a natural product (thaspine) as the most potent inhibitor at reducing $P2X_4$ activation. Further characterisation experiments revealed that thaspine had an IC_{50} value of 3.8 ± 0.2 µM and showed an allosteric mode, time-dependent and irreversible inhibition. Thaspine was similarly potent at mouse $P2X_4$, but not effective at human $P2X_2$, $P2X_{2/3}$ and $P2X_7$. It was also inactive at human $P2Y_2$ and $P2Y_6$ at concentrations below 10 µM and 30 µM respectively. In primary microglial cell model (BV2), it inhibited ivermectin-potentiated responses but not normal ATP-evoked responses. Meanwhile, 5-BDBD was found to be inhibiting $P2X_4$ receptor competitively and diazepinone was a pivotal group of the structure to cause inhibition. The binding pocket of 5-BDBD at $P2X_4$ was also predicted using molecular docking. In this study, a novel compound thaspine, has been shown to be effective at inhibiting human $P2X_4$ and thus may have potential therapeutic applications while novel information about 5-BDBD was also acquired.

Table of Contents

List of Figures

List of Tables

List of Schemes

Abbreviations

5-BDBD	5-(3-Bromophenyl)-1,3-dihydro-2H-benzofuro[3,2-e]-1,4-diazepin-2-one
AA	Arachidonic acid
ADP	Adenosine diphosphate
AM	Acetoxylmethyl ester
AMD	Age-related macular degeneration
AMP	Adenosine monophosphate
APC	Antigen-presenting cell
APII	Alveolar type II epithelial cells
ATP	Adenosine triphosphate
BDNF	Brain-derived neurotrophic factor
BMD	Bone mineral density
BSA	Bovine serum albumin
BzATP	2'(3')-O-(4-Benzoylbenzoyl)adenosine-5'-triphosphate tri(triethylammonium) salt
Ca^{2+}	Calcium ion
Cd^{2+}	Cadmium ion
Cu^{2+}	Copper ion
$CaCl_2$	Calcium chloride
cAMP	Cyclic adenosine monophosphate
CCL	CC chemokine ligand
CCR	CC chemokine receptor
cPLA2	Cytosolic phospholipase A2 α
DI	Deionised water
DMEM	Dulbecco's Modified Eagle Medium
DMSO	Dimethyl sulfoxide
DNA	Deoxyribonucleic acid
DTP	Developmental Therapeutic Program
E_{anion}	Anion reversal potential
ECs	Endothelial cells
EDTA	Ethylenediaminetetraacetic acid

ERK	Extracellular signal-regulated protein kinase (ERK)
FTIR	Fourier transform infrared spectroscopy
GABA	γ-amino butyric acid
GABA$_A$	γ-amino butyric acid type A
GABAR	γ-amino butyric acid receptor
GABA$_A$R	γ-amino butyric acid type A receptor
GPCR	G protein-coupled receptor
GvHD	Graft-versus-host disease
HBPS	HEPES-buffered physiological saline
HEK	Human embryonic kidney
Hg^{2+}	Mercury
HMC	Human mesangial cells
HPLC	High performance liquid chromatography
HRMS	High resolution mass spectrometer
IFN-γ	Interferon gamma
IFN-γR	Interferon gamma receptor
iNOS	inducible nitric-oxide synthase
IUPAC	The International Union of Pure and Applied Chemistry
KCC2	Potassium chloride cotransporter
KCl	Potassium chloride
LB	Lamellar bodies
LTP	Long-term potentiation
LPS	Lipopolysaccharide
MCP-1	Monocyte chemoattractant protein 1 (also known as CCL2)
MFI	Median fluorescence intensity
MgCl$_2$	Magnesium chloride
NaCl	Sodium chloride
NaOH	Sodium hydroxide
NCBI	National Center for Biotechnology Information
NCI	National Cancer Institute
NMR	Nuclear magnetic resonance
PBS	Phosphate buffered saline
PGE2	Prostaglandin E2
PNI	Peripheral nerve injury

PWT	Paw withdrawal threshold
RMSD	Root-mean-square deviation of atomic positions
ROS	reactive oxygen species
SFK	Src-family kinases
SNP	Single nucleotide polymorphisms
SOC	Super optimal broth with catabolite repression
UDP	Uridine Diphosphate
UTP	Uridine triphosphate
IVM	Ivermectin
TAE	Tris-Acetate-EDTA
TCR	T cell receptor
TLC	Thin layer chromatography
TLR2	Toll-like receptor 2
TNF-α	Tumour necrosis factor alpha
TRITC	Tetramethylrhodamine
UV	Ultraviolet
VSV	Vesicular Stomatitis Virus
zfP2X$_4$	Zebrafish P2X$_4$
Zn^{2+}	Zinc ion

Conference Abstract

Listed below is published work resulting from the work in this thesis.

Conference Abstract

Nadzirin, I. A., Searcey, M., Fountain, S. J. (2016). Identification of Small Molecule Inhibitor of Human P2X$_4$ by Rational Drug Design. Abstracts of the 1st (2016) UK/Italian Purine Club Meeting. *Purinergic Signalling*. In Press. 28

Acknowledgement

First and foremost, I would like to offer my sincerest gratitude to my supervisor, Dr. Samuel J. Fountain and co-supervisor Professor Mark Searcey for their guidance, advice, knowledge and supervision throughout my PhD candidacy. My special thanks also go to Dr. Marco Cominetti who contributed a lot to the success of this study. Constructive comments on this thesis, made by them, are tremendously appreciated and without them, this thesis would not have been completely written.

My special appreciation and gratitude go to my beloved mother (Kamariah) for the love and support. Unlimited thanks to my wife (Fazlina) for always being supportive and inspiring. She had been a good listener and spirit booster for me to complete this research. Her love and care motivated and encouraged me to finish my experiments and thesis. She is also the heart of my family; without her I would not have been able to finish this. The sacrifice she has made, is priceless. We have been through lots of ups and downs during this period of study. May the memories remain to be cherished and may Allah give you lots of rewards. Thank you sayang. Thank you to all my children; Darwisy, Danish, and Delisha for being there in this journey. In addition, I would also like to thank parents in law for the prayers and support that they gave throughout my study and lots of thanks to all my siblings, family members, and Malaysian family friends for giving me hope and prayers.

I also want to express my gratitude to my colleagues; Dr. Janice Layhadi, Seema Ali, Jonny Micklewright, Dr. Lisa Burrows, Dr. David Richards, and Dr. Priscilla Day for their guidance and assistance during my work. They had offered a lot of advice and insight on my work. Finally, I would like to thank everybody who directly or indirectly contributed to the successful realisation of my thesis, as well as expressing my apology to those that I could not mention personally one by one.

To those who are reading this, the journey of my PhD was not easy. There were lots of hurdles to reach the end. If you're doing a PhD as well, I know you can do this! Never give up, persevere, believe in yourself and pray hard too! Alhamdulillah.

Dedication

In the name of God, the most Beneficent, the most Merciful

To my beloved mother, wife and children

(Kamariah, Fazlina sayang, Darwisy, Danish, Delisha)

CHAPTER 1

INTRODUCTION

1.1 Purinergic signalling

Purine nucleotides and nucleosides, adenosine triphosphate (ATP), and adenosine were first proposed as extracellular signalling molecules in a seminal paper by Drury and Szent-Györgyi (1929). The scientists observed the potent action of these molecules on the heart and blood vessels. Emmelin and Feldberg (1948) provided more evidence on the involvement of ATP in producing systemic effect on cat, particularly on the circulatory and respiratory systems. There were several other studies suggested the involvement of ATP and other purines nucleotides as neurotransmitters, as reviewed by Burnstock (1998). These allowed the proposal of *purinergic* term by Burnstock (1971) to refer ATP and other related purine nucleotides, in an effort to simplify the nomenclature of the mentioned compounds.

In 1972, the term *purinergic signalling* was proposed by Geoffrey Burnstock. He defined the term *purinergic receptors* in 1976 as the receptors that bind to purine molecules (Burnstock, 2006). In 1978, the term was formally used and purinergic receptors were divided into two families, P1 and P2, by Burnstock based on the natural ligands they bind to. P1 purinoreceptors bind to adenosine while P2 purinoceptors bind to ATP and ADP (Ralevic & Burnstock, 1998). The P2 family was further subdivided based on their pharmacological characteristics which were ligand-gated ion channel P2X and G protein-coupled P2Y receptors (GPCR) (Burnstock & Kennedy, 1985). The early development of purinergic signalling has received a significant amount of challenge because of the global reluctance to accept that a nucleotide, like ATP, can act as a neurotransmitter. The reluctance could be due to the fact that ATP is ubiquitously present and as the main currency of energy in human body, it was hard to digest the notion of ATP being a messenger (Burnstock, 2006).

1.1.1　P1 receptors

P1 receptors can be categorised into four subtypes and their natural ligand is adenosine. These receptors share one common feature with P2Y in which they are coupled to a G protein. The activation of A_{2A} and A_{2B} receptors leads to the production of cyclic AMP (cAMP) while activation of A_1 and A_3 receptors results in the inhibition of cAMP production (Abbracchio et al., 2009). These receptors have been reported to play various roles related to the central nervous system, cerebral blood flow, pain regulation, respiration, functions of basal ganglia, and sleep (Jaakola et al., 2008).

1.1.2　P2Y receptors (P2YR)

The first member of the P2Y family, i.e., $P2Y_1$ (formerly known as P_{2Y}) was introduced by Webb et al. (1993). Since then, several other P2Y receptors have been identified and named in a consecutive order based on the time of their discovery. To date, there are eight established subtypes of P2Y namely $P2Y_1$, $P2Y_2$, $P2Y_4$, $P2Y_6$, and $P2Y_{11-14}$ (Abbracchio et al., 2003, 2006; Communi et al., 2001; Hollopeter et al., 2001; Zhang et al., 2002). The current accepted classification of the P2Y family was established after the discovery and reclassification of the last three receptors ($P2Y_{12-14}$) between the year of 2000 and 2003 (Burnstock, 2007).

P2Y receptors are G protein-coupled receptors (GPCR) which are composed of seven hydrophobic transmembrane domains with an intracellular C-terminus and extracellular N-terminus. The transmembrane domains are connected by three extracellular and intracellular loops. The seven subunit transmembrane motifs form a pocket for ligand binding (Burnstock, 2004; Ralevic & Burnstock, 1998). The P2Y receptors have been reported to respond towards both endogenous and exogenous purine and pyrimidine nucleotides (ATP, ADP, UTP, UDP, and UDP-glucose). Dissimilar to P2X, the calcium influx caused by these receptors is not caused by the direct opening of the receptors, rather the cascade involves secondary signalling pathway.

P2Y receptors are divided into two groups based on their structural and functional features. The first group consists of $P2Y_1$, $P2Y_2$, $P2Y_4$, $P2Y_6$, and $P2Y_{11}$ which signals

through $G\alpha_{q/11}$ to activate phospholipase C (PLC) and the second group consists of $P2Y_{12}$, $P2Y_{13}$, and $P2Y_{14}$ which signals through $G\alpha_{i/0}$ to inhibit adenylyl cyclase (AC) (von Kügelgen & Hoffmann, 2016). The activation of the first group of P2Y receptors by nucleotides causes the dissociation of heterotrimeric G protein, i.e., separation of $G\beta\gamma$ dimer from $G\alpha$ subunit. This leads to the activation of PLC by $G\alpha_{q/11}$ subunit and PLC subsequently hydrolyses the phosphatidylinositol-4,5-bisphosphate (PIP_2) to inositol-1,4,5-trisphosphate (IP_3). The IP_3 then acts on its receptor (IP_3R) at the endoplasmic reticulum (ER) which then leads to the release of calcium ion from ER into cytosol. Meanwhile, the activation of the second group of P2Y receptors causes the inhibition of AC that results in the alteration of cyclic adenosine monophosphate (cAMP) level. $P2Y_{11}$ has also been reported to couple to $G\alpha_s$ proteins that results in the stimulation of AC (Abbracchio et al., 2006; Bridges & Lindsley, 2008; von Kügelgen & Hoffmann, 2016).

The functions of P2Y have been demonstrated in various literatures and one of them was explained by Hechler et al. (1998). The study revealed that $P2Y_1$, which was found on platelets, in co-operation with $P2Y_{12}$ (Hollopeter et al., 2001) were crucial for ADP-induced platelet aggregation. Both receptors were found to be important in the aggregation of platelets in response to damaged vessels. Meanwhile, the function of $P2Y_2$ has been investigated by several studies that proved the involvement of $P2Y_2$ in the amplification of signals to recruit more neutrophils for phagocytic activity (Chen et al., 2006) and during the development of intimal hyperplasia in response to vascular injury (Seye et al., 2002). A more recent study highlighted the role of $P2Y_2$ in graft-versus-host disease (GvHD) after allogeneic hematopoietic cell transplantation (allo-HCT). The researchers found that $P2Y_2$-deficient recipient mice could survive longer than wild-type mice after receiving the allogeneic wild-type bone marrow and T cells. However, the GvHD was independent of the donor because both $P2Y_2$ wild-type and deficient donors produced the same GvHD-related mortality rate (Klämbt et al., 2015). The detailed characteristics of P2Y receptors are shown in Table 1.1.

Table 1.1 P2Y receptor characteristics

P2YR subtype	Primary distribution	Agonist	Antagonist	Downstream signalling pathways
$P2Y_1$	Epithelial and endothelial cells, platelets, immune cells, osteoclasts	2-MeSADP=ADPβS>2-MeSATP=ADP>ATP, MRS2365	MRS2179, MRS2500, MRS2279, PIT	$G\alpha_{q/11}$; PLC-β activation
$P2Y_2$	Immune cells, osteoblasts, epithelial and endothelial cells, kidney tubules	UTP=ATP, UTPγS, INS 37217, INS365	suramin>RB2, ARC126313	$G\alpha_{q/11}$ and $G\alpha_{i/0}$; PLC-β activation
$P2Y_4$	Endothelial cells	UTP≥ATP, UTPγS, INS 37217	RB2>suramin	$G\alpha_{q/11}$; PLC-β activation
$P2Y_6$	Some epithelial cells, placenta, T cells, thymus	UDP>UTP>>ATP, UDPβS, IDP	MRS2578	$G\alpha_{q/11}$; PLC-β activation
$P2Y_{11}$	Spleen, intestine, granulocytes	ARC67085MX>BzATP≥ATPγS>ATP	suramin>RB2, NF157, 5'-AMPS	$G\alpha_{q/11}$ and $G\alpha_s$; PLC-β activation, AC activation
$P2Y_{12}$	Platelets, glial cells	2-MeSADP≥ADP>>ATP	CT50547, AR-C69931MX, INS49266, AZD6140, PSB0413, ARL66096, 2-MeSAMP	$G\alpha_{i/o}$; AC inhibition
$P2Y_{13}$	Spleen, brain, lymph nodes, bone marrow	ADP=2-MeSADP>> ATP=2-MeSATP	MRS2211, 2-MeSAMP	$G\alpha_{q/11}$ and $G\alpha_i$; PLC-β activation, AC inhibition
$P2Y_{14}$	Placenta, adipose tissue, stomach intestine, discrete brain regions	UDP glucose=UDP-galactose	-	$G\alpha_{i/o}$; AC inhibition

Adapted from Burnstock (2007).

1.1.3 P2X receptors (P2XR)

P2X receptors are ionotropic receptors which involved in fast excitatory neurotransmission (Burnstock & WIlliams, 2000). The length of the receptors ranges from 384 to 595 amino acids across the subtypes (North, 2002). They are known to be distributed throughout the human body (Surprenant & North, 2009). There are seven subtypes of P2X receptors identified, namely $P2X_1$, $P2X_2$, $P2X_3$, $P2X_4$, $P2X_5$, $P2X_6$, and $P2X_7$. The receptor family members shared few common characteristics. The first one is their N- and C- termini are located intracellularly and connected by a large extracellular loop comprised of 10 conserved cysteine residues across the family. Secondly, all P2X receptor subunits have two transmembrane regions (TM1 and TM2) and ATP-binding site (Burnstock, 2004), and are activated by ATP (Figure 1.1) (Hernandez-Olmos et al., 2012). Lastly, they share a common topology in which they consist of three subunits either as homotrimers or heterotrimers (Burnstock & WIlliams, 2000). The first evidence indicating the organisation of P2X heterotrimers was demonstrated by Lewis et al. (1995) where the co-expression of $P2X_2$ and $P2X_3$ formed a new phenotype. A subsequent immunoprecipitation study predicted eleven form of heteromers involving all P2X receptors except $P2X_7$ (Torres et al., 1999), however only six have been functionally established which are $P2X_{1/2}$, $P2X_{1/4}$, $P2X_{1/5}$, $P2X_{2/3}$, $P2X_{2/6}$, and $P2X_{4/6}$ (Burnstock, 2007). The detailed characteristics of P2X receptors are shown in Table 1.2.
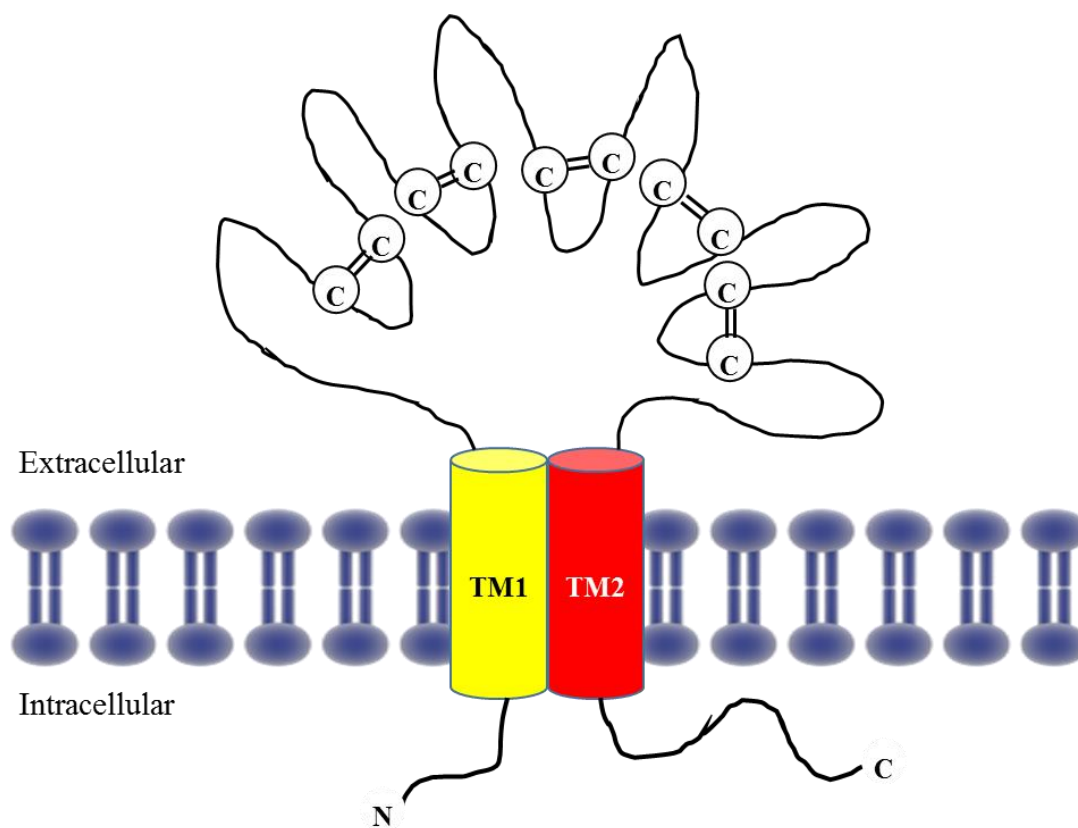
Figure 1.1 General structure of P2X receptors.

All P2X receptor subunits have two transmembrane domains of TM1 and TM2, which are connected by a large extracellular loop consisting of 10 cysteine residues that keep the extracellular structure stable via disulphide bridges. Both N- and C- termini are located intracellularly.

Table 1.2 P2X receptor characteristics

P2XR subtype	Primary distribution	Agonist	Antagonist	Downstream signalling pathways
P2X$_1$	Smooth muscle, platelets, cerebellum, dorsal horn spinal neurons	α,β-meATP=ATP=2-MeSATP, L-β,γ-meATP (rapid desensitisation)	MRS2220, MRS2159, NF449, NF279, Ro-0437626, Suramin, PPADS, TNP-ATP	Increase in cytosolic calcium level
P2X$_2$	Smooth muscle, CNS, retina, chromaffin cells, autonomic and sensory ganglia	ATP≥ATPγS≥2-MeSATP>>α,β-meATP (pH + zinc-sensitive)	Suramin, PPADS, RB2, NF770, NF279, NF776, NF778, PSB-12011, PSB-10211	Increase in cytosolic calcium level
P2X$_3$	sensory neurones, nucleus tractus solitarius, some sympathetic neurons	2-MeSATP≥ATP≥α,β-meATP ≥Ap$_4$A (rapid desensitisation)	NF023, NF279, NF449, RO-4, RO-3, MRS2159, MRS2257, Suramin, PPADS, A317491, NF110, Ip$_5$I,	Increase in cytosolic calcium level
P2X$_4$	CNS, testis, colon	ATP>> α,β-meATP, CTP	5-BDBD, PSB12062, BX430, NP-1815-PX, Suramin, PPADS, Paroxetine, TNP-ATP	Increase in cytosolic calcium level
P2X$_5$	Skin, gut, bladder, thymus, spinal cord	ATP>> α,β-meATP, ATPγS	Suramin, PPADS, BBG, TNP-ATP	Increase in cytosolic calcium level
P2X$_6$	CNS, motor neurons in spinal cord	ATP > 2-meSATP (does not function as homomer)	TNP-ATP, PPADS	Increase in cytosolic calcium level
P2X$_7$	Immune cells, pancreas, skin	BzATP>ATP≥2-MeSATP>> α,β-meATP	KN62, KN04, A-438079, A-740003.0, A-804598, AZ11645373, Brilliant blue G	Increase in cytosolic calcium level

Adapted from Burnstock (2007)

1.2   P2X$_4$ receptor

P2X$_4$ receptors were originally cloned from the brain of rat by Bo et al. (1995) and Soto et al. (1996). Both reported that rat P2X$_4$ was insensitive to known P2X antagonists, suramin and pyridoxal-phosphate-6-azophenyl-2`,4`-disulfonic acid (PPADS). Subsequently, P2X$_4$ was cloned from the brain of human (Garcia-Guzman et al., 1997) and mouse (Simon et al., 1999). Heterologous expression of both P2X$_4$ orthologues yielded ATP-evoked responses which were blocked by suramin (weak blockade at mouse P2X$_4$) and PPADS, in contrast to the rat P2X$_4$. The human P2X$_4$ was found to exhibit broad tissue expression. The order of agonist potency reported for the human P2X$_4$ receptor was ATP $\gg$ 2-methylthio-ATP (2meSATP) $\geq$ CTP > $\alpha\beta$-meATP > dATP (Garcia-Guzman et al., 1997). The P2X$_4$ receptors were also demonstrated to form functional heterotrimers with other P2X subtypes, i.e., P2X$_{1/4}$ (Nicke et al., 2005) and P2X$_{4/6}$ (Le et al., 1998), where both showed increased sensitivity to suramin.

1.2.1   Molecular structure of P2X$_4$

The P2X$_4$ receptor consists of three subunits that cluster together and become a trimeric receptor. It is an ion channel primarily modulated by ATP as the physiological agonist, of which activation results in the fluxes of Ca^{2+}, Na^+, and K^+. The reported EC$_{50}$ of ATP at the human P2X$_4$ receptor was 1.4 µM (Jones et al., 2000). The first ever solved crystal structure of P2X$_4$ was from zebrafish (zfP2X$_4$) in its closed, resting state and this has significantly improved the insight of the structure of P2X receptor family (Kawate et al., 2009). The shape of homotrimeric zfP2X$_4$ can be analogised to a goblet. A relatively big portion of extracellular loop (~70 Å) protruding from the lipid bilayer of the plasma membrane resembles the cup portion of a goblet while the stand looks like the relatively small portion of transmembrane motifs embedded in the membrane (~28 Å) (Figure 1.2). The structure of each subunit resembles a dolphin shape. The flukes are similar to the two transmembrane helices and the upper body resembles the extracellular portion of the subunit (Figure 1.3). Kawate et al. (2009) also proposed two ways that extracellular cations can enter cells through the receptor. The first way was through the openings known as lateral fenestrations which are

slightly above the transmembrane motifs. In the closed state, the diameter of the fenestrations is ~8 Å, which is sufficient for Ca^{2+}, Na^+, and K^+ ion fluxes. This route was also suggested by Samways et al. (2011) through cysteine-scanning mutagenesis study. The second proposal was through the upper vestibule of the receptor, surrounded by the three subunits. Though the opening was too small (~2.3 Å) for hydrated ions to go through in the closed state, it was hypothesised that the opening may enlarge after activation by agonist (Figure 1.4) (Kawate et al., 2009).
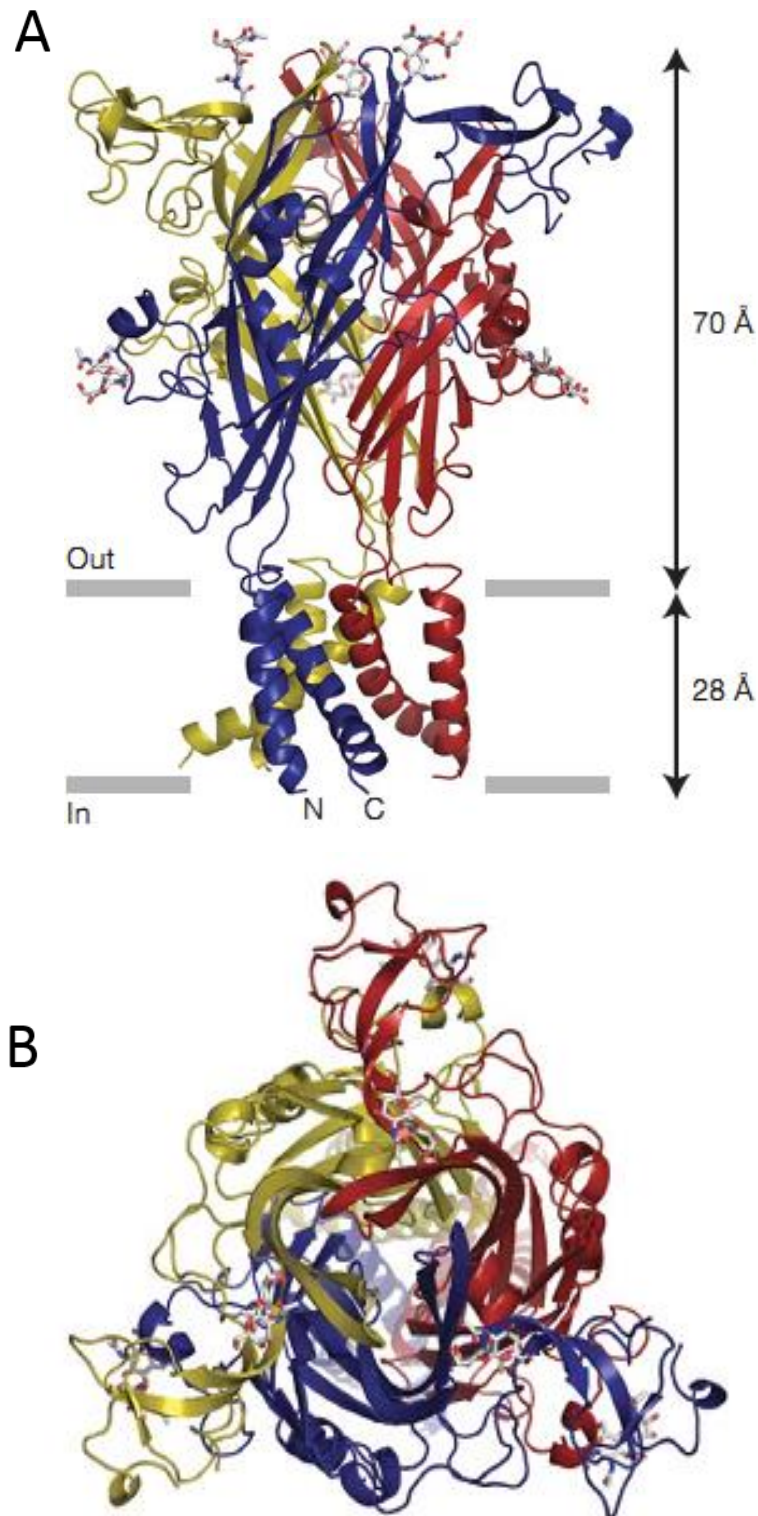
Figure 1.2 Stereo view of zfP2X$_4$ from the side (A) and the top (B).
(Kawate et al., 2009)
P2X$_4$ receptor consists of three subunits, coded with different colours (red, blue, and yellow). Panel A shows side view (parallel to the plasma membrane) of P2X$_4$ receptor. The grey bars indicate the outer and inner membranes. Panel B shows top view (from the extracellular space) of the receptor.
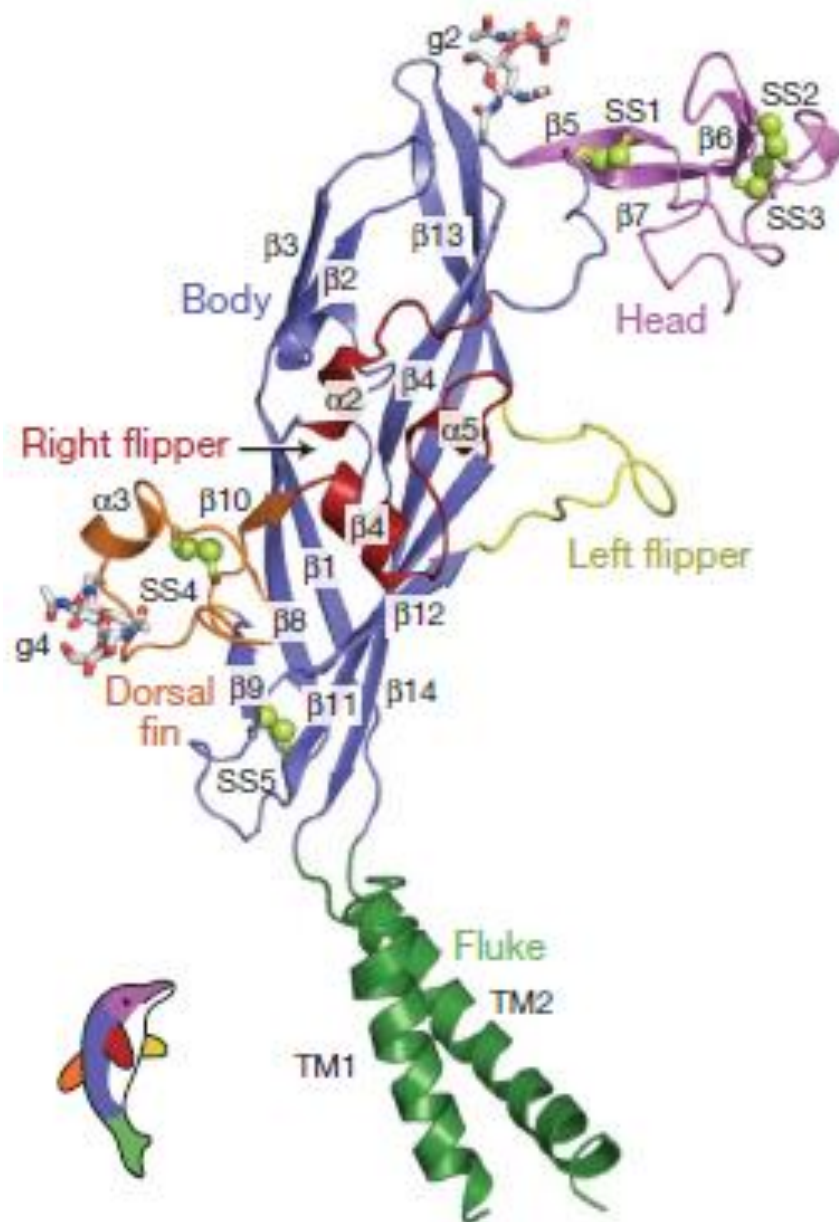
Figure 1.3 Crystal structure of a subunit of P2X$_4$ resembling dolphin.
(Kawate et al., 2009)
The figure shows the resemblance of one P2X$_4$ subunit to a dolphin. Each part of dolphin is colour-coded according to the parts of P2X$_4$ subunit.
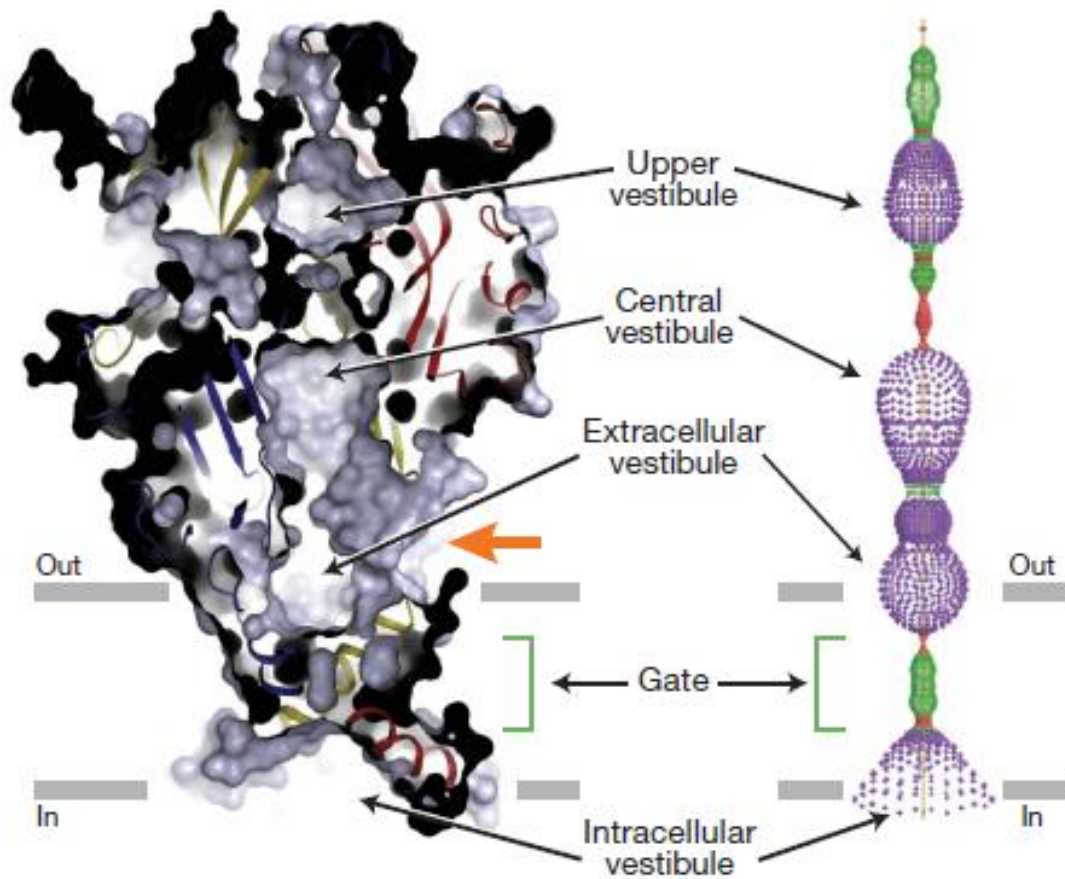
Figure 1.4 Conformation of closed state P2X₄.

(Kawate et al., 2009)

The left panel shows sagittal plane of P2X₄ and reveals four vestibules (as shown schematically on the right panel) in the middle of receptor, surrounded by three subunits. The first proposed ion channel is marked with the orange arrow which is connected to extracellular vestibule and the second proposal is through the green opening on top of upper vestibule (right panel).

In 2012, the same group solved the crystal structure of zfP2X$_4$ in an open state with bound ATP at the ligand binding site at a resolution of 2.8 Å, together with another closed, resting state at higher resolution of 2.9 Å (Hattori & Gouaux, 2012). This study benefitted researchers with a vast amount of information about the ATP binding site of P2X$_4$ that is very important in drug screening. With the crystal structures, they could identify the exact location of ATP binding and vital residues that make up the binding. Also, they could confirm the hypothesised routes of ion transfer.

Through this unearthing, the binding sites were identified to be pockets in the middle of two subunits. Between the two subunits, there was one binding site. Thus, there are three binding sites in a P2X$_4$ receptor. This observation was in agreement with a theory hypothesised by Bean (1990) based on his experiments, where the stoichiometry of ATP binding to P2X$_4$ was at least 3:1. These findings were also in line with previous studies at other P2Xs. Wilkinson et al. (2006) proved that the ATP binding site of P2X$_{2/3}$ was made up of two subunits and Marquez-Klaka et al. (2007) also reported the same finding for P2X$_1$.

Based on the ATP-bound P2X$_4$ crystal structure, the zfP2X$_4$ residues that interacted with ATP were Asn296, Arg298 and Lys316 of the first subunit and Lys70, Lys72, and Thr189 of the adjacent subunit. The residues established direct polar interaction with ATP molecules while Lys193 of the adjacent subunit interacted indirectly with ATP through interaction with glycerol molecule. There were a few other residues that have hydrophobic interactions with ATP which were Ala291 and Ala292 of the first subunit, and Arg143, Ile232, Leu217, and Leu191 of the adjacent subunit.

The crystal structure also revealed that the first proposal regarding ion transfer channel was revealed true. When ATP binds to the binding site, the size of upper, extracellular, and intracellular vestibules is enlarged while the top middle opening remains relatively unchanged and thus, not allowing ions to pass through (Figure 1.5). The acidic environment of the extracellular vestibule also helps to repel anions and attract cations to transport them into the cytosol (Hattori & Gouaux, 2012). At P2X$_3$, the extracellular and intracellular boundaries are gated by Ile323 and Thr330 respectively, as well as Val326 that also contributes to the occlusion of the vestibules. However, the desensitised state is not the reverse of open state, rather the movement of

transmembrane motifs towards the extracellular surface by 4.4 Å and an inward rotation of Val334 cause the pore to close (Mansoor et al., 2016).

Nevertheless, there was a concern regarding the gating mechanism proposed by Hattori and Gouaux (2012) because both terminal domains were truncated in their crystal constructs (Mansoor et al., 2016). Based on the study on the rat $P2X_2$, Habermacher et al. (2015) found that there was a discrepancy in the fenestration observed in the crystal structure of ATP-bound $zfP2X_4$, where such fenestration was absent in the rat $P2X_2$ receptor. Molecular dynamics simulations also showed that such opening was smaller than that observed in the ATP-bound crystal structure of $zfP2X_4$ (Heymann et al. 2013). Mansoor et al. (2016) gave a new insight into the gating mechanism by solving crystal structures of human $P2X_3$ in its apo/resting, agonist-bound/open-pore, agonist-bound/closed-pore/desensitized, and antagonist-bound/closed states. They described the changes during the transition from the resting to open and from open to desensitised states, and also revealed the existence of a cytoplasmic cap anchor which was absent in the crystals of $zfP2X_4$ because of the truncated termini. It was hypothesised that this cytoplasmic cap affects the rate of desensitisation of P2X receptors. In short, the pore opening observed in the zfP2X4 crystal was not accurate because of the truncation of the termini, however the path of ion fluxes was true. Later studies provided new information on important residues that were involved in the gating mechanism and most importantly, the cytoplasmic cap that influenced the desensitisation state of P2X receptors (Habermacher et al., 2016; Heymann et al., 2013; Mansoor et al., 2016).
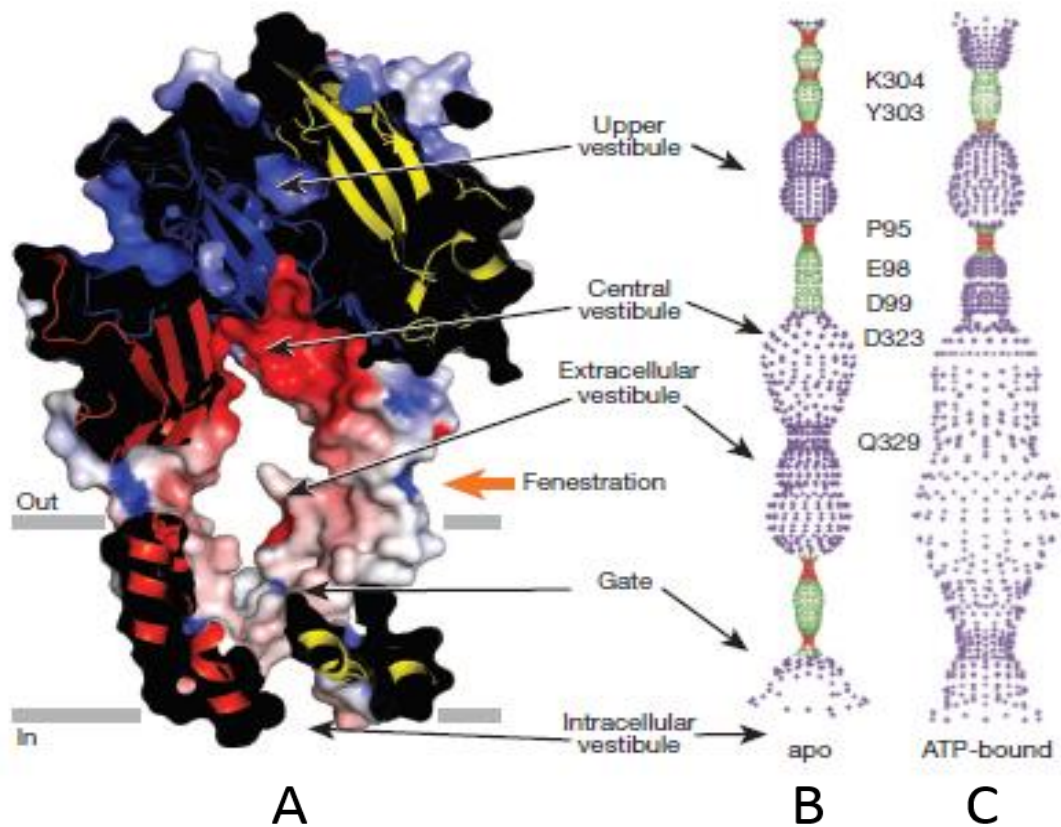
Figure 1.5 Differences between open and closed conformation of P2X₄.
(Hattori & Gouaux, 2012)

Panel A shows sagittal plane of zfP2X₄ in open state, revealing even larger vestibules compared to apo state as schematically represented in panel B and C. The crystal structure confirms that ion transfer occurs through the fenestration marked with orange arrow. Ions then enter the enlarged extracellular and intracellular vestibules before going into the cytosol.

1.2.2 Polymorphisms in P2X$_4$

The *P2RX4* gene contains a few single nucleotide polymorphisms but not many studies were done to identify its functional impact on the P2X$_4$ receptor. Stokes et al. (2011) were the first to demonstrate the impact of *P2RX4* gene polymorphisms. They investigated four nonsynonymous coding single nucleotide polymorphisms (SNP) which were identified from the National Centre for Biotechnology Information Single Nucleotide Polymorphism database (build 126). It was found that one SNP (mutation at Tyr315>Cys (rs28360472)) appeared to have a profound effect on current amplitude compared to wild-type (WT) P2X$_4$. Subsequent epidemiological study on 2,874 subjects from the Victorian Family Heart Study revealed that 1.4 % from that population carried the minor allele mutation. Further analysis showed a positive correlation between the mutation and increased pulse pressure which may reflect reduced large arterial compliance because of vasodilation failure by large arterial vascular endothelial cells.

Further study by Gu et al. (2013) also found a correlation between the same mutation at *P2RX4* gene and Gly150>Arg mutation in the *P2RX7* gene, with age-related macular degeneration (AMD) patients. This medical condition is the main factor for blindness in western countries which is characterised by the deposition of yellow substance called drusen, beneath retina. These deposits are physiologically scavenged by phagocytosis which is controlled by P2X$_7$. Based on a population of 744 AMD patients and 557 control patients, they discovered that those mutations form a unique haplotype that is associated with increased susceptibility to AMD (odds ratio = 4.05).

In another study, the researchers examined the effect of three non-synonymous SNPs at *P2RX4* gene on bone mineral density (BMD) in an association with the risk of osteoporosis (Wesselius et al., 2013). The risk of osteoporosis was assessed by measuring BMD at different locations. The study was done on 921 patients with bone fractures which were divided into two groups; osteoporotic and non-osteoporotic. They found that patients with this polymorphism (Tyr315>Cys) in the *P2RX4* gene have a 2.68-fold higher risk of osteoporosis compared to wild-type subject, with a significant decrease in BMD at the lower lumbar spine. They also found an anomaly

with another polymorphism (Ser242>Gly) where the affected patients gave contrary measurements of BMD at lumbar spine compared to the wild-type subject.

1.2.3   Roles of P2X$_4$

P2X$_4$ is widely distributed throughout many tissues of human body. The evidence of their tissue-specific roles have been highlighted by several studies, which will be discussed in greater detail below.

1.2.3.1   Roles in the cardiovascular system

Studies utilising the transgenic mouse model overexpressing P2X$_4$ by Hu et al. (2001) illustrated that these mice have a higher basal level of cardiac output when compared to wild-type mice. This highlights the role of P2X$_4$ in stimulating cardiac contractility in the human heart muscles. In addition to this, Yang et al. (2014) established a more sophisticated role of P2X$_4$ in myocytes. Their finding was that P2X$_4$ serves as protection against heart failure. This was based on their observation on cardiac-specific P2X$_4$ knock-out and overexpressed mouse models which showed a clear difference on the impact of contractile performance and pressure overload between those models after infarction. The knock-out mice exhibited reduced contraction and pressure overload while the overexpressed mice showed the opposite.

In addition to this, Northern blot analysis by Yamamoto et al. (2000) demonstrated that P2X$_4$ was abundantly present in human vascular endothelial cells (ECs), e.g., aorta, pulmonary artery, and umbilical cord vein. Functionally, it was found to be responsible for the sustained phase of calcium influx in ECs (Yamamoto et al., 2000). Later, the same group showed a more detailed study on the functions of P2X$_4$ in the ECs. P2X$_4$ receptors were shown to play an important role in adapting the ECs structure and function in response to physical development and exercise. It was reported that the presence of P2X$_4$ in ECs holds the key for blood vessel adaptation to blood flow and that there was no calcium influx that in turn leads to the production of nitric oxide (NO, a vasodilator) in P2X$_4$ knock-out mice as well as a marked increase in blood pressure (Yamamoto et al., 2006).

In addition to that, Harhun et al. (2014) contributed the evidence of heteromeric $P2X_{1/4}$ presence in vascular smooth muscle cells. It has been understood that ATP is implicated in cerebral vasospasm via activation of rapidly-desensitising $P2X_1$. However, it was unclear how the pathological condition sustains as $P2X_1$ was rapidly desensitised. Therefore, the researchers discovered that $P2X_{1/4}$ was involved with the process in which $P2X_4$ contributed to the sustained phase of vasospasm.

1.2.3.2 Roles in the respiratory system

$P2X_4$ receptors have also been found in various parts of the respiratory system, including in lamellar bodies (LBs) of alveolar type II epithelial cells (APII). Lamellar bodies are the large organelles that store insoluble surfactant which function to ease the surface tension. The surfactant is not easily released into the alveolar space. Miklavc et al. (2013) found that the $P2X_4$ receptor facilitated the process. When LBs fuse with the APII membrane, the extracellular ATP from the alveolar space comes into the LBs and activates $P2X_4$ which in turn promotes the release of Ca^{2+} and Na^+ into APII cells surrounding the fused vesicle. This further enlarges the pore of exocytosis and helps the release of surfactant.

Recently, $P2X_4$ has also been implicated in the development of allergic asthma (Zech et al., 2016). The study discovered that $P2X_4$ played a role in causing airway inflammation that leads to asthma. $P2X_4$ knock-out and 5-BDBD-treated wild-type mice were exposed to albumin in order to develop the allergen-induced airway inflammation (AAI) (that resembles allergic asthma). All mice were reported to exhibit increased expression of $P2X_4$ and $P2X_7$, as well as increased production of IL-1β following ATP stimulation. However, both $P2X_4$ knock-out and wild-type mice treated with $P2X_4$ antagonist (5-BDBD) showed reduced expression of $P2X_7$ and IL-1β production along with reduced inflammation. The findings suggested that $P2X_4$ played a role in the progression of allergic asthma and mediated the $P2X_7$ expression in response to allergen. These findings were also in agreement with a previous study (Nagaoka et al., 2009) that proposed a link between $P2X_4$ and bronchial asthma.

1.2.3.3 Roles in the nervous system

In the nervous system, $P2X_4$ receptors are abundantly present in glial cells and throughout the central nervous system. For example, microglia are the immune effector cells that naturally present in a ramified condition under physiological condition. In response to stimuli, microglia undergo morphological changes into a motile amoeboid form which then migrate to lesion sites, and subsequently release certain substances. Ohsawa et al. (2007) reported low $P2X_4$ expression in normal brain and spinal cord, however the expression was enhanced in activated microglia following nerve injury. This finding was later verified by Li and co-researchers (2011) which suggests that the chemotactic microglial cells in postnatal rat brain were also mediated by $P2X_4$.

$P2X_4$ has also been reported to be expressed at various regions of the central nervous system. This includes the CA1 region of hippocampus, in which $P2X_4$ receptors are concentrated at the perisynaptic region of pre- and post-synaptic membranes (Rubio & Soto, 2001). This localisation of $P2X_4$ receptors was shown to be involved in long-term potentiation (LTP) (Sim et al., 2006). The stimulation of Schaffer collaterals in *P2X4R* knock-out mice produced significantly lower LTP magnitude compared to wild-type mice. This was further confirmed when ivermectin (IVM, a $P2X_4$ allosteric positive modulator) further increased the LTP magnitude in wild-type mice. Unaltered LTP magnitude in knock-out mice, on other hand, ruled out the possibility of IVM potentiation on other receptors such as $GABA_A$ ($GABA_AR$) and $\alpha7$ nicotinic receptors. Thus, it was deduced that calcium influx through $P2X_4$ receptor could enhance the long-term synaptic plasticity of hippocampal CA1 neurons. It was also postulated that $P2X_4$ may be responsible for incorporating more AMPA receptors to subsynaptic membrane that result in LTP (Baxter et al., 2011).

$P2X_4$ receptor has also been directly associated with the neurotransmission process by interacting with $GABA_AR$ that might affect synaptic plasticity (Jo et al., 2011). Moreover, an interaction between $P2X_4$ and dopamine transmission has recently been established (Khoja et al., 2016), where $P2X_4$-deficient mice showed altered level of pre-synaptic markers such as dopamine transporter and post-synaptic markers such as

dopamine receptors. This remarkable finding provides a ground for new insights to treat the dopamine-related diseases such as psychiatry disorders.

Apart from P2X$_4$ receptor involvement in neurotransmission and synaptic plasticity, growing evidence indicates that P2X$_4$ was also involved in alcohol-related issues (Yardley et al., 2012). It was initially shown that ethanol inhibited purinergic receptors, particularly P2X receptors (Li et al., 1993, 1998). Later, ethanol was shown to inhibit P2X$_4$ expressed in *Xenopus* oocytes (Xiong et al., 2005, 2000) and HEK293 cells (Ostrovskaya et al., 2011). Converging lines of evidence suggested alcohol-related problems could be due to the P2X$_4$ inhibition by ethanol. P2X$_4$ knock-out mice displayed increased alcohol intake in relative to wild-type (Franklin et al., 2015), in agreement with a finding that reported the low expression of P2X$_4$ receptors in alcohol-preferring mice (Kimpel et al., 2007). The localisation of P2X$_4$ receptors within mesolimbic pathway including the ventral tegmental area (VTA) of the midbrain, amygdala, and hippocampus supported the hypothetical link between P2X$_4$ receptors and reward- and aversion-related neurotransmission (as reviewed by Franklin et al. (2014)).

1.2.3.4 Roles in the immune system

The expression of P2X$_4$ receptor has been shown to be upregulated during inflammatory conditions. One of the discoveries of P2X$_4$ in pathological conditions was described by Solini et al. (2007) who suggested the involvement of P2X$_4$ in the apoptosis of human mesangial cells (HMC). Extracellular ATP activates the highly expressed P2X$_4$ receptor in HMC that in turn triggers the cell death in case of chronic renal disease.

P2X$_4$ receptor was also found to be highly expressed in peripheral myeloid cells (Wang et al., 2004). It was thought that P2X$_4$ was involved during inflammatory processes, which contributed the release of prostaglandin E2 (PGE2), a regulator for inflammatory responses. The synthesis of inflammation-linked PGE2 is a result of cytosolic phospholipase A2 α (cPLA2) that releases arachidonic acid (AA). The enzymatic reaction of cPLA2 is highly dependent on intracellular calcium and ATP is one of several extracellular signalling molecules that can trigger calcium rise and

therefore, an activator for cPLA2 (Balboa et al., 1999). Ulmann et al. (2010) investigated the possibility of P2X$_4$ activation in cultured macrophages to cause AA production and consequently PGE2 production and their finding was in accordance with the theory that P2X$_4$ activation lead to PGE2 release through cPLA2 activity which in turn, caused the inflammation.

P2X$_4$ was also reported to be related with immune response stimulation involving T cell activation and proliferation. It is known that T cell activation requires an immunological synapse with antigen-presenting cells (APC) which subsequently activates a signalling cascade that includes ATP release as one of intermediates. The release of ATP is facilitated by pannexin-1, a gap junction hemichannel, once the T cell receptor (TCR) communicates with APC. The P2X$_4$ receptor has also been shown to take part in T cell activation (Schenk et al., 2008). Therefore, Woehrle et al. (2010) investigated the relationship between pannexin-1, P2X$_1$, and P2X$_4$ in relation to T cell stimulation. It was found that the pannexin-1 and P2X$_4$ were involved during the amplification of T cell activation and proliferation, despite the limited number of TCR at immune synapse that may restrict T cell activation.

1.2.3.5   Roles in the endocrine system

Many reports indicated that P2X$_4$ receptors are present at various sites of the endocrine system and contribute in the activities of gonadotrophin-releasing hormone neuron, thyroid gland, adrenal cortex, lactotrophs, and anterior pituitary gland, as reviewed by Bjelobaba et al. (2015). Despite its ubiquitous expression throughout the endocrine system, its role at various locations have been largely unexplored. Zemkova et al. (2010), among others, investigated the expression of P2X receptors in anterior pituitary cells using quantitative RT-PCR analysis and found that P2X$_4$ was the most abundant in the cells. The receptors were suggested to trigger secretory pathways involving thyrotropin-releasing hormone-responsive cells and lactotrophs by initiating and regulating the electrical activity and recruiting calcium influx.

1.2.4   P2X$_4$ and tactile allodynia

Tactile allodynia, as understood so far, is a type of neuropathic pain which is believed to be resulted from peripheral nerve injury (PNI). This disease is primarily characterised by persistent pain or recurrence of pain independent of stimulus (Murphy et al., 2017). Pain experienced by patients includes a feeling of burning, and shooting pain. The sufferers are highly sensitive to pain, that in some extreme cases, even a light touch can result in a great pain. The aetiology and mechanism by which this disease occurs are largely unexplained. It might be caused by a collection of mechanisms or one mechanism that could lead to many conditions (Scholz & Woolf, 2002; Woolf & Mannion, 1999). However, numerous outstanding discoveries over the past decade have produced a mutual consensus that the PNI causes microglial activation which leads to its pathogenesis. The underlying mechanisms on the process of microglial cells activation and subsequent cascades are the interesting issues that demand further exploration.

The first association between P2X$_4$ and tactile allodynia was demonstrated by Tsuda et al. (2003). A non-selective P2X$_4$ antagonist, TNP-ATP, was used to demonstrate that inhibition of P2X$_4$ receptor reduces the hypersensitivity in animals with nerve injury. They also ruled out the involvement of other P2X receptors using low concentration of PPADS which was sufficient to block other P2X receptors. They found that PPADS failed to attenuate pain hypersensitivity in the animals used, indicating P2X$_4$ was the only receptor responsible for hypersensitivity.

There were many other studies that revealed historical findings in understanding tactile allodynia development which will be discussed in the next three sections. The first section will discuss on the signalling cascades that lead to P2X$_4$ receptor upregulation, the second section will scrutinise the downstream pathway resulted from P2X$_4$ upregulation, and the third section will summarise the first two sections.

1.2.4.1   Signals which upregulate P2X$_4$

There are several studies have been done to elucidate the possible processes that lead to the upregulation of P2X$_4$ receptors. One such study was carried out by Zhang and

De Koninck (2006). They demonstrated that chemoattractant protein-1 (MCP-1), also known as CCL2, was responsible for microglial cell activation after PNI. CCL2 was induced in a few parts of the spinal cord that is ipsilateral to the injury site and the induction subsequently leads to the activation of microglial cells, which is confirmed through the morphological changes of microglia and antibody-labelled $P2X_4$ receptors. Later, they asserted that the interaction between CCL2 and its receptor, CCR2, is essential during the microglial activation, not only on the resident microglia at the spinal cord, but also macrophages/monocytes that migrated into the spinal cord, proliferated, and differentiated into microglia. The CCR2-deficient model (native receptor for CCL2) did not display the symptoms of neuropathic pain or even microglial activation when the CCL2 was injected intrathecally. Moreover, neutralising CCL2 also inhibited the infiltration of macrophages into spinal cord (Zhang et al., 2007).

Kim et al. (2007) explained another component that might be involved in the progression of tactile allodynia. They showed the participation of toll-like receptor 2 (TLR2) during the activation of glial cells, which is vital for the development of allodynia. They also showed that the expression of interleukin-1β, interleukin-6, tumour necrosis factor-α (TNF-α), and inducible nitric-oxide synthase (iNOS) were induced in spinal cord glial cells after sensory neurons were damaged. Later, the same group further investigated the involvement of TLR2 in tactile allodynia. They demonstrated that the receptor was also responsible for the upregulation of NADPH oxidase 2 (Nox2) (Lim et al., 2013) and interferon regulatory factor (IRF8) (Lim et al., 2016).

Nox2 has been shown to be induced in spinal cord microglia after PNI. The induction of Nox2 in turn stimulates the production of reactive oxygen species (ROS) which is required for microglia activation and pain hypersensitivity (Lim et al., 2013). Meanwhile, IRF8 is a main transcription factor in microglial activation after PNI. They discovered the TLR2 knock-out mice did not display the upregulation of IRF8, and potentiating the TLR2 with an agonist marked an increase in IRF8 transcription (Lim et al., 2016). Earlier, the importance of IRF8 in microglial activation was implicated by Masuda et al. (2012) who proposed that the IRF8 is an important transcription factor that increases the transcription of genes required for activated microglia.

In addition to IRF8, Masuda et al. (2014) also found another transcription factor that is crucial for P2X$_4$ receptor upregulation, namely interferon regulatory factor-5 (IRF5). It was reported that its expression was induced after PNI and that it bound directly to the promoter region of *P2RX4* gene. Observation on IRF5-deficient mice proved that P2X$_4$ was not upregulated after PNI and that hypersensitivity was compromised. Moreover, they demonstrated a relationship between the two transcription factors where IRF8 regulated the expression of IRF5 in microglia. Together, IRF5 and IRF8 are two major transcription factors that are directly responsible for upregulating the P2X$_4$ receptors in microglia.

Tsuda et al. (2008b) found that the Src-family kinases (SFK), particularly Lyn, was key players in the development of allodynia. Lyn was the most abundant SFK in the central nervous system. Lyn expression was found to be confined to microglia and increased after PNI. Apart from that, Lyn knock-out mice also displayed reduced upregulation of P2X$_4$ receptor expression following PNI, indicating that the kinases were one of many possible signals in causing the P2X$_4$ receptor upregulation.

The same group also delineated the involvement of fibronectin/integrin in P2X$_4$ upregulation at the spinal cord after PNI. Fibronectin is a molecule in the extracellular matrix and it has been shown to regulate the microglial functions. The receptor for fibronectin is integrin, which can be a heterodimer between 18 α subunits and 8 β subunits (Campbell & Humphries, 2011). In case of tactile allodynia, fibronectin was found to upregulate the expression of P2X$_4$ receptor (Tsuda et al., 2008a). The blockade of integrin using echistatin in an *in vivo* study revealed failed upregulation of P2X$_4$ receptors, while introduction of fibronectin into normal rats induced P2X$_4$ upregulation prior to development of tactile allodynia.

Later, the same team made another discovery regarding the possible cytokine or receptor which involved in microglia activation. They unearthed the involvement of cytokine IFN-γ together with its receptor (IFN-γR). The receptors are present in naïve microglia and upon activation of receptors, the microglia become activated and tactile allodynia develops. Meanwhile, the IFN-γR knock-out mice exhibited reduced sensitivity of some microglia (not all) to PNI. This might be explained through the fact

that microglia activation is not a result of IFN-γ/IFN-γR signalling alone, rather it involves a collection of mechanisms that can lead to its activation. Interestingly, the activation of IFN-γR also increases the expression of Lyn tyrosine kinase and P2X$_4$ receptors, which indicates that the IFN-γ/ IFN-γR cascade occurs during the pre-SFK activation (Tsuda et al., 2009).

Besides, Biber et al. (2011) elucidated another molecule that is important in P2X$_4$ receptor upregulation. CCL21 expression was found to be induced at the nerve injury site and it is transported to their central terminals in the dorsal horn. In CCL21 knock-out mice, the P2X$_4$ receptor expression level remains unchanged after nerve injury, and injection of CCL21 into CCL21 knock-out model induces the overexpression of P2X$_4$ receptor. CXCR3 and CCR7 are the receptors for CCL21, however this study indicated that neither is crucial for CCL21 cascade signalling since knock-out mice of either receptor produced similar reduction in paw withdrawal threshold (PWT), a characteristic of model with hyperalgesia. This finding presented a direct evidence that CCL21 is indeed a very crucial factor during the upregulation of expression of P2X$_4$.

1.2.4.2 Signalling downstream of P2X$_4$

Tsuda et al. (2004) associated tactile allodynia with the activation of p38 mitogen-activated protein kinase (p38MAPK) in spinal microglia of rat model (Tsuda et al., 2004). Immunofluorescence assay revealed that this protein kinase is overexpressed in the dorsal horn at the injury site, particularly in microglia, but not in the opposite side. Moreover, the use of a p38MAPK inhibitor, 4-(4-fluorophenyl)-2-(4-methylsulfonylphenyl)-5-(4-pyridyl)-1H-imidazole (SB203580) inhibited the development of nerve injury-associated tactile allodynia.

Coull et al. (2005) addressed another remarkable finding in understanding neuropathic pain development. They found that activated microglia following PNI changes the anion reversal potential (E_{anion}) in spinal lamina I neurons, and that application of brain-derived neuropathic factor (BDNF) to a naïve rat model resembles the E_{anion} changes. The receptor for BDNF, TrkB, has been shown to interact with BDNF that subsequently causes E_{anion} changes. In addition, under normal condition, GABA (γ-amino butyric acid) causes the inhibition of action potentials which results in the

inhibition of nociceptive signals. However, in this case, GABA through its receptor (GABAR) causes the opposite outcome, instead of being inhibitory, it excites action potentials and sequentially transmits more pain signals. This was observed on some, but not all, lamina I neurons when GABA is applied.

In agreement with previous discovery by Coull et al. (2005), Ulmann et al. (2008) identified additional knowledge on the consequence of $P2X_4$ receptor upregulation. They presented direct evidence showing that the $P2X_4$ upregulation and activation by ATP subsequently cause the release of BDNF, which has been indicated to be a vital signalling molecule between activated microglia and neurons in hypersensitivity cases. The release of BDNF from microglia is likely to mediate the downregulation of K^+/Cl^- cotransporter KCC2 in inhibitory neurons, which results in allodynia.

Trang et al. (2009) further investigated the process of BDNF release from microglia upon $P2X_4$ receptor stimulation by ATP. They made several interesting discoveries in their study. Upon activation of $P2X_4$ receptor by ATP, the influx of calcium in turn activates p38MAPK, a signalling mechanism as implicated by Tsuda et al. (2004). The p38MAPK activation then causes the upregulation of BDNF expression as well as the release of BDNF from microglia. They also found that the BDNF release occurs through soluble N-ethylmaleimide-sensitive factor attachment protein (SNAP) receptor (SNARE)-dependent exocytosis. These findings are also in agreement with Xiaodi et al. (2010) who found the same signalling cascade in rat model with mechanical hypersensitivity.

In addition to that, Slack et al. (2005) demonstrated the presence of TrkB, a high-affinity receptor for BDNF in spinothalamic tract, a route where nociceptive information was transmitted in the spinal cord. The presence of TrkB supports previous findings which stated that the BDNF was crucial in neuropathic progression. Microinjection of BDNF and capsaicin introduction to naïve rats stimulate the PNI and subsequently produce BDNF, both cause the activation of extracellular signal-regulated protein kinase (ERK) phosphorylation in TrkB containing neurons. Induction of ERK phosphorylation was earlier observed by Ji et al. (1999) (as cited in Slack et al. (2005)) as an important sequential event in hyperalgesia development.

Next, Katsura et al. (2006) documented another possible signalling mechanism in the tactile allodynia development. They reported PNI stimulated the activation of SFK, including Src, Lck, and Lyn at the microglia of spinal dorsal horn. The activation in turn rises the phosphorylation of ERK and contributes to the pathogenesis of mechanical hypersensitivity. Blocking SFK with 4-amino-5-(4-chlorophenyl)-7-(t-butyl)pyrazolo[3,4-d]pyrimidine (PP2) signifies a halt on the activation of ERK and mechanical hypersensitivity caused by nerve injury, but not by cold and heat.

1.2.4.3 Summary of tactile allodynia signalling cascade

After extensive in-depth studies about the disease over decades, a unifying mechanism for its development was proposed by Beggs and Salter (2010) and Trang and Salter (2012). After PNI, several proteins and cytokines such as CCL2, CCL21, IFN-γ, and fibronectin are upregulated and activated. Although some studies argued against the hypothesis of CCL2 upregulation since its receptor (CCR2) is absent in microglia, its involvement during the development of nerve-injury induced neuropathic pain is evident (Biber & Boddeke, 2014). The involvement of CCL21 was clear based on several convincing evidences that link the CCL21 with $P2X_4$ receptor upregulation although its receptors (CCR21 and CXCL3) are not important in the process. Instead, it was proposed that it could be another unknown CCL21 receptor that is activated during this signalling mechanism (Biber & Boddeke, 2014). Meanwhile, the binding of IFN-γ to its receptor, IFN-γR, subsequently activates the SFK signalling (Lyn particularly) cascade and phosphorylation of ERK (Tsuda et al., 2009).

Fibronectin, on the other hand, has been quite well elaborated. Its binding to its receptor, integrin, stimulates microglia to their activated form and that upregulates the IRF5 expression. In addition to that, the activation of TLR2 by an unknown protein upregulates another transcription factor, IRF8. The upregulation of IRF5 is controlled by IRF8, which then induces the upregulation of de novo expression of $P2X_4$ receptors by directly binding to promoter region of *P2X4R* gene. Together, the CCL2, CCL21, IFN-γ, and fibronectin are all being stimulated in response to PNI and the stimulation activates microglia with the upregulated $P2X_4$ receptor expression (Trang & Salter, 2012).

Following the upregulation of P2X$_4$ and its activation by ATP, presumably released as neurotransmitter, P2X$_4$ activates p38MAPK. The activation of p38MAPK induces synthesis and release of BDNF via SNARE exocytosis. The BDNF then binds to its high affinity receptor, TrkB on the neurons and further causes changes in E_{anion}. The changes in anion reversal potential might be due to the downregulation of KCC2 which causes the accumulation of Cl$^-$ in neurons. High neuronal [Cl$^-$] causes the impairment in GABA receptor function which, under normal condition, plays its role to compensate the loss of Cl$^-$ by extrusion through KCC2 and accordingly causes inhibition in transmission. The impairment, however, disinhibits the transmission and rather potentiates the nociceptive transmission that turns innocuous stimuli into noxious stimuli, which consequently results in tactile allodynia (Beggs & Salter, 2010; Stokes et al., 2017; Trang & Salter, 2012).
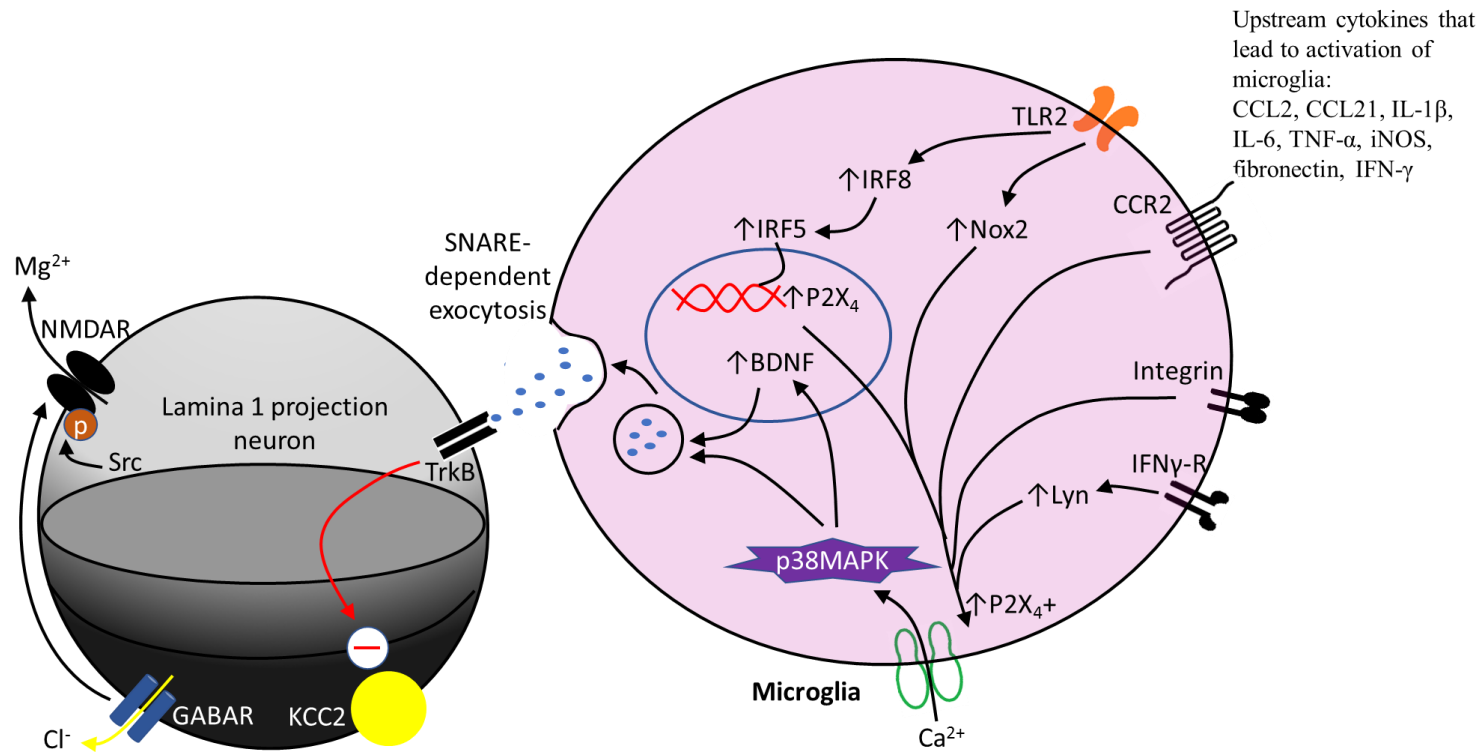
Figure 1.6 Schematic presentation of signalling involved in hypersensitivity

The figure illustrates signals involved in the process of hypersensitivity. Several cytokines are released in response to PNI and act on their respective receptors on microglia cells. The activation of those receptors causes the P2X$_4$ to be upregulated, particularly TLR2 that has been directly associated with upregulation of IRF8 and IRF5. Both regulate the transcription of *P2X4R* gene. Increased calcium influx through upregulated P2X$_4$ receptors in turn activates the p38MAPK, that subsequently causes overexpression of BDNF in addition to release BDNF through SNARE-dependent exocytosis. BDNF interacts with its receptor (TrkB) which then downregulates the KCC2 and causes alteration on membrane properties of dorsal horn lamina 1 neuron. This change can then potentiate the firing of impulse through NMDAR potentiation which eventually leads to hypersensitivity.

1.2.5   P2X$_4$ subcellular localisation and trafficking

P2X receptors are continuously recycled between the plasma membrane and intracellular compartments. It was postulated that this is the way the cells control the up or downregulation of receptors. The seven members of P2X receptors show different cellular distribution due to different receptor trafficking properties. The receptors are predominantly localised at the plasma membrane or within endosomes and lysosomes while some are localised within the endoplasmic reticulum (Bobanovic et al., 2002; Qureshi et al., 2007; Robinson & Murrell-Lagnado, 2013).

The investigation on P2X$_4$ subcellular distribution revealed that the predominant distribution of P2X$_4$ receptors is within the late endosomes and lysosomes. The ability of P2X$_4$ receptors to resist proteolytic environment of the lysosomes is attributed to N-linked glycans which can be found within the intra-luminal loop of the receptor (Bobanovic et al., 2002; Boumechache et al., 2009; Qureshi et al., 2007). The receptors are rapidly internalised from the plasma membrane through a dynamin-dependent mechanism as an evidence showed that mutated dynamin-1 increases the surface expression of P2X$_4$ as well as ATP-evoked response (Bobanovic et al., 2002). In macrophages, P2X$_4$ receptors in the lysosomes are exocytosed to the plasma membrane, stimulated by intracellular calcium increase and this has been hypothesised to be a mechanism of which surface P2X$_4$ is upregulated (Qureshi et al., 2007).

Molecular studies showed that the internalisation involves a non-canonical tyrosine-based endocytic motif of the form YXXGL at C terminal of the P2X$_4$ receptor which interacts with a clathrin- and AP2-dependent pathway (Royle et al., 2002, 2005). Recently, Xu et al. (2014) generated mouse P2X$_4$ carrying a pHluorin tag that shows the same characteristics with wild-type P2X$_4$. This can greatly facilitate the research of P2X$_4$ trafficking through live imaging experiments.

1.2.6 Pharmacology

1.2.6.1 Agonists

All homomeric and heteromeric P2X receptors are activated by ATP but the affinity for ATP is receptor-specific with the EC_{50} values ranging from nanomolar to submillimolar concentrations (Coddou et al., 2011). At the rat $P2X_4$ heterelogously expressed in *Xenopus* oocytes, ATP acts as the most potent agonist with an EC_{50} value of 10 µM and this is followed by ATPγS, 2-methylthio ATP (2meSATP), ADP, and αβ-methylene ATP (the last two have similar potency) (Bo et al., 1995). A subsequent study by Soto et al. (1996) using rat $P2X_4$ also revealed a similar potency order of ATP > 2meSATP ≥ CTP > α,β-meATP > dATP but no response was evoked by ADP, AMP, GTP, adenosine, or β,γ-methylene-ATP analogue. The concentration-response analysis displayed an EC_{50} value of 6.9 ± 0.8 µM for ATP. Early studies of the human $P2X_4$ receptor expressed in *Xenopus* oocytes demonstrated a similar agonist potency order of ATP > 2meSATP ≥ CTP > α,β-meATP > dATP and a similar value of ATP EC_{50} value, i.e., 7.4 ± 0.5 µM (Garcia-Guzman et al., 1997). A study using three $P2X_4$ orthologues (human, rat, and mouse) expressed in HEK293 displayed EC_{50} values of 5.5 µM, 1.5 µM, and 2.3 µM, respectively (Jones et al., 2000). BzATP has also been discovered to be a partial agonist of rat and human $P2X_4$ receptors (Stokes et al., 2017).

1.2.6.2 Positive modulators

Positive allosteric modulators are the compounds that increase response by binding to an allosteric site of a receptor. One of the best positive allosteric modulators for $P2X_4$ is ivermectin (IVM). Ivermectin is a derivative of a macrocyclic lactone which is highly lipophilic. It has long been used as an antiparasitic and anthelmintic drug but it has also been reported to positively modulate several ligand-gated ion channels including $GABA_AR$ (Kru˚šek & Zemkova´, 1994) and α7 neuronal nicotinic acetylcholine receptor (Krause et al., 1998). Ivermectin's potentiation at $P2X_4$ was recorded to be attributed via two effects; it slowly deactivates the receptor and increases the magnitude of agonist-evoked response (Khakh et al., 1999). Ivermectin was reported to be selective to $P2X_4$ (Khakh et al., 1999) but recently, Norenberg and

co-authors (2012) found that IVM can also positively modulate human $P2X_7$, but not mouse $P2X_7$.

The IVM mechanism of action has been extensively elaborated by numerous researches. There are several theories explaining its mechanism of action. Priel and Silberberg (2004) stated that IVM binds allosterically to outer region of the $P2X_4$ receptor and there are two possible allosteric sites for IVM binding, identified as higher and lower affinity sites based on their EC_{50} values. It was postulated that IVM at the higher affinity site reduces channel desensitisation and thereby increases the current magnitude, while IVM at the lower affinity site stabilises the open state of the receptor and thereby slows the deactivation time. This hypothesis was progressively supported by later studies that discovered, rather than acting on the outer region of $P2X_4$ receptor, that IVM enters the bilayer plasma membrane through lateral fenestration of the open state receptor, binds, and jams the opening of $P2X_4$ receptor at allosteric site in transmembrane helices. This allows more calcium to enter and slows the decay kinetics. (Jelínková et al., 2006; Silberberg et al., 2007).

In agreement with previous findings, Jelínkova et al. (2008) brought more evidence showing the action of IVM is indeed through the binding with transmembrane domain. Their cysteine-scanning mutagenesis study revealed that IVM was not sensitive at $P2X_4$ with mutations at one of these residues: Arg33, Gln36, Leu40, Val43, Val47, Trp50 of TM1 and Asn338, Gly342, Leu346, Ala349, Cys353, Ile356 of TM2. Comparing the residues with the topological structure of $P2X_4$ receptors, those residues appeared to line the outer helical side of transmembrane domain in addition to principally a hydrophobic-nonpolar region. These two statements provide more evidence that hydrophobic IVM binds to the transmembrane domain. In addition to this, Zemkova and colleagues (2014) also proposed that the binding of IVM may involve two neighbouring subunits, inferred from the fact that a single mutation of the abovementioned residues failed to totally diminish IVM action in the previous study.

In contrary to Silberberg et al. (2007), Toulmé et al. (2006) earlier reported a slightly different view for the mechanism. The $P2X_4$ receptors are continuously cycled between the intracellular environment and the plasma membrane. In their experiment, it was demonstrated that IVM acted by increasing the surface expression of $P2X_4$

receptors due to a mechanism that involves a constitutive AP2/clathrin-dependent internalisation, and the potentiation characteristic of IVM (in comparison to untreated) is absent when the clathrin-dependent endocytosis mechanism is compromised. However, IVM still causes delayed deactivation in deficient clathrin-dependent internalisation model. Thus, they proposed that IVM potentiates magnitude of $P2X_4$ response via increasing surface expression of $P2X_4$ receptors. In congruity with Toulmé et al. (2006), Stokes (2013) observed the same finding in a study. It was suggested that the action of IVM is indeed dependent on the internalisation mechanism.

Nevertheless, the two findings did not oppose each other, but are rather complementary. Stokes (2013) stated that IVM may bind to the transmembrane region of $P2X_4$ receptor and stabilise the open state. This in turn may prevent the endocytosis of receptors into the cytosol. On the other hand, $P2X_4$ receptors are continually reinserted into the plasma membranes. Together, these situations — prevention of internalisation of IVM-bound $P2X_4$ receptors and the continuous reinsertion of $P2X_4$ receptors — may be interpreted as increased surface expression.

In short, IVM potentiates $P2X_4$ response during an open state and it alone cannot cause channel activation. Once $P2X_4$ receptor is activated, IVM enters the membrane lipid bilayer through lateral opening and binds to transmembrane domain between two neighbouring subunits. The hydrophobic regions of TM1 and TM2 are the most possible binding site for IVM as the compound is lipophilic and the molecular structure configuration of both transmembrane region and IVM complement each other (Jelínkova et al., 2008). Once bound to the higher affinity binding site, it increases the response, while binding to the lower affinity region prolongs deactivation time by blocking the closure of receptor. It is also possible to deduce that the binding of IVM also prevents the internalisation of surface receptor while reinsertion of the receptors causes elevated surface $P2X_4$ receptor expression.

Ivermectin was also reported to antagonise the ethanol effect of $P2X_4$ receptor expressed in *Xenopus* oocytes. The electrophysiology data showed that IVM can overcome the inhibition by ethanol (Asatryan et al., 2010). Yardley et al. (2012) also found that when IVM is injected into mice, it can reduce their alcohol intake and

preference. Recent findings showed that an analogue of IVM, moxidectin, could also potentiate the $P2X_4$ response and antagonise the inhibition of ethanol as well as alleviate alcohol intake by mice (Huynh et al., 2017). Other IVM analogues that have been reported to potentiate the $P2X_4$ responses include avermectin, doramectin, and emamectin (Silberberg et al., 2007). Avermectin showed comparable potentiation to IVM while the last two compounds displayed potentiation to a lesser extent (Silberberg et al., 2007).

1.2.6.3 Non-selective antagonists of $P2X_4$

The research into $P2X_4$ has been hampered due to the lack of selective antagonists. The scientists depend on broad-spectrum antagonists such as suramin, PPADS, and brilliant blue G (BBG) together with other inhibitory techniques such as divalent cations, pH, and several drugs (anti-depressants and statins). Table 1.3 shows the summary of non-selective antagonists identified so far.

1.2.6.3.1 Broad-spectrum antagonists

It has been demonstrated that 2'(3')-O-(2,4,6-trinitrophenyl)adenosine 5'-triphosphate (TNP-ATP) competitively blocked the activation of human $P2X_4$ receptor with an IC_{50} value of 15.0 μM, however it is at least 2000-fold more potent at $P2X_1$, $P2X_3$, and $P2X_{2/3}$ (Hernandez-Olmos et al., 2012; Virginio et al., 1998). Suramin is another broad-spectrum antagonist of purinergic receptors and it shows a very weak inhibition at human, mouse, and rat $P2X_4$ orthologues. Jones et al. (2000) reported that the inhibition was only 11 – 35 % across the $P2X_4$ orthologues when 100 μM suramin was used. In addition to this, human and mouse $P2X_4$ were reported to be sensitive to PPADS with IC_{50} values of 9.6 μM and 10.5 μM, respectively but relatively less sensitive at rat $P2X_4$ with an inhibition of ~50 % when 100 μM PPADS was used.

Table 1.3 The list of P2X4 antagonists

Name	IC$_{50}$ value (μM) (Species)	Type of expressing cells	Mode of action	Selectivity (human paralogues)	Reference
5-BDBD	0.5-1.2 (human, current) 0.35 (human, calcium) 3.47 (rat, calcium) 2.04 (mouse, calcium)	HEK293	Competitive	Not reported	(Abdelrahman et al., 2017; Balazs et al., 2013; Fischer et al., 2004)
Paroxetine	1.87 (human, calcium) 2.45 (rat, calcium)	Human astrocytoma	Noncompetitive	Not reported	(Nagata et al., 2009)
N,N-diisopropyl-5H-dibenz[b,f]azepine-5-carboxamide	3.44 (human, calcium) 54.6 (rat, calcium) 14.9 (mouse, calcium)	Human astrocytoma	Noncompetitive	>1.5-fold (P2X$_1$, P2X$_3$) >30-fold (P2X$_2$) >27-fold (P2X$_7$)	(Tian et al., 2014)
PSB12054	0.19 (human, calcium) 2.10 (rat, calcium) 1.77 (mouse, calcium)	Human astrocytoma	Allosteric	>34-fold (P2X$_1$) >50-fold (P2X$_2$, P2X$_3$, P2X$_7$)	(Hernandez-Olmos et al., 2012)
PSB12062	1.38 (human, calcium) 0.93 (rat, calcium) 1.76 (mouse, calcium)	Human astrocytoma	Allosteric	>50-fold (P2X$_1$, P2X$_2$, P2X$_3$, P2X$_7$)	
TNP-ATP	15.2 (human, current)	HEK293	Competitive	More potent at P2X$_1$, P2X$_2$, P2X$_{2/3}$ and P2X$_3$ (IC$_{50}$ <2 μM) >2-fold (P2X$_7$)	(Hernandez-Olmos et al., 2012; Virginio et al., 1998)
NP-1815-PX	0.26 (human, calcium)	Human astrocytoma	Not reported	>100-fold (P2X$_1$, P2X$_{2/3}$, P2X$_7$ >28-fold (P2X$_2$)	(Matsumura et al., 2016)

				>10-fold (P2X$_1$, P2X$_2$, P2X$_3$,	
BX430	0.55 (human, current) 1.89 (zebrafish, current)	HEK293	Noncompetitive	P2X$_4$, P2X$_5$) >100-fold (P2X$_7$)	(Ase et al., 2015)
Duloxetine	1.59 (human, calcium)	Human astrocytoma	Not reported	Not reported	(Yamashita et al., 2016)

1.2.6.3.2 Divalent cations and pH

Several divalent cations have been shown to cause modulation on ATP-evoked response at $P2X_4$ receptors. Zn^{2+} was reported to potentiate ATP-evoked response at low concentrations $(0.1 – 10\,\mu M)$ but it inhibited the response at higher concentrations $(30\,\mu M – 1\,mM)$ (Acuña-Castillo et al., 2000; Garcia-Guzman et al., 1997; Wildman et al., 1999). Further investigation on other transition metals from the same group in the periodic table as Zn^{2+} revealed that Cd^{2+} demonstrated slightly less potentiation compared to Zn^{2+}, while Cu^{2+} and Hg^{2+} inhibited the ATP-evoked response (Acuña-Castillo et al., 2000). In addition to this, the ATP-evoked response of $P2X_4$ was also affected by pH. A high concentration of H^+ (pH 6.5 and pH 5.5) progressively reduced the potency of ATP in evoking the response and the efficacy was also reduced at pH 6.5 (Clarke et al., 2000) and pH 5.5 (Wildman et al., 1999).

1.2.6.3.3 Antidepressants

Nagata and co-researchers (2009) investigated some antidepressant drugs to observe the ability of those drugs to inhibit $P2X_4$. This was due to the clinical evidences that showed the drugs were effective in modulating pain. They tested paroxetine, fluoxetine, maprotiline, and clomipramine on 1321N1 cells stably expressing human $P2X_4$ receptor. It was observed that those drugs inhibited the $P2X_4$ activity and paroxetine showed the most potent inhibition with an IC_{50} value of $1.87\,\mu M$. This was also supported by a recent study that showed paroxetine has a direct inhibition on $P2X_4$ (Abdelrahman et al., 2017). However, another study claimed that those four antidepressants did not significantly inhibited the $P2X_4$ receptor even at high concentrations up to tens of micromolars, tested on activated mouse cerebellar immortalised microglial C8-B4 cell line. Nonetheless, it was noticed that the antidepressants (at small concentration of 500 nM) reduced the upregulation of cell membrane $P2X_4$ receptor by impairing lysosomal function and subsequently lead to smaller response (Toulme et al., 2010). These contradictory results might be explained by the fact that the cell systems used in both experiments were different. The 1321N1 cells may be more susceptible to the antidepressants and thus, cause reduced upregulation of cell membrane $P2X_4$.

1.2.6.3.4 Statins and cholesterol depleting agents

An HMG-CoA reductase inhibitor, fluvastatin, was discovered by Li and Fountain (2012) to inhibit the activation of P2X$_4$ through a calcium-based assay on heterologously expressed P2X$_4$ in HEK293 cells and native P2X$_4$ in human THP-1 monocytes. The inhibition of P2X$_4$ was postulated to occur through cholesterol depletion that might interfere with the receptor trafficking.

1.2.6.4 Selective antagonists

The researchers have been using the non-selective antagonists of P2X$_4$ such as suramin and TNP-ATP for a considerable amount of time. This has impeded the development of pharmacological insight into P2X$_4$ receptors. Since 2006, there have been several novel compounds identified, which are selective to P2X$_4$ and this has provided a new avenue for scientists to selectively target P2X$_4$. Table 1.3 shows the summary of selective antagonists identified so far.

1.2.6.4.1 Carbamazepine derivatives

A total of 47 carbamazepine derivatives including 32 novel compounds were investigated for P2X$_4$ receptor antagonists study. A compound, N,N-diisopropyl-5H-dibenz[b,f]azepine-5-carboxamide, was reported to potently and allosterically block P2X$_4$ activity with an IC$_{50}$ value of 3.44 μM. The compound was not fully selective for P2X$_4$ as it showed a considerable blockade at P2X$_1$ and P2X$_3$, but was selective versus P2X$_2$ and P2X$_7$ which indicates that more optimisation is needed. The compound was found to be less potent at mouse and rat (IC$_{50}$ values: 14.9 μM and 54.6 μM, respectively) (Tian et al., 2014).

1.2.6.4.2 N-substituted phenoxazine

Two phenoxazine derivatives were reported to exhibit potent inhibition at P2X$_4$ which were PSB12054 (N-(Benzyloxycarbonyl)phenoxazine (II)) with IC$_{50}$ value of 0.189 μM and PSB12062 (N-(pMethylphenylsulfonyl)phenoxazine) with IC$_{50}$ value of 1.38 μM, at the human P2X$_4$ receptor expressed in human astrocytoma cells (Hernandez-

Olmos et al., 2012). The former compound was reported to be less potent on rat (IC_{50} value of 2.1 µM) and mouse (IC_{50} value of 1.77 µM) $P2X_4$ and the latter is similarly potent at all $P2X_4$ orthologues tested (IC_{50} values: rat = 0.928 µM, mouse = 1.76 µM). PSB12054 blocks noncompetitively and is highly selective for the human $P2X_4$ receptor with over 50-fold selectivity against $P2X_2$, $P2X_3$, and $P2X_7$ and over 30-fold against $P2X_1$. PSB12062 is also an allosteric blocker with 35-fold selectivity towards $P2X_4$ versus $P2X_1$, $P2X_2$, $P2X_3$, and $P2X_7$.

1.2.6.4.3 BX430

Ase et al. (2015) recently revealed a novel compound that negatively modulates $P2X_4$ receptor. The discovery was a consequence of high throughput screening of a compound library of 26,240 compounds. The compound, known as BX430, was claimed to have an IC_{50} value of 0.54 µM. Further testing on other P2X paralogues unearthed its selectivity for $P2X_4$ only, with effective dose at other P2Xs about 10 – 100 times to its IC_{50} value at $P2X_4$. However, BX430 was proven to inhibit the $zfP2X_4$ and $hP2X_4$, but not $rP2X_4$ and $mP2X_4$ despite their high similarity in amino acid sequence among all those orthologues.

1.2.6.4.4 NP-1815-PX

A recent discovered antagonist of $P2X_4$ receptor, NP-1815-PX (5-[3-(5-thioxo-4H-[1,2,4]oxadiazol-3-yl)phenyl]-1H-naphtho[1, 2-b][1,4]diazepine-2,4(3H,5H)-dione), was identified from a high throughput screening of a chemical library using calcium-based assay on human astrocytoma cells stably expressing human $P2X_4$ receptor with an IC_{50} value of 0.26 µM. The compound was claimed to fit some characteristics that previous compounds did not, in which it is highly potent, selective, and effective across $P2X_4$ orthologues, as well as high water solubility and in addition, has been shown to be effective in attenuating pain on chronic pain mouse model (Matsumura et al., 2016).

1.2.6.4.5 Duloxetine

Yamashita et al. (2016) discovered another antagonist of $P2X_4$ receptor as a result of high throughput screening of 1,979 compounds obtained from Drug Discovery

Initiative, University of Tokyo. The compound, duloxetine, was reported to have an IC_{50} value of 1.59 µM at $P2X_4$ and was also found to ameliorate pain hypersensitivity on spinal nerve injury rat model but did not completely remove the mechanical allodynia. The identified $P2X_4$ antagonists and their characteristics are listed in Table 1.3.

1.2.6.4.6 5-BDBD

5-BDBD was first reported by Fischer et al. (2004) in a form of commercial patent but no information was found in any scientific report. It was only recorded academically through a review article by Donnelly-Roberts et al. (2008). However, there was no additional information about the compound other than the stated IC_{50} value of 5-BDBD as in the patent, which is 0.5 µM. The experiment was done on Chinese hamster ovarian (CHO) cell. Other than that, the detailed report about the characteristics of the compound are not available neither in the patent nor the article. Also, 5-BDBD has long been claimed to be selective for $P2X_4$ but there is no evidence to prove that (Ase et al., 2015; Jacobson & Müller, 2016).

Since then, there were several studies that incorporated 5-BDBD in their experiments involving $P2X_4$ inhibition such as Wu et al. (2011). They used 30 µM of 5-BDBD on ECs of spiral ligament (SL) capillaries to prove the existence of $P2X_4$ receptor in these cells. Later, Kwon (2012) discovered that $P2X_4$ was the main P2 receptor involved in pre-chondrogenic condensation, which was a vital process in skeletal patterning, using 10 µM of 5-BDBD to revoke the pre-chondrogenic condensation. Besides, Norenberg et al. (2012) also used 5-BDBD on HEK293-stably-expressing human $P2X_4$ receptor cell line. They found that it was effective for $P2X_4$ by inhibiting 70 % of normal response at 5 µM and that it did not cause any modulation on human $P2X_7$.

Hung et al. (2013) used 50 µM of 5-BDBD on human immortalised gingival keratinocyte to explain the role of $P2X_4$ in the production of reactive oxygen species in response to microbial infection. So far, 5-BDBD has been used in studies involving various types of cells at various concentrations. In addition to that, there was also a study (Vavra et al., 2011) that claimed that the compound did not inhibit $P2X_4$, at least

on endogenously expressed $P2X_4$ receptors after 3 and 30 µM of 5-BDBD were tested on primary supraoptic neuron that were freshly isolated from rat brain slices.

Until this point, the use of 5-BDBD is only focused on its application on various settings of experiments but none of the studies offers any insight on the compound behaviour. Thus, Balazs et al. (2013) explored the potency and mode of inhibition of 5-BDBD. They identified the IC_{50} value of 1.2 µM when tested on human $P2X_4$ overexpressing HEK293 cells and the inhibition was due to competitive inhibition. Their electrophysiology data also showed that 5-BDBD blocked the ion current. Another observation made was that 5-BDBD and TNP-ATP have similar potency on the tested cell line.

A recent article on 5-BDBD by Abdelrahman et al. (2017), however, contradicted the previous finding. It is widely and commonly accepted that 5-BDBD blocks $P2X_4$ competitively. Nevertheless, this team unveiled a quite surprising finding that the inhibition of $P2X_4$ by 5-BDBD was noncompetitive rather than competitive. They made use of a radioligand $[^{35}S]ATP\gamma S$ that binds to the active site of $P2X_4$. They measured the displacement of the radioligand as an indication for the type of binding. Interestingly, 5-BDBD did not displace the radioligand and that suggested 5-BDBD binds to an unknown allosteric site on the $P2X_4$ receptor, not at the orthosteric site. Up until now, there is a limited knowledge on 5-BDBD despite it is being widely used in various studies.

1.2.7 Structure activity relationship study

To date, there have been two structure activity relationship (SAR) studies of the P2X$_4$ antagonists performed by the same group (Hernandez-Olmos et al., 2012; Tian et al., 2014). In the first study, a total of 54 compounds were synthesised based on the parent compounds of phenoxazine and acridone, as well as 47 carbamazepine derivatives in the second study. The modification of the derivatives involved the substitution with different functional groups including amide, amine, urea, and carbamate. As a result of the studies, three novel compounds were identified to potently inhibit the activation of P2X$_4$ which were PSB12062, PSB12054 (Hernandez-Olmos et al., 2012), and N,N-diisopropyl-5H-dibenz[b,f]azepine-5-carboxamide (Tian et al., 2014).

1.3 Objectives

Assessing the current situations, two gaps have been identified in P2X$_4$ research. Firstly, there is a lack of selective and potent inhibitors of P2X$_4$ that impacts the development of P2X$_4$ receptor-related studies. Another gap identified is the lack of information about 5-BDBD. Despite this it is being used in numerous studies involving P2X$_4$, very little information is available. Hence, this project aimed to solve these two recognised gaps in existing knowledge. The first major objective of this study was to search for a potential inhibitor of P2X$_4$ that can be used as a therapeutic tool in research and as a template to design more potent and selective inhibitors which could be used therapeutically in the future. The second main objective was to study the structure activity relationship of 5-BDBD derivatives at P2X$_4$ receptor. Throughout this project, several specific objectives were hoped to be achieved as follows:

1. To produce 1321N1 cells stably expressing human and mouse P2X$_4$ and human P2X$_7$.
2. To screen the NCI diversity set and natural product library (1,710 compounds), and identify hit compounds in a receptor activity assay with P2X$_4$ overexpressing cells.
3. To characterise a lead compound to understand its properties, selectivity, and mechanism of action.
4. To produce chemical orthologues of 5-BDBD in order to explore its structure activity relationship of a known antagonist at P2X$_4$.

5. To use in silico docking for generating hypothesis of 5-BDBD binding sites in human P2X$_4$ receptor.

CHAPTER 2

MATERIALS AND METHODS

2.1 Materials

All general salts, reagents, and solvents were purchased from Sigma-Aldrich or Thermo Scientific unless otherwise stated. All buffers were prepared in deionised water unless otherwise stated. All screened compounds were obtained from National Cancer Institute library, except for 5-BDBD analogues which were purchased commercially and synthesised in-house. Tables below provide the lists of materials used in this study.

Table 2.1 P2 receptor ligands.

Compound	Target receptor	Function	Supplier	Vehicle	Final concentration (μM)
5-BDBD	$P2X_4$	Antagonist	Tocris	DMSO	0.03 – 30
ATP	All P2 receptors except $P2Y_6$ and $P2X_7$	Agonist	Abcam	DI	0.01 – 100
BzATP	$P2X_7$	Agonist	SA	DI	0.01 – 500
UDP	$P2Y_6$	Agonist	SA	DI	0.01 – 30
IVM	$P2X_4$	Positive allosteric modulator	Tocris	DMSO	0.01 – 10
PPADS	$P2X_4$	Antagonist	SA	DI	0.01 – 100
PSB12062	$P2X_4$	Antagonist	SA	DMSO	10

Note. DMSO = dimethyl sulfoxide, DI = deionised water, SA = Sigma Aldrich

Table 2.2 Antibodies.

Antibody	Epitope	Host	Target species	Supplier
Goat anti-Rabbit IgG (H+L) Secondary Antibody, Alexa Fluor 488	-	Goat	R	Invitrogen
P2X$_4$ antibody	Intracellular	Rabbit	H, M, R	Alomone
P2X$_4$ antibody	Extracellular	Rabbit	H, M, R	Alomone
Rabbit (DA1E) mAb IgG XP® Isotype Control	-	-	-	CST
Human BD Fc blocker	-	-	H	BD Pharmingen

Note. H = human, M = mouse, R = rat, CST = Cell Signalling Technology

Table 2.3 Other calcium pathway mediators.

Compound	Function	Supplier	Vehicle	Final concentration (µM)
Carbachol	It causes phosphatidylinositol hydrolysis resulting in calcium release from intracellular store (Chough et al., 1993)	SA	DI	100
Ionomycin	Ionophore that allows calcium gets into the cell (Caridha et al., 2008)	SC	DMSO	1

Note. DMSO = dimethyl sulfoxide, DI = deionised water, SC = Santa Cruz

Table 2.4 Starting molecules for 5-BDBD analogues syntheses.

Compound	Supplier	Molecular weight (g/mol)	Purity (%)
2-hydroxy-5-trifluoromethylbenzonitrile	Fluorochem	187.12	95
3-(trifluoromethyl)phenacyl bromide	Fluorochem	267.05	98
3-bromophenacyl bromide	Fluorochem	277.94	97
3-chlorophenacyl bromide	Fluorochem	233.49	90
3-fluorophenacyl bromide	SA	217.04	97
5-bromo-2-hydroxybenzonitrile	Fluorochem	198.02	98
5-chloro-2-hydroxybenzonitrile	SA	153.57	NM
5-fluoro-2-hydroxybenzonitrile	Fluorochem	137.11	95
Ammonia, 0.5M solution in 1,4-dioxane	FS	17.03	99
Bromoacetyl bromide	AG	201.84	98
Sodium ethoxide	SA	68.05	95

Note. SA = Sigma Aldrich, AG = Acros Organics, FS = Fisher Scientific, NM = not mentioned

Table 2.5 List of 5-BDBD analogues that available commercially.

Compound	Catalogue number	Molecular weight (g/mol)	Purity (%)
5-(4-bromophenyl)-1,3-dihydro-2H-[1]benzofuro[3,2-e][1,4]diazepin-2-one	STK775918	355.19	> 90
5-Phenyl-1,3-dihydro-2H-[1]benzofuro[3,2-e][1,4]diazepin-2-one	STK045532	276.30	> 90
5-(4-methylphenyl)-1,3-dihydro-2H-[1]benzofuro[3,2-e][1,4]diazepin-2-one	STK027946	290.32	> 90
5-(4-fluorophenyl)-1,3-dihydro-2H-[1]benzofuro[3,2-e][1,4]diazepin-2-one	STK747973	294.29	> 90
9-bromo-5-phenyl-1,3-dihydro-2H-[1]benzofuro[3,2-e][1,4]diazepin-2-one	STK731427	355.19	> 90
9-methoxy-5-phenyl-1,3-dihydro-2H-[1]benzofuro[3,2-e][1,4]diazepin-2-one	STK864662	306.32	> 90
5-(4-chlorophenyl)-1,3-dihydro-2H-[1]benzofuro[3,2-e][1,4]diazepin-2-one	STK079751	310.74	> 90
2-benzoyl-5-chloro-1-benzofuran-3-amine	STK021512	271.70	> 90

*All compounds were purchased from Vitas-M Laboratory and dissolved in DMSO.

2.2 Methods

2.2.1 Cell culture

The main cell line used for this study was the human 1321N1 cells which was readily available in-house. This astrocytoma cell line was previously isolated from 1181N1 line, a subline of parent U-118 MG (Pontén & Macintyre, 1968). The cells have been tested and showed no response upon nucleotide stimulation in calcium-based experiments (Communi et al., 1996). The two other types of cell line used were the HEK293T/17 and murine microglial (BV2) cell lines.

All cell types were cultured in Dulbecco's Modified Eagle Medium containing 0.6 g/L L-Glutamine and 4.5 g/L glucose (DMEM, Lonza) supplemented with 10 % (v/v) Foetal Bovine Serum (FBS, HyClone) and 1 % (v/v) penicillin-streptomycin (Gibco) solution containing 50 units/mL of penicillin and 50 μg/mL of streptomycin (this will be referred as cell culture medium from hereon). All cell lines were the adherent type, cultured in vented T75 flasks (Nunc), and were kept in a humidified incubator (Nuaire) at 37 °C with 5 % of CO_2. When the cells were 80 – 90 % confluent, they were rinsed with 5 mL PBS (Lonza) and subsequently detached from bottom of the flask by incubating the cells with 3 mL Trypsin EDTA (Lonza) containing 170,000 U trypsin/L at 37 °C for 3 minutes. After incubation, the flasks were tapped gently to ensure all cells were detached and afterwards, 7 mL of cell culture medium was added into the flask to stop the enzymatic reaction. The cells were then centrifuged at $805 \times g$ for 7 minutes at room temperature and supernatant was discarded. The pellet was resuspended with 10 mL of cell culture medium and utilised for further experiments, which was either reseeded into a new T75 flask or cryopreserved.

Cryopreservation is a technique to preserve cells for future use without causing loss of viability. The cryopreservation mixture constituted of 45 % cell culture medium with cells (~1 – 2 million cells), 45 % of FBS, and 10 % of DMSO which were added together in a 1.8 mL cryotube (Thermo Scientific). The cryotubes were then placed in a freezing container (Sigma Aldrich) to allow slow freezing and the container was stored at −80 °C for one day and later were transferred to a liquid nitrogen facility. When the cryopreserved cells were to be used, the cells were thawed by swirling the

tube in lukewarm water and immediately transferred the suspension into a falcon tube containing 10 – 15 mL of cell culture medium. The cells were washed twice by centrifugation and resuspension before they were seeded in a new flask per requirement.

2.2.1.1   Activation of BV2 cells

BV2 cells were used to model primary microglial cells under physiological and inflamed conditions. Henn et al. (2009) made a comparison between BV2 cells and primary microglial cells in vitro and in vivo in terms of their response towards bacterial lipopolysaccharide (LPS, *E. coli* 0127:B8, Sigma). It was found that BV2 cells respond similarly to primary microglia and thus the cells serve as a good model for primary microglia. The cells in the physiological state was termed as quiescent cells and used as it were after splitting. On the other hand, to render the cells from quiescent state to pathological state (termed as activated), the LPS was used. After being seeded, the cells were exposed to 1 µg/mL LPS in cell culture medium for 24 hours and incubated at 37 °C humidified with 5% of CO_2. After the incubation, the cells were ready to be used for further experiment.

2.2.2   Generation of DNA recombinant plasmid

$P2X_4$ recombinant DNA in pcDNA3.1 vector was available in-house. The recombinant DNA was restricted and the DNA was ligated into pLVX-IRES-mCherry vector for transfection. The pLVX-IRES-mCherry is a lentiviral expression vector based on HIV-1 which allows its expression in most mammalian cell types. It is a bicistronic vector that can carry two DNA sequences; one is the DNA of interest and another is DNA for fluorescing mCherry protein. The use of mCherry protein was useful because it could be used to indicate the transfection success and sort the transfected cells. Figure 2.1 shows the map for the vector and its multiple cloning sites. BamHI was chosen as the restriction enzyme as it was also present in the pcDNA3.1 vector as shown in Figure 2.1 and Figure 2.2. The whole procedure for generation of $P2X_4$ recombinant plasmid is described below.
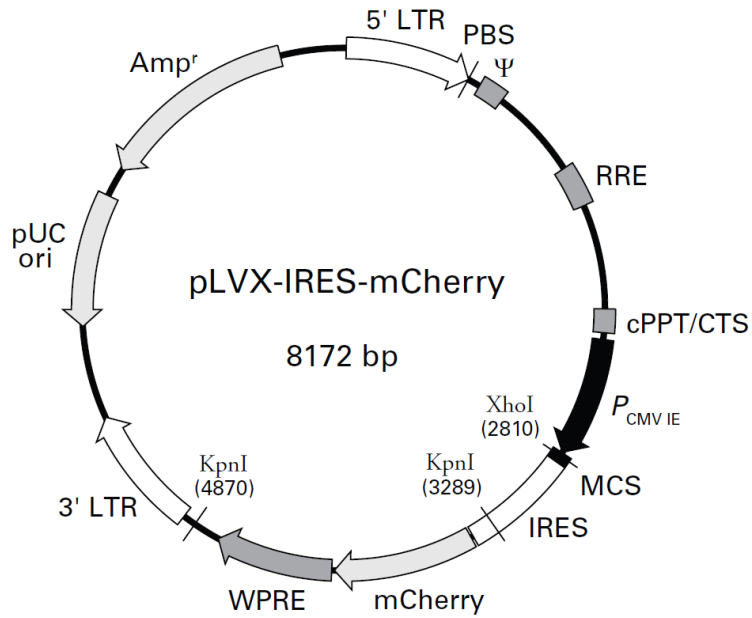
Figure 2.1 pLVX-IRES-mCherry vector map and multiple cloning sites (MCS)
This bicistronic vector was used to express P2X$_4$ together with mCherry protein for selection purpose. The vector was restricted using BamHI for inserting the P2X$_4$ DNA.
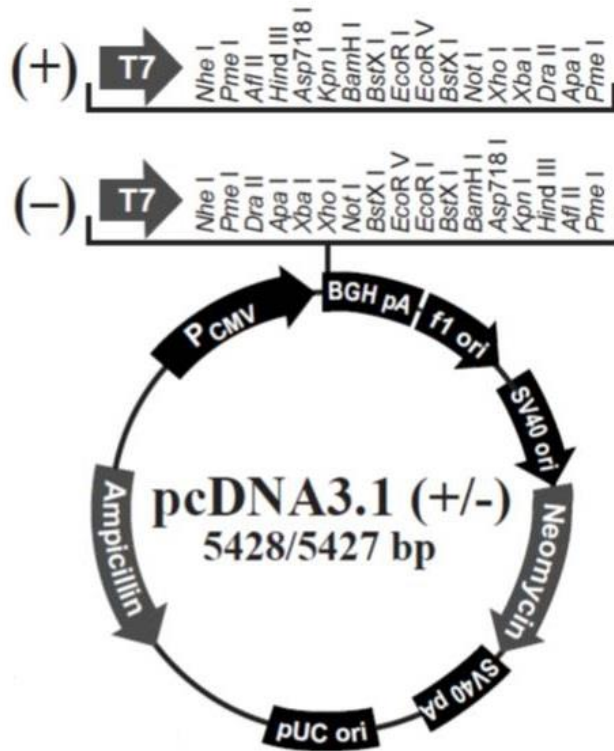
Figure 2.2 pcDNA3.1 (+/-) vector map and multiple cloning sites (MCS).
In-house human P2X$_4$ DNA was in pcDNA3.1 vector. Therefore, the DNA was restricted using BamHI and further ligated into pLVX-IRES-mCherry. Both pcDNA3.1 and pLVX-IRES-mCherry vectors contained BamHI restriction sites, hence the BamHI was selected.

2.2.2.1 Restriction analysis of P2X₄ DNA

The P2X$_4$ recombinant DNA in pcDNA3.1 and pLVX-IRES-mCherry vectors were both digested using the restriction enzyme, BamHI, in two separate tubes. The digestion mixture consisted of 20 units (1 µL) of BamHI restriction enzyme, 5 µL of 10X CutSmart buffer, 5 µg of plasmid (1 µg for pLVX-IRES-mCherry vector), and molecular grade water (topped up to 50 µL). The mixtures were mixed by gentle tapping and incubated at 37 °C for two hours. Afterwards, the restricted pLVX-IRES-mCherry vector was purified using E.Z.N.A Cycle Pure Kit (OMEGA bio-tek) according to manufacturer's protocol. The resulting product was quantified using a NanoDrop (Thermo Scientific) and stored at −20 °C until further use.

For P2X$_4$ DNA in pcDNA3.1, the digestion mixture was run on an agarose gel using electrophoresis (will be discussed in Section 2.2.2.6). After visualising the gel under UV light, the corresponding size of DNA was carefully excised from gel and weighed. The DNA in the excised gel was extracted and purified using gel extraction kit (OMEGA bio-tek) per manufacturer's protocol. The resulting product was quantified and stored at −20 °C until further use.

2.2.2.2 Insertion of DNA into selected vector

Two products generated following the process mentioned in Section 2.2.2.1 were thawed on ice and used in the ligation process to produce a recombinant plasmid. Ligation mixture consisted of 400 units (1 µL) of T4 DNA ligase (BioLabs Inc.), 1 µL of 10X T4 DNA ligase buffer (BioLabs Inc.), 50 ng of P2X$_4$ DNA, 50 ng of vector (pLVX-IRES-mCherry), and molecular grade water (topped up to 10 µL). The ligation mixture was mixed by flicking and briefly centrifuged to collect remaining liquid from the tube wall, and then incubated at 16 °C overnight (up to 24 hours). After overnight incubation, the product was proceeded to the next step.

2.2.2.3 Transformation of recombinant plasmid

The product obtained (as described in Section 2.2.2.2) was promptly followed by transformation. This step was done to allow *E. coli* to uptake the recombinant DNA for the multiplication of DNA copies. Prior to this process, the ligation reaction from previous section was chilled on ice while the Super Optimal broth with Catabolite repression (SOC) outgrowth medium (BioLabs Inc.) and LB agar (Sigma) plates (with 100 µg/mL ampicillin) were warmed up to 37 °C. A vial of commercially available 50 µL of high efficiency competent *E. coli* (BioLabs Inc.) was thawed on ice. Then, 5 µL of recombinant plasmid was added into the *E. coli* vial, mixed by gentle tapping, and incubated on ice for 30 minutes. Afterwards, the vial was heat-shocked at 42 °C for 30 seconds and immediately returned to ice for 2 minutes. Subsequently, 250 µL of pre-warmed SOC outgrowth medium was added into the vials which were then placed into universal tubes and shaken at 225 rpm for an hour at 37 °C. After shaking, 200 µL and 50 µL of the culture were plated on separate pre-warmed agar plates, respectively and then incubated at 37 °C in an upside-down position overnight. Colonies were observed on the agar following overnight incubation. Eight single colonies were selected and inoculated in 10 mL of LB broth (with 100 µg/mL ampicillin, Sigma) to increase the possibility of getting successful ligation. Next, the cultures were incubated overnight at 37 °C on a shaker at 225 rpm. This procedure was done in a sterile environment.

2.2.2.4 Purification and confirmation of recombinant plasmid

After the incubation, 750 µL from each culture tube and 250 µL of glycerol (Sigma) were added into separate cryotubes (Thermo Scientific) in a sterile setting and stored at −80 °C. These glycerol stocks were intended for future use if more recombinant plasmids were required. The remaining cultures were centrifuged at $805 \times g$ for 10 minutes at room temperature and the supernatant was discarded. The remaining pellet was then purified using E.Z.N.A Plasmid Mini Kit I (OMEGA bio-tek) according to manufacturer's protocol. The obtained recombinant plasmids from bacterial culture were then quantified. All plasmids were then run on a gel to determine whether these plasmids contained the DNA of interest. This was confirmed by comparing the size of the bands on the gel. If the plasmid size was larger than the unrestricted pLVX-IRES-mCherry vector, this might be an indication of successful ligation. This was further

confirmed with DNA sequencing using CMV promoter and pIRES reverse primers. Successful recombinant plasmid was then carried forward for the next procedure which was the generation of P2X$_4$ overexpressing cell line.

2.2.2.5   LB broth and agar preparation

LB broth and agar powder (both from Sigma) were dissolved using distilled water according to manufacturer's recommendation and then autoclaved to sterilise the solution. The autoclaved solution was stored at room temperature until future use. For making culture, 10 mL of broth was added into a universal tube and 10 µL of ampicillin from 100 mg/mL stock (final concentration = 100 µg/mL) was added into broth and mixed. These cultures were freshly prepared before use. Meanwhile, for making agar plates, LB agar was liquefied by heating it in microwave. Then, 12 µL of ampicillin from 100 mg/mL stock (final concentration = 100 µg/mL) was placed at the centre of the petri dish and 12 mL of lukewarm LB agar was added into the petri dish and mixed with ampicillin. Bubbles were removed as much as possible. The plates were left to solidify at room temperature and then stored at 4 °C in an upside-down position, and it can be used within two weeks. All steps were done under a sterile condition.

2.2.2.6   Gel electrophoresis

Gel electrophoresis is a procedure to separate DNA of different sizes. With the help of electricity through an electrophoretic system, DNA fragments are separated based on their size, where bigger fragment will travel slower than the lighter fragments. Three main ingredients were needed to make a gel, 1X Tris-Acetate-EDTA (TAE) buffer, 1 % agarose, and ethidium bromide (Sigma, 10 mg/mL). 1X TAE buffer was prepared by diluting 50X TAE solution (Fisher Scientific) with deionised water. The 1 % agarose gel was prepared by dissolving and heating 1 g of agarose (Fisher Scientific) with 100 mL of 1X TAE buffer. When the gel solution was lukewarm, 4 µL of ethidium bromide (final concentration = 40 ng/mL) was added as the intercalation dye to enable gel visualisation under UV light.

The 1 % agarose gel solution was poured into a cast with the desired comb and allowed to solidify (approximately 20 minutes). To start the electrophoresis, the gel was

transferred into the gel electrophoresis system and 1X TAE buffer was added into the system until the surface of solidified gel was fully submerged. Samples were prepared by mixing them with 6X blue loading dye at a ratio of 1:6 (dye:sample) and then loaded into the wells of the gel. One of the wells was filled with a 1 kb ladder which was mixed with the loading dye. The ladder served as the reference for DNA size. The gel electrophoresis was run for approximately an hour at 95 V and the gel was visualised under UV illumination using a ChemiDoc™ XRS visualiser (Bio-Rad).

2.2.3 Generation of P2X$_4$ overexpressing cell lines

The DNA product (obtained following process explained in Section 2.2.2.4) was used to generate the P2X$_4$ overexpressing cell line in a process called transfection. Transfection is a process whereby transfected cells take up the recombinant DNA, incorporate it into its genome, and starts expressing the protein. There are many ways of transfecting DNA into cells which are categorised into three classes, which are biological, chemical, and physical (Kim & Eberwine, 2010). In this study, the biological way of transfection was employed which involved the packaging of recombinant DNA into lentiviral particles. Subsequently, the virus infected human astrocytoma cells and plasmid DNA were incorporated into human astrocytoma cells' DNA.

2.2.3.1 Production of lentiviral particles

The production of lentiviral particles was achieved by co-transfecting the three plasmids, namely lentiviral vector coding the viral genome with the transgene, psPAX2 containing a robust CAG promoter for packaging protein expression, and pMD2.G which encoded the Vesicular Stomatitis Virus (VSV) envelope glycoprotein. Those three plasmids were co-transfected into the HEK293T/17 cells.

On Day 0, nine million HEK293T/17 cells were seeded into a 150 mm culture dish in 20 mL cell culture medium and incubated at 37 °C overnight, supplemented with 5 % of CO$_2$. On Day 1, two Eppendorf tubes were filled with 1.2 mL of Opti-MEM® Reduced-Serum Medium (Gibco) each. The three plasmids; 9 µg of transgene DNA, 12 µg of psPAX2 packaging vector, and 3 µg of pMD2.G envelope vector (a total of

24 µg DNA) were added into one of the tubes while 36 µL of transfection reagent Lipofectamine 2000 (Invitrogen, 1 mg/mL stock) was added into the other tube. Both tubes were then incubated at room temperature for 5 minutes. Afterwards, the tubes were mixed together and incubated at room temperature for 20 minutes. In the meantime, the medium in HEK293T/17 culture dish from the Day 0 was replaced with 20 mL DMEM (Lonza) supplemented with 1 % (v/v) FBS (will be referred as virus collection medium from hereon). After 20 minutes, the plasmids and transfection reagent mixture were added in a drop-wise manner into the HEK293T/17 cells culture dish. The cells were incubated at 37 °C for 6 hours, supplemented with 5 % CO_2. After 6 hours, the medium was replaced with 20 mL of virus collection medium and incubated at 37 °C overnight with 5% of CO_2 supplementation.

On Day 2 until 4, 20 mL of virus collection media in the culture dish was collected each day and passed through a 0.45 µm polyethersulfone (low protein binding) filter (Whatman) to remove cells/debris. The filtered media was stored at 4 °C. After each collection, 20 mL fresh virus collection medium was added to the HEK293T/17 cells. On Day 4 after the last day of media collection, there was 60 mL of virus-containing media in total. The media was split into two falcon tubes containing 30 mL each. The virus was then concentrated by adding 10 mL of Lenti-X Concentrator (Clontech Laboratories) into each tube. The mixture was mixed thoroughly by gentle inversion and kept for 72 hours at 4 °C. After three days, the tubes were centrifuged at $1500 \times g$ for 45 minutes at 4 °C. After centrifugation, an off-white pellet of virus was visible. The supernatant was carefully removed, taking care not to disturb the pellet. The pellet was then gently resuspended in 0.5 mL of DMEM and the suspension was quantified. The remaining suspension was aliquoted and stored at −80 °C.

2.2.3.2   p24 ELISA and determination of viral titre

The lentivirus produced (as described in Section 2.2.3.1) was quantified using QuickTiter™ Lentivirus Titer Kit (Lentivirus Associated HIV p24) according to manufacturer's protocol (Cell Biolabs Inc.). The kit can only quantify lentivirus associated with p24 protein but not free p24 generated by HEK293T/17 cells during transfection and thus, it was an accurate kit for measuring viral titre. The kit has a detection sensitivity limit of 1 ng/mL HIV p24, or about 10,000 to 100,000 TU/mL

VSVG-pseudotyped lentivirus samples. The lentivirus p24 formed complexes with ViraBind™ lentivirus reagents while free p24 remained in the supernatant and lentivirus associated p24 were measured by a HIV p24 ELISA. The antibodies were reacted with FITC-conjugated anti-p24 monoclonal antibody and subsequently HRP-conjugated anti FTIC-monoclonal antibody. The absorbance was measured using a FlexStation 3 Multi-Mode Microplate Reader (Molecular Devices) at 450 nm.

2.2.3.3 Transfection of P2X$_4$ into human astrocytoma cells

The transfection procedure was used to introduce the P2X$_4$ recombinant plasmid into human astrocytoma cells. Prior to transfection, the polybrene reagent was prepared. Polybrene is a cationic polymer that facilitates more efficient gene transfer into target cells, i.e., astrocytoma cells (Davis et al., 2002). This was done by dissolving the hexadimethrine bromide (or polybrene, Sigma) in deionised water to a concentration of 100 mg/mL. The solution was then filtered using sterile 0.20 µm polyethersulfone filter (Whatman) in a sterile environment and aliquoted (1 µL per tube). The 1 µL aliquot was subsequently diluted with 61.5 µL of cell culture medium, yielding 1.6 µg/µL of polybrene concentration which was stored at −20 °C until further use.

The transfection process began with the splitting of human astrocytoma cells as described in Section 2.2.1 and the cell suspension was diluted to a concentration of 5×10^5 cells/mL. Then, 400 µL of the cell suspension (final cell count of 2×10^5 cells) was added into a 15 mL falcon tube containing 1.6 mL of cell culture medium and 10 µL of polybrene (final concentration = 8 µg/mL). Finally, 10 µL of virus media (obtained from the steps explained in Section 2.2.3.1) was added into the tube. The mixture was then spinoculated at $1400 \times g$ for 1 hour at 37°C. The supernatant was discarded and disposed of accordingly, and the pellet was resuspended with 1 mL of cell culture medium. The suspension was then transferred into T25 flask containing 4 mL of cell culture medium. The flask was incubated at 37 °C supplemented with 5 % CO_2 until the cells fluoresced brightly as observed with a fluorescence microscope with the TRITC filter. The cells were then sorted according to the intensity of their mCherry fluorescence. Cell that strongly produced mCherry indicated the high expression of P2X$_4$ receptors.

2.2.3.4 Sorting the P2X4 highly expressing cells

Not all cells are able to successfully express the protein of interest. Hence, the highly expressed cells are required to be sorted according to their expression of protein of interest. The cells with high expression of mCherry, i.e., that fluoresced brightly, were physically selected BD FACSAria III Sorter and collected in a tube whereas the cells with low expression were discarded.

Briefly, the transduced cells (obtained from steps done in Section 2.2.3.3) were split and the cell suspension was diluted with cell culture medium to a concentration of 1×10^6 cells/mL. A clean tube with 1 mL of cell culture medium was prepared for cell collection purpose. The cells were then passed through the instrument, excited at 587 nm wavelength, and emitted at 610 nm wavelength. The highest 1 % of fluorescing cells were then selected and collected into the collection tube. The collected cells were added into a T75 flask containing 20 mL of cell culture medium and incubated at 37 °C with 5 % CO_2 until the cells reached 80 – 90 % confluency. When it reached confluency, the cells were split and remaining cells were cryopreserved as described in Section 2.2.1.

2.2.4 Measurement of intracellular calcium responses

2.2.4.1 Calcium indicator

Indicators can be classified into two groups; single wavelength such as Fluo-4 and ratiometric dye such as Fura-2. The advantage of ratiometric dye over the other class is that it circumvents common problems associated with chemical calcium indicators which include photobleaching, uneven dye loading and cell thickness, leakage, and changes in cell volume (Paredes et al., 2008).

Fura-2 is a membrane impermeable indicator but when it is esterified with acetoxymethyl (AM) group, it becomes more lipophilic and cell permeant. Once Fura-2 AM (used in this study) enters the cytosol, the AM group is cleaved by intracellular esterases, leaving Fura-2 trapped in the cells to bind with free intracellular calcium (Hirst et al., 1999; Tsien, 1981). The Fura-2 was initially synthesised from a

combination of stilbene fluorophore and calcium chelator, ethylene glycol tetraacetic acid (EGTA). When Fura-2 bound with calcium, its excitation spectra shifts in peak fluorescence from $\lambda_{ex} = 362$ nm in unbound states to $\lambda_{ex} = 335$ nm in calcium-bound states while the emission wavelength remains the same ($\lambda_{em} = 510$ nm) (Grynkiewicz et al., 1985). It has high affinity towards calcium compared to other cations with a K_d value of ~145 nM (Paredes et al., 2008).

2.2.4.2   Buffer preparation

The buffer used in this experiment was HEPES-buffered physiological saline (HBPS). The buffer contained 137 mM of sodium chloride (NaCl), 4 mM of potassium chloride (KCl), 10 mM of HEPES, 8 mM of D-glucose, 1.2 mM of magnesium chloride ($MgCl_2$), and 1.5 mM of calcium chloride ($CaCl_2$) in deionised water. The buffer was pH-adjusted using sodium hydroxide (NaOH) to pH of 7.4. The buffer was then used to make the loading buffer, i.e., a buffer used to load Fura-2 AM into the cells. To make the loading buffer, 0.02 g of Pluronic F-127 was weighed and dissolved in 200 mL of HBPS (0.01 % w/v). Pluronic helped with the internalisation of Fura-2 AM by making the plasma membrane more permeable. Both buffer solutions were stored at 4 °C and used within one week of preparation.

2.2.4.3   Concentration-response experiments

2.2.4.3.1   ATP concentration-response experiment

The ATP concentration-response relationship experiment was done to describe the intracellular calcium change in the human P2X$_4$ overexpressing cells upon stimulation with ATP. The data could also be used to plot a concentration-response relationship curve in which, the EC$_{50}$ value could be determined. The EC$_{50}$ value is the concentration of ATP that causes the 50 % activation, i.e., half of the maximum response recorded, at the P2X$_4$ receptor. In this study, the ATP EC$_{50}$ value was used for compound screening experiment so that the screening would not exclude the potential competitive inhibitors that might not be able to compete with ATP. The

response of P2X$_4$ receptors upon activation by ATP was assessed by measuring the fluorescence from Fura-2, which was the indicator for calcium influx into the cells.

The human P2X$_4$ overexpressing cells were split and seeded in a 96-well clear flat bottom black plate (Molecular Devices) at a density of 25,000 cells/well in 200 μL of cell culture medium, and incubated overnight in a 37 °C incubator supplemented with 5 % of CO$_2$. The following day, Fura-2 AM (TEFLabs) was mixed with loading buffer (final concentration = 2 μM, 0.2 % DMSO) and warmed at 37 °C. The seeded cells were then taken out of the incubator, washed gently with 200 μL of pre-warmed HBPS once, and then loaded with 200 μL of the prepared loading buffer containing Fura-2 AM. Next, the plate was wrapped with aluminium foil because Fura-2 was photosensitive and can be bleached by prolonged exposure to light; and incubated at 37 °C for an hour.

During the 1 hour incubation, the ATP solution was prepared by dissolving ATP disodium salt (Abcam) with deionised water to make up 50 mM of stock solution. The stock was further diluted with HBPS into 14 concentrations; 500, 300, 150, 50, 30, 15, 5, 3, 1.5, 0.5, 0.3, 0.15, 0.05, and 0.03 μM. Then, each of the different concentrations of ATP was added into a clear round bottom plate in triplicate. After the 1 hour incubation, the cells were washed gently with HBPS twice and loaded with 200 μL of HBPS. Both plates were then placed in the FlexStation3 at 37 °C. ATP solution (50 mL) was added to each column using the instrument at 17th second (final ATP concentration was one fifth of the concentrations prepared) and the fluorescence was recorded for 250 seconds. The data obtained were analysed using Origin® version 9.1.

With regards to the instrument, there were two excitation wavelengths set up because Fura-2 is excited at two wavelengths which are 340 nm and 380 nm, and emits at 510 nm light. The ratio of readings from the two wavelengths will give an accurate measurement of calcium influx. This ratiometric reading provides accurate reading because it is independent of Fura-2 concentration loaded into the cells (Kong & Lee, 1995).

2.2.4.3.2 Inhibitor concentration-response experiment

This experiment aimed to observe the inhibition potency of a compound. The cells splitting, Fura-2 loading, and FlexStation3 set-up followed the same procedure as described previously. However, only the first six columns of the 96-well plate were used. While the cells were loaded with Fura-2, different concentrations of an inhibitor were prepared using DMSO, HBPS, and vehicle control. The compounds were usually dissolved in final concentration of 0.1 % DMSO but some hydrophobic compounds were dissolved in 1 % DMSO. After final wash following Fura-2 loading, the 96-well and compound plates containing different concentrations of inhibitor were placed in FlexStation3. The compound (10 µL) was injected into column 1 until 6 using the instrument and the fluorescence of each column was recorded for 250 seconds. These took 30 minutes for the compound delivery. Immediately after, the cells were injected with 0.6 µM of ATP (in the case of human P2X$_4$ overexpressing cells) into column 1 until 6 and fluorescence was recorded for 250 seconds for each column. This was done to ensure a constant 30 minute-incubation time for the inhibitor of each column.

2.2.4.3.3 Statistical analysis

In all calcium-based experiments, peak responses were recorded and used for statistics. Peak responses are the maximum peak recorded after ATP was added. The value was in the form of F ratio which was the ratio of fluorescence from two wave lengths (340/380 nm). Meanwhile, for the inhibitor concentration-response curve, the percentage of response was normalised to the peak response of the vehicle control.

Data from the calcium experiments was presented in two forms, which are the concentration-response curve establishment and decay kinetics. The concentration-response curves were fitted using the Hill equation as follows:

$$y = A1 + \frac{A2 - A1}{1 + 10^{(Logx0-x)p}}$$

where;

A1 = bottom asymptote

A2 = top asymptote

Logx0 = centre of curve

p = Hill slope

The IC_{50} or EC_{50} values was the value of Logx0 as the value represented the centre of the curve, which also corresponded to the half of maximal response concentration. To get the *x* value (concentration of ATP in log10) at any magnitude of response, the above equation was rearranged and *y* was substituted accordingly, and the value was base-10 anti-logged to get a value in molar.

$$x = -1 \left(\frac{\sqrt[10]{\frac{A2 - A1}{y - A1} - 1}}{p} + Logx0 \right)$$

Decay kinetics was measured in the form of tau value (τ). Tau value is defined as the time constant of a single exponential decay fitted to the desensitisation phase. It was determined using the exponential decay 1 function in Origin software and the equation was:

$$y = y_0 + A_1 e^{-(x-x_0)/t_1}$$

where;

y_0 = offset

x_0 = centre

A_1 = amplitude

t_1 = time constant

2.2.5   High throughput screening

2.2.5.1   Compound library

The compounds for high throughput screening were obtained from the National Cancer Institute (NCI). It is the primary agency for cancer research and training under the federal government of United States of America and is a part of the National Institute

of Health. It is located at Rockville Pike, Bethesda, Maryland, USA. Generally, as its name implies, it manages programs related to cancer by conducting and supporting research, managing health-related issues of cancer, and continuing to take care of cancer sufferers as well as their families (NCI, *n. d.*-a).

One example of the programs operated by the institute is the Development Therapeutics Program (DTP). This programme was first established in 1955 by Congress. It aims to help academic and private-sector researchers in their research and development by providing services and resources to facilitate drug discovery and development. Since then, more than 40 compounds have been developed and licenced in the USA as anti-cancer agents with the support of DTP. This would not be achieved without the close relationship and collaborations between DTP, academics, biotechnological industries, and pharmaceutical companies. Among the licensed anti-cancer agents are paclitaxel, romidepsin, eribulin, sipuleucel-T, and dinutuximab (NCI, *n. d.*-b).

DTP also holds a big library of compounds comprised of synthetic and natural compounds. The library consists of more than 200,000 compounds either submitted by third parties for biological assessment or synthesised under DTP protection. They are available to be used by researchers for research purpose (NCI, 2015). Some of those compounds are available in plates which are classed into four sets — Approved Oncology Drugs Plated, Diversity, Mechanistic, and Natural Products Sets. During the commencement of this study, the Natural Products Set was in the third version (current version is fourth), which lacks 302 compounds compared to the fourth version (NCI, 2016). All compounds in those sets were supplied in 96-well plates, dissolved in 20 µL DMSO at 10 µM, and shipped in a frozen state.

2.2.5.1.1 Diversity Set V (DSv)

In this study, the Diversity Set V (DSv) was used for compound screening in the search for potential inhibitors of human $P2X_4$ receptor. Out of 140,000 compounds available in DTP, 1,594 compounds were extracted based on few parameters and categorised into the DSv. The parameters include the drug-like criteria as outlined by Lipinski's research team (1997) and as a result, compounds that were relatively rigid, with 5 or

fewer rotatable bonds, with tendency to be planar, one or less chiral centres, and pharmacologically desirable features were included into the set. All compounds included in this set have a purity of > 90 % as analysed by LCMS (NCI, 2016).

2.2.5.1.2 Natural Products Set III (NPiii)

As opposed to the currently available Natural Products Set IV, this study used NPiii which was available at the beginning of the study. It differed in terms of the number of compounds where the latter set contains 302 more compounds than the previous set. Set III came with 117 compounds while set IV had 419 compounds. This set was also extracted from 200,000 compounds that meet certain criteria. The first criterion was that the compounds must be extracted from natural sources. Other criteria were that the compounds must have > 90 % purity and correct mass ion, depending on the compound structural diversity, and availability of the compound itself. This set was established in response of growing enthusiasm among researchers for various scaffold structures having multiple functional groups for drug discovery purposes, as observed in natural products (NCI, 2016).

2.2.5.1.3 Studies involving DTP compound plates

Several studies were carried out using these DTP compound libraries. Li et al. (2004) screened, in silico and in vitro, the NCI diversity set to search for 5-aminoimidazole-4-carboxamide ribonucleotide (AICAR) transformylase inhibitors. They found 19 compounds with inhibitory properties at AICAR which can be a good template/scaffold to design more potent compounds. Another cancer-related study was done by Sukkurwala et al. (2014) in which they screened 879 compounds from the Mechanistic Diversity Set. They tested the compounds for the ability to enhance immunogenic cell death (ICD). They unveiled one lead compound, septacidin which is an antifungal antibiotic produced by *Streptomyces fibriatus*, that can act as an ICD inducer and regulate anti-tumour effect. Other than that, NCI libraries have also been reported in an antimicrobial study by Feng and co-researchers (2015). They tested Diversity Set V, Mechanistic Diversity Set II, and Natural Products Set III on a species of bacteria, *Borrelia burgdorferi persisters*, which is the cause of Lyme disease. From the screening, they discovered a few compounds from the libraries with the detrimental

activity on the non-growing stationary and growing phases of *B. burgdorferi* cultures. Yet, there were no studies that used the NCI compound libraries in the purinergic receptor field. Thus, this study was the first to use the compound library from NCI to see if any compounds has a modulation potency at P2X$_4$ receptor.

2.2.5.2 Compound screening experiment

The compounds obtained from NCI were in 100 % DMSO with a concentration of 10 mM. Prior to the experiment, the compounds were diluted with HBPS to reach a concentration of 210 µM (DMSO concentration = 2.1 %). This experiment followed the same procedure as the ATP concentration-response experiment (Section 2.2.4.3), but there were few differences. After the cells were treated with Fura-2 AM and washed, 10 µL of 210 µM compound (final concentrations of sample and DMSO were 10 µM and 0.1 %, respectively) was added into each well. The delivery of the compound into each well was automatically performed by FlexStation 3 at 37 °C. The instrument delivered compound into a column of wells each time and the fluorescence of respective column was recorded for 120 seconds. This action was repeated for 10 columns. By the end of compound delivery process, the first column of wells was incubated with the compound for 30 minutes. Immediately after the compound delivery process, 50 µL of 3.12 µM of ATP (final concentration = 0.6 µM) was added to the cells using Flexstation 3 at 37 °C and the fluorescence was recorded for 120 seconds (the same time interval with compound delivery). The rationale of this arrangement was to ensure that the cells were incubated with the compounds at a constant duration of 30 minutes across the plate. A schematic presentation of the plate layout is shown in Figure 2.3 (top panel). The peak responses recorded for each compound were normalised to the vehicle control responses in order to evaluate the response modulation.

2.2.6 Reversibility experiment

This experiment aimed to determine the reversibility of thaspine blockade. The plate layout is shown in Figure 2.3 (lower panel). The experiment consisted of two parts. The first part was performed according to the procedure for compound screening experiment except that the maximal ATP concentration was used (final concentration

= 3 µM) and the recording time was extended to 250 seconds (instead of 120 seconds) for both compound delivery and ATP addition. After the first part of the experiment, the wells were washed twice with HBPS. This was done to remove thaspine and ATP from the buffer. After washing, the plate was incubated at 37 °C for 5 minutes. Then, the cells in the first column were stimulated with ATP for the second time by adding 50 µL of 15.6 µM ATP (final concentration = 3 µM) using Flexstation 3 and the fluorescence was recorded for 250 seconds. This was repeated until column number 6. The arrangement allowed a gradual 5 minutes increase in the incubation time across the plate which meant that the last column was incubated for 30 minutes after washing. The peak response for each well was recorded and used for statistics.
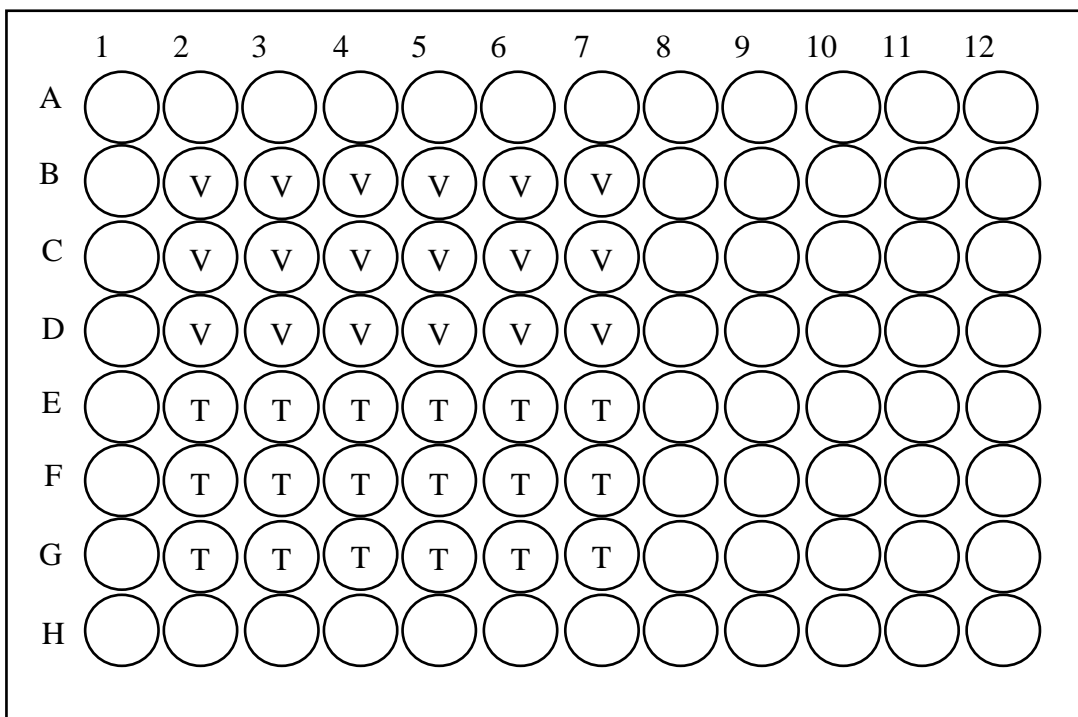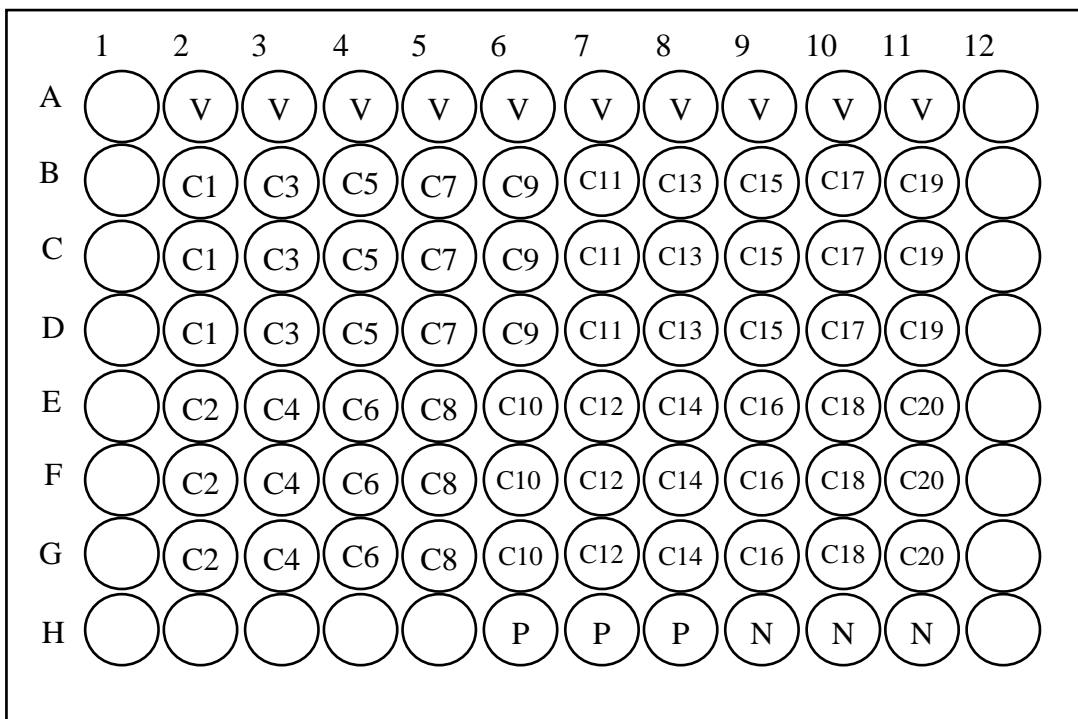
Figure 2.3 The layout of 96-well plate for compound screening and reversibility experiment.

The top panel shows the layout of 96-well plate used for compound screening. V was the vehicle control, C1 – C20 were the different compounds in triplicate, P and N were both positive controls for positive modulators (IVM) and antagonists (PPADS), respectively. Each plate consisted of 20 different compounds. Meanwhile, the lower panel shows the plate layout for reversibility experiment. V represented the vehicle control (0.1 % DMSO) and T represented thaspine (10 µM).

2.2.7 Flow cytometry

This experiment was done to test the hypothesis of thaspine causing the internalisation of surface P2X$_4$ receptors that resulted in the decrease of calcium response. This was done by tagging the external epitope of membrane-bound P2X$_4$ receptor with rabbit anti-human P2X$_4$ (extracellular epitope) (Alomone) and then coupled with a secondary antibody carrying fluorophore that was excited at 488 nm wavelength, namely goat anti-rabbit Alexa Fluor 488 (Thermo Fisher). The fluorescence was then measured using a CytoFLEX Flow Cytometer (Beckman Coulter).

The highly expressing human P2X$_4$ receptor cells were split and diluted in PBS to a concentration of 1×10^7 cells/mL. Next, 100 µL of the cell suspension (1 million cells) was added into two suitable tubes. Afterwards, thaspine or DMSO (test and vehicle controls, respectively) were added into each of tubes to reach a final concentration of 10 µM or 0.1% DMSO, respectively. Both conditions were accompanied with their own negative control, which was the rabbit isotype control. The concentration of thaspine was chosen based on calcium experiment data. The tubes were then incubated at 37 °C for 30 minutes. Following incubation, the cells were washed by adding 3 mL of PBS into each tube and centrifuged at $400 \times g$ for 5 minutes at room temperature. Supernatant was removed and pellet was resuspended with 100 µL of PBS.

Subsequently, 5 µL of human Fc blocker (BD Bioscience) was added into each tube to block all Fc receptors to avoid the non-specific binding. This was incubated for 10 minutes at room temperature before 1 µL of rabbit anti-human P2X$_4$ (extracellular) (1/100 dilution, 0.85 mg/mL stock) was added into each tube. For isotype control, a rabbit monoclonal antibody IgG (0.85 µg) was added into each tube. After 1 hour incubation at room temperature, the cells were washed in the same way as described earlier. The pellet was then resuspended with 500 µL of PBS and then 1 µL (1/500 dilution) of secondary antibody was added. The tubes were incubated in dark condition for 1 hour. Later, the cells were washed twice (as previously described) and resuspended in 500 µL of PBS.

CytoFLEX Flow Cytometer was then used to measure the fluorescence of antibody. The cells were kept in dark during transport to avoid bleaching of the fluorophore. The

excitation and emission wavelengths used were 490 and 525 nm, respectively and FITC filter was applied. The fluorescence was recorded for 10,000 events for each condition. The data were then analysed using CytExpert Software and student t-test was used for statistics.

2.2.8 Synthesis of 5-BDBD analogues

Ten analogues were synthesised based on parent compound, 5-BDBD to study the structure relationship between 5-BDBD and P2X$_4$. The general formula for the synthesised compounds is shown in Figure 2.4, in which R$_1$ and R$_2$ differed in each compound. The analogues synthesised are listed in Table 2.6.
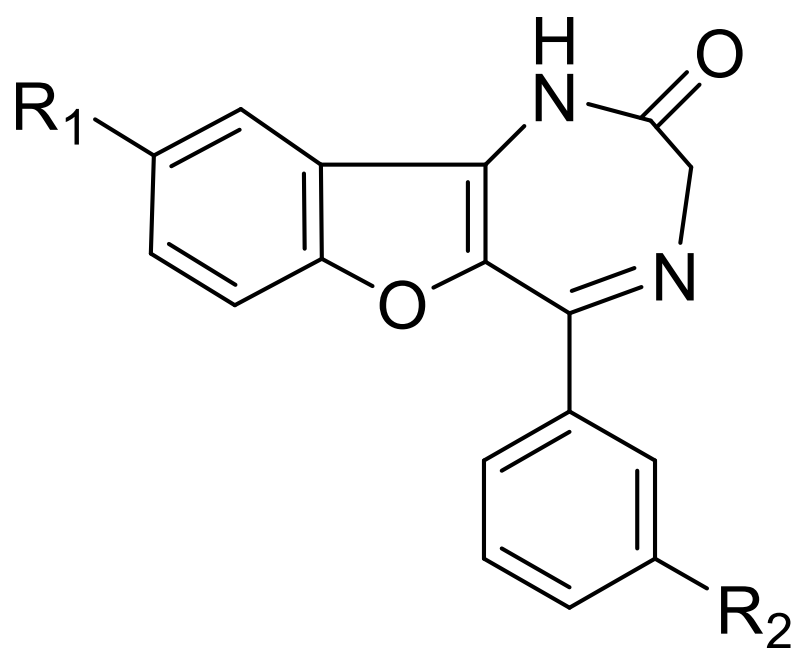
Figure 2.4 General formula of synthesised 5-BDBD analogue.
The chemical formula shows the backbone of the analogue investigated in this study. There were two sites of chemical modification, which were R_1 and R_2, which are either H, F, Cl, Br, or CF_3.

Table 2.6 List of synthesised compounds with chemical variabilities.

Compound ID	Compound name	R_1	R_2
IA1	5-(3-chlorophenyl)-1,3-dihydro-2H-benzofuro[3,2-e]-1,4-diazepin-2-one	H	Cl
IA2	9-bromo-5-(3-bromophenyl)-1,3-dihydro-2H-[1]benzofuro[3,2-e][1,4]diazepin-2-one	Br	Br
IA3	5-(3-trifluoromethyl)-1,3-dihydro-2H-benzofuro[3,2-e]-1,4-diazepin-2-one	H	CF_3
IA4	9-trifluoromethyl-5-(3-trifluoromethylphenyl)-1,3-dihydro-2H-[1]benzofuro[3,2-e][1,4]diazepin-2-one	CF_3	CF_3
IA6	9-fluoro-5-phenyl-1,3-dihydro-2H-[1]benzofuro[3,2-e][1,4]diazepin-2-one	F	H
IA7	9-trifluoromethyl-5-phenyl-1,3-dihydro-2H-[1]benzofuro[3,2-e][1,4]diazepin-2-one	CF_3	H
IA8	9-chloro-5-(3-chlorophenyl)-1,3-dihydro-2H-[1]benzofuro[3,2-e][1,4]diazepin-2-one	Cl	Cl
IA9	9-chloro-5-phenyl-1,3-dihydro-2H-[1]benzofuro[3,2-e][1,4]diazepin-2-one	Cl	H
IA10	9-fluoro-5-(3-fluorophenyl)-1,3-dihydro-2H-[1]benzofuro[3,2-e][1,4]diazepin-2-one	F	F
IA11	5-(3-fluorophenyl)-1,3-dihydro-2H-benzofuro[3,2-e]-1,4-diazepin-2-one	H	F

Note. Br = bromine, Cl = chlorine, H = hydrogen, F = fluorine, CF_3 = trifluoromethyl

2.2.8.1 Compound synthesis

The synthesis of ten compounds was performed by two persons. I synthesised three compounds (IA1, IA2, and IA3) and the rest were synthesised by Dr Marco Cominetti, a postdoctoral researcher in School of Pharmacy and Chemistry, University of East Anglia. The synthesis which consisted of four major steps were based on methods outlined by Fischer et al. (2004). Two starting materials were required to synthesise each compound which were purchased from either Sigma-Aldrich or Fluorochem. The general chemical structure for the starting materials is shown in Figure 2.5. The following procedure is the example of IA2 synthesis.

In Step 1, 4 mmol (1.11 g) of 3-bromophenacyl bromide (compound **1**) and 4 mmol (0.792 g) of 5-bromo-2-hydroxybenzonitrile (compound **2**) were weighed and put into a V-vial with silicone septa-equipped open top cap. Then, 4.4 mmol (0.445 g) of triethylamine (Sigma-Aldrich) was added into the vial and lastly 5 mL of dimethylformamide (Fischer Scientific) was added. All ingredients were stirred at 70 °C for 2 – 3 hours. The reaction mixture was checked with thin layer chromatography (TLC) after 2 hours to check the extent of reaction. The solvent system used for TLC was ethyl acetate:hexane (3:7). After TLC indicated a complete reaction, the reaction mixture was washed with water and saturated sodium chloride solution. The reaction mixture was poured into a separating funnel, then 95 mL of ethyl acetate and 200 mL of water was added to it. The mixture was shaken to wash off impurities from the reaction mixture and allowed to stand until two distinct layers were formed; ethyl acetate containing product and water containing impurities. The water underneath was removed and another 200 mL of water was added again into the separating funnel, shaken, and removed. This was repeated three times and an additional two times with saturated sodium chloride solution. The organic phase was dried over sodium sulphate and the solvent was vaporised under reduced pressure. The product was then tested for ^{1}H-NMR to check its purity and chemical content.

Next, 2.8 mmol (1.067 g) of product from Step 1 was added into V-vial and dissolved with 7 mL of ethanol (Fischer Scientific). Then, 3.08 mmol (0.210 g) of sodium ethoxide (Sigma-Aldrich) was added into the vial which was heated under reflux for 2 – 3 hours. The reaction mixture was checked on TLC after two hours to determine the

extent of reaction. Solvent system used for TLC was dichloromethane:hexane (3:7). When the reaction was completed, the reaction mixture was washed with water and saturated sodium chloride solution for three and two times, respectively, and the remaining steps explained in previous paragraph were repeated. The dried product was weighed and the mole number was determined. The product was then tested for ^{1}H-NMR to check its purity and chemical content.

In Step 3, 1.9 mmol (0.751 g) of product from Step 2 was dissolved in 60 mL of chloroform (Fischer Scientific) and stirred at 0 °C. Next, 2.09 mmol (0.422 g) of bromoacetyl bromide (Sigma-Aldrich) and 7.6 mmol (0.638 g) of sodium bicarbonate were added into the mixture to start the reaction. The reaction mixture was stirred for 1 – 2 hours at 0 °C, with TLC checking after 1 hour of stirring. When the reaction was completed, the solvent was removed under reduced pressure and the dried product was redissolved with 50 mL of ethyl acetate. The solution was then washed with 100 mL of sodium bicarbonate solution and 100 mL of saturated sodium chloride solution, once each. The organic phase was dried over sodium sulphate and solvent was removed under reduced pressure. The dried product was weighed and mole number was determined. The product was then tested for ^{1}H-NMR to check its purity and chemical content.

Finally, 1.3 mmol (0.671 g) of product from Step 3 was dissolved in 30 mL diethyl ether (Fischer Scientific) and stirred at room temperature in a V-vial. Sodium sulphate (5.0 g) was also added into the reaction to absorb water formed during the reaction. The air in the V-vial was flushed with nitrogen gas to make the environment inert because dioxane can form explosive peroxide with prolonged exposure to air. Then, in an inert environment, 13 mmol (25.89 mL) of 0.5 M solution of ammonia in dioxane was added into the mixture to start the reaction and the reaction mixture was stirred at room temperature for 3 – 4 days. The mixture was checked on TLC after three days with solvent system of ethyl acetate:hexane (4:6). When the reaction was completed, 30 mL of ethyl acetate was added to the reaction mixture and it was washed with 150 mL of water and 150 mL of saturated sodium chloride for thrice and once, respectively. The organic phase was dried over sodium sulphate and the solvent was removed under reduced pressure. The final product was weighed and mole number was determined. The product was then tested for ^{1}H-NMR to check its purity and chemical content.

Two modifications on the synthesis protocol were made to make the synthesis more efficient. Firstly, the duration for each reaction step was increased by up to 1 hour on top of reported duration (Fischer et al., 2004) for Step 1 – 3 and additional 1 – 2 days for Step 4. This was done because TLC test indicated that the reaction was incomplete at the end of reported reaction period, hence the reaction was allowed to proceed longer. Another modification made was the addition of anhydrous Na_2SO_4 into reaction vial during Step 4 because the reactions were reversible. Therefore, to prevent the product from hydrolysing, Na_2SO_4 was added to dry up water by-product.

Secondly, the yield of final product from each synthesis was extremely low. From an initial amount of 4 mmol at the beginning of reaction, the yield decreased after each reaction step and the yield of final product was approximately 1 % of theoretical yield of each compound. This could be due to many factors; lack of competency in organic synthesis, incomplete reaction, but mostly due to sample being taken out after each step for analysis purposes. Another factor that contributed to low yield was the presence of impurities together with the compound that demanded purification using HPLC in which caused more product to lose.

Basically, the main reactions involved throughout the synthesis were nucleophilic substitution and acid-base reactions. The detailed mechanism of each reaction step is shown in Scheme 2.1 to 2.4.
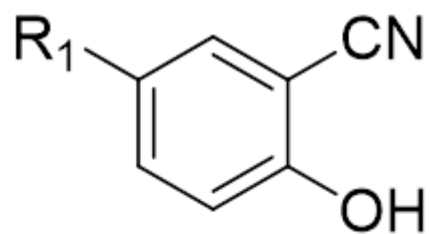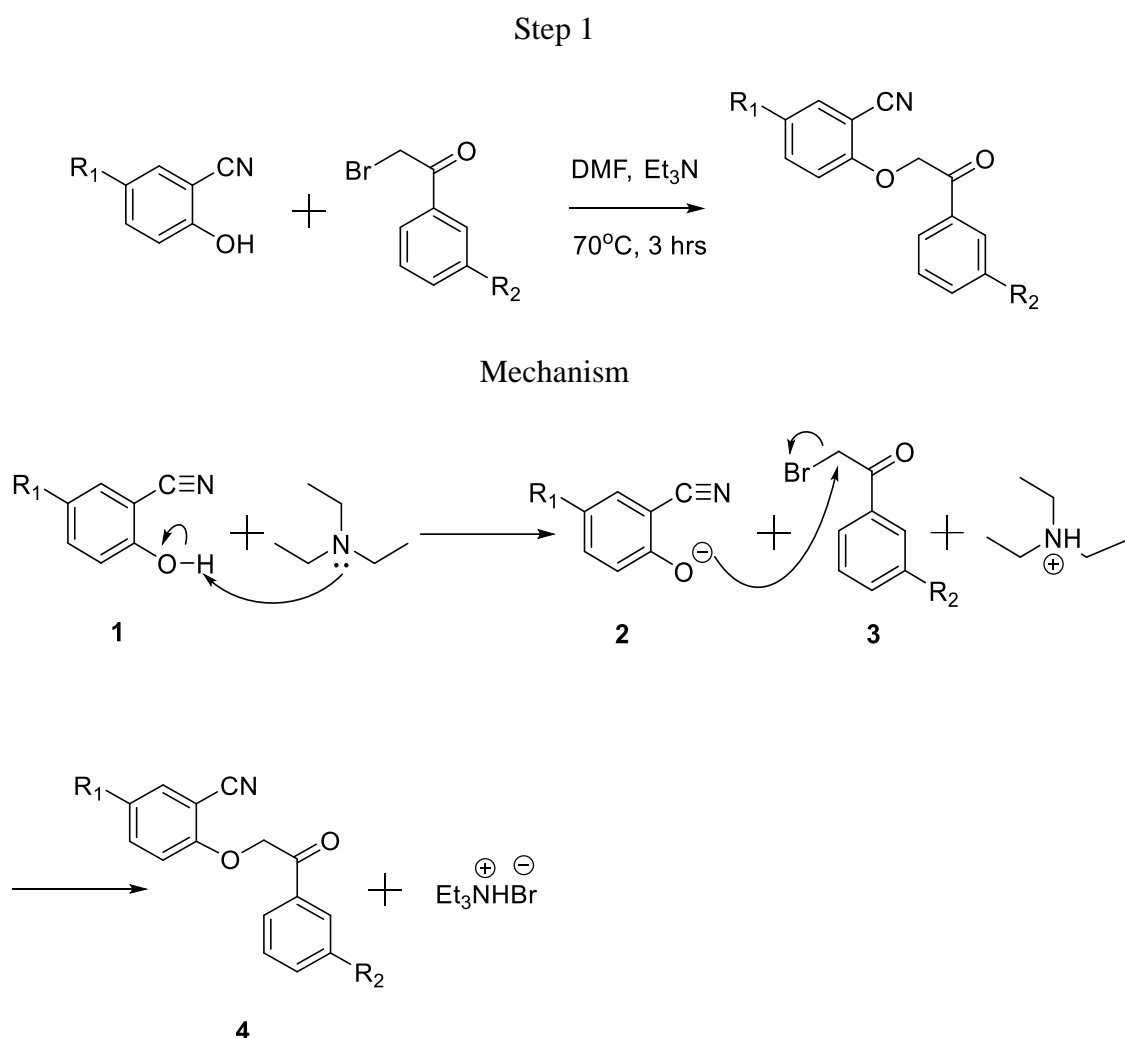
Compound 1
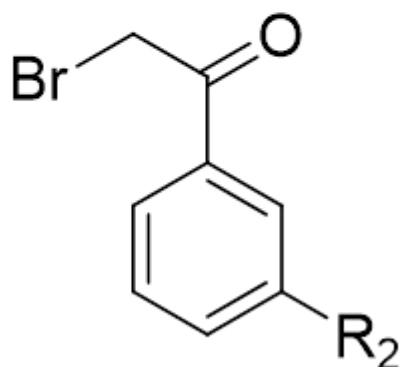
Compound 2

**Figure 2.5 General chemical formula of starting materials.**

Compound 1 and 2 were reacted in certain conditions as a starting reaction to produce final products. R_1 and R_2 were determined based on required final product chemical structure.
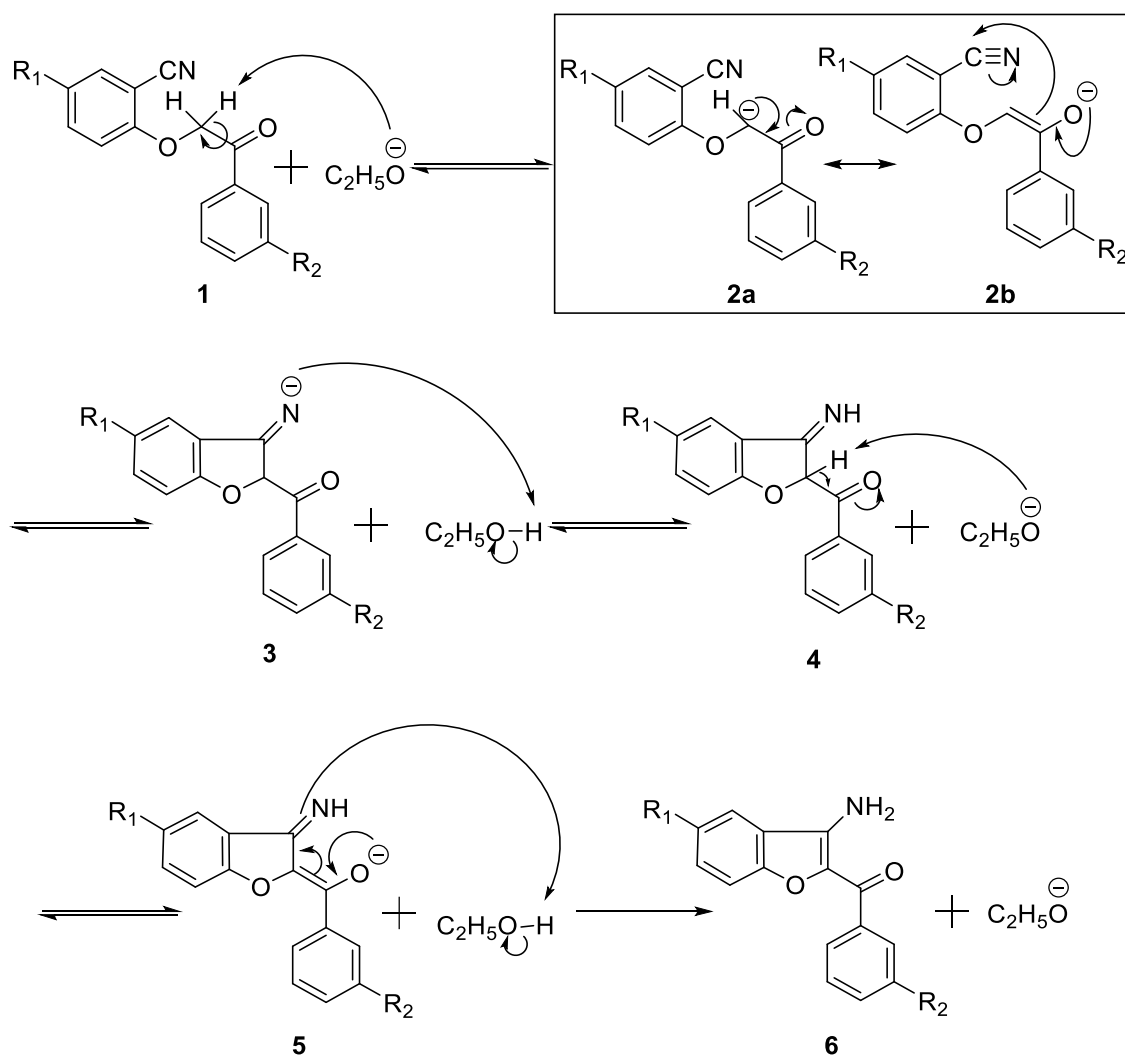
Step 1

Mechanism

Scheme 2.1 Mechanism of reaction during Step 1 synthesis.
Two starting materials were reacted in dimethylformamide in the presence of triethylamine at 70 °C for 3 hours. The hydroxyl group at Reactant **1** was deprotonated by triethylamine through acid-base reaction. The resulting nucleophilic phenoxy ion (O⁻) at Intermediate **2** attacked the electrophilic carbon at Reactant **3** which in turn caused Br⁻ to leave through S_N2 reaction to form Product **4**.
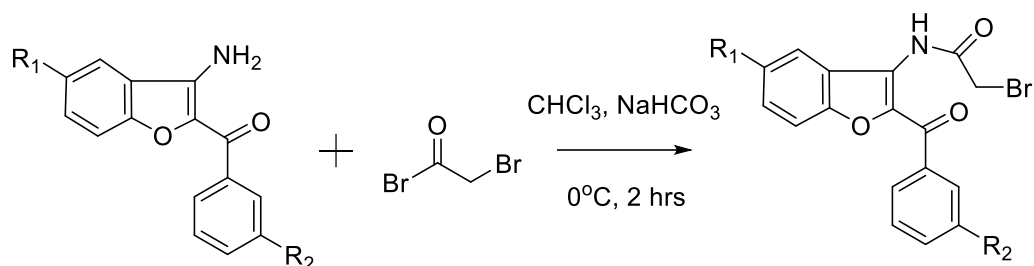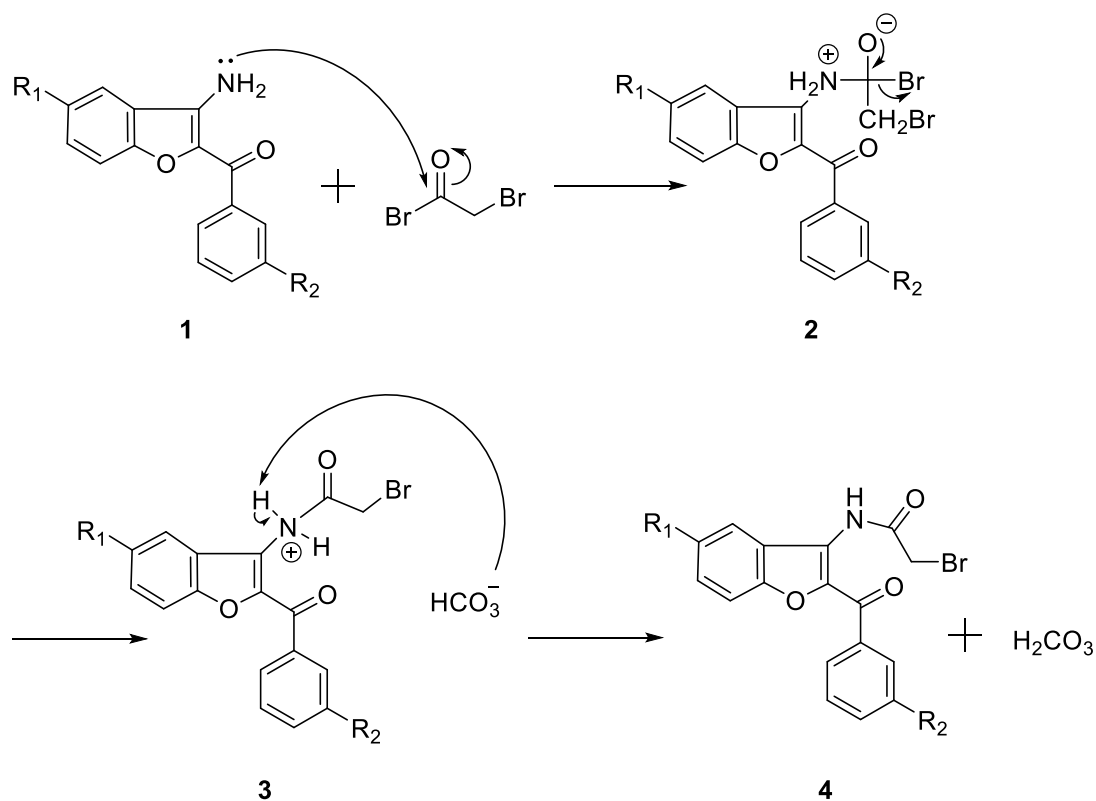
Step 2
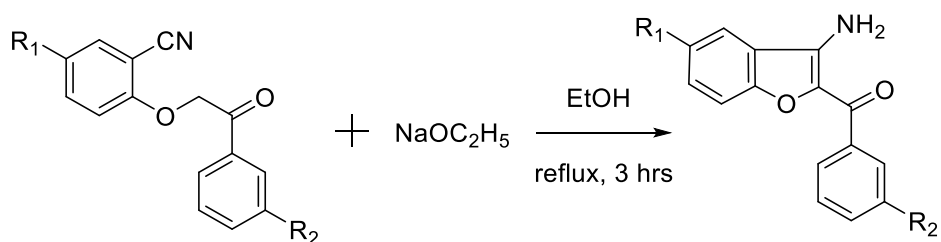
Mechanism

Scheme 2.2 Mechanism of reaction during Step 2 synthesis.
The product from Step 1 was then reacted with sodium ethoxide in ethanol under reflux for 3 hours. Sodium ethanoate deprotonated the alpha carbon to carbonyl at Reactant **1** and the resulting enolate was stabilised by resonance. The nucleophile at Resonant **2b** attacked the neighbouring electrophilic carbon through S_N2 reaction to yield Intermediate **3**. The nitrogen was then reprotonated by ethanol to give Intermediate **4**. As in Step 1, deprotonation by enolate led to Intermediate **5**. Subsequent rearrangement and proton transfer led to aromatization of the furan ring and restoration of neutrality (**6**).
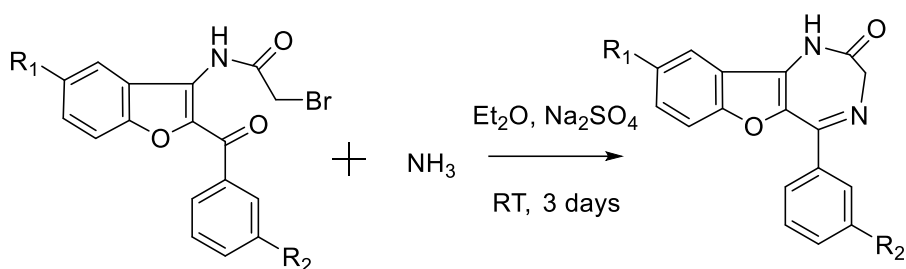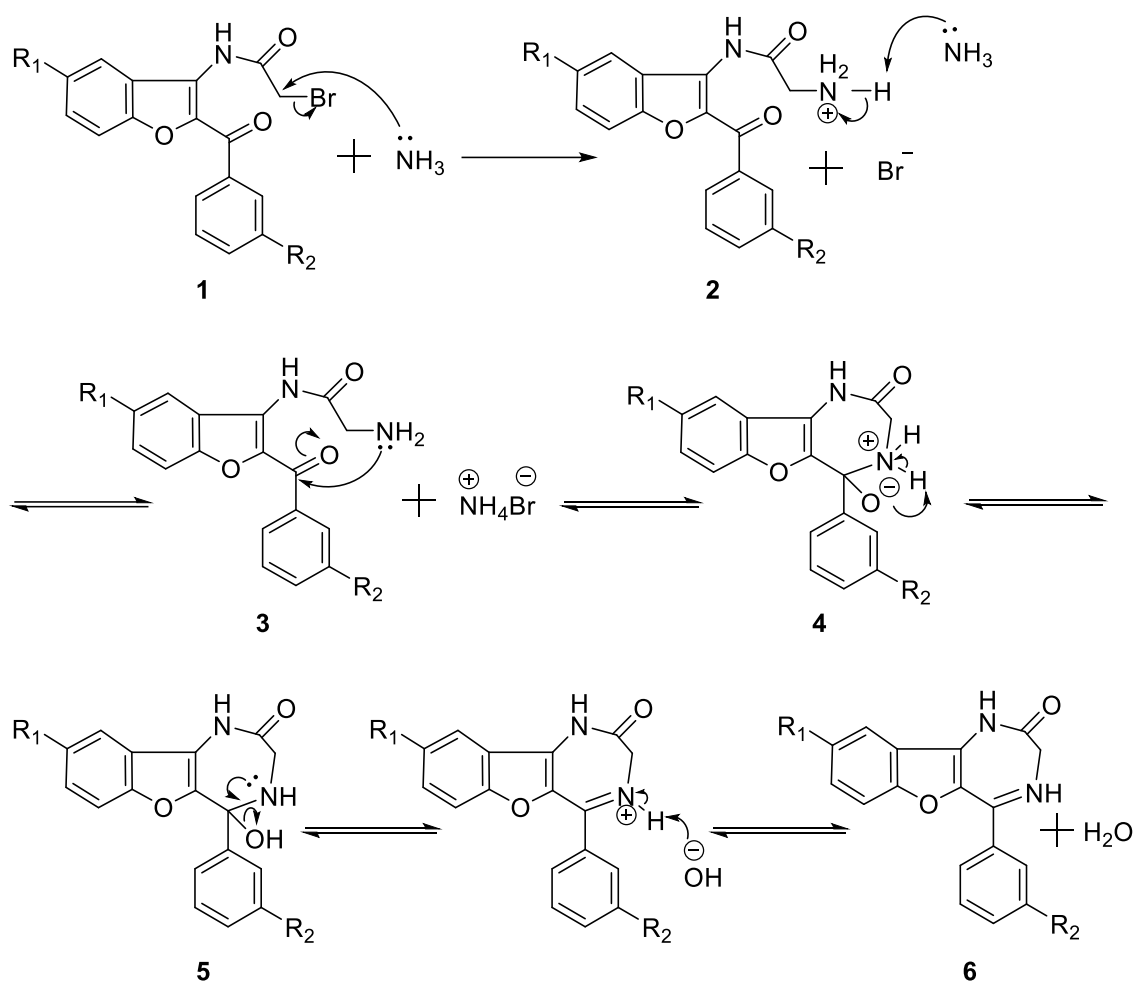
Step 3

Mechanism

Scheme 2.3 Mechanism of reaction during Step 3 synthesis.
The product from Step 2 was then reacted with bromoacetyl bromide in chloroform and sodium bicarbonate for 2 hours at 0 °C. Nucleophile at Reactant **1** attacked the electrophilic δ^+ carbon of bromoacetyl bromide and caused Br$^-$ to leave through S_N2 reaction (**2**). The amide nitrogen at Intermediate **3** was then deprotonated by bicarbonate yielding the final Product **4**.

Step 4

Mechanism

Scheme 2.4 Mechanism of reaction during Step 4 synthesis.

Finally, the Step 3 product was reacted with ammonia in diethylether together with sodium sulphate, to absorb water by-product, for 3 days at room temperature. Nucleophilic ammonia attacked the electrophilic carbon at Reactant **1** and caused subsequent loss of Br⁻. Then, Intermediate **2** was deprotonated by ammonia. Nucleophilic amine at Intermediate **3** attacked the carbonyl and formed the benzodiazepinone ring. Proton transfer at Intermediate **4** led to the hydroxyl group at Intermediate **5**, which was then eliminated to yield final Product **6**.

2.2.8.2 Analysis and purification of synthesised compounds by HPLC

Both the analysis and purification were performed by Dr Marco Cominetti. The analysis of final compounds was done using high performance liquid chromatography (HPLC, Agilent Technologies 1200 Series) using reverse phase column Agilent Eclipse XDB-C18 with a pore size of 5 µm and dimension of 4.6 ×150 mm, heated at 40 °C. The eluted compounds were detected using UV light at 210 nm. The samples were eluted using a gradient system using solvent A (water added with 0.05 % trifluoroacetic acid) and solvent B (acetonitrile added with 0.05 % trifluoroacetic acid). Two gradient methods were used to analyse the compound, which were short and long. The short method was firstly used for all compounds. The long method was employed if there were the presence of integrated peaks, in order to obtain better peaks separation. Both gradient elution methods are shown in Table 2.7. Data analysis was performed using OpenLAB CDS ChemStation Edition by Agilent Technologies. The blank was subtracted from the signal of the analysis prior to integration.

For purification, the compounds were purified using preparative HPLC (Agilent Technologies 1200 Infinity Series). The column used was the Agilent Eclipse XDB-C18 with a pore size of 5 μm and dimension of 21.2 × 150 mm. The eluted compounds were detected using UV light at 210 nm. The sample was separated using a gradient system adjusted from the analytical HPLC gradient system but with slightly different solvents; Solvent A was water/acetonitrile 95/5 added with 0.05 % trifluoroacetic acid while Solvent B was water/acetonitrile 5/95 added with 0.05 % trifluoroacetic acid. The gradient elution system for purification is shown in Table 2.8. The fractions containing the product were collected and acetonitrile was removed by evaporation under reduced pressure. The remaining water was freeze dried to yield the dry product.

Table 2.7 Gradient elution system used for HPLC analysis.

Time (min)		Solvent A (%)	Solvent B (%)
Short method	Long method		
0 – 2	0 – 3	100	0
2 – 5	3 – 10	100 – 5	0 – 95
5 – 10	10 – 15	5	95
10	15	100	0

Table 2.8 Gradient elution system used for HPLC purification.

Time (min)	Solvent A (%)	Solvent B (%)
0 – 3	100	0
3 – 10	100 – 5	0 – 95
10 – 15	5	95
15	100	0

2.2.8.3   Other analyses for the synthesised compounds

All final compounds were also analysed by Dr Marco Cominetti using ^{1}H NMR, ^{13}C NMR, ^{19}F NMR (where applicable), melting point determination equipment (Stuart), and Fourier transform infrared spectroscopy (FTIR). The molecular weight of the compounds was determined using high resolution mass spectrometry (HRMS, Thermo Scientific LTQ Orbitrap XL) carried out by EPSRC UK National Mass Spectrometry Facility.

2.2.9   Docking of 5-BDBD and its analogues

Docking was done by Dr Marco Cominetti. The ligands were prepared for docking with UCFS Chimera (Pettersen et al., 2004) and AutodockTools4 (Morris et al., 2009), each one in two different conformations to account for flexibility of the diazepinone ring. The rotation of phenyl group was allowed. The human homology model of P2X$_4$ in its closed, resting state was kindly modelled by Associate Professor Dr Ralf Schmid from University of Leicester based on closed state of zfP2X$_4$ (PDB ID: 4DW0) (Hattori & Gouaux, 2012). The protein was cleaned, hydrogens were added with UCFS Chimera (Pettersen et al., 2004), and relaxed with GROMACS 4.6.5 (Pronk et al., 2013). The AutoDockTools4 (Morris et al., 2009) was used to convert the files for docking. The side chains of residues near the active site were made flexible.

The homology model of human P2X$_4$ receptor in its ATP-bound, open state was created using MODELLER 9.18 (Webb & Sali, 2014). The crystal structure of *Danio rerio* P2X$_4$ (PDB: 4DW1) was used as template. Sequence alignments were obtained through BLASTP 2.6.1+ from the NCBI website (Altschul et al., 1997; Altschul et al., 2005; National Institute of Health, *n. d.*). Due to the number of halogens present in the structures under investigation, docking was performed with AutoDock VinaXB (Koebel et al., 2016). Considering the competitive activity of these compounds with ATP, each compound was docked into the ATP binding pocket of protein in its closed, apo state. Considering the slight different conformation of three ATP binding pockets on P2X$_4$, the process was repeated for each pocket to increase the sampling.

All binding poses of every docked analogue were clustered hierarchically by the

RMSD relative to rigid, flat part of the molecule present in all analogues to identify the similar binding poses throughout the series of compounds. This was repeated for each of the three ATP binding pockets. The clustering was performed with the single-linkage clustering method provided in MATLAB 8.5. The manual inspection of clusters led to the identification of a redundant binding mode across all three binding pockets. This mode was also presented a prevalence of active compounds versus non-active compounds. The ability of the model to reproduce and explain the activity in relation to the different substitutions led to the proposal of this model as the binding mode.

2.2.10 Statistical analysis

All data were analysed using Origin® version 9.1 software (Origin Lab Corporation, USA). The distribution of data was determined using the Shapiro-Wilk test. If the data was normally distributed, statistical analysis was done using paired t-tests and if otherwise, the paired-sample Wilcoxon signed rank test was done. All experiments were repeated three times, at least, which was indicated by number of n. If $n = 3$, for instance, the experiment was done in three individual experiments, each in triplicates, using cells from three different flasks. The confidence interval was set at 95 % and statistical significance was labelled with asterisk where $*p < 0.05$, $**p < 0.01$, and $***p < 0.001$. All concentration-response curves were fitted using the Hill equation and desensitisation period (tau value (τ)) was determined using the exponential decay 1 function in the Origin software.

CHAPTER 3

IDENTIFICATION OF THASPINE AS A P2X$_4$ INHIBITOR THROUGH HIGH THROUGHPUT SCREENING

3.1 Introduction

A total of 1,710 compounds were used for screening and they came in two different sets namely Natural Products Set III (NPiii) and Diversity Set V (DSv) which were obtained from the NCI. The NPiii consists of 116 compounds; and the set is derived from DTP repository and put together by NCI based on their origin, purity, structural diversity, and availability of compound in the repository. However, this set was recently updated to Natural Products Set IV with additional compounds ("National Cancer Institute Development Therapeutics Program," 2016). Meanwhile, DSv consists of 1,594 compounds which are carefully selected from 140,000 compounds available in DTP repository, based on their pharmacophoric properties such as the number of hydrogen bond acceptors and donors, electric charge, and hydrophobicity. Another criterion for the selection is that the compounds should be relatively rigid, with five or less rotatable bonds, having tendency to be planar, having one or less chiral centres, and possessing pharmacologically desirable features; all of which contribute to the favourability of compounds to bind with biological proteins. Those properties are important because they represent drug-like properties, which are vital in this study.

Before the screening experiment, a few steps were carried out for the preparation of compound screening. Stable P2X$_4$ and other P2 receptor overexpressing cells were either generated in the lab or supplied by third parties as gifts. All overexpressing cells were characterised before being used in high throughput screening. After the stable P2X$_4$ overexpressing cells were generated and characterised, the high throughput screening was performed of which its process is illustrated in Figure 3.18. The process started with screening of 1,710 compounds using a calcium response assay. Any compound that met two criteria (will be discussed later) were considered as hits which were then further characterised. After the hit characterisation, lead compound was

identified and taken forward for further investigation. In this study, thaspine was identified as the lead compound and investigated further for its pharmacological properties.

3.2 Aim

The main objective of this experiment was to find any potential compound with the potential of antagonising the human $P2X_4$ receptor and to further characterise this lead compound.

3.3 Results

The results for section are divided into three sections. The first section will discuss the generation of stable $P2X_4$ overexpressing cell line. The second section will describe on the high throughput screening while the third section will explain the characterisation of lead compound, thaspine.

3.3.2   Generation of stable cell lines

3.3.2.1   Cloning of DNA

To generate stable cell lines, the DNAs of interest were first introduced into pLVX-IRES-mCherry vector. The DNAs were already available in-house with different vectors. Therefore, they were restricted using suitable restriction enzymes for insertion into the new vector. The size of DNAs was determined by running the DNA on gels. The DNAs were then inserted into pLVX-IRES-mCherry vector and transformed inside bacteria. The DNA extracted from bacterial colonies were then run on a gel to check for successful transformation. Based on Figure 3.1B, for mouse $P2X_4$, the DNA from bacterial colony 1 was observed to travel less on gel compared to the uncut vector, which suggested that it contained the DNA of interest because theoretically it had a bigger size in comparison with the uncut vector and thus, travelled less. As for the human $P2X_7$, all five colonies travelled less compared to uncut vector and it was deduced that all of them contained the human $P2X_7$ DNA. The DNAs from colony 1 from both mouse $P2X_4$ and human $P2X_7$ cloning were then sent for DNA sequencing and the data showed that they both contained the right sequence for mouse $P2X_4$ and human $P2X_7$, respectively, with correct orientation.
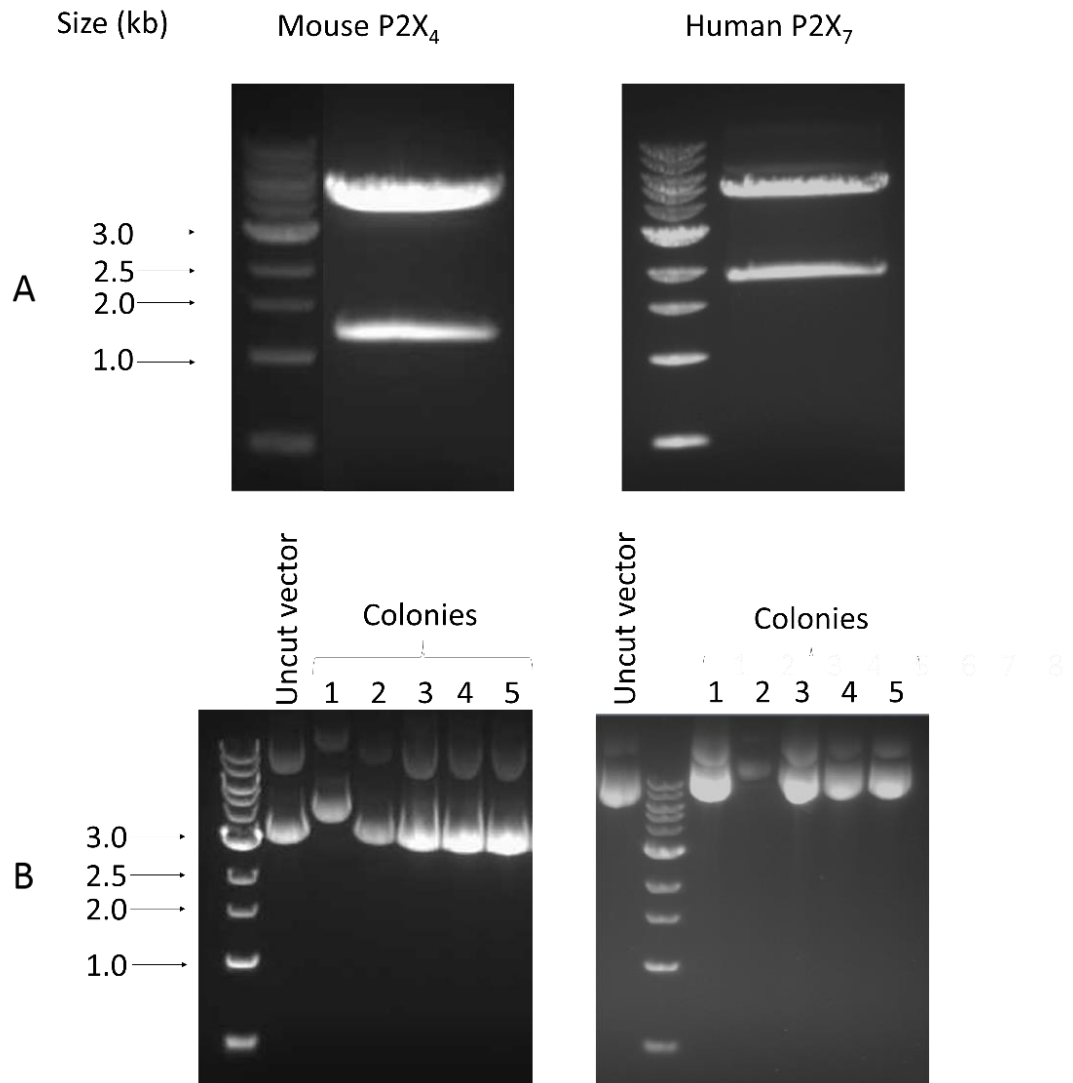
Figure 3.1 Gels showing bands after restriction and ligation.
Panel A shows the bands of restricted mouse P2X$_4$ DNA and human P2X$_7$ DNA, and their vectors after restriction with EcoRI-HF and NotI-HF (for mouse P2X$_4$), and NotI-HF (for human P2X$_7$). Mouse P2X$_4$ and human P2X$_7$ had a size of ~1.2 and ~1.9 kb, which were both confirmed by the gels. The bigger bands on top of DNA in both gels were the vectors. Gels in panel B show the size of circular DNA extracted from five colonies which had been transformed with DNA of interest. On the left, DNA from bacterial colony 1 travelled less than the uncut vector, indicating a successful ligation. On the right, the DNA from all bacterial colonies moved relatively less than uncut vector, which was an evident of successful ligation. The DNAs from colony 1 of both clones were verified further using DNA sequencing.

3.3.2.2   Transfection with Fugene HD

Once the correct recombinant DNAs were obtained, they were transfected into the astrocytoma cells. To achieve that, a transfecting agent called Fugene HD was used. Optimisation experiments were done to determine the best Fugene HD (µL):DNA (µg) ratio, seeding density (two seeding densities chosen based on manufacturer's protocol, i.e., 50,000 and 125,000 cells/well in a 24-well plate) and transfection duration. GFP-tagged recombinant DNA was used in this experiment to assess the success of transfection by observing the fluorescence under a fluorescence microscope as well as a more accurate quantitative evaluation using FlexStation 3. Basically, the more fluorescence recorded indicated that more cells were being successfully transfected.

Figure 3.2 shows the amount of fluorescence measured by FlexStation 3 at different Fugene HD:DNA ratio and seeding densities. At a ratio of 3:2, there was no fluorescence observed at low cell density and minimal fluorescence measured at high cell density after 48 and 72 hours. At 4:2 ratio, no or minimal fluorescence detected from cells at low seeding density at both time points. On the contrary, at high seeding density, the fluorescence was markedly higher with slightly more intense fluorescence after 72 hours compared to 48 hours. As the Fugene HD:DNA ratio increased to 5:2 and 6:2, the fluorescence remained similar with that 4:2 ratio.

However, at 7:2 ratio, the fluorescence was further reduced at high seeding density after 48 and 72 hours in relative to lower Fugene HD:DNA ratio, while fluorescence at low seeding density remained undetected. Again, the transfection was better when the cells were left with transfecting agent for 72 hours rather than 48 hours. Surprisingly, further ratio increase had turned down the fluorescence lower than 7:2 ratio, with no or minimal detection of fluorescence at low seeding density. Based on the results, it was deduced that the optimum conditions for transfection using Fugene HD were 7:2 ratio (Fugene HD:DNA), 125,000 cells/well density and 72 hours incubation with Fugene HD.
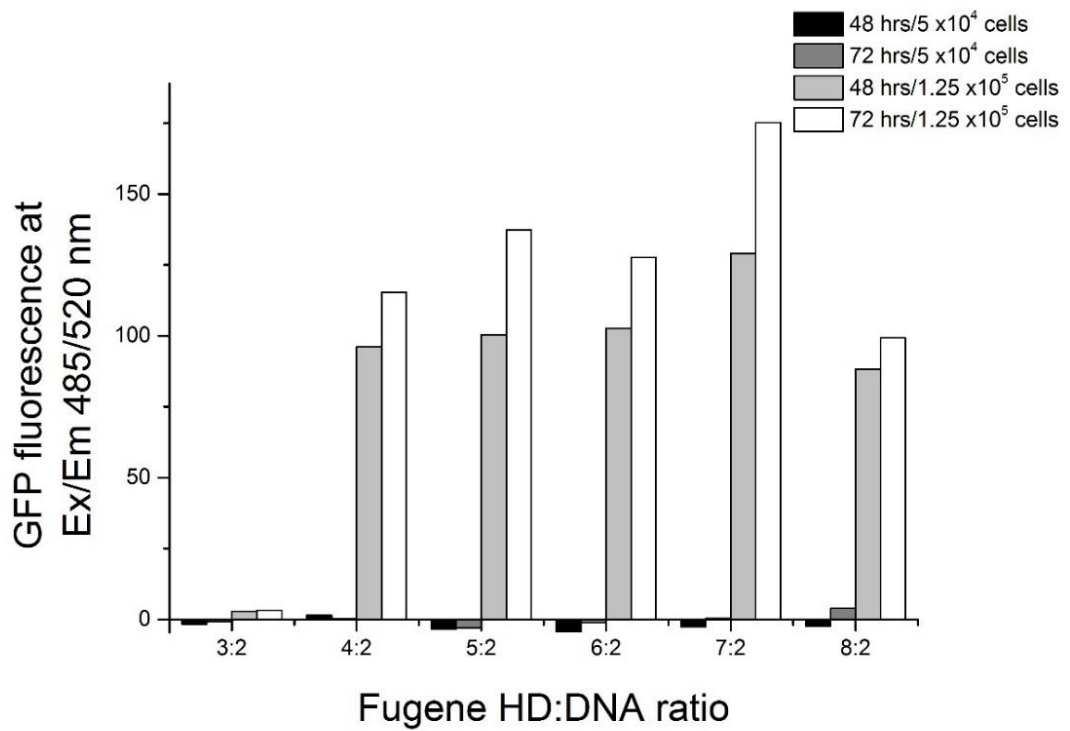
Figure 3.2 Optimisation of Fugene HD:DNA ratio for transfection.
The figure shows the optimisation process to determine the optimum condition for transfection using Fugene HD. The variables tested were Fugene HD:DNA ratio, duration of transfection, and seeding density. The tests were done in a 24-well plate. Black and dark grey bars represent the fluorescence measured after 48 and 72 hours of transfection duration, respectively, at low cell density. Light grey and white bars represent the fluorescence measured after 48 and 72 hours of transfection, respectively, at high cell density. ($n = 1$)

Afterwards, a kill curve experiment was carried out to determine the resistance of astrocytoma cells towards puromycin. This was important at later stages of the transfection process because puromycin was used to select the successfully transfected cells which carry the puromycin-resistant gene. The viable cells after puromycin selection were quantitated using an MTS assay as they can reduce MTS tetrazolium compound into a coloured formazan product which was subsequently measured by absorbance reading at a wavelength of 490 nm. Based on Figure 3.3, the cells multiplied on Day 1 of treatment except at 10 and 30 µg/mL of puromycin, where the cells died straight after puromycin treatment. Meanwhile at 1.0 µg/mL, the proliferation rate was greatly reduced to almost balance between cell proliferation and death.

On Day 2, the cells at all concentrations started to die. Throughout four days of puromycin treatment, astrocytoma cells were only resistant towards 0.1 and 0.3 µg/mL of puromycin and survived. On the contrary, at higher concentrations, the cells died from Day 1 onwards. Generally, the rate of cell death gradually increased as the puromycin concentration increased. At 1.0 and 30 µg/mL, the cells did not survive after four days of puromycin treatment, whereas at 3.0 and 10 µg/mL, the cells died after three days of treatment. Consequently, it was deduced that the optimum condition for puromycin selection for post-transfection was 1.0 µg/mL for four days.

After all this important information was retrieved from the experiments, the outcomes were used to transfect the recombinant DNA into blank astrocytoma cells. When the transfected cells were treated with 1.0 µg/mL puromycin, visually, 99 % cells died after five days. Only a few cells survived after five days and the remaining cells were maintained at the same puromycin concentration. However, the rate of multiplication was extremely slow. It took about a month to get a sufficient number of cells for the ATP concentration-response experiment which is shown in Figure 3.4. Based on the concentration-response, the calculated EC_{50} value was 6.64 µM with a maximal ATP concentration of 100 µM, which produced a response of 0.96 F ratio.

However, the experiment was only performed once because the cells did not survive after subsequent splitting. That might have been caused by the low cell number after

splitting. That was also the cause for the inability to provide the standard error of mean for EC_{50} value. Afterwards, numerous attempts were done to repeat transfection process including up-scaling the transfection process but only resulted in numerous failures. Having continuous disappointment with the current technique of transfection, another technique was employed, which will be discussed shortly.
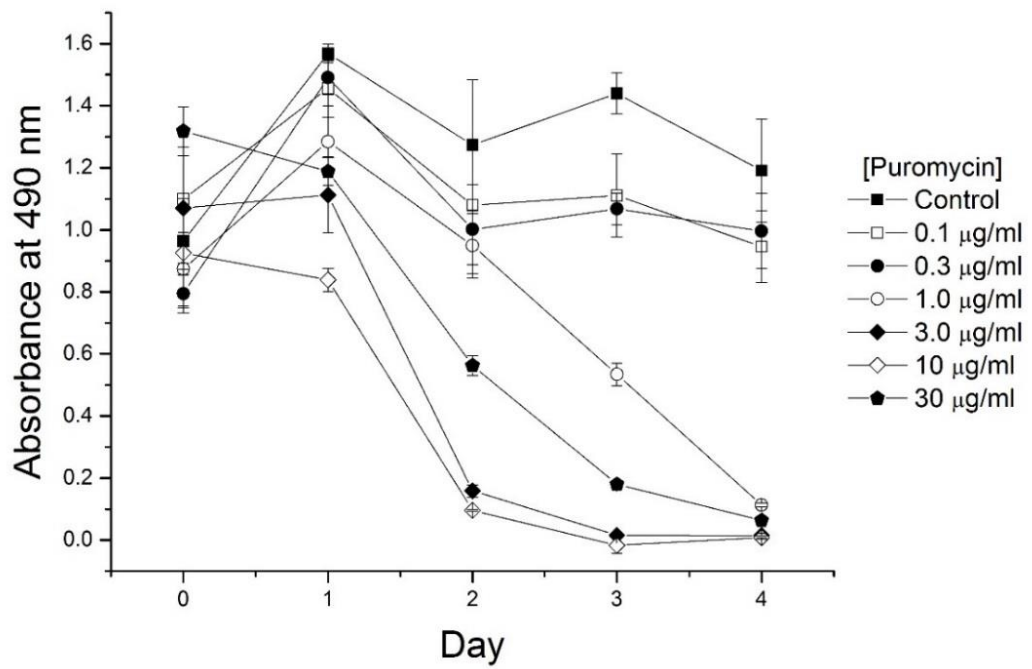
Figure 3.3 Puromycin kill curve on astrocytoma cells.

The graph shows the absorbance of MTS-reagent after puromycin treatment on astrocytoma cells for 4 days. The absorbance represents the number of viable cells; higher absorbance indicates more viable cells. ($n = 1$)
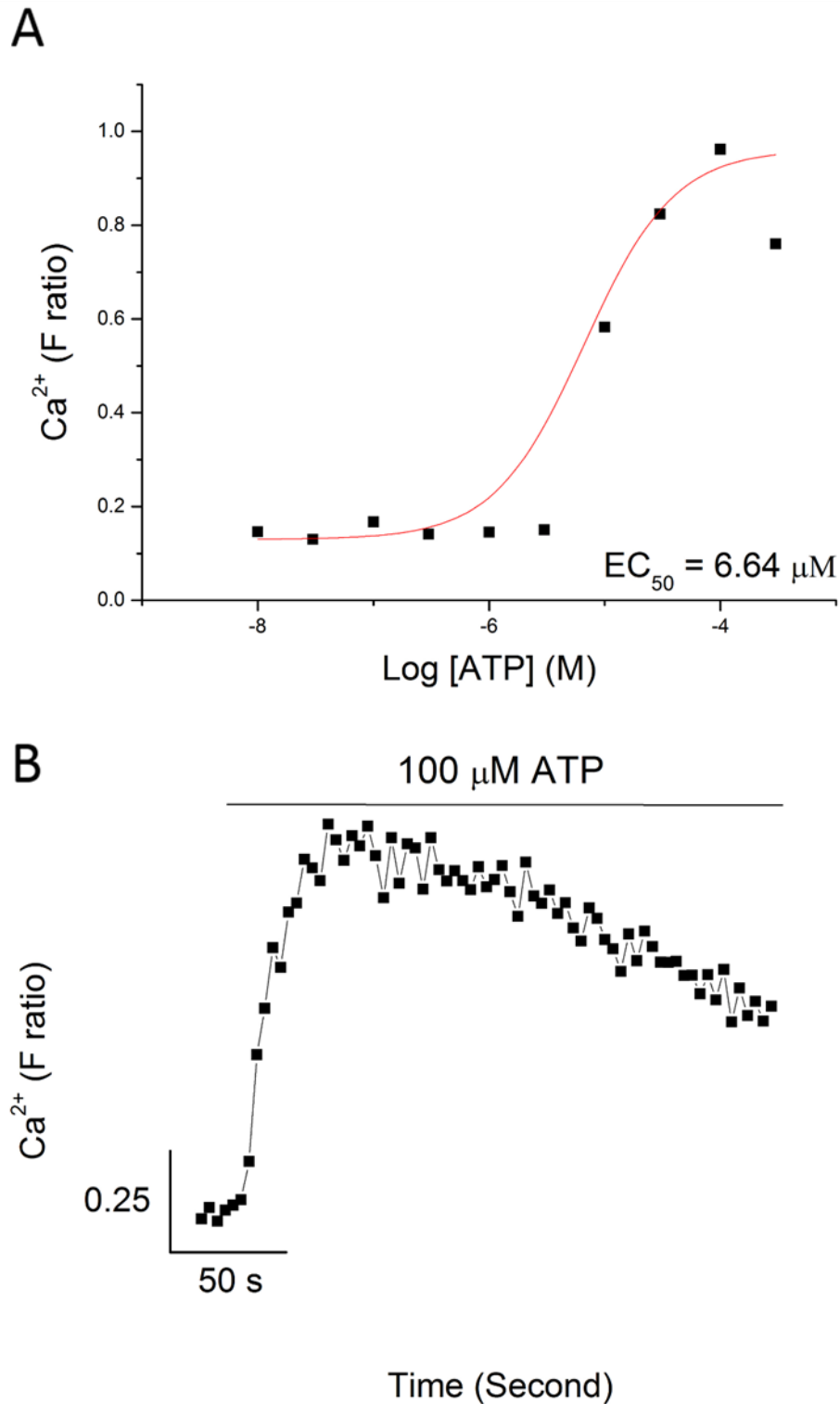
Figure 3.4 ATP concentration-response of the human P2X4 puromycin-resistant overexpressing cell.

Panel A shows the ATP concentration-response at human P2X$_4$ puromycin-resistant overexpressing cells and panel B shows the representative trace when the cells were stimulated with 100 µM of ATP. ($n = 1$)

3.3.2.3 Viral transfection

As the transfection using Fugene HD failed, the transfection strategy was changed to viral transfection. In this technique, the recombinant DNA was delivered into the blank astrocytoma cells using lentivirus. The number of lentiviral particles for each lentivirus produced was determined using p24 standard curve, as shown in Figure 3.5. The plasmid packaged in lentivirus contained mCherry gene that after being transcribed, would produce a fluorescent protein that emitted light when being excited at 587 nm wavelength. Thus, the selection of successfully transfected cells was based on the amount of fluorescence produced by the cells. The cells that highly fluoresced relative to non-transfected astrocytoma cells were sorted and grown in cell culture medium.

Figure 3.6 shows the distribution of cell population and histogram of fluorescence for the transfected cells in flow cytometry. Dot plots show the size and granularity of the cells while the histograms show fluorescence of the transfected cells of (A) human $P2X_7$, (B) mouse $P2X_4$, and (C) human $P2X_4$, respectively. Fluorescent cells were most likely to express the genes of interest although it was not guaranteed. The fluorescence histogram was divided into two regions, which P8 was the region that overlapped with fluorescence from non-transfected astrocytoma cells while P7 marked the fluorescence region outside non-transfected cell fluorescence. Cells that highly fluoresced and fell into P7 region were collected and cultured in flasks for future experiments. The percentage of highly expressing cells collected from the total population were 0.2, 2.3, and 1.0 % for human $P2X_7$, mouse, and human $P2X_4$, respectively.

All sorted cells for each P2X subtype were then cultured, expanded, and cryopreserved. The growth of cells after sorting was relatively slow but when it reached about 50 % confluency, the growth became faster. After the first splitting, the cells proliferated at the same rate as non-transfected astrocytoma cells and still showed fluorescence under fluorescence microscope as indicated in Figure 3.7.
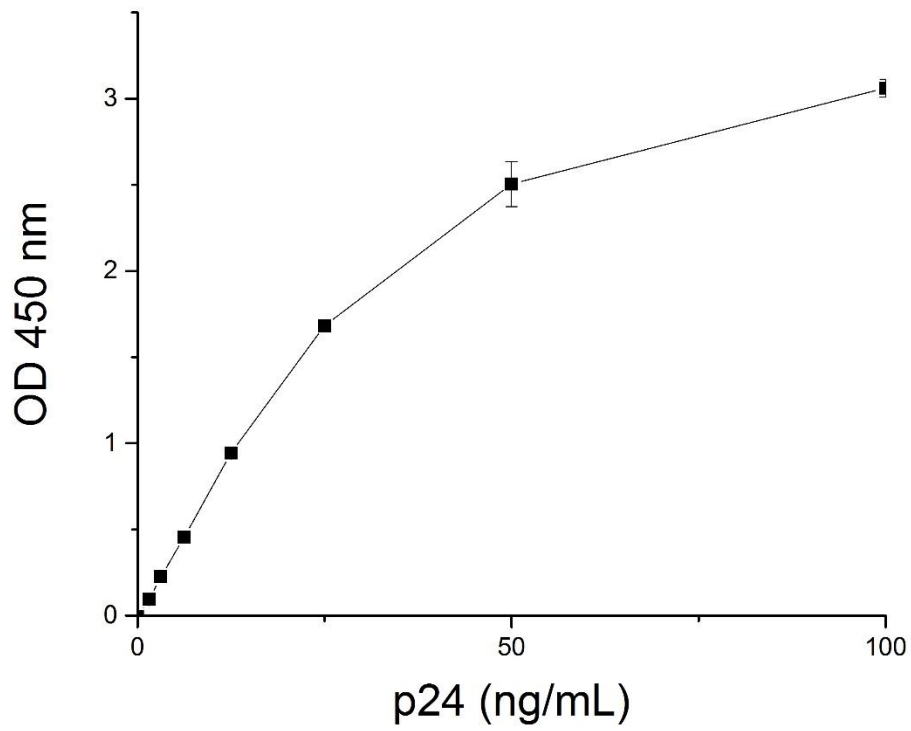
Figure 3.5 HIV p24 ELISA standard curve of recombinant HIV-1 p24 antigen. The amount of p24 associated particles of each lentiviral produced was calculated using this p24 standard curve and formula given by the manufacturer. The resulting figure was the amount of virus-containing gene in 1 mL of virus suspension.
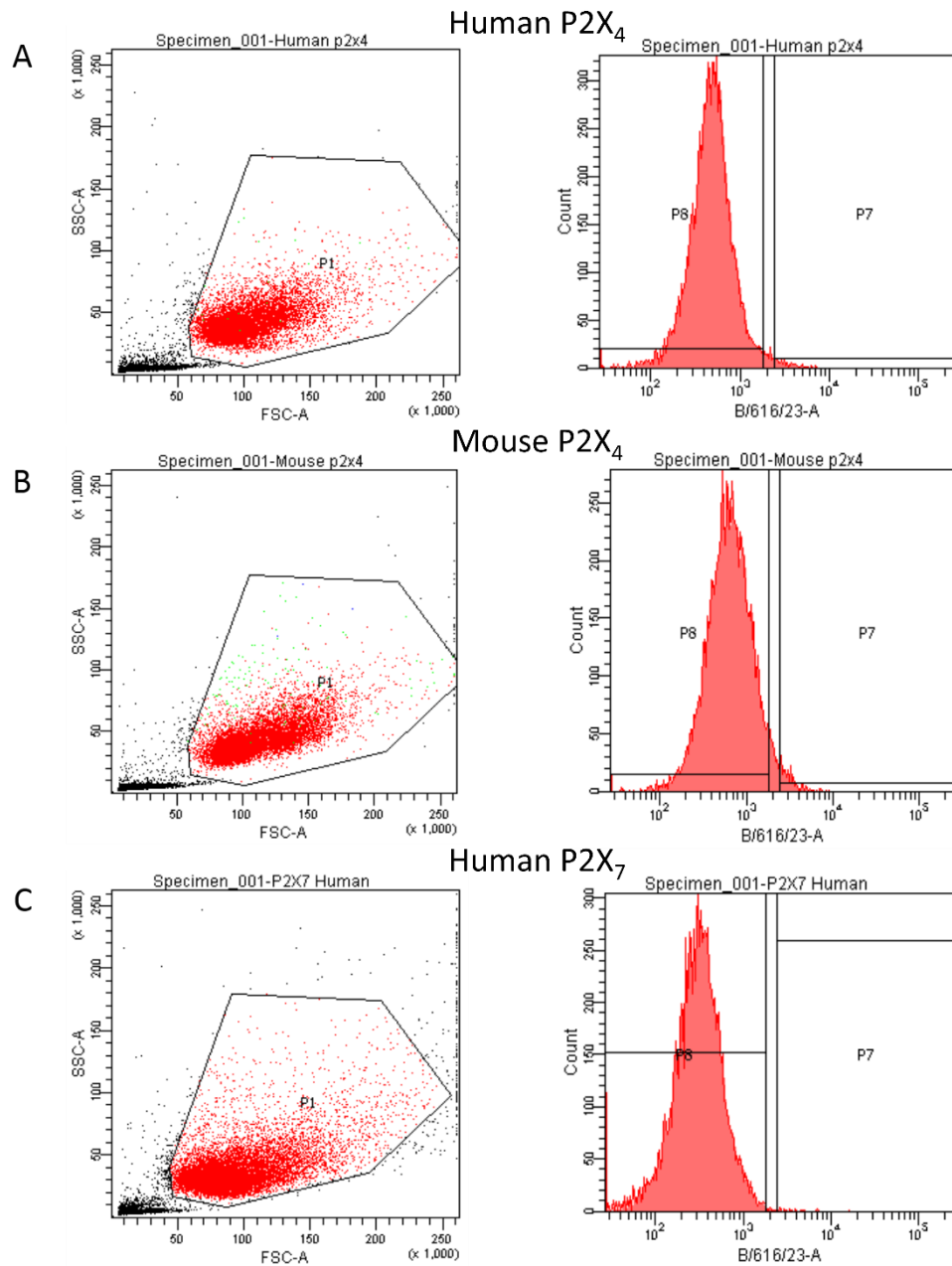
Figure 3.6 Distribution of P2X overexpressing cells and mCherry fluorescence. These are the flow cytometry histograms of (A) human P2X$_4$, (B) mouse P2X$_4$, and (C) human P2X$_7$. The left panel shows the distribution of cells being transfected for each transfected DNA. The target population was gated as P1 region and coloured in red and the small black population in the lower left side of the plot was regarded as dead cells. The right panel of the figure shows the fluorescence of mCherry protein. Since the vector used to carry the P2X DNAs also contained mCherry gene, the cells that were highly fluorescent indicated successful transfection. P7 region was regarded as the overexpressing cells and sorted for future experiments.
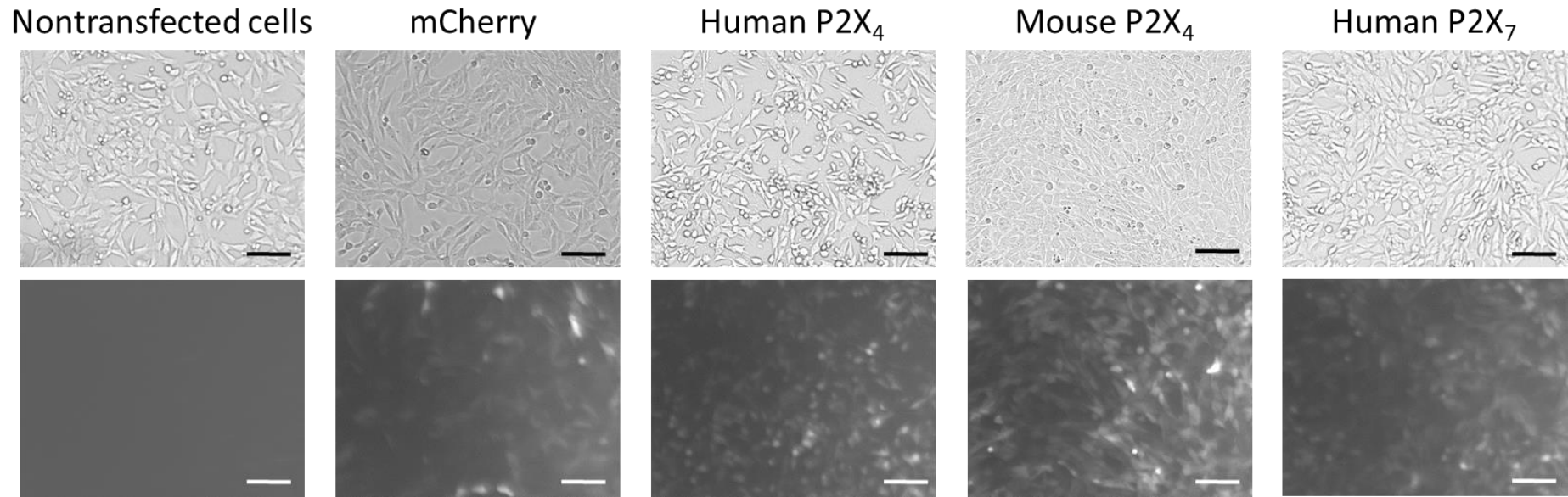
Figure 3.7 Images of overexpressing cells under fluorescence microscope
The images show the non-transfected astrocytoma cells, mCherry overexpressing cells (positive control), human P2X$_4$, mouse P2X$_4$, and human P2X$_7$ overexpressing cells under the fluorescence microscope post-sorting. The top panels are the bright-field images and bottom panels are the fluorescence images under TRITC laser. The scale bar represents 10 µm and magnification was 100x.

3.3.2.4 Characterisation of overexpressing cells

After the overexpressing cells were successfully generated, they were characterised for preparation to be used in high throughput screening. The performed characterisation tests comprised of the optimum seeding density determination, ATP concentration-response, determination of cell tolerability towards DMSO, PPADS inhibition concentration-response, and IVM potentiation concentration-response. All characterisation mentioned was only done on the human P2X$_4$ overexpressing cells; and for the overexpressing cells of other receptors, only nucleotide concentration-response was done.

Figure 3.8 shows the data on the optimum seeding density for a maximal calcium response. Based on the data, it showed that the highest response (0.69 ± 0.04 F ratio) was observed at a density of 2.5×10^4 cells/well. The responses remained unchanged at the densities of $\leq 10 \times 10^4$ cells/well but significantly lower at density of $> 10 \times 10^4$ cells/well ($p < 0.05$, $n = 3$). Therefore, the optimum seeding density chosen for the next experiments was 2.5×10^4 cells/well.

The potency of ATP on the human P2X$_4$ overexpressing cell line was determined through the concentration-response experiment and the results are shown in Figure 3.9. The first significant response was recorded when the cells were applied with 0.1 μM of ATP which yielded a response of 0.042 ± 0.008 F ratio ($p < 0.001$, $n = 12$). The response exponentially increased to a plateau at 3 μM of ATP. The calculated EC$_{50}$ value was 0.56 ± 0.13 μM ($n = 12$ experiments).
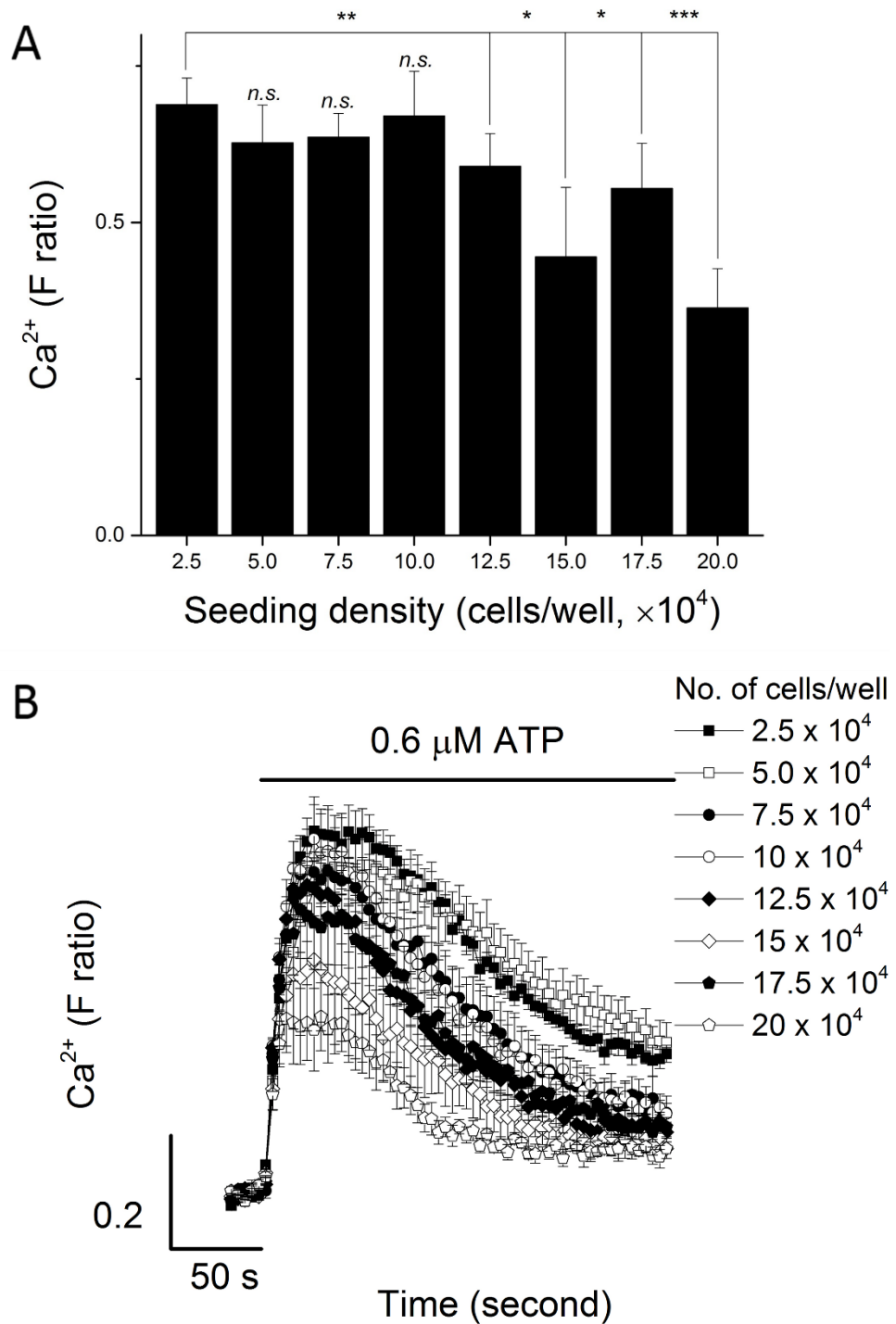
Figure 3.8 Effects of seeding density on ATP-evoked calcium response on the human P2X$_4$ overexpressing cells.

Panel A shows the peak response recorded within a recording period of 250 seconds when the cells were stimulated with 0.6 μM ATP at different seeding cell density, and panel B shows representative at each seeding density. The lowest seeding density tested was 2.5×10^4 cells/well and the maximum was 20×10^4 cells/well. The statistical analysis was performed against the ATP-evoked response elicited at the cell density of 2.5×10^4 cells/well. ($n = 3$)

A

B
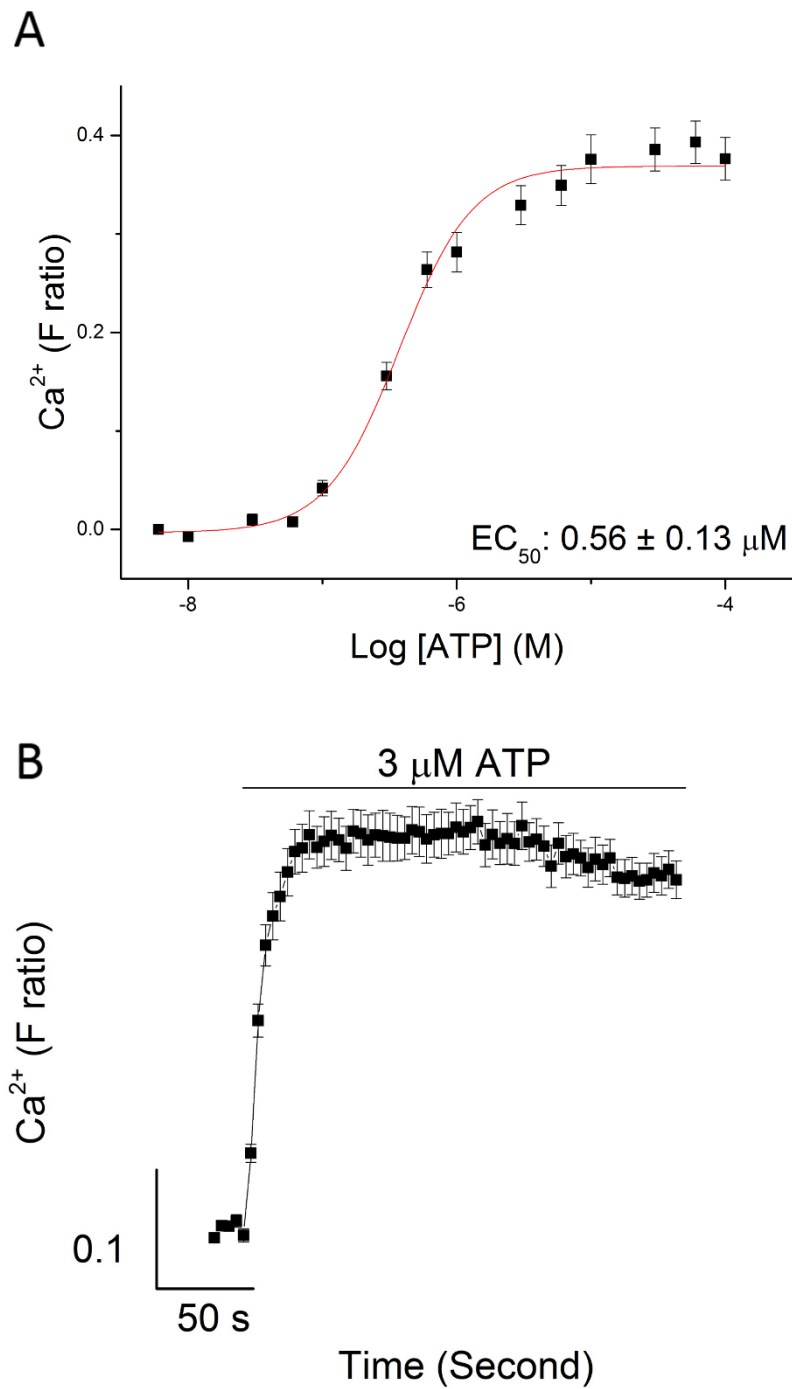
Figure 3.9 ATP concentration-response of the human P2X$_4$ overexpressing cells.
Panel A shows a complete ATP concentration-response at human P2X$_4$ receptors and panel B shows its representative trace for 250 seconds when stimulated with a saturating concentration of ATP (3 µM). ($n = 12$)

Subsequently, various concentrations of DMSO were tested to determine its toxicity on the human P2X$_4$ overexpressing cells. The cells were pre-incubated with various percentages of DMSO for 30 minutes and stimulated with 0.6 µM of ATP. This experiment was required because all compounds to be screened were dissolved in 0.1 % DMSO (final concentration), however higher DMSO concentration might be needed if certain compounds were insoluble in 0.1 % DMSO. Figure 3.10 shows the effect of different DMSO percentages on ATP-evoked response. Up to 0.1 % of DMSO (final concentration), there was no significant change on the response in relation to the no DMSO control. However, at 0.3 % of DMSO, the response was seen to be potentiated significantly (32.6 ± 9.3 % potentiation, $p < 0.05$, $n = 3$) while at the highest concentration of 3 % of DMSO, it significantly reduced the response by 70.9 ± 17.7 % ($p < 0.01$, $n = 3$). Therefore, 0.1 % DMSO content was chosen to dissolve all compounds. However, in case of insolubility issue, the compounds were dissolved in 1 % DMSO with proper controls.

Figure 3.11 shows the inhibition concentration-response of PPADS on the human P2X$_4$ overexpressing cells. It was shown that PPADS started to reduce the response at 0.1 µM by 17.2 ± 5.2 % ($p < 0.05$, $n = 3$), and further inhibited until it abolished the response and reached plateau at 30 µM of PPADS. The IC$_{50}$ value determined from the curve was 14.9 ± 5.2 µM ($n = 3$). Therefore, for high throughput screening, 100 µM of PPADS was used as a positive control for inhibitor. Meanwhile, Figure 3.12 shows the potentiation concentration-dependent curve of a selective positive allosteric modulator of P2X$_4$, IVM. The value of EC$_{50}$ determined from the curve was 1.7 ± 0.3 µM ($n = 3$). From the curve, it was decided that 3 µM of IVM should be used for the positive control for the positive modulator.
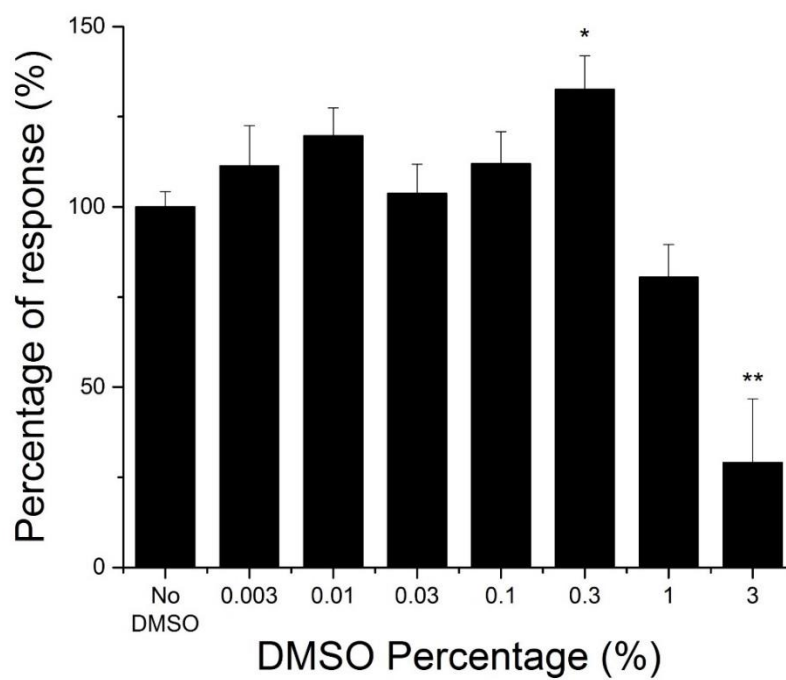
Figure 3.10 Effects of DMSO incubation on ATP-evoked response.
The bar chart shows the effect of DMSO on peak responses recorded within 250 seconds when the cells were pre-incubated with different percentage of DMSO for 30 minutes, and stimulated with 0.6 µM of ATP at human P2X$_4$. All responses were normalised to mean of no DMSO. ($n = 3$)
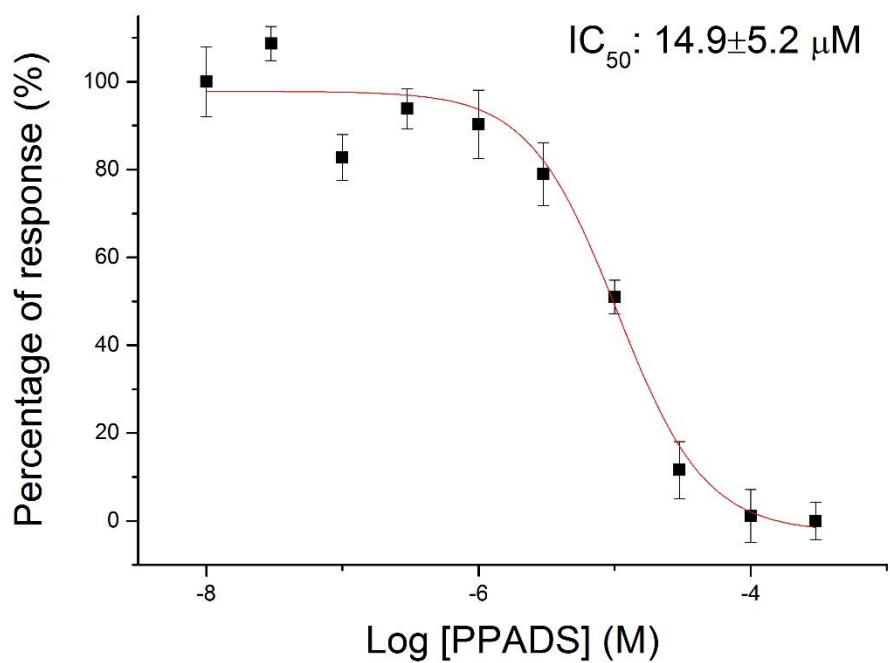
Figure 3.11 PPADS inhibition concentration-response at human P2X$_4$.
The curve shows the PPADS inhibition concentration-response at human P2X$_4$. Concentrations of PPADS used were from 0.01 to 300 µM, while the agonist ATP concentration was 0.6 µM, corresponded to EC$_{50}$ value of the human P2X$_4$ overexpressing cells. All data were normalised against vehicle response. ($n = 3$)
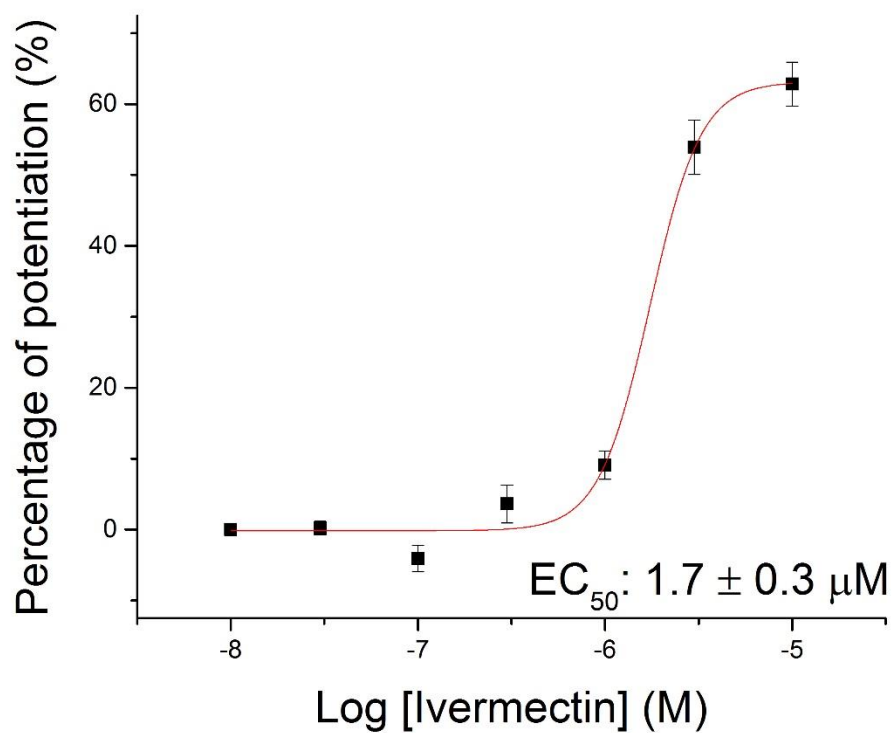
Figure 3.12 Ivermectin potentiation concentration-response at human P2X₄.
The curve shows IVM potentiation concentration-response at human P2X₄. Concentration of IVM used was from 0.01 to 300 µM, while ATP concentration was 0.6 µM, corresponded to EC_{50} value of the human P2X₄ overexpressing cells. All data were normalised against vehicle response. ($n = 3$)

3.3.2.4.1 Characterisation of P2X and P2Y overexpressing cell lines

Concentration-response curves for agonists were performed on all available P2X and P2Y overexpressing cell lines to identify the maximal and EC_{50} concentrations required for the activation of receptors. ATP was used as the nucleotide for human $P2X_2$, $P2X_{2/3}$, $P2Y_2$, and mouse $P2X_4$ overexpressing cell lines while UDP and BzATP were used for human $P2Y_6$ and $P2X_7$ overexpressing cell lines, respectively. Although ATP is the physiological nucleotide for $P2X_7$, BzATP was used as the agonist because $P2X_7$ was only responsive to high concentration of ATP (millimolar range) (Bianchi et al., 1999) while the use of millimolar concentrations of ATP produced an endogenous response from non-transfected astrocytoma cells (data not shown), hence the ATP was replaced with BzATP. In the non-transfected astrocytoma cells, there was no response recorded at high BzATP (500 µM) concentration (data not shown).

In the human $P2X_2$ overexpressing cell line (Figure 3.13), ATP elicited a concentration-dependent increase in calcium level (EC_{50}: 0.51 ± 0.1 µM, $n = 3$). The lowest ATP concentration that elicited response was 0.06 µM and the response plateaued at 3 µM. The maximal calcium influx was obtained from the application of 3 µM of ATP which produced a magnitude of 1.77 ± 0.06 F ratio at 43.7 seconds.

The human $P2X_{2/3}$ receptor used in this study was a chimeric receptor. This was used because the instrument (FlexStation 3) could not detect any fluorescence from the activation of $P2X_3$ expressing cell lines due to rapid desensitization. The amino acid sequence of the chimeric $P2X_{2/3}$ ectodomain followed the sequence of $P2X_3$ while the tail of C terminus followed the $P2X_2$ residue segment. Therefore, activation of this chimeric $P2X_{2/3}$ receptor followed the characteristic of $P2X_3$ but desensitisation followed $P2X_2$ behaviour because the tail of C terminus played a big role for desensitisation (Koshimizu et al., 1999). The use of ATP as an agonist in this overexpressing cell line produced a concentration-dependent influx of calcium (Figure 3.14). The concentration-response curve revealed an EC_{50} value of 0.12 ± 0.03 µM ($n = 3$). The lowest concentration that receptor responded to was 0.06 µM and maximal concentration (1 µM) elicited a peak response of 1.54 ± 0.15 F ratio at 40.3 seconds.

The agonist BzATP elicited a concentration-dependent response in the human $P2X_7$ overexpressing cells (Figure 3.15). The first increase in intracellular calcium level was detected from the application of 10 µM of BzATP and the response plateaued at 300 µM. The concentration-response curve revealed an EC_{50} value of 46.0 ± 4.0 µM ($n = 3$). At the maximal concentration of 300 µM, the peak response recorded was 0.7 ± 0.04 F ratio ($n = 3$) at 38.9 seconds.

In the mouse $P2X_4$ overexpressing cell line, the increase in calcium response was ATP concentration-dependent (Figure 3.16). The lowest response was detected with the application of 0.06 µM of ATP and the response plateaued at 1 µM. The calculated EC_{50} value was 0.22 ± 0.01 µM ($n = 3$). At the maximal concentration of 1 µM, the peak response recorded was 1.62 ± 0.06 F ratio ($n = 3$) at 40.4 seconds.

Next, the ATP concentration-response for human $P2Y_2$ is displayed in Figure 3.17. $P2Y_2$ was more sensitive to ATP compared to P2X receptors tested in this study with a calculated EC_{50} value of 27.0 ± 7.3 nM ($n = 3$). The first response observed was when the cells were stimulated with 3 nM of ATP and the magnitude exponentially increased at higher ATP concentrations until it reached plateau at 0.3 µM. At a maximal concentration of 0.3 µM, the peak response recorded was about 1.5 ± 0.1 F ratio ($n = 3$) at 28.6 seconds.
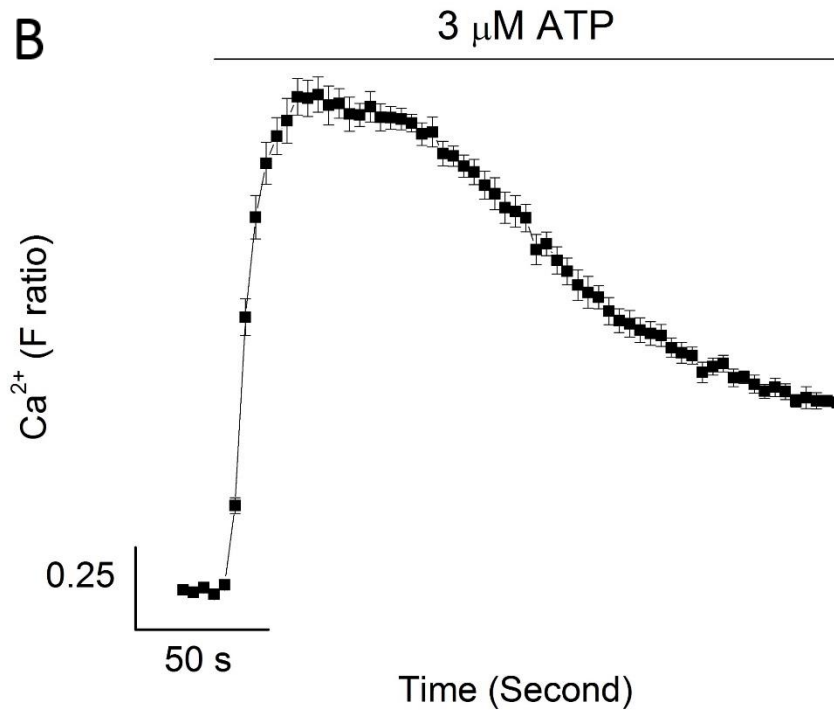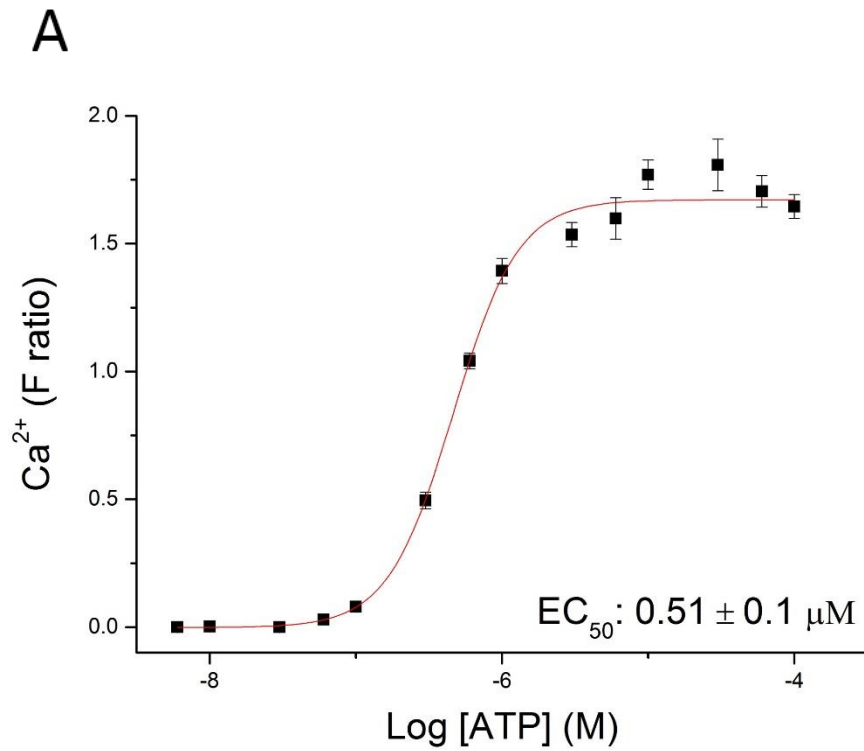
Figure 3.13 ATP concentration-response of the human P2X$_2$ overexpressing cells.

The curve in panel A shows the concentration-response curve at human P2X$_2$ receptor with ATP as an agonist and panel B shows the representative trace at super maximal concentration of 3 µM ATP. All responses were normalised to the mean peak response of vehicle control. ($n = 3$)
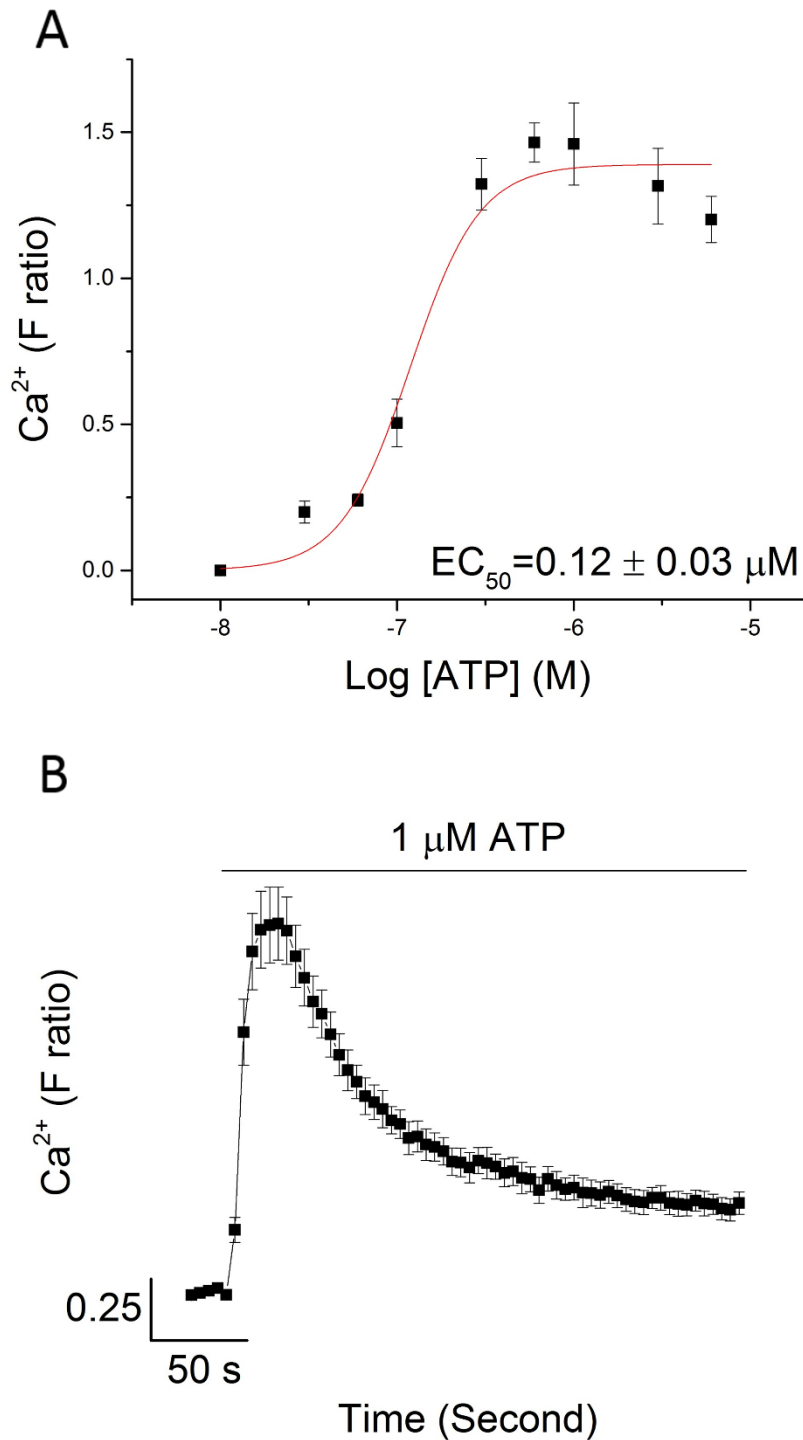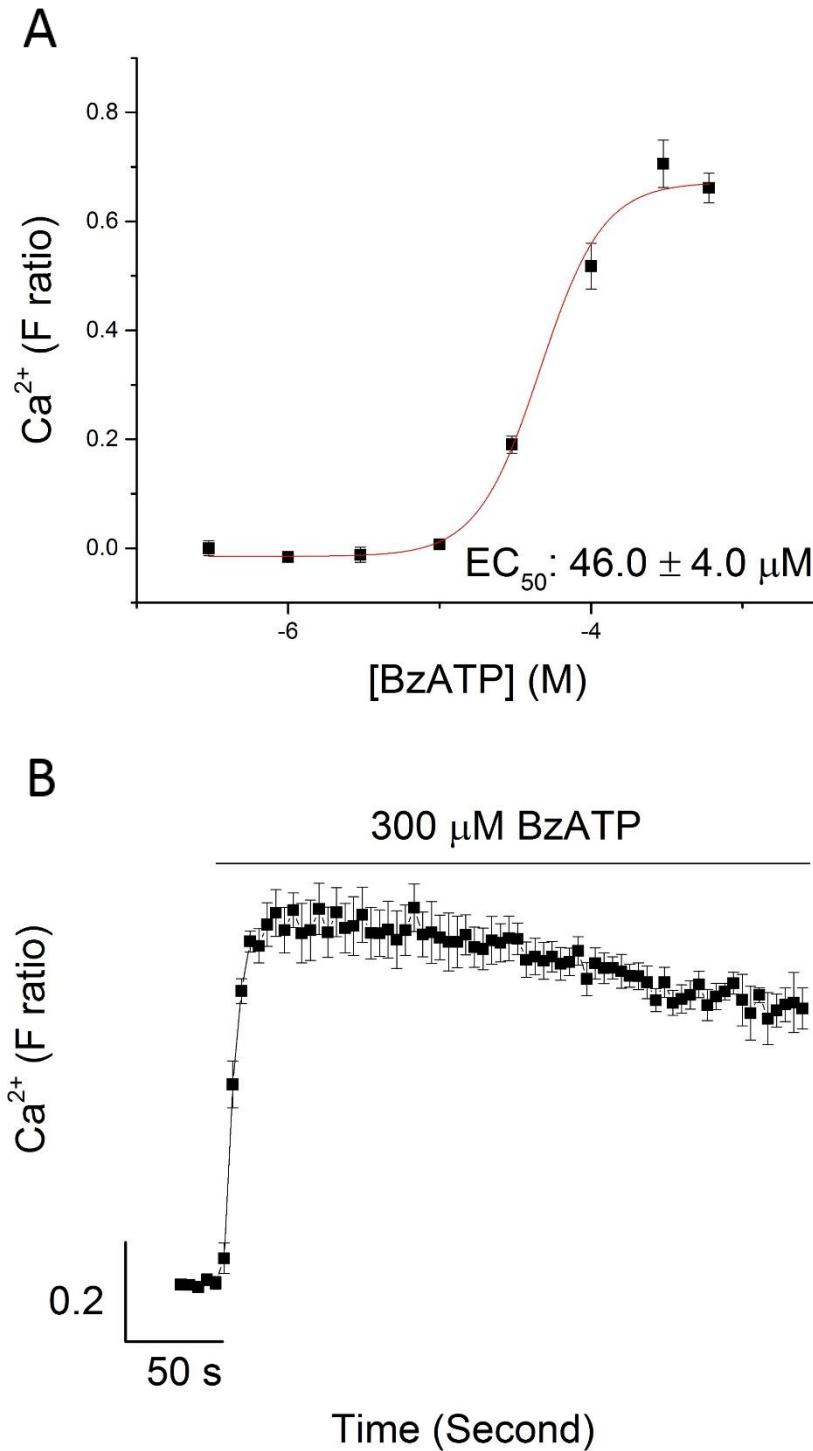
A

$EC_{50}=0.12 \pm 0.03\ \mu M$

B

1 μM ATP

Figure 3.14 ATP concentration-response of the human P2X$_{2/3}$ overexpressing cells.

The curve in panel A shows the concentration-response curve at human P2X$_{2/3}$ receptor with ATP as an agonist and panel B shows the representative trace at super maximal concentration of 1 μM of ATP. All responses were normalised to the mean peak response of vehicle control. ($n = 3$)
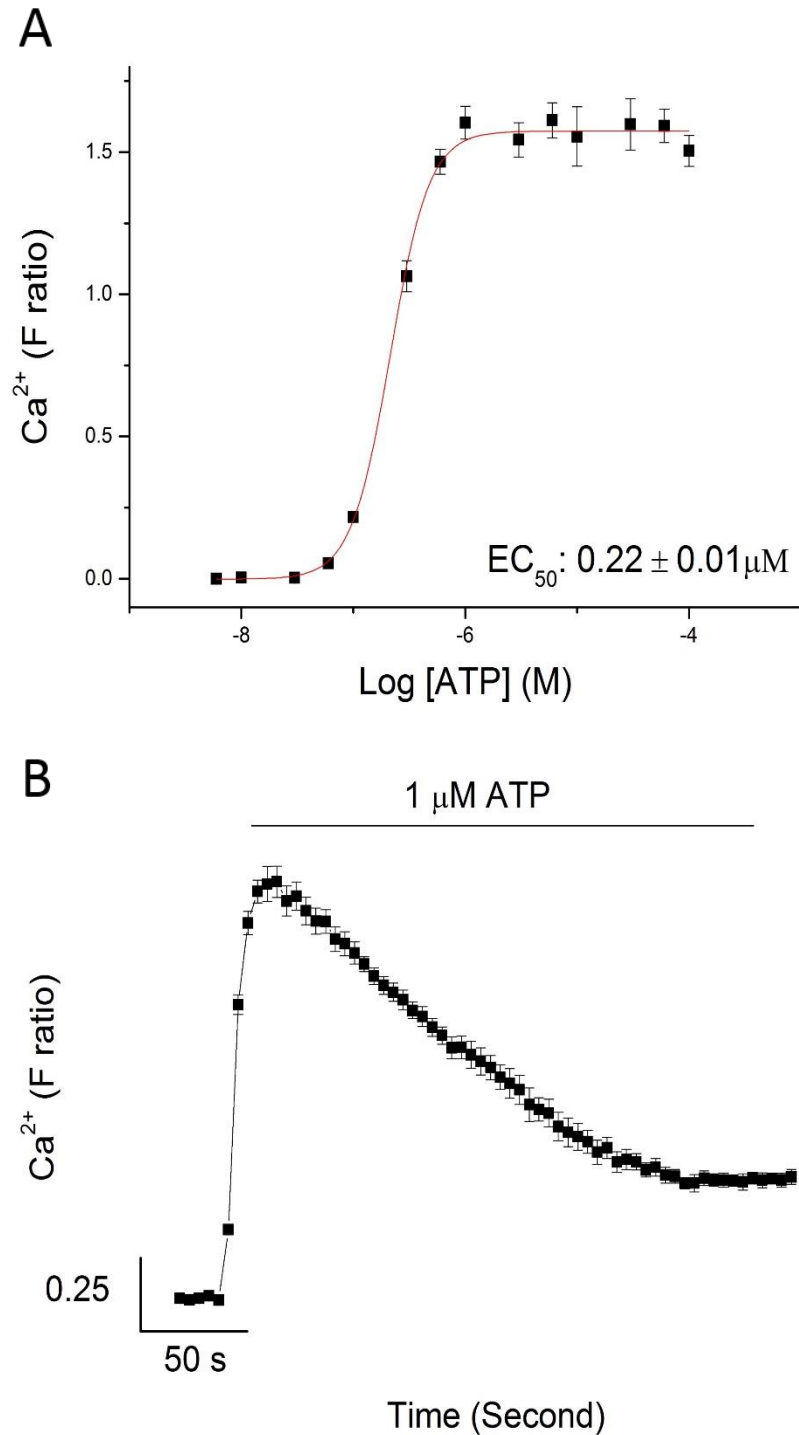
Figure 3.15 BzATP concentration-response of the human P2X$_7$ overexpressing cells.

The curve in panel A shows the concentration-response curve at human P2X$_7$ receptor with BzATP as an agonist and panel B shows the representative trace at super maximal concentration of 300 μM of BzATP. All responses were normalised to the mean peak response of vehicle control. ($n = 3$)
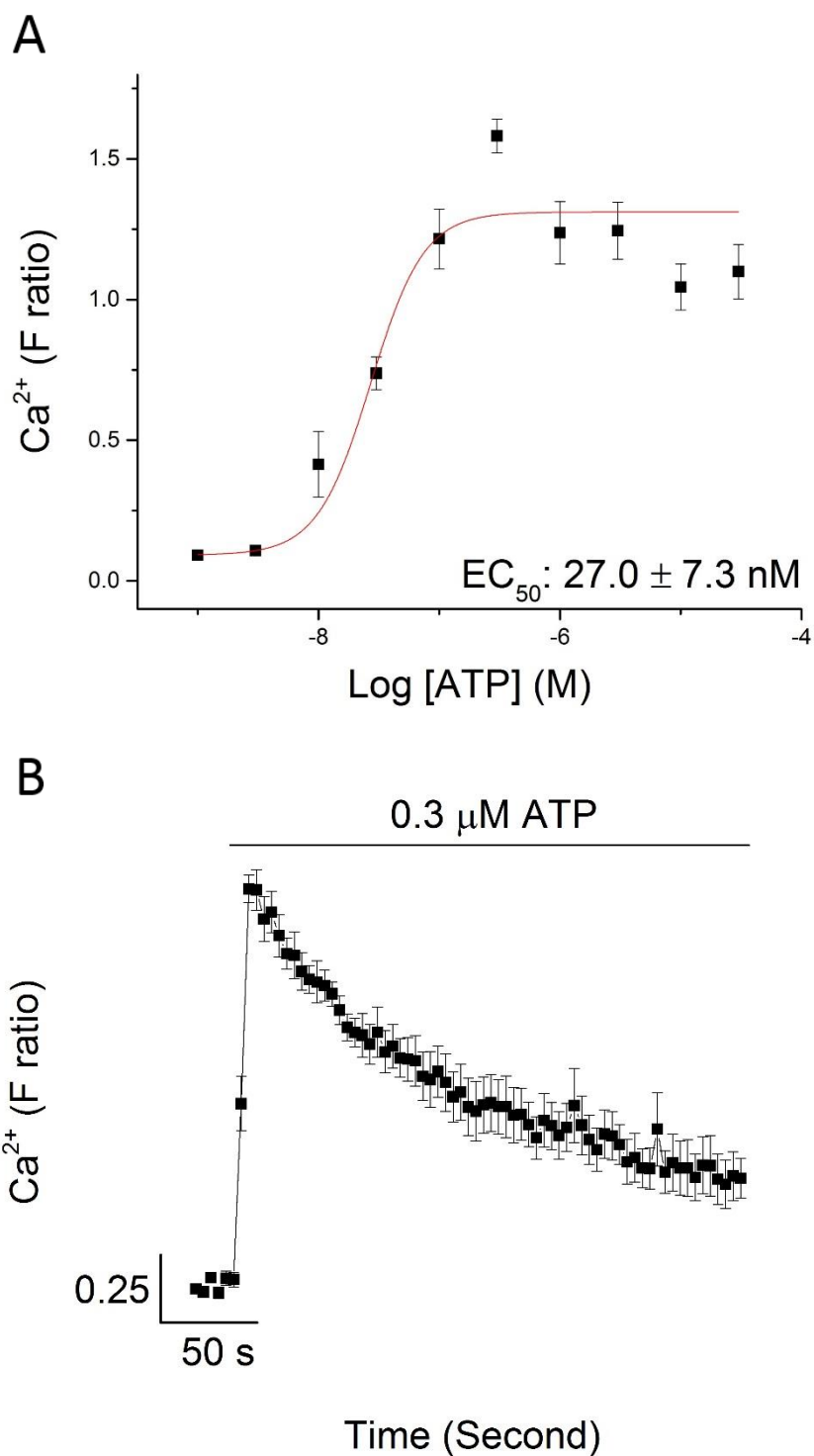
Figure 3.16 ATP concentration-response of the mouse P2X$_4$ overexpressing cells.

The curve in panel A shows the concentration-response curve at mouse P2X$_4$ receptor with ATP as an agonist and panel B shows the representative trace at super maximal concentration of 1 µM of ATP. All responses were normalised to the mean peak response of vehicle control. ($n = 3$)

A

B

0.3 μM ATP

Figure 3.17 ATP concentration-response of the human P2Y$_2$ overexpressing cells.

The curve in panel A shows the concentration-response curve at human P2Y$_2$ receptor with ATP as an agonist and panel B shows the representative trace at super maximal concentration of 0.3 µM of ATP. All responses were normalised to the mean peak response of vehicle control. ($n = 3$)

3.3.3 High throughput screening

High throughput screening is a way to search for potential compounds that can be developed as the potential modulator, either positive or negative modulation. The flow of high throughput screening in this study is illustrated in Figure 3.18. The compounds obtained from NCI were screened in fluorescence-based assays using FlexStation 3. Subsequently, the hits were identified and several criteria were imposed to filter out the false positive hits. The hits were then characterised further before only one compound known as the lead was taken forward.

Figure 3.19 shows the distribution of 1,710 compounds screened in this study in terms of response modulation. It was observed that most compounds lay in the region of 80 – 150 % response, i.e., close to the 100 % mark of vehicle control. Since the screening was performed once in triplicate, the 80 – 150% region might be a result of variability. Thus, two filtering criteria were imposed to exclude the false positive results. The first criterion was the magnitude of potentiation or inhibition. Any compounds must have potentiated at least 75 % or inhibited at least 60 % of the control response to pass the first criterion. The control response was normalised to 100 % which was marked with a straight horizontal line in the figure. The potentiation percentage was calculated by subtracting the control response of 100 % from the remaining response displayed on the chart, while the percentage of inhibition was calculated by subtracting the remaining response displayed on the chart from 100 % control response.

In the figure, the first criterion was marked with dashed lines (upper line for potentiation cut-off value and lower line for inhibition cut-off value). By applying the first criterion, 31 compounds were identified to potentiate the response while 56 compounds showed the inhibitory properties. The three highest recorded potentiation were 1030.4 % (1130.4 % response), 534.1 % (634.1 % response), and 381.6 % (481.6 % response) which were recorded from the application of NSC179822, NSC375997, and NSC186067, respectively. The three biggest inhibition recorded were 97.5 % (2.5 % response), 96.7 % (3.3 % response), and 96.3 % (3.7 % response) ($n = 1$) which were recorded from the application of NSC122131, NSC639174, and NSC28080, respectively.
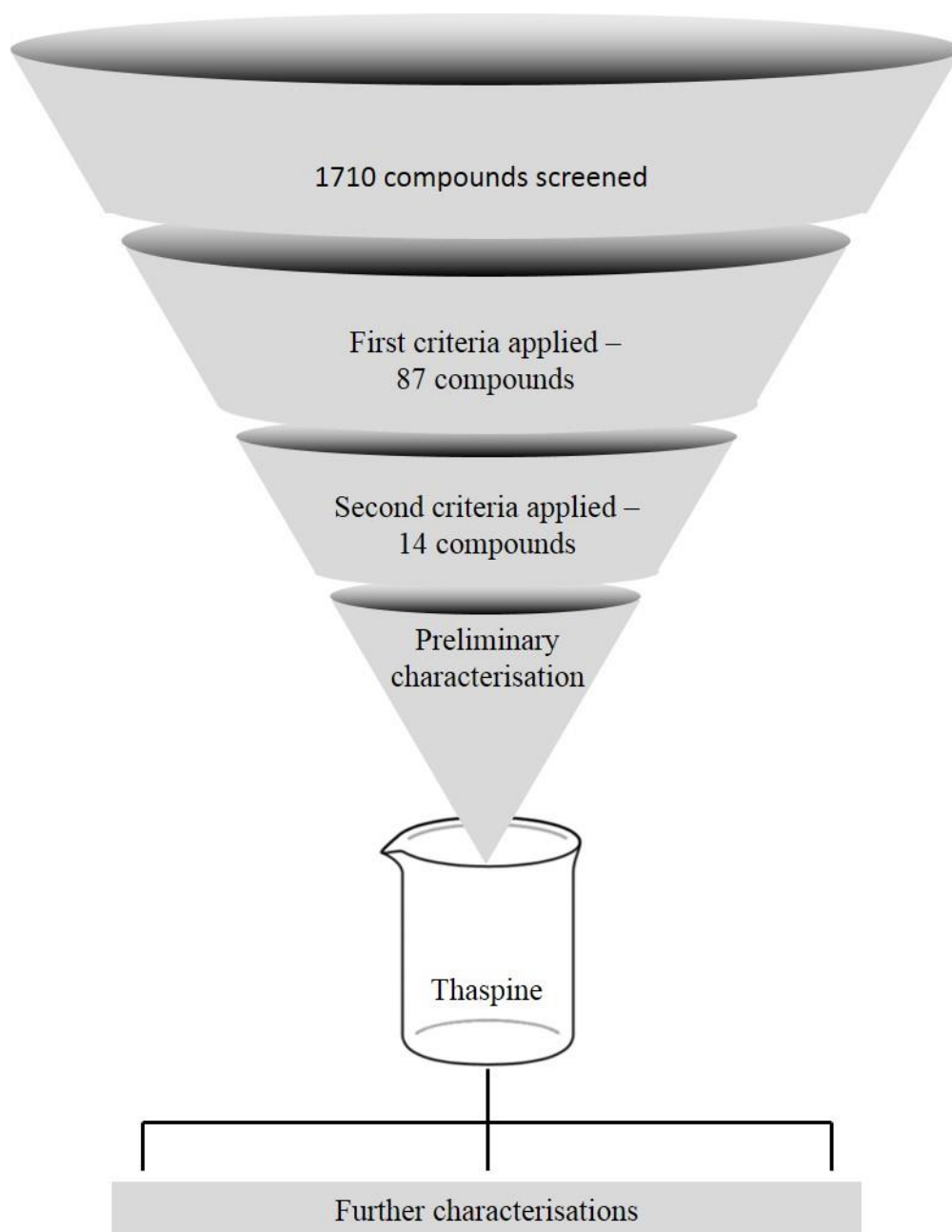
Figure 3.18 Flow chart of high throughput screening.
The figure illustrates the process of high throughput screening from the testing of 1,710 compounds until the discovery of lead compound and its characterisation.
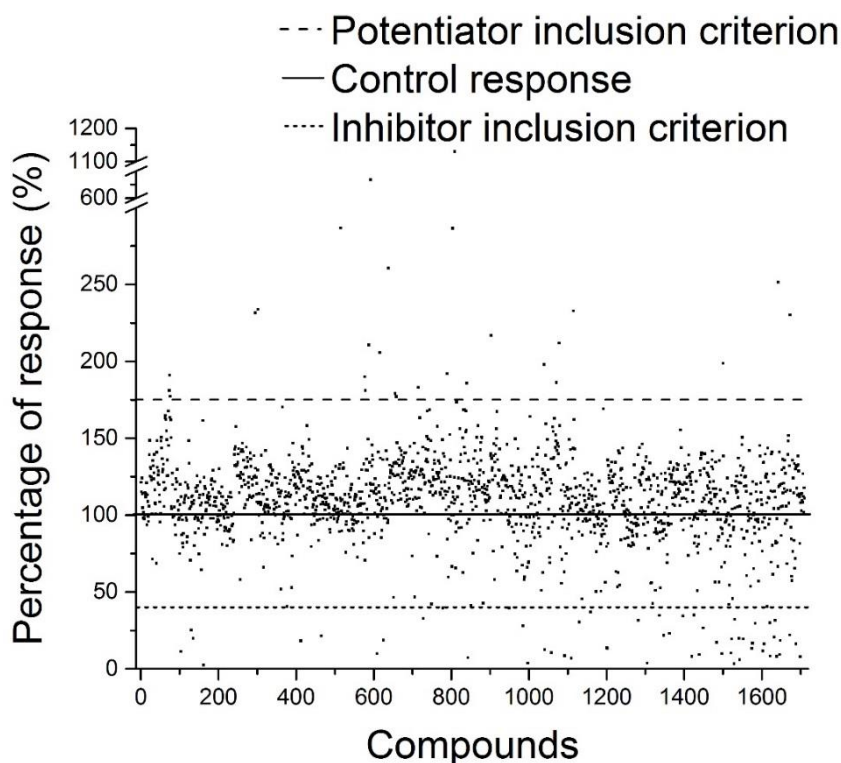
Figure 3.19 Modulation of ATP-evoked calcium response in the human P2X₄ overexpressing cells treated with the screened compounds.

The figure shows the distribution of all screened compounds in terms of their peak response in comparison to control response. The screening was done in triplicate. The solid line represents the control response normalised as 100 %. The long dash line represents the inclusion criterion for potential positive modulator. Compounds above the line ($\geq$ 75 % potentiation) was regarded as potential positive modulators. Meanwhile, the short dash line represents the inclusion criterion for potential inhibitors. Compounds that had response below 40 % (i.e. $\geq$ 60 % inhibition) were carried forward for further experiments. In short, compounds between the long and short dashed lines were excluded from consideration. ($n = 1$)

The second criterion restricted the compounds that showed fluorescence baseline change after compound addition into the cells. This could be because of auto-fluorescent compounds, quenching effect of compounds, and/or toxicity. To exclude those probabilities, the second criterion applied was that the compounds must not have altered the baseline ± 0.25 F ratio. The basis for selecting the value was that, a known human $P2X_4$ blocker, PPADS, also shifted the baseline at a maximum of -0.25 F ratio. The second criterion is shown in Figure 3.20 where panel (A) shows the inclusion criterion for positive modulators and panel (B) for the inhibitors. The compounds populated in the figure were the compounds that passed the first inclusion criteria. The grey box highlights the compounds that passed the second criterion.

As a result, eight positive modulator hits were identified: NSC9489, NSC14771, NSC27389, NSC34910, NSC211336, NSC48443, NSC369066, and NSC90749. The percentages of potentiation recorded were 81.04, 91.05, 77.20, 82.96, 85.76, 86.12, 111.88, and 132.78% ($n = 1$), respectively. As for the modulation of baseline, all compounds did not cause baseline alteration except for two compounds: NSC34910 and NSC211336 which shifted the baseline +0.2 and +0.06 F ratio, respectively.

Meanwhile, the inhibitor hits identified were NSC345647, NSC116339, NSC50688, NSC17055, NSC5426, and thaspine, and their percentages of inhibition were 94.71, 89.75, 65.18, 60.48, 81.40, and 69.96%, respectively. As for modulation shift, five from the six compounds altered the baseline. Compound NSC345647, NSC116339, NSC50688, NSC17055, and NSC5426 shifted the baseline by -0.15, -0.1, -0.25, +0.2, and -0.12 F ratio, respectively. Only thaspine indicated stable baseline upon compound addition. Thus, these eight positive modulator and six inhibitor hits were brought forward for preliminary testing.
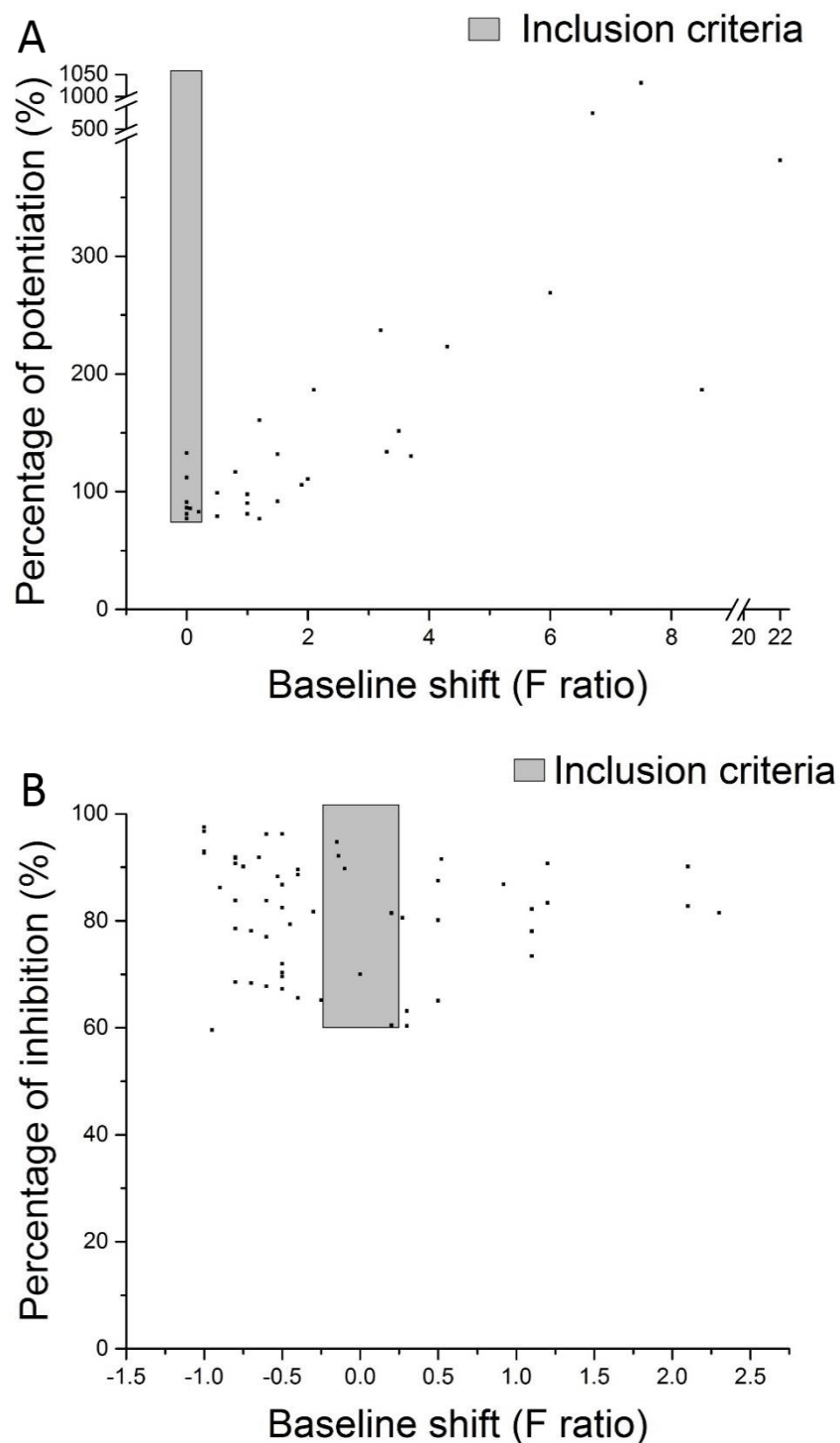
Figure 3.20 Change in baseline fluorescence upon compound addition to the human P2X$_4$ overexpressing cells.

The dots in the figure represent the compounds that met the first criteria which was the percentage of potentiation and inhibition of more than 75 and 60 %, respectively (panel A and B, respectively). The y-axis represents the percentage of potentiation or inhibition while x-axis represents the fluorescence baseline alteration after compound addition, recorded at wavelength 340 and 380 nm excitation, and 510 nm emission. The acceptable value of baseline shift was within ±0.25 F ratio, which was set as the second inclusion criterion. The grey box marks the compounds that met both first and second criteria, known as hits. The hits were taken forward for further tests.

3.3.3.1 Preliminary characterisation of hits

Further testing on the positive modulator hits revealed that none of the compounds tested potentiated the response more than 42 % despite the increasing concentration of the compounds (Figure 3.21), in contrast to the observation made in the high throughput screening. The highest significant potentiation observed among all the positive modulator hits was exhibited by NSC14771 which had 41.4 ± 12.6 % ($p < 0.05$, $n = 3$) potentiation at a concentration of 0.5 µM. The data also showed that the potentiation was even lower at 10 µM which suggested that the potentiation was concentration-independent. This was also observed in other tested compounds. Therefore, further work on positive modulator hits were put to an end.

While for the inhibitor hits, the results were more promising compared to positive modulator hits. Five out of six hits showed similar inhibition at 10 µM as observed in the screen, i.e., NSC345647, NSC116339, NSC17055, NSC5426, and thaspine. At 5 µM, the reduction in response were 37.9 ± 5.7 % (NSC5426), 81.8 ± 1.3 % (NSC17055), 27.2 ± 7.3 % (NSC116339), 59.7 ± 7.7 % (NSC345647), and 29.1 ± 12.8 % (thaspine) ($n = 3$). When the compound concentrations were reduced further, only NSC17055 still showed an inhibition of 46.5 ± 4.9 % and 26.6 ± 3.8 % at 1 and 0.5 µM ($n = 3$), respectively. No inhibition was observed by all compounds at 0.1 µM. Overall, all compounds showed a concentration-dependent inhibition. Therefore, the lead compound, NSC17055, was selected for further characterisation as it showed the most potent inhibition at P2X$_4$ receptor.
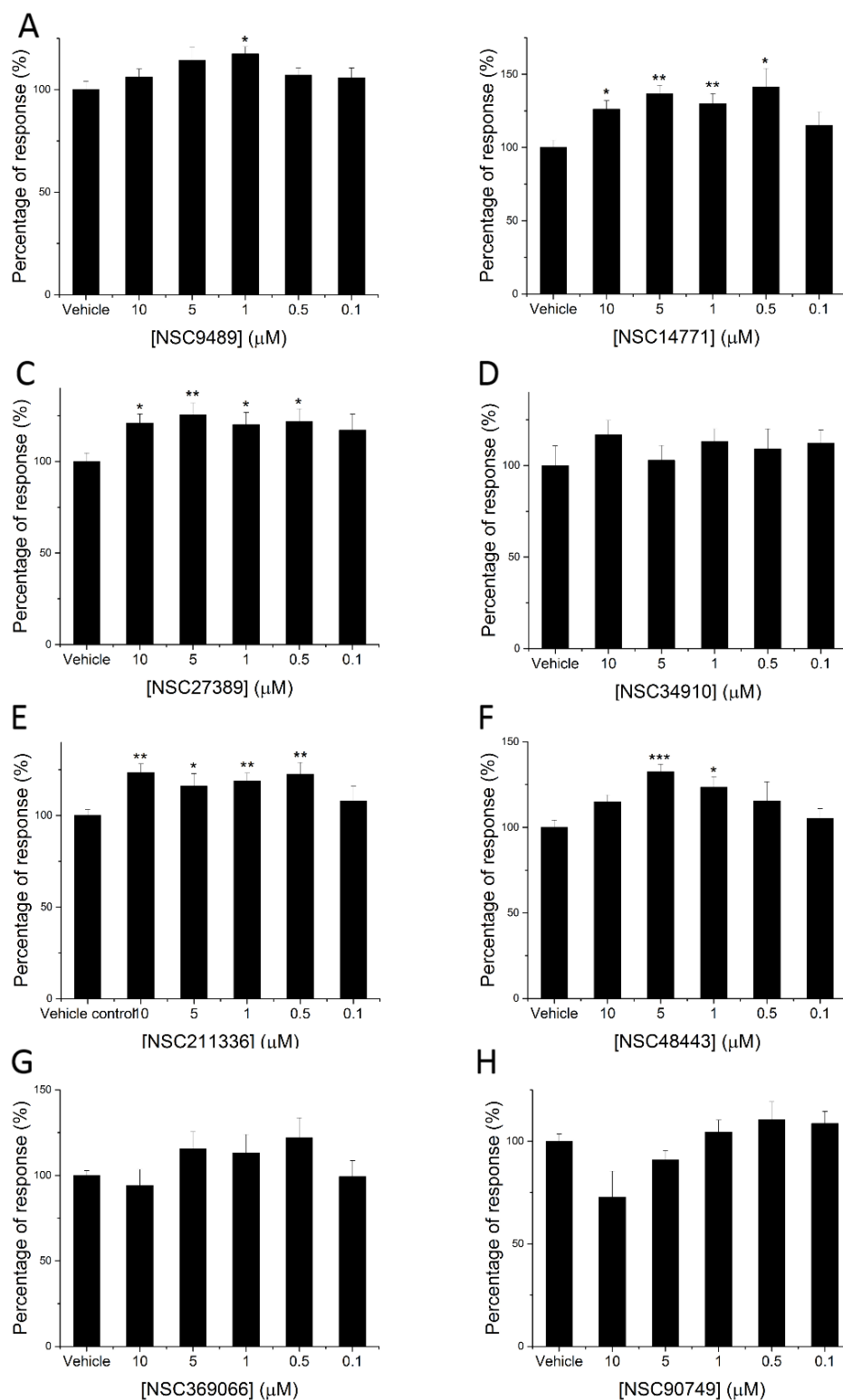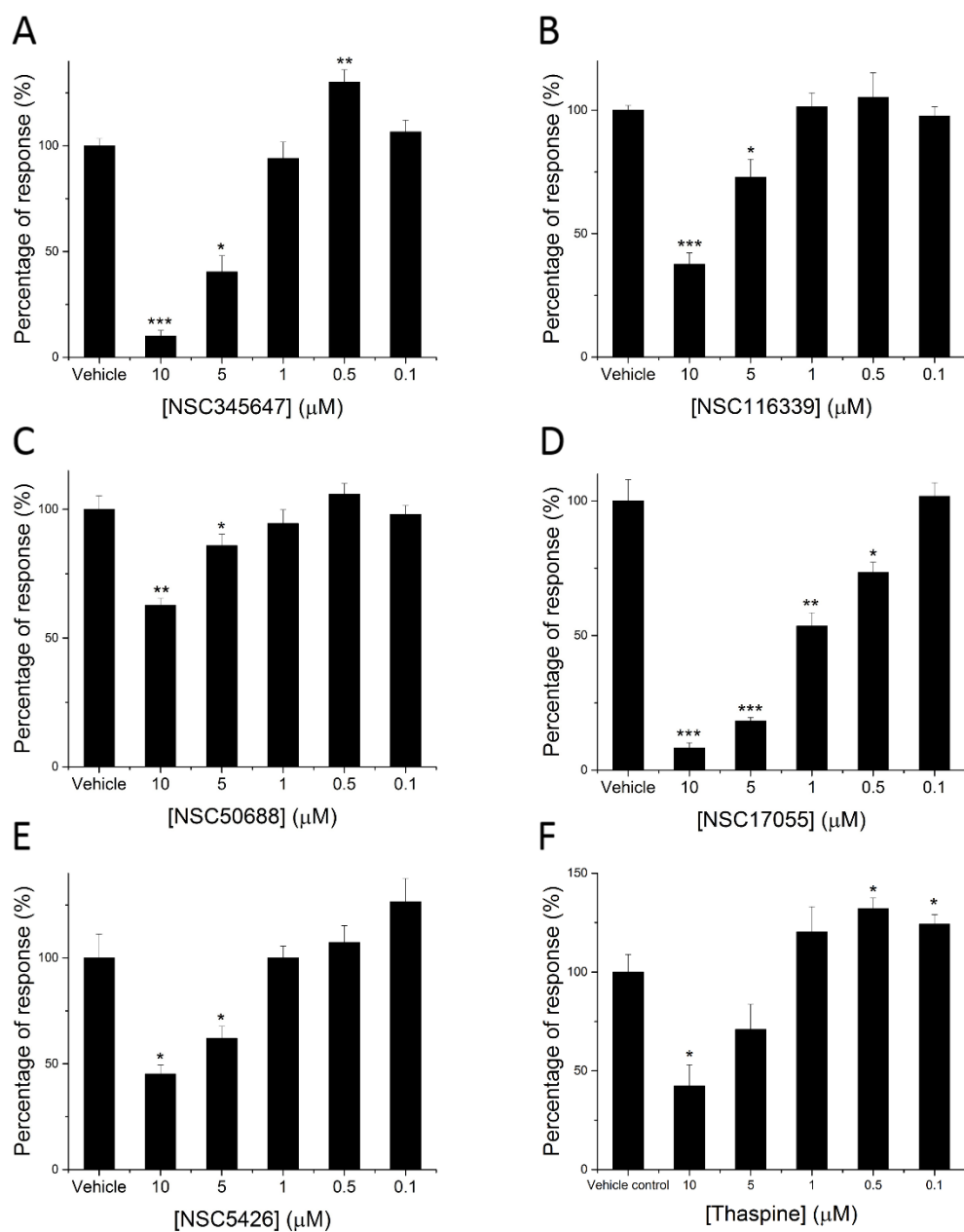
Figure 3.21 Concentration-response for compounds that went through second filter for positive modulators.

The bar charts show the effects of eight positive modulator hits using five different concentrations: 0.1, 0.5, 1, 5, and 10 μM on the ATP-evoked response of the human P2X$_4$ overexpressing cell. The concentration of ATP used was 0.6 μM, corresponded to EC$_{50}$ value. All responses were normalised to the mean of vehicle response. Chemical structure of each compound is shown in Appendix I. Asterisks denote p-value: * = < 0.05, ** = < 0.01, *** = < 0.001. (n = 3)

Figure 3.22 Concentration-response for compounds that went through second filter for inhibitors.

The bar charts show the effects of six inhibitor hits using five different concentrations: 0.1, 0.5, 1, 5 and 10 µM on the ATP-evoked response of the human P2X$_4$ overexpressing cell. The concentration of ATP used was 0.6 µM, corresponded to EC$_{50}$ value. All the responses were normalised to mean peak response of the mean peak response of vehicle control. Chemical structure of each compound is shown in Appendix II. Asterisks denote *p*-value: * = < 0.05, ** = < 0.01, *** = < 0.001. (*n* = 3)

3.3.3.2 Characterisation of NSC17055

The first characterisation of NSC17055 was done to determine its inhibitory potency by establishing the inhibition concentration-response (Figure 3.23). The response elicited by the maximal concentration of ATP (3 µM) was blocked by NSC17055 in a concentration-dependent pattern. The fist inhibition was observed with the treatment of 0.3 µM of NSC17055 (6.9 ± 2.3 % inhibition, $n = 3$, $p < 0.01$) and a complete blockade was observed with 60 µM of NSC17055. From the concentration-response curve, the calculated IC_{50} value was 1.26 ± 0.08 µM. Based on the representative trace, it can be seen that the response magnitude was inhibited by 90.3 ± 0.6 % at 10 µM of NSC17055.

The second characterisation was to determine its mode of inhibition, whether the blockade was competitive or noncompetitive. As shown in Figure 3.24, the inhibition from the treatment of 10 µM of NSC17055 was insurmountable regardless of increasing ATP concentration used which was up to 100 µM (13.9 ± 2.8 % response, $n = 3$) and the EC_{50} value of ATP was not significantly different between the untreated and treated cells (0.2 ± 0.03 µM versus 0.1 ± 0.01 µM, $p > 0.05$ $n = 3$). These indicated that the NSC17055 blocked the response noncompetitively and that the inhibition was an insurmountable antagonism.

Looking at the potency of NSC17055, it was decided to look at its analogues to see if there were other variants that might inhibit better than NSC17055 while preserving its main backbone structure. The search for the analogues were done via MolPort web-based server. The search was set up to show similar compounds with NSC17055 by 0.8 similarity (Tanimoto index). Ten compounds with the highest similarity to NSC17055 and met drug-like properties as outlined by Lipinski et al. (2007) were then purchased from MolPort SIA and screened at 10 µM, and the chemical structure of each can be found in Appendix III. During the first replicate of experiment, there was a discrepancy in the data recording for STK331042. During the 250 seconds calcium response recording, there was no fluorescence detected and these were not observed in any other compounds. This raised a question whether the inhibition was an actual inhibition or just an artefact caused by the compound. Therefore, the experiment was put on hold and not replicated.
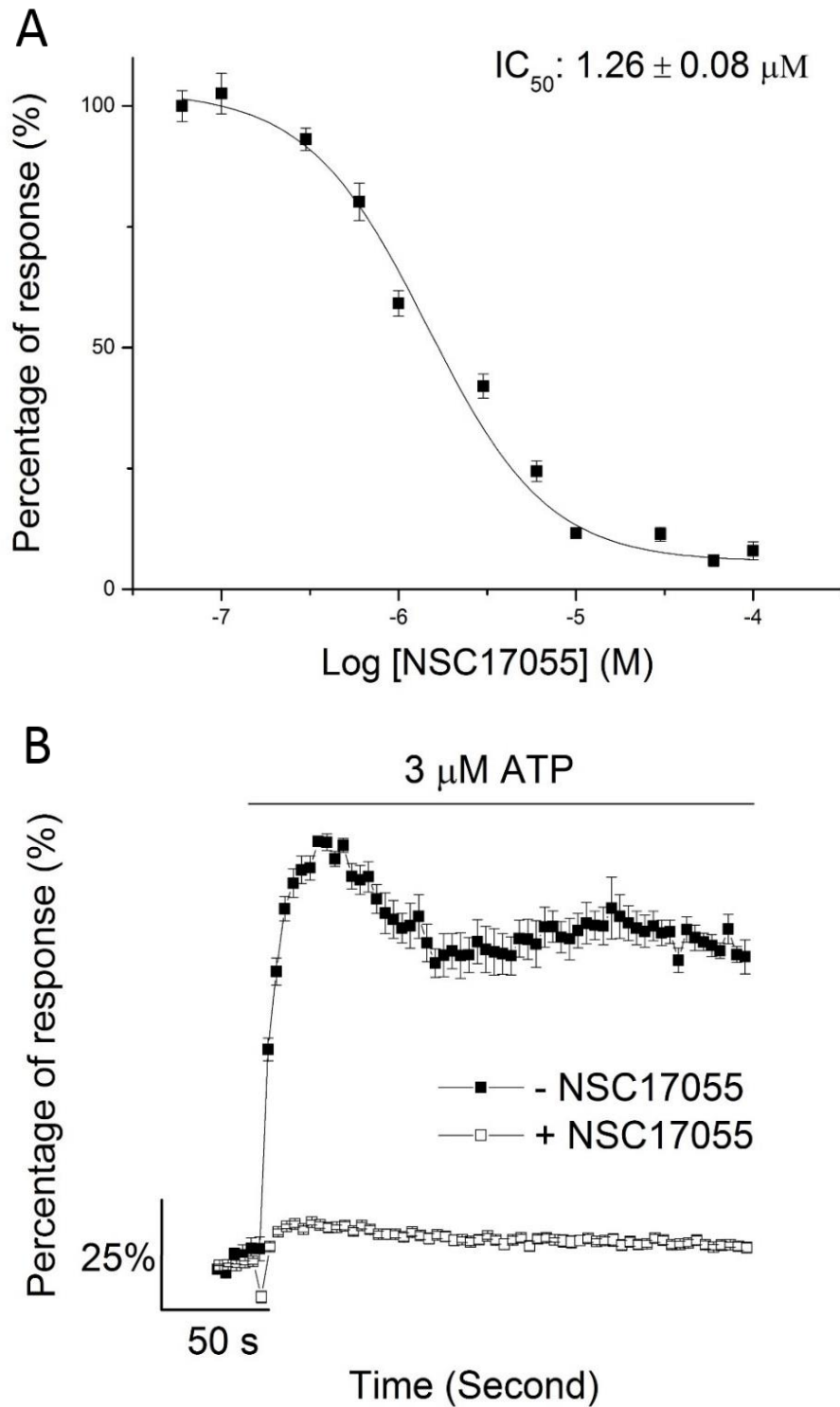
Figure 3.23 Inhibition concentration-response of NSC17055 at human P2X₄.
Panel A shows the complete inhibition concentration-response of NSC17055 on ATP-evoked response of the human P2X$_4$ overexpressing cells, plotted using peak response reading within 250 seconds recording post ATP activation. Panel B shows the representative trace with and without 10 μM NSC17055. ($n = 3$)
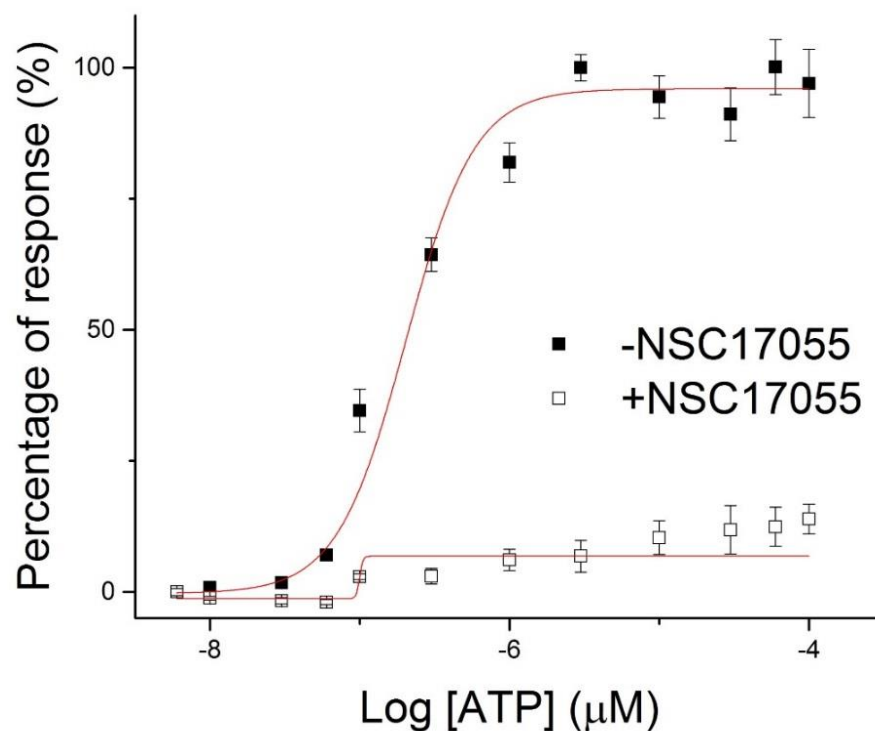
Figure 3.24 Determination of NSC17055 mode of action.

The curve above displays the ATP concentration-responses with and without 10 µM of NSC17055. This experiment was aimed to study the mode of inhibition of compound, whether it was competitive or noncompetitive. Concentrations of ATP used were from 6 nM to 100 µM. The insurmountable inhibition by the compound indicated that it inhibited noncompetitively. ($n = 3$)

To verify whether NSC17055 was a true inhibitor, it was tested to check its effect on ionomycin- and carbachol-evoked responses. Ionomycin and carbachol are the compounds that can cause influx of calcium into the cytosol when they are applied on cells. However, ionomycin- and carbachol-evoked responses do not activate the P2X$_4$ receptor. Ionomycin was earlier hypothesised to physiochemically translocate the extracellular calcium into cells, but recent findings revealed that it also caused the release of calcium from intracellular store (Müller et al., 2013). Meanwhile, carbachol was reported to be an agonist for muscarinic acetylcholine receptors that mediated extracellular calcium influx through voltage-dependent calcium channels and also calcium release from intracellular store (Blackwood & Bolton, 1993). Therefore, both compounds can increase the level of calcium in the cytosol independent of P2X$_4$ receptor activation.

In this experiment, ATP was replaced with either ionomycin or carbachol. It was hypothesised that the blockade of P2X$_4$ receptor would not affect the ionomycin- and carbachol-evoked responses which are the results of activation of other receptors other than P2X$_4$ activation. Therefore, the effect of NSC17055 treatment on the responses was investigated to ensure that the inhibition observed in P2X$_4$ cell line was true. The cells were treated with 10 µM of NSC17055 for 30 minutes before being stimulated with 1 µM of ionomycin or 100 µM of carbachol.

The data indicated that the antagonism of NSC17055 was not only specific to P2X$_4$ receptor since it significantly inhibited the ionomycin- and carbachol-evoked responses (Figure 3.25) by 87.2 ± 2.3 % and 81.0 ± 1.5 % ($p < 0.001$, $n = 3$), respectively. This may imply a possibility that NSC17055 was a fluorescence quencher that quenched Fura-2 fluorescence, and in turn gave low reading of F ratio. The quenching effect was also previously reported by Żamojć et al. (2014) who claimed that some coumarin derivatives caused the fluorescence quenching. Following the observed inhibition by NSC17055 on ionomycin- and carbachol-evoked response, the characterisation of NSC17055 was put to an end and the study turned back to other inhibitor hits.

To avoid the same problem, all inhibitor hits were tested to observe their effects on ionomycin- and carbachol-evoked responses. The results (Figure 3.26) showed that

five out of six compounds inhibited the responses significantly. The percentage of inhibition ranged from 32.9 – 93.0 % for ionomycin and 17.8 – 81.2 % for carbachol, ($p < 0.05$, $n = 3$). These suggested that all potential inhibitor hits were false positives and that their inhibitory effect might be due to fluorescence quenching or via a non-P2X4 mediated pathway, except for one compound, thaspine. Thaspine did not significantly cause a reduction in ionomycin- and carbachol-evoked responses compared to vehicle control. Therefore, thaspine was selected as the new lead compound as it showed 60 % inhibition of calcium-evoked response in the human P2X$_4$ overexpressing cells at 10 µM in addition to its lack of effect on ionomycin- and carbachol-evoked responses.
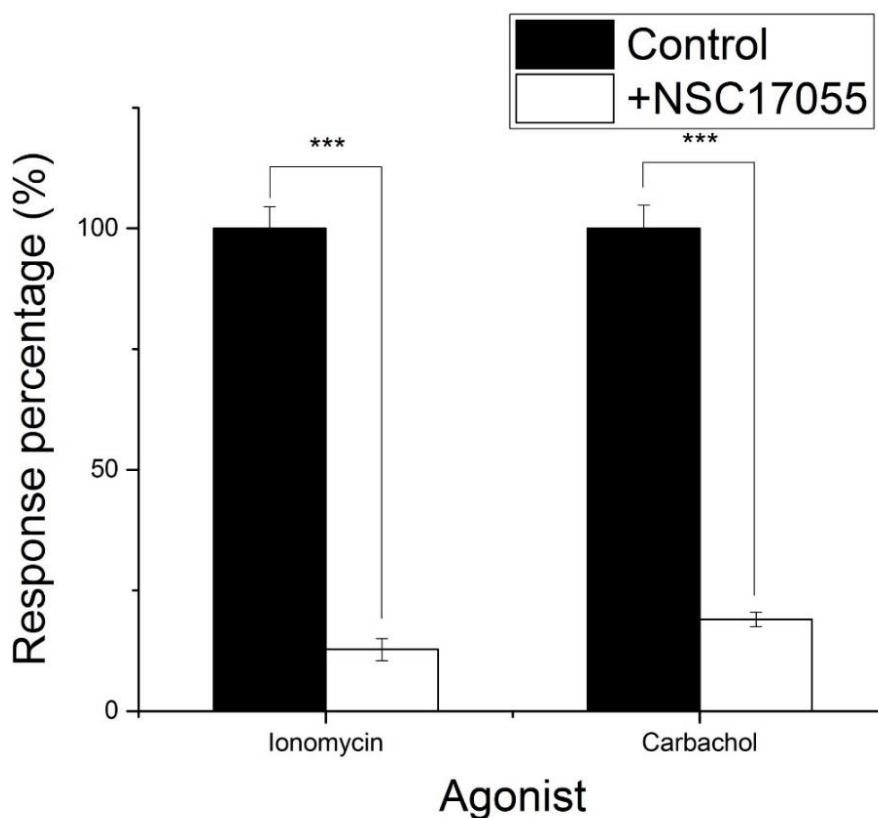
Figure 3.25 Effect of NSC17055 on ionomycin- and carbachol-evoked response.
The bar chart shows the responses of human P2X$_4$ when challenged with 1 µM of ionomycin and 100 µM of carbachol in the presence and absence of 10 µM of NSC17055. Black bar represents the peak response of vehicle control recorded for each condition without the compound and the response was normalised to 100 %. Meanwhile, white bar shows the peak response of each condition when 10 µM of compound was present and the responses were normalised to control response. Asterisks denote *p*-value: * = < 0.05, ** = < 0.01, *** = < 0.001. (*n* = 3)
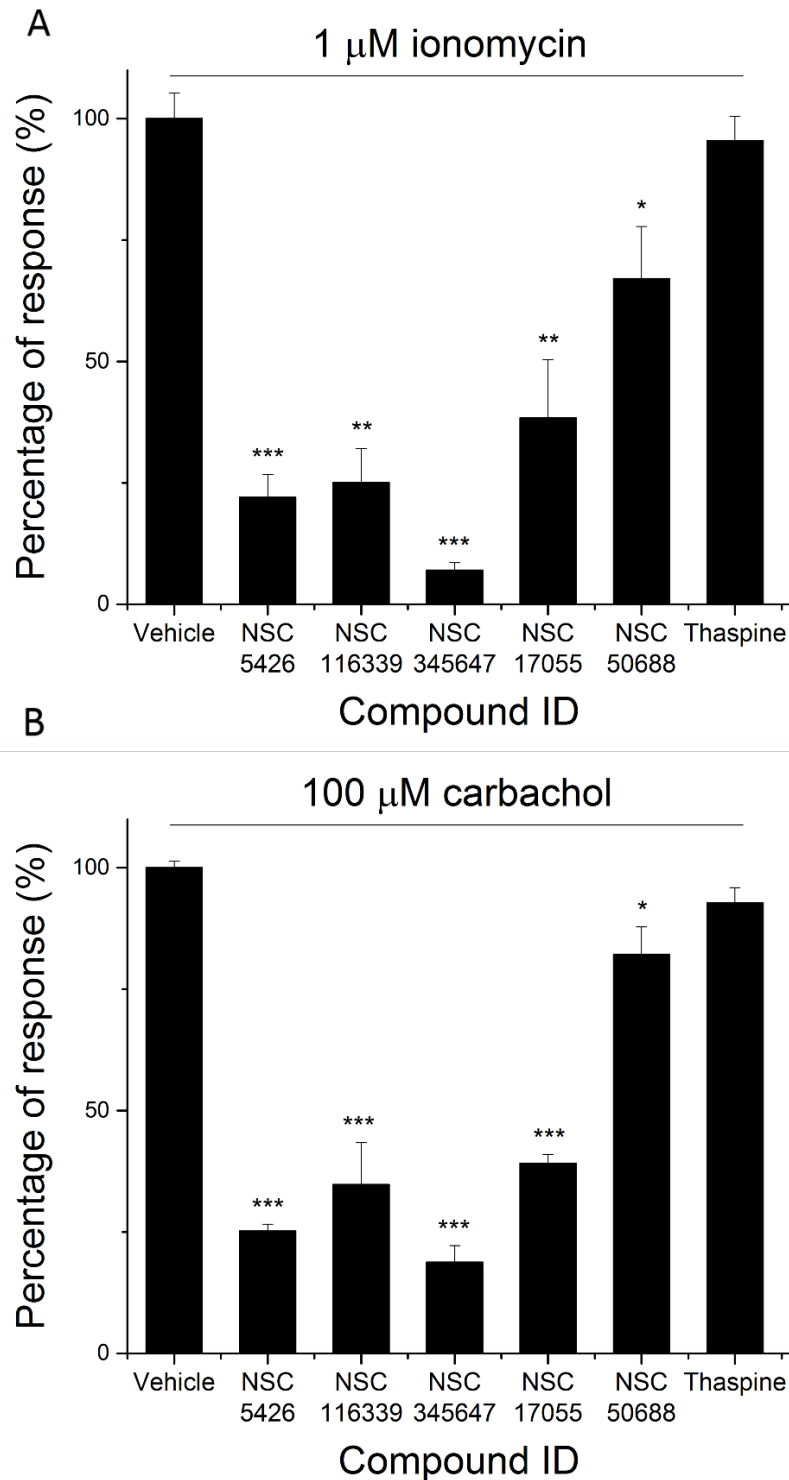
Figure 3.26 Effects of potential inhibitor hits on ionomycin- and carbachol-evoked responses.

The bar charts show the effect of all inhibitor hits on ionomycin- and carbachol-evoked responses of the human $P2X_4$ overexpressing cells. The concentrations of ionomycin, carbachol, and potential compounds used in this experiment were 1, 100, and 10 μM, respectively. All responses were normalised to mean peak response of the vehicle control (0.1 % DMSO). The differences in percentage of responses between each compound and vehicle response were statistically calculated. Asterisks denote *p*-value: * = < 0.05, ** = < 0.01, *** = < 0.001. (*n* = 3)

3.3.3.3 Characterisation of thaspine

Several characterisation experiments on thaspine were done to fully understand its properties. The first characterisation done was the inhibition concentration-response to study its potency at inhibiting human P2X$_4$ receptor. As shown in Figure 3.27, thaspine started to inhibit at a concentration of 3 µM, where it significantly inhibited 33.0 ± 3.0 % ($p < 0.001$, $n = 3$) of the response elicited by 3 µM of ATP and at 100 µM, it almost abolished the response (95.0 ± 1.1 % inhibition, $p < 0.001$, $n = 3$). From the data, the value of IC$_{50}$ determined was 3.81 ± 0.2 µM ($n = 3$) and it could be clearly seen that thaspine only affected the magnitude of response while maintaining the decay kinetics, represented by tau value. The tau values for response with and without thaspine were not significantly different (106.8 ± 34.7 and 100.4 ± 10.3 seconds, respectively, [thaspine] = 10 µM, [ATP] = 3 µM, $p > 0.05$, $n = 3$).

To test the dependency of thaspine inhibition on the cell system used for overexpressing the P2X$_4$ receptors, it was tested on human P2X$_4$ expressed in HEK293 cells which were kindly donated by MedImmune. Due to HEK293 having endogenous P2Y receptors that were also responsive to ATP, cytidine triphosphate (CTP) was used as it only activates P2X$_4$ and partially activates P2X$_1$ (Roberts & Evans, 2004; Soto et al., 1996). Based on the data shown in Figure 3.28, it showed that thaspine blocked 100 µM CTP-evoked response in concentration-dependent pattern. The first significant inhibition was observed when the cells were treated with 3 µM of thaspine (40.2 ± 8.0 % inhibition, $p < 0.01$, $n = 3$). At 30 µM of thaspine, the response was almost completely inhibited (92.4 ± 1.3 % inhibition, $p < 0.001$, $n = 3$). Its potency was also similar to that in 1321N1 cells overexpressing human P2X$_4$ (IC$_{50}$ value of 3.99 ± 1.0 µM versus 3.81 ± 0.2 µM, $p > 0.05$, $n = 3$). These indicated that the inhibition of thaspine was not dependent on the use of nucleotide and cell system that overexpresses human P2X$_4$.

Next, thaspine was tested on mouse orthologue to see if it was also effective at blocking other P2X$_4$ orthologue. Mouse P2X$_4$ has an 88 % similarity with human P2X$_4$ in terms of amino acid sequence and thus, it was expected that thaspine would have similar effect. Figure 3.29 shows thaspine inhibition concentration-response at mouse P2X$_4$ receptor (overexpressed in astrocytoma cells) and representative traces of

responses in the absence and presence of 10 µM of thaspine. The calculated IC_{50} value based on the curve was 3.53 ± 0.26 µM ($n = 3$) which was similar with the human $P2X_4$ expressed in 1321N1 and HEK293 cells ($p > 0.05$, $n = 3$).

The fourth characterisation was to determine the mode of inhibition. The result showed that the highest ATP concentration tested (30 µM) did not overcome the inhibition by 10 µM of thaspine (Figure 3.30). The ATP EC_{50} values in the absence and presence of thaspine were also not significantly different (0.44 ± 0.1 µM versus 0.48 ± 0.2 µM, respectively, $p > 0.05$, $n = 3$). Together, the data suggested that the inhibition was noncompetitive.

A

IC$_{50}$: 3.81 ± 0.2 μM

B

3 μM ATP

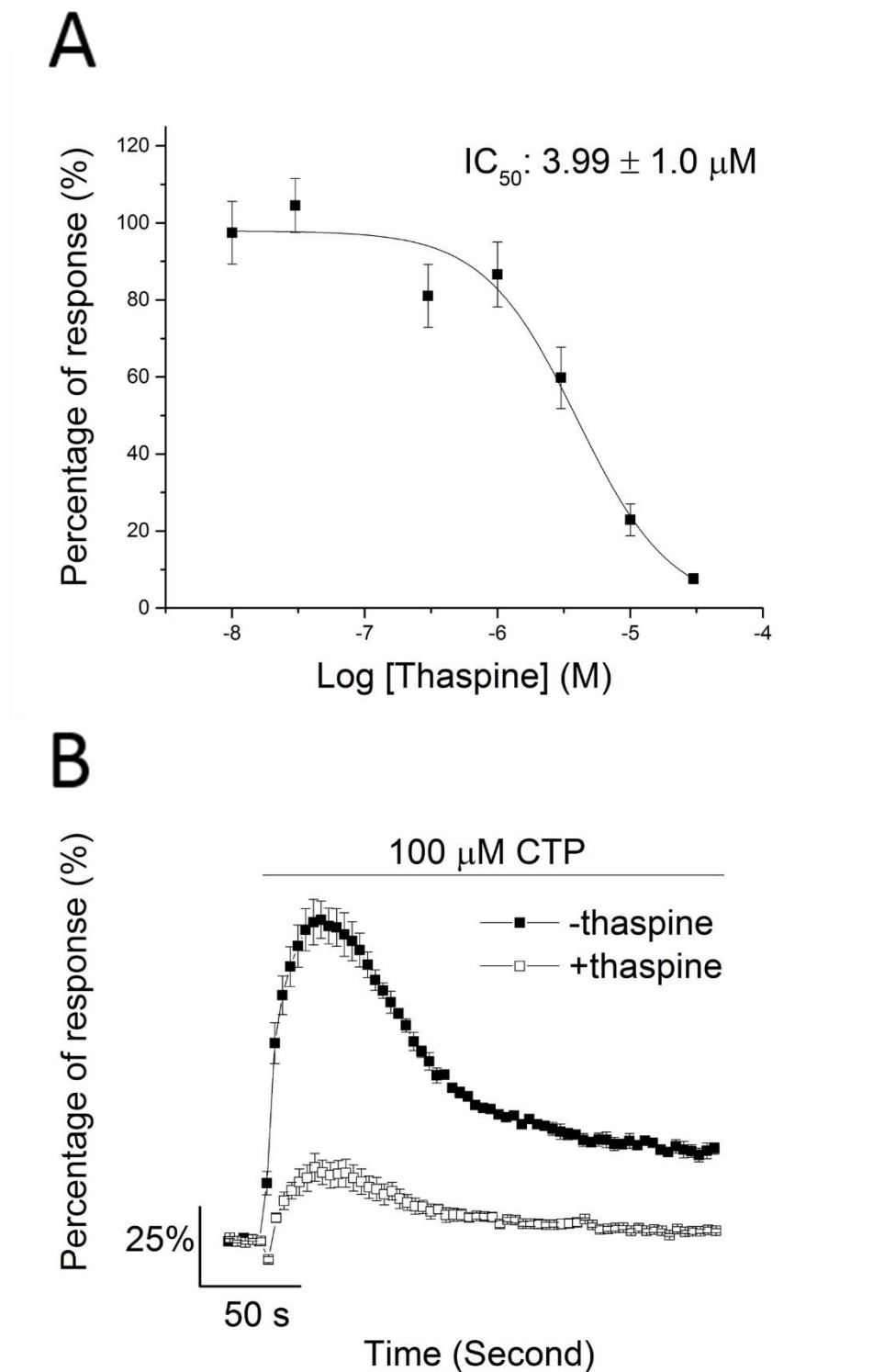- -thaspine
- +thaspine

25%

50 s

Time (Second)
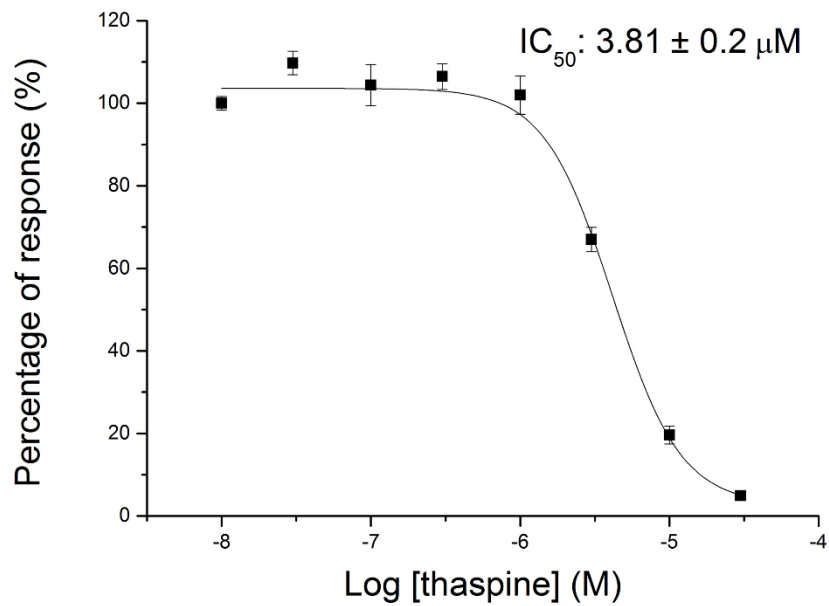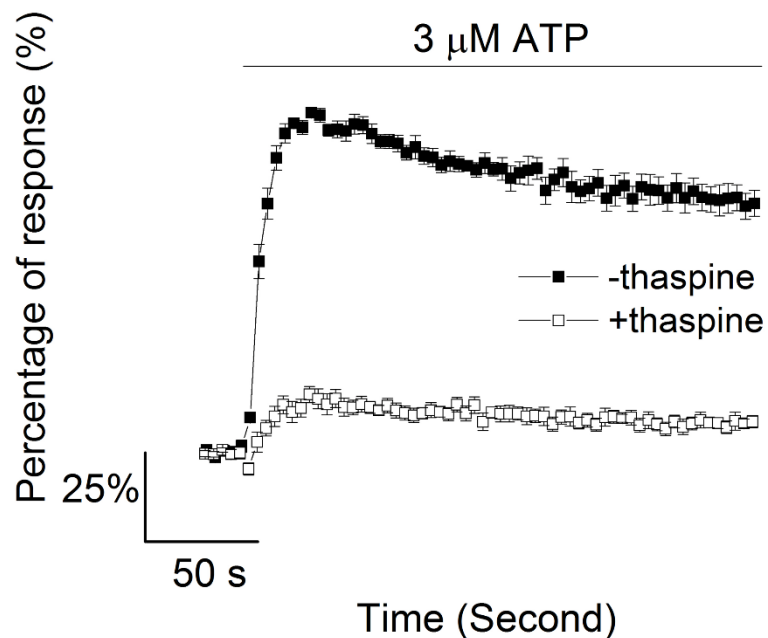
Figure 3.27 Inhibition concentration-response of thaspine at human P2X$_4$ receptor overexpressed in astrocytoma cells.

Panel A shows thaspine inhibition concentration-response at human P2X$_4$. The lowest thaspine concentration was 10 nM and the highest was 30 μM. Panel B shows the representative trace of calcium response for 250 seconds recording with the presence and absence of 10 μM of thaspine. The cells were challenged with maximal agonist (ATP) concentration which was 3 μM. All responses were normalised to the maximum response of vehicle control. ($n = 3$)
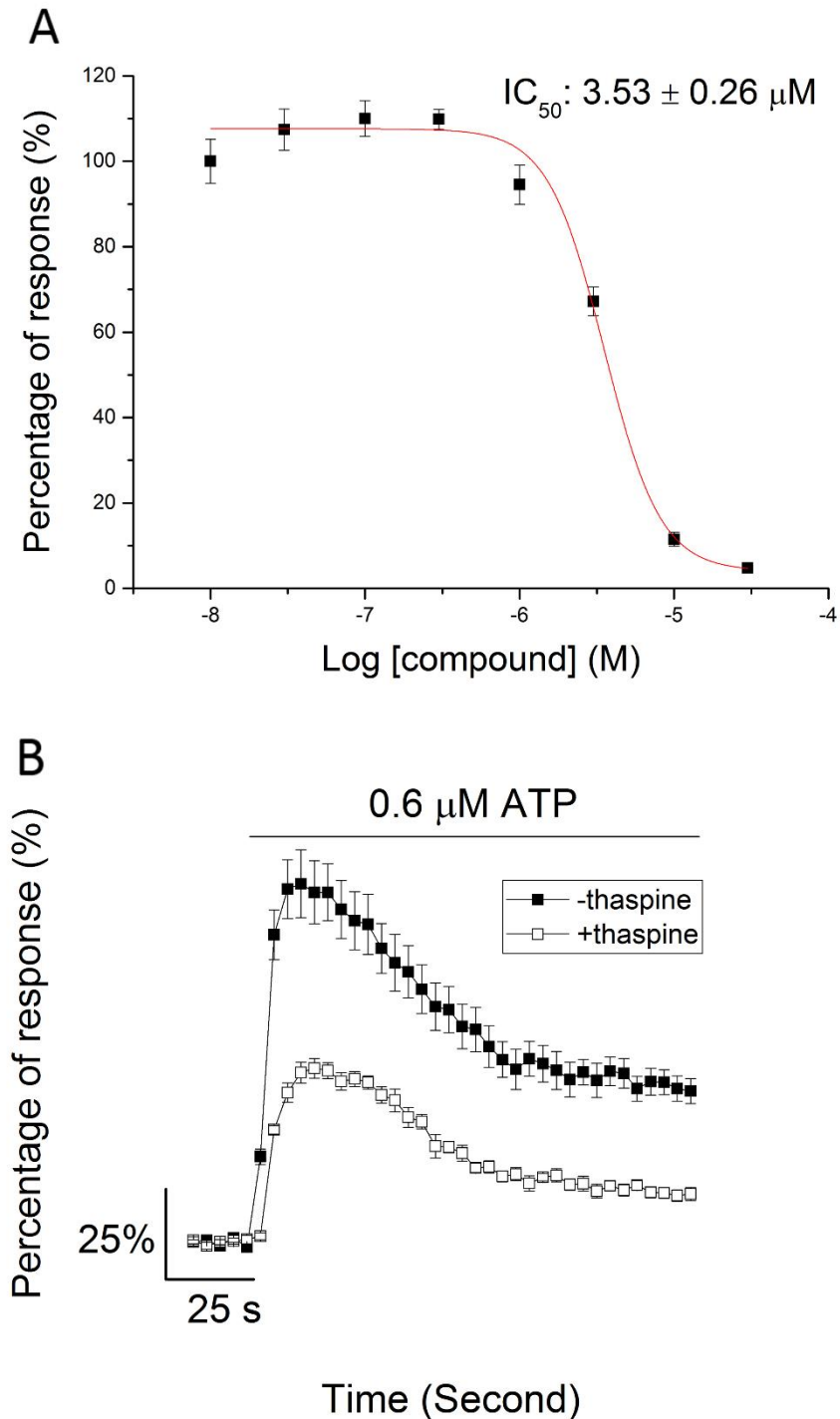
Figure 3.28 Inhibition concentration-response of thaspine at human P2X4 receptor overexpressed in HEK293 cells.

Panel A shows thaspine inhibition concentration-response at human P2X$_4$ receptor overexpressed in HEK293 cells. The lowest thaspine concentration was 10 nM and the highest was 30 µM. Panel B shows the representative trace of the response for 250 seconds recording in the presence and absence of 10 µM of thaspine. The cells were challenged with a maximal CTP concentration which was 100 µM. All responses were normalised to the maximum response of vehicle control. ($n = 3$)

Figure 3.29 Inhibition concentration-response of thaspine at mouse P2X4.
Panel A shows thaspine inhibition concentration-response at mouse P2X4 receptor. The lowest thaspine concentration was 10 nM and the highest was 30 µM. Panel B shows the representative traces of the response for 250 seconds recording between untreated and treated cells with 10 µM of thaspine. The cells were stimulated with a maximal concentration of 0.6 µM of ATP. All responses were normalised to the maximum response of vehicle control. ($n = 3$)
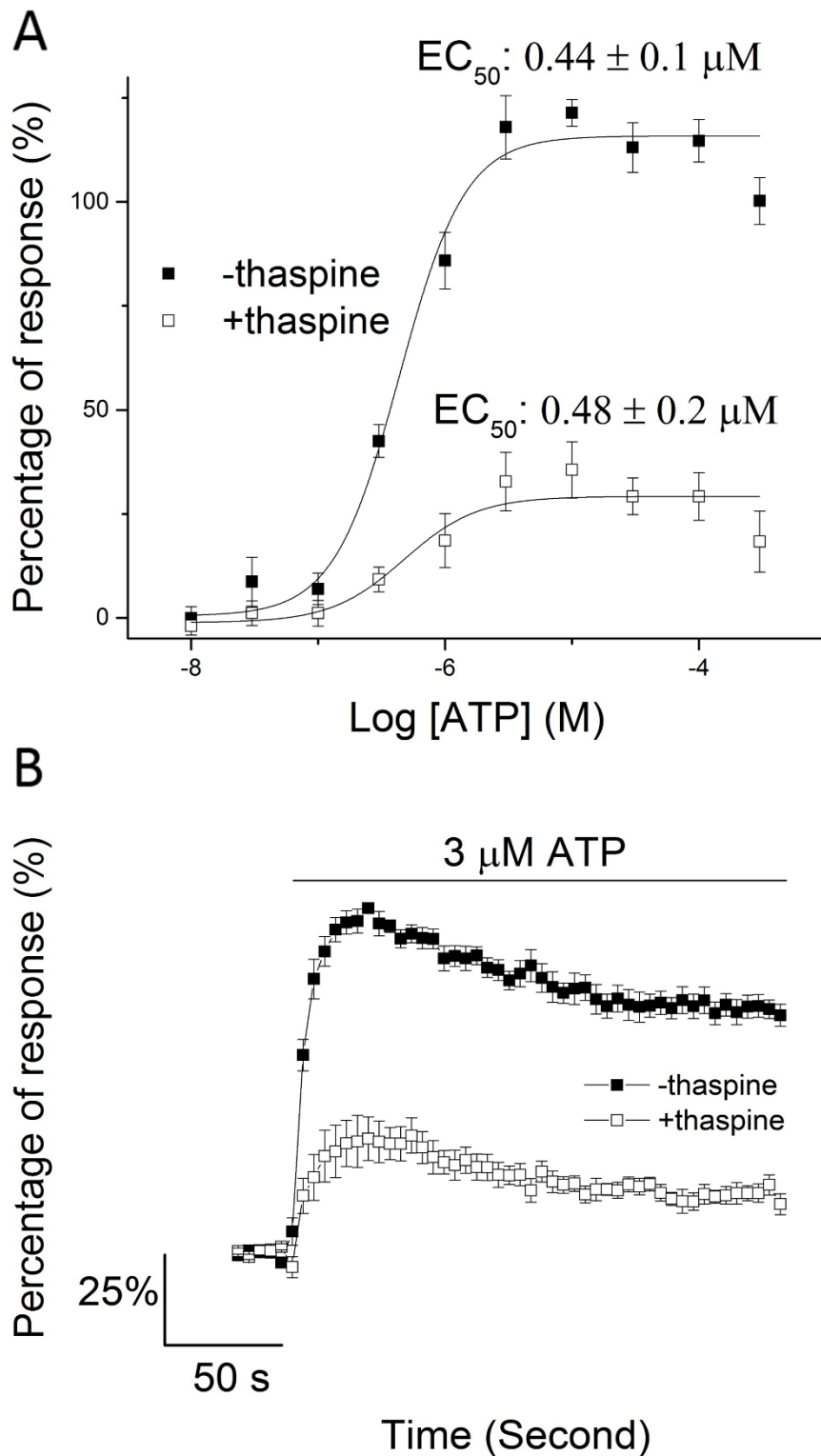
Figure 3.30 Determination of thaspine mode of inhibition.
Panel A shows the ATP concentration-response at human $P2X_4$ receptor with and without 10 µM of thaspine (open and closed squares, respectively). Panel B shows the representative trace of response when the cells were challenged with 3 µM of ATP in the absence and presence of 10 µM of thaspine for a period of 250 seconds. The inability of maximal ATP concentration to surmount thaspine inhibition and unchanged EC_{50} values were both the indicators of a noncompetitive antagonism. All responses were normalised to the response of vehicle control (without ATP). ($n = 3$)

Next, the bar chart in Figure 3.31 shows the effect of different pre-incubation periods of thaspine (10 µM) on ATP-evoked calcium response at human P2X$_4$. The data showed that thaspine had no significant effect on the calcium response after 5 minutes pre-incubation where the inhibition was only 3.7 ± 4.5 % ($p > 0.05$, $n = 3$). The first significant inhibition was observed after 10 minutes pre-incubation with 19 ± 3.0 % inhibition ($p < 0.001$, $n = 3$) and the blockade was gradually increased as the pre-incubation time increased. The maximum inhibition was observed after 40 minutes pre-incubation and the inhibition with periods longer than 40 minutes produced similar inhibition with that of 40 minutes ($p > 0.05$, $n = 3$). The incubation period versus percentage of inhibition were as follows: incubation period (minute) – percentage of inhibition (%): 10 – 19.1 ± 3.0, 15 – 21.3 ± 4.0, 20 – 30.5 ± 5.8, 25 – 37.4 ± 7.3, 30 – 50.0 ± 8.4, 35 – 55.0 ± 9.1, 40 – 63.6 ± 9.1, 45 – 60.2 ± 10.3, 50 – 66.7 ± 6.5, 55 – 70.0 ± 5.5, and 60 – 65.9 ± 4.5 ($n = 3$). The curve revealed that the time taken to produce 50 % of its inhibitory activity was 15.2 ± 11 ($n = 3$) minutes.

Figure 3.32 shows the results of reversibility experiment. This was achieved by stimulating the cells with 3 µM ATP twice. Between the stimulations, the cells were washed with HBPS and incubated at 37 °C for 5 – 30 minutes. The hypothesis was if thaspine was a reversible inhibitor, it would be displaced from its binding site during the wash, and the second ATP stimulation should produce the same response between thaspine-treated cells and vehicle control. Based on the results, the second ATP stimulation of vehicle control yielded 41.0 ± 2.0 % ($n = 3$, normalised to the first ATP stimulation) after 5 minutes incubation. The percentage of response gradually increased as the incubation time increased and the highest response was recorded when the cells were incubated for 15 minutes after washing (61.9 ± 2.5 %, $n = 3$). The fitting of responses at each time point revealed that the receptors took 10.4 ± 1.0 minutes to achieve 50 % of its recovery fraction.

However, the second ATP stimulation on thaspine-treated cells did not show the same magnitude of response as the vehicle control. After 5 minutes incubation, the percentage of response (normalised to the first ATP stimulation of vehicle control) recorded was only 8.2 ± 1.5 % ($n = 3$). The responses gradually increased as the incubation time increased and the highest point was recorded after 30 minutes

incubation (16.8 ± 2.1 %, $n = 3$). The percentage of responses after the second ATP stimulation between thaspine-treated cells and vehicle control was significantly different ($p < 0.001$, $n = 3$). This indicated that thaspine was not removed during the wash, and that it was a long-acting or irreversible inhibitor.
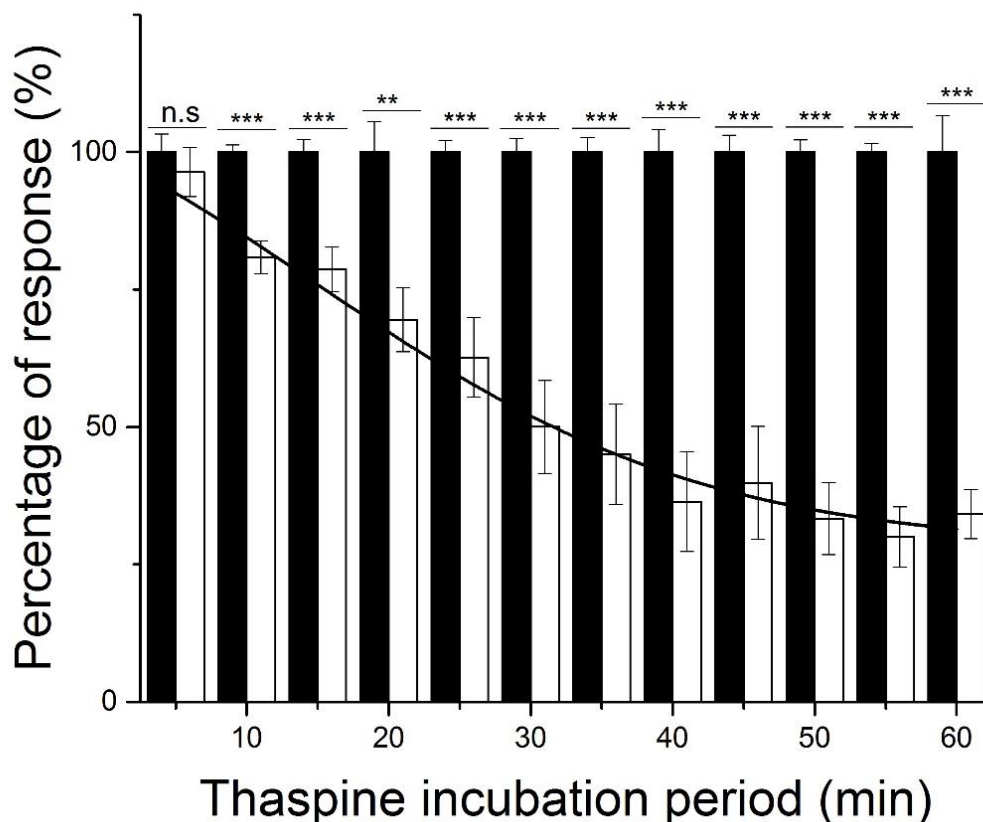
Figure 3.31 Effects of different thaspine incubation periods on calcium response.

The bar chart represents the effect of different thaspine pre-incubation periods on the human P2X$_4$ overexpressing cells after being stimulated with 3 µM of ATP. The shortest incubation period was 5 minutes and the period gradually increased by 5 minutes up to 60 minutes. Black bar is the vehicle control response of untreated cells while white bar represents the response of treated cells. All responses were normalised to the vehicle control response at each time point. Statistics were calculated based on responses of untreated and treated cells at each respective time point. Black line is the curve fit of the treated cells data. The fitting revealed that the time taken to produce 50 % of its inhibitory activity was 15.2 ± 11 minutes. Asterisks denote p-value: * = < 0.05, ** = < 0.01, *** = < 0.001, n.s. = not significant. (n = 3)
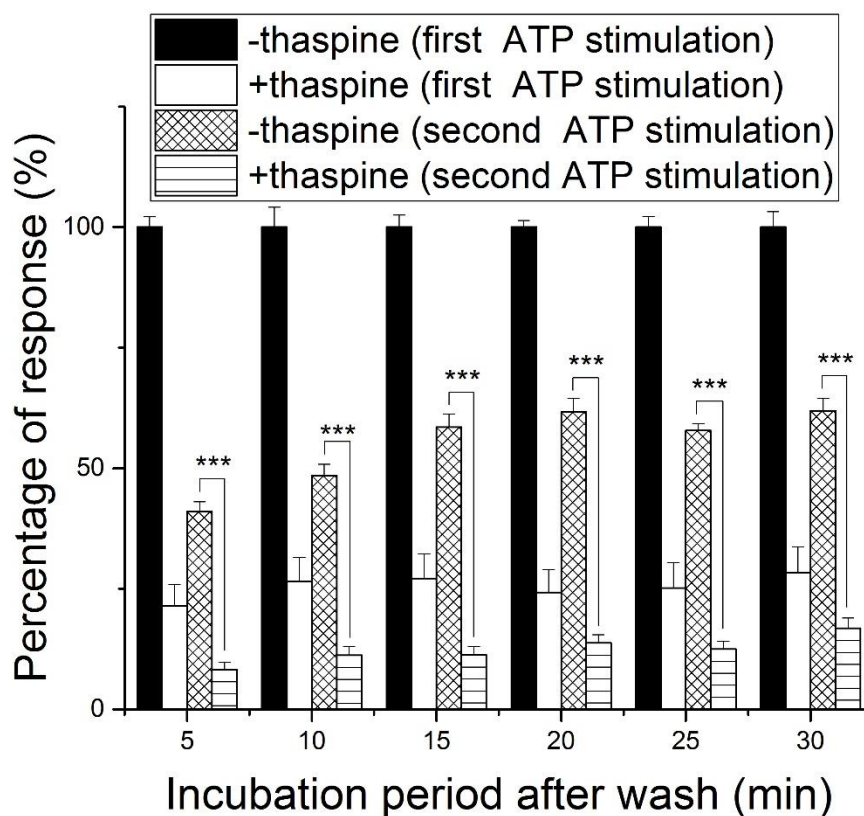
Figure 3.32 Reversibility experiment of thaspine at human P2X₄.
The bar chart shows the amount of calcium response elicited by four conditions. Black bar represents the response of vehicle control in the first ATP stimulation while crossed bar represents the second ATP stimulation. White bar represents the response of thaspine-treated cells in the first ATP stimulation, while bar with horizontal lines shows the second ATP stimulation. The responses were normalised to the response of vehicle control in the first ATP stimulation (black bar). The x-axis represents the duration of incubation after washing, i.e., before the second ATP stimulation. The statistics show the difference in response magnitude in the second ATP stimulation between the vehicle control and thaspine-treated cells. The data shows that thaspine-treated cells did not recover the response as high as the vehicle control. This shows that thaspine was not removed during the wash and the inhibition remained in the second ATP stimulation. Asterisks denote *p*-value: * = <0.05, ** = <0.01, *** = <0.001. (*n* = 3)

3.3.3.4 Effects of thaspine at P2X$_4$ paralogues and P2Ys

Then, thaspine was tested to determine its selectivity. Several P2X and P2Y overexpressing cell lines were tested with the compound. Figure 3.33 – 3.37 show the effect of thaspine treatment on each cell line: the human P2X$_2$, P2X$_{2/3}$, P2X$_7$, P2Y$_2$, and P2Y$_6$, respectively. In the experiment, two concentrations were used, which were the EC$_{50}$ and maximal agonist concentrations.

At human P2X$_2$, P2X$_{2/3}$, and P2X$_7$, there was no significant inhibition observed with the treatment of 10 µM of thaspine either at EC$_{50}$ or maximal concentrations of agonist ($p > 0.05$, $n = 3$). On the other hand, the inhibition observed at human P2Y$_2$ was significant either at EC$_{50}$ or maximal concentrations of ATP with a magnitude of 79.9 ± 4.7 % and 74.4 ± 6.0 % ($p < 0.001$, $n = 3$), respectively. The inhibition was also observed at human P2Y$_6$ with an inhibition of 19.1 ± 7.3 % ($p < 0.05$, $n = 3$) and 39.6 ± 5.7 % ($p < 0.001$, $n = 3$) when the cells were stimulated with 23 and 100 nM of UDP, respectively.
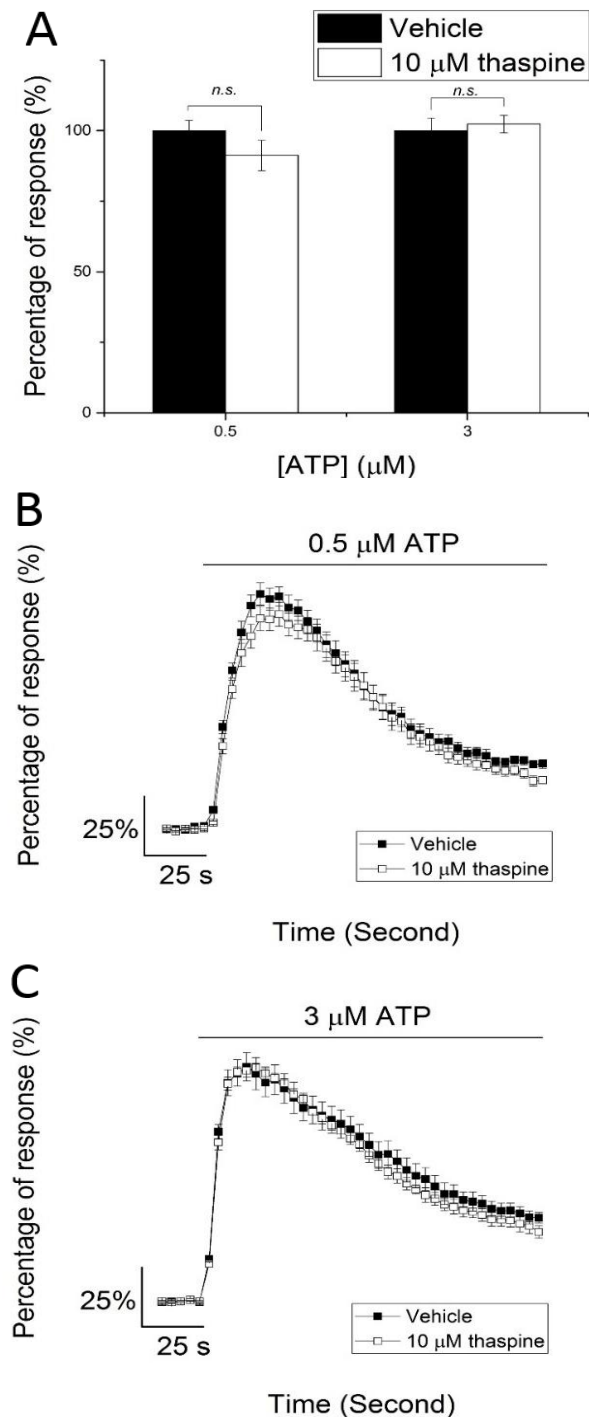
Figure 3.33 Effect of thaspine on ATP-evoked response at human P2X$_2$.
Panel A shows the effect of thaspine on ATP-evoked response at human P2X$_2$ receptor when challenged with EC$_{50}$ and maximal concentrations of ATP. The black bars represent the vehicle control peak response and white bars represent the peak responses of thaspine-treated cells. Panel B and C illustrate the representative trace for 250 seconds when the cells were challenged with EC$_{50}$ and super maximal ATP concentration, respectively. Close square is the trace for vehicle while the open square is for thaspine-treated cells. All responses were normalised to mean peak response of vehicle control for each concentration. n.s. = not significant. ($n = 3$)
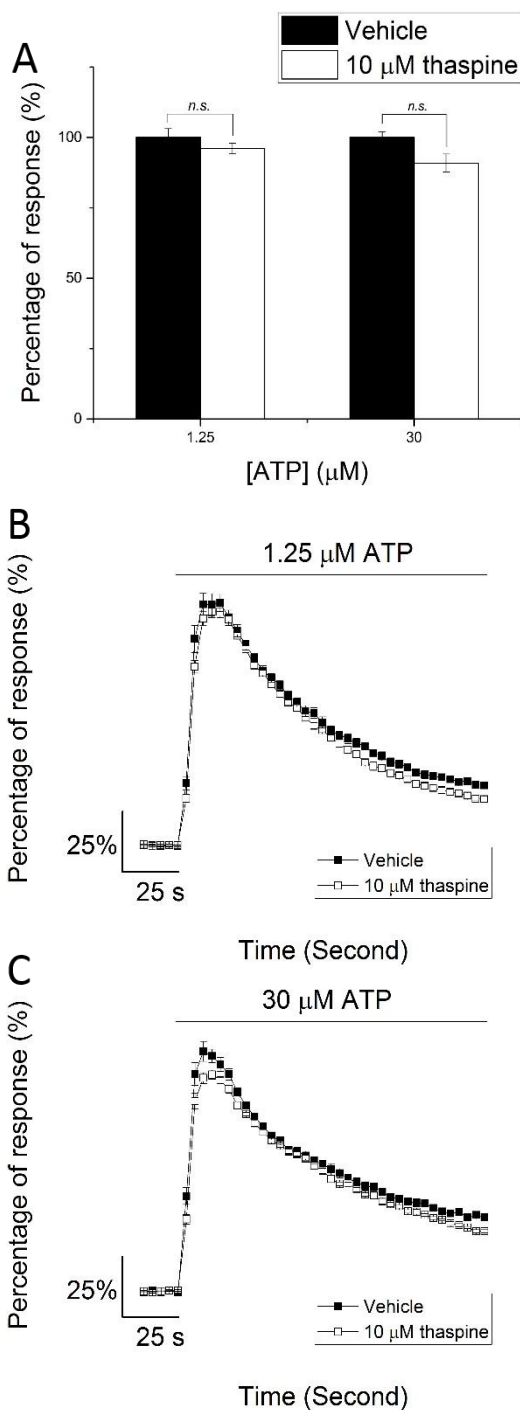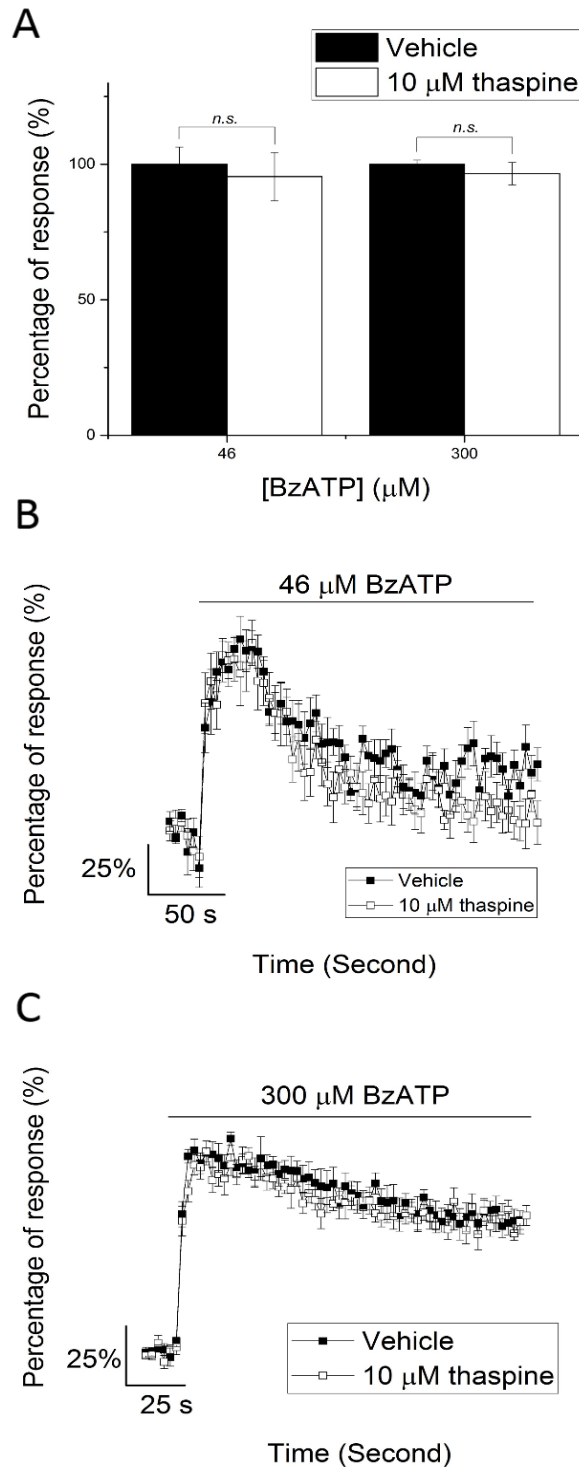
Figure 3.34 Effect of thaspine on ATP-evoked response at human P2X$_{2/3}$

Panel A shows the effect of thaspine on ATP-evoked response at human P2X$_{2/3}$ receptor when challenged with EC$_{50}$ and maximal concentrations of ATP. The black bars represent the vehicle control peak response and white bars represent the peak responses of thaspine-treated cells. Panel B and C illustrate the representative trace for 250 seconds when the cells were challenged with EC$_{50}$ and super maximal ATP concentration, respectively. Close square is the trace for vehicle while open square is for thaspine-treated cells. All responses were normalised to mean peak response of vehicle control for each concentration. n.s. = not significant. ($n = 3$)

Figure 3.35 Effect of thaspine on BzATP-evoked response at human P2X$_7$
Panel A shows the effect of thaspine on BzATP-evoked response at human P2X$_7$ receptor when challenged with EC$_{50}$ and maximal concentrations of BzATP. The black bars represent the vehicle control peak response and white bars represent the peak responses of thaspine-treated cells. Panel B and C illustrate the representative trace for 250 seconds when the cells were challenged with EC$_{50}$ and super maximal BzATP concentration, respectively. Close square is the trace for vehicle while open square is for thaspine-treated cells. All responses were normalised to mean peak response of vehicle control for each condition. n.s. = not significant. ($n = 3$)
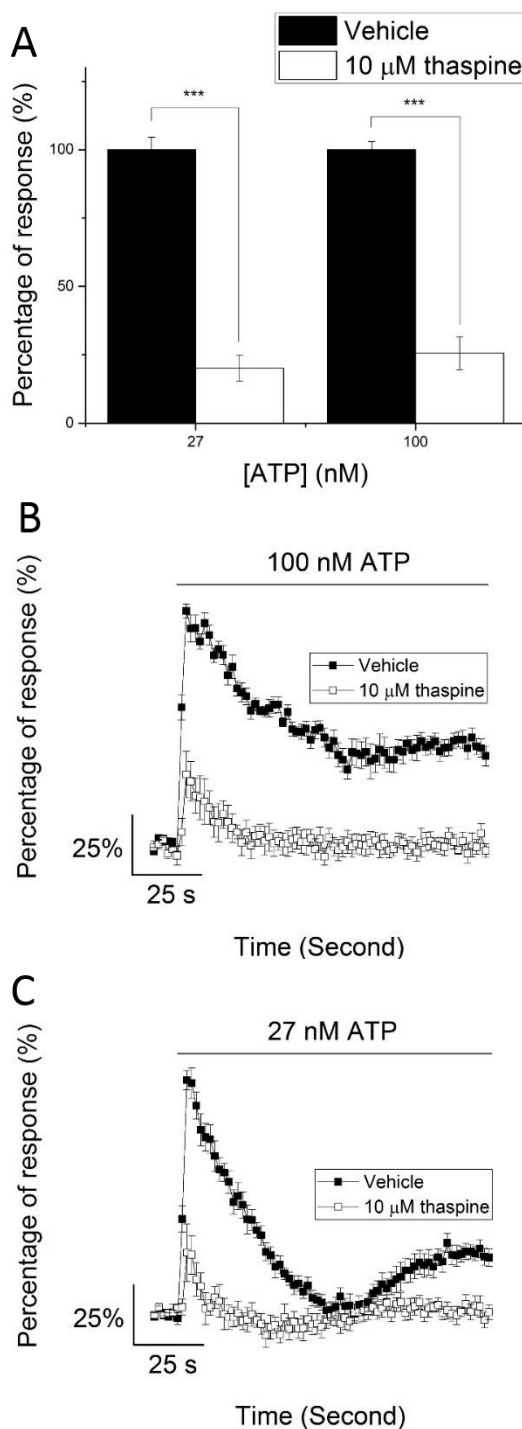
Figure 3.36 Effect of thaspine on ATP-evoked response at human P2Y$_2$

Panel A shows the effect of thaspine on ATP-evoked response at human P2Y$_2$ receptor when challenged with EC$_{50}$ and maximal concentrations of ATP. The black bars represent the vehicle control peak response and white bars represent the peak responses of thaspine-treated cells. Panel B and C illustrate the representative trace for 250 seconds when the cells were challenged with EC$_{50}$ and super maximal ATP concentration, respectively. Close square is the trace for vehicle while open square is for thaspine-treated cells. All responses were normalised to mean peak response of vehicle control for each concentration. Asterisks denote *p*-value: $*$ = < 0.05, $**$ = $<$ 0.01, $***$ = < 0.001. ($n = 3$)
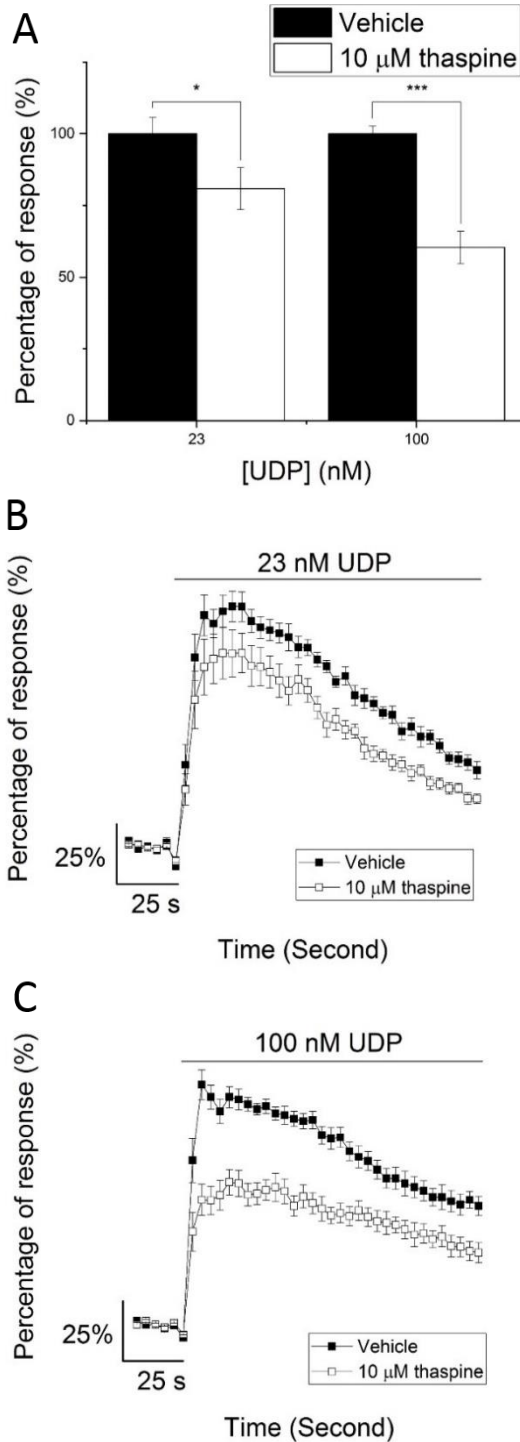
Figure 3.37 Effect of thaspine on UDP-evoked response at human P2Y$_6$
Panel A shows the effect of thaspine on UDP-evoked response at human P2Y$_6$ receptor when challenged with EC$_{50}$ and maximal concentrations of UDP. The black bars represent the vehicle control peak response and white bars represent the peak responses of thaspine-treated cells. Panel B and C illustrate the representative trace for 250 seconds when the cells were challenged with EC$_{50}$ and super maximal UDP (values based on Campwala (2015)) concentrations, respectively. Close square is the trace for vehicle while open square is for thaspine-treated cells. All responses were normalised to mean peak response of vehicle control for each condition. Asterisks denote p-value: $* = < 0.05$, $** = < 0.01$, $*** = < 0.001$. ($n = 3$)

To further investigate the potency of thaspine in inhibiting $P2Y_2$ and $P2Y_6$, an inhibition concentration-response was generated for both receptors which are shown in Figure 3.38. For $P2Y_2$, there was no modulation of response observed at concentrations of lower than 10 µM. At only 10 µM, the response elicited by 100 nM of ATP was almost abolished (95.2 ± 0.8 % inhibition, $n = 3$) and the same effect was also observed at 30 µM of thaspine (96.1 ± 1.0 % inhibition, $n = 3$). On the other hand, there was a significant potentiation at 1 µM of thaspine (23.1 ± 13.6 % potentiation, $p < 0.05$, $n = 3$). At $P2Y_6$, the UDP-evoked response was not changed with the treatment of ≤ 10 µM of thaspine ($p > 0.05$, $n = 3$), but it was significantly blocked with the application of 30 µM of thaspine by 94.7 ± 0.5 % ($p < 0.001$, $n = 3$). Together, the data showed that thaspine was not effective at human $P2Y_2$ and $P2Y_6$ at the concentrations of below 10 µM and 30 µM, respectively.
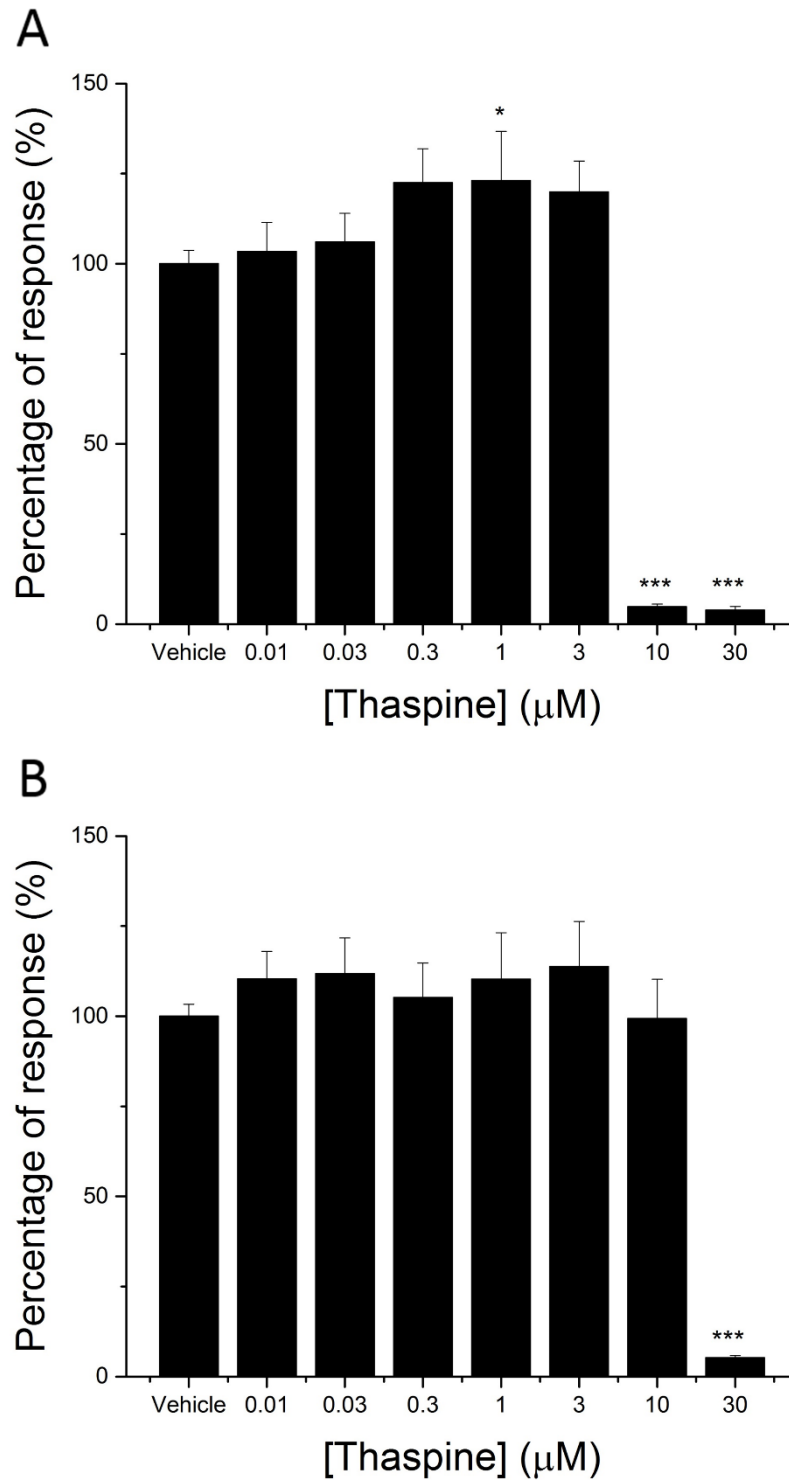
Figure 3.38 Thaspine inhibition concentration-response at human P2Y$_2$ and P2Y$_6$ receptors.

The figure shows thaspine inhibition concentration-response at (A) human P2Y$_2$ and (B) human P2Y$_6$. Thaspine was ineffective at human P2Y$_2$ at concentration of below than 10 µM and below than 30 µM at human P2Y$_6$. The responses were normalised to the mean peak response of vehicle and the error bars show the standard error of mean. Asterisks denote *p*-value: * = < 0.05, ** = < 0.01, *** = < 0.001. (*n* = 3)

3.3.3.5 Effects of thaspine on microglial cells

Up to this point, all characterisation experiments were performed on the stable overexpressing cell lines and this might not be reflected in primary cells or in vivo setting. To reflect the finding on primary cells, murine microglial cell line or BV2 cells were used. Although they were not the primary cells, Henn et al. (2009) proposed that BV2 cells behaved similar to primary microglial cells. Moreover, since thaspine also blocked ATP-evoked calcium response at mouse $P2X_4$ as shown in Figure 3.29, BV2 cell was a suitable model to examine such effect on mouse microglial cell line.

Figure 3.39 shows the complete ATP concentration-response of BV2 cells. The calculated EC_{50} was 1.8 ± 0.65 µM and maximal concentration was 10 µM ($n = 3$). It is worth noting, however, BV2 cells contain other P2X and P2Y receptors and thus the observed response was a result of stimulation of multiple types of purinergic receptor (Gendron et al., 2003).

To test whether thaspine had any effect on the response liberated by specifically $P2X_4$ receptors in BV2 cells, the cells were potentiated with IVM, which is a selective positive allosteric modulator. Theoretically, IVM will only potentiate the response yielded by $P2X_4$ and if thaspine inhibits the $P2X_4$ receptor, it will reduce the potentiated response by IVM. The tests were done on two states of cells, quiescent and activated cells. The activated cells were induced by LPS, of which increased the expression of $P2X_4$ (Raouf et al., 2007). This was done to imitate the actual situation where hypersensitivity to pain was a consequence of overexpression of $P2X_4$ receptors. The activity of thaspine was compared to a known $P2X_4$ inhibitor, PSB12062, to see if they share common characteristics when exposed to BV2 cells. The concentration used for both compounds was 10 µM whereas 3 µM for IVM.
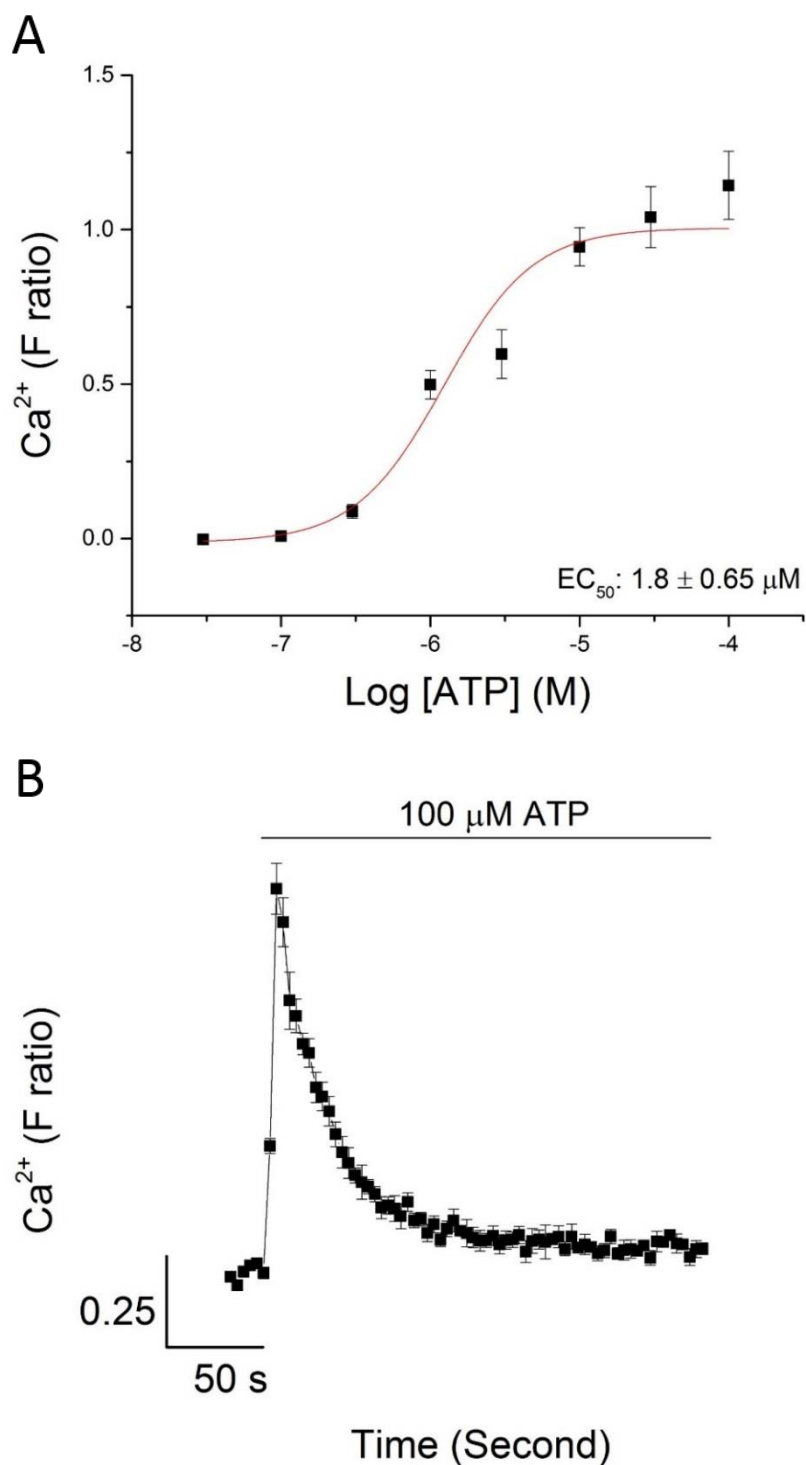
Figure 3.39 ATP concentration-response of BV2 cells.
The curve in panel A shows the complete ATP concentration-response of BV2 cells challenged (25,000 cells/well) with multiple concentrations of ATP and panel B shows the representative trace at 100 µM of ATP which corresponded to saturated concentration. The EC_{50} value determined from the graph was 1.8 ± 0.65 µM. The error bars show the standard error of mean. ($n = 3$)
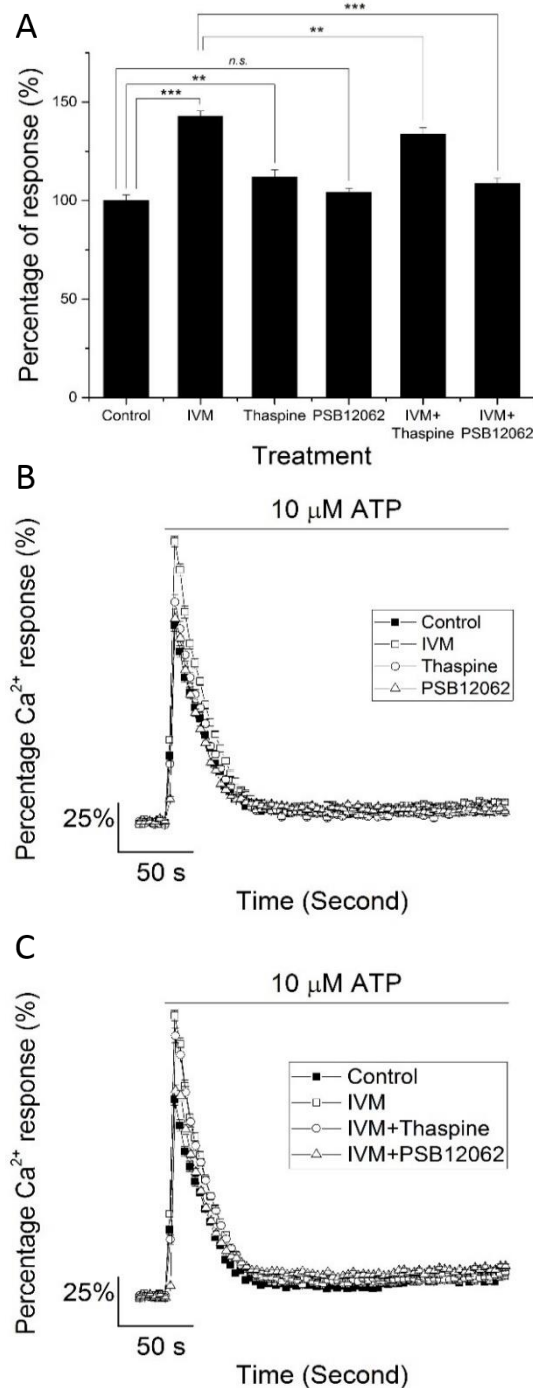
Figure 3.40 Effects of thaspine and PSB12062 on quiescent BV2 cells.
Panel A shows the effect of thaspine and PSB12062 on ATP-evoked response of quiescent BV2 cells. The effects were measured in terms of percentage of peak response normalised to control response. The effects of both compounds were observed on normal ATP response and on IVM-potentiated response. Panel B shows the effects of IVM, thaspine, and PSB12062 on the representative traces of ATP-evoked response while Panel C shows the effect of thaspine and PSB12062 on IVM-potentiated representative traces. The concentration of compounds used in this experiment was 10 µM for thaspine and PSB12062, 3 µM for IVM, and 10 µM for ATP. Asterisks denote p-value: $* = < 0.05$, $** = < 0.01$, $*** = < 0.001$, n.s. = not significant. ($n = 6$)
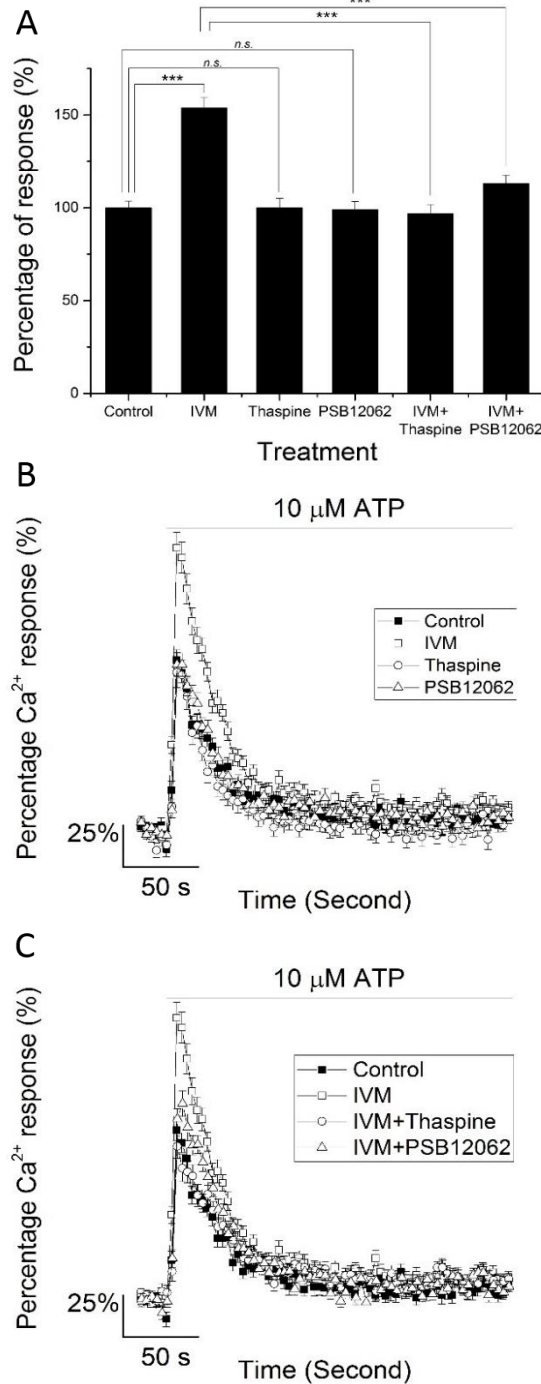
Figure 3.41 Effects of thaspine and PSB12062 on LPS-activated BV2 cells.
Panel A shows the effect of thaspine and PSB12062 on ATP-evoked response of LPS-activated BV2 cells. The effects were measured in terms of percentage of peak response normalised to control response. The effects of both compounds were observed on normal ATP response and on IVM-potentiated response. Panel B shows the effect of IVM, thaspine, and PSB12062 on the representative traces of ATP-evoked response while panel C shows the effects of thaspine and PSB12062 on IVM-potentiated representative traces. The concentration of compounds used in this experiment was 10 µM for thaspine and PSB12062, 3 µM for IVM, and 10 µM for ATP. Asterisks denote p-value: * = < 0.05, ** = < 0.01, *** = < 0.001. n.s. = not significant. ($n = 6$)

Figure 3.40 shows the effects of thaspine and PSB12062, as positive control, on quiescent BV2 cells. Ivermectin significantly potentiated the response by 42.8 ± 2.6 % ($p < 0.001$, $n = 6$) compared to control. In terms of representative trace, there was no difference in the decay kinetic (τ) between the vehicle control and IVM-potentiated response (16.5 ± 0.7 versus 16.7 ± 0.5 seconds respectively, $p > 0.005$, $n = 6$). In thaspine-treated cells, the response significantly increased by 11.9 ± 3.7 % ($p < 0.01$, $n = 6$) while there was no difference observed when the cells were treated with PSB12062. However, when IVM and thaspine or IVM and PSB12062 were co-treated, both inhibitors significantly reduced the response in comparison to IVM-potentiated response by 8.7 ± 2.6 % ($p < 0.01$, $n = 6$) and 33.6 ± 3.4 % ($p < 0.001$, $n = 6$), respectively.

On the other hand, Figure 3.41 shows the effects of thaspine and PSB12062 on LPS-activated BV2 cells. Similar pattern was observed as in quiescent cells except there was no effect on the response, in comparison with control, when the cells were treated with either thaspine or PSB12062. Ivermectin positively modulated the response by 53.7 ± 5.6 % relative to control ($p < 0.001$, $n = 6$). When thaspine or PSB12062 was applied, there was no effect on the ATP-evoked response. Interestingly, when thaspine or PSB12062 was co-treated with IVM, both decreased the IVM-potentiated response by 56.9 ± 5.0 % and 40.6 ± 4.4 % (both $p < 0.001$, $n = 6$), respectively.

Taken from the two sets of data of quiescent and LPS-activated cells, several deductions could be made. Ivermectin positively modulated ATP-evoked response on both cell conditions but there was a clear difference in the magnitude of potentiation between the two cell states. The potentiation in LPS-activated cells was significantly greater than quiescent cells (by 10.9 %, $n = 6$). That was in agreement with Raouf et al. (2007) who discovered that IVM-potentiation was stronger in activated cells and attributed to the increase in upregulated expression of $P2X_4$ in activated cells. Meanwhile, there was no significant difference in response when PSB12062 was added to both cell conditions. However, the application of thaspine slightly potentiated the quiescent cells but did not affect LPS-activated cells. In terms of IVM-potentiated response, both thaspine and PSB12062 blocked the potentiation by IVM in both cell states. While the blockade strength by PSB12062 remained unchanged between the

two cell states (in relative to IVM-potentiated response), thaspine inhibition was stronger in activated cells.

3.3.4   Understanding the mechanism of action of thaspine

Subsequently, the mechanism of action of thaspine was investigated. Since thaspine was a slow acting compound, it was hypothesised that the reduction of response might not be due to a direct blockade of ATP binding. Rather, thaspine might cause the internalisation of $P2X_4$ receptors from the plasma membrane and that resulted in less receptors on the surface. Consequently, less calcium channels were present on the membrane that led to less calcium influx into the cells.

A flow cytometry experiment was used to test the hypothesis. In the experiment, the cells were labelled with an antibody that recognised extracellular epitope of $P2X_4$ receptors. The idea was to treat the cells with either 10 µM of thaspine or vehicle (0.1 % DMSO) to see the effect of the treatments. If the hypothesis were true, the fluorescence from the antibody would be less than the vehicle control, indicating a lower number of $P2X_4$ receptors on the plasma membrane.

To test the binding specificity of anti-$P2X_4$ antibody used, the non-transfected astrocytoma cells were labelled with the antibody to see if there was fluorescence. Figure 3.42 (panel A) shows that there was a significant increase in the median fluorescence intensity (MFI) ($p < 0.01$, $n = 3$) of the labelled non-transfected cells relative to isotype control which suggested that there were non-specific bindings. However, the increase in the MFI of human $P2X_4$ overexpressing cells was significantly higher than that of non-transfected cells (compare panel A and C of Figure 3.42, $p < 0.05$, $n = 3$) which suggested that the difference was the result of antibody binding to overexpressed $P2X_4$ receptors.

Figure 3.42 (panel C) shows the mean fluorescence intensity of isotype control and anti-$P2X_4$ labelled human $P2X_4$ overexpressing cells when treated with 0.1 % DMSO (vehicle control) or 10 µM of thaspine. In the presence of thaspine, the fluorescence was not significantly different from the vehicle control ($p > 0.05$, $n = 3$) which suggested that the number of $P2X_4$ receptors on the plasma membrane was not

reduced. Figure 3.42 (panel E) represents the histogram of anti-$P2X_4$ labelled human astrocytoma cells when treated with DMSO and thaspine. Both histograms overlapped each other indicating that the level of antibody binding was similar between the treatments.

An alternative explanation for these results was that the effect of thaspine was overcome during the course of experiment as the antibody labelling process took approximately 3 hours. Therefore, another experiment was designed for FlexStation 3 recording. The cells were treated and washed using the same protocol as the flow cytometry experiment, but they were challenged with ATP at the end of the procedure. This was to see if thaspine-treated cells regained their response as much as the control response because if the internalised receptors re-emerged, the inhibition would not be observed. Upon analysis, the results showed that the responses were still supressed compared to the control response even after 3 hours following thaspine treatment (36.3 ± 2.4 %, $p < 0.001$, $n = 3$), suggesting that the inhibition caused by thaspine was long term (Figure 3.43). Together, these suggested that thaspine did not alter the number of $P2X_4$ receptors on the plasma membrane.
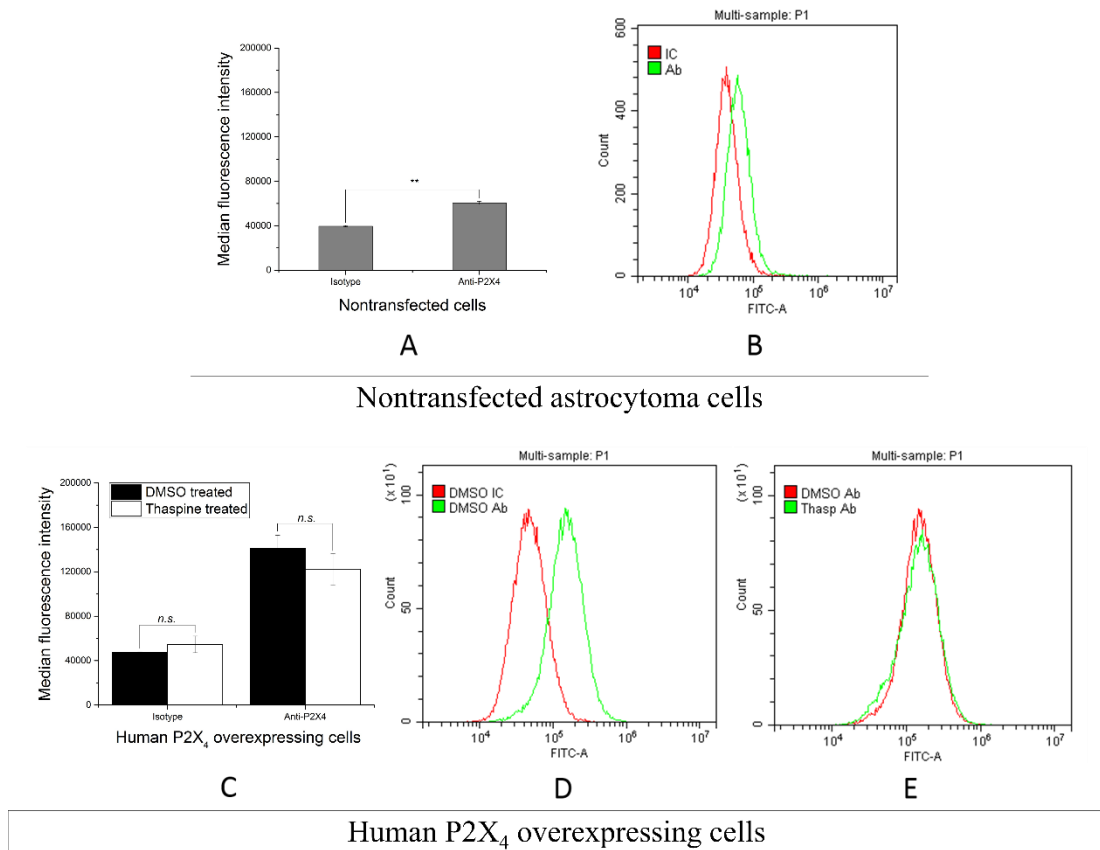
Nontransfected astrocytoma cells

Human P2X$_4$ overexpressing cells

Figure 3.42 Flow cytometry of the non-transfected astrocytoma and human P2X$_4$ overexpressing cells

The charts summarise the fluorescence of the non-transfected astrocytoma and human P2X$_4$ overexpressing cells when labelled with anti-P2X$_4$ antibody. A) MFI of isotype control and anti-P2X$_4$ labelled non-transfected astrocytoma cells, B) representative histogram of non-transfected astrocytoma cells where red curve is for isotype control and green is for anti-P2X$_4$ labelled cells, C) MFI of the human P2X$_4$ overexpressing cells that were treated with 0.1 % DMSO or 10 µM of thaspine, D) representative histogram of the human P2X$_4$ overexpressing cells where red curve is for isotype control and green is for anti-P2X$_4$ labelled cells, and E) representative overlaid histograms between DMSO- and thaspine-treated human P2X$_4$ overexpressing cells where red is for DMSO treatment and green is for thaspine treatment. The experiments were repeated three times and the histograms are representative from one repetition.
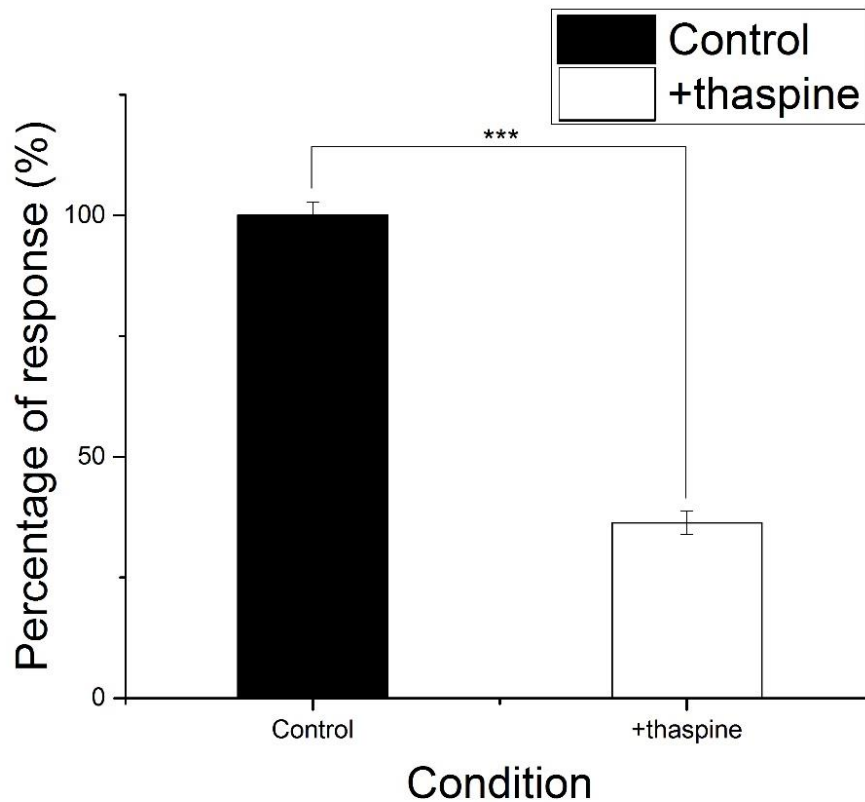
Figure 3.43 ATP-evoked response of the human P2X$_4$ overexpressing cells after being treated according to flow cytometry protocol.

The bar chart shows the ATP-evoked response of thaspine-treated P2X$_4$ overexpressing cells after using the same protocol as the flow cytometry experiment and being stimulated with 3 μM of ATP at the end of the protocol. The results showed that the response was still inhibited after a 3 hours protocol. The response was normalised to control response. Asterisk denotes p-value: $* = < 0.05$, $** = < 0.01$, $*** = < 0.001$. ($n = 3$)

Another proposed mechanism was based on its chemical properties. It was found that it has an XLogP3 value of 2.8 which suggested that the compound was a moderately lipophilic compound. Therefore, it was postulated that thaspine diffused through the plasma membrane and subsequently bound to the $P2X_4$ receptor on the internal epitope and changed the $P2X_4$ structure conformation. The theory was also based on the fact that it was a slow-acting drug as shown in Figure 3.31. The idea behind this theory was that thaspine required certain amount of time to penetrate into the plasma membrane and bind to intracellular epitope of $P2X_4$ before starting to effect the ATP-evoked calcium response.

To test this theory, thaspine was incubated with cells for 10 minutes in different percentages of DMSO. According to Williams and Barry (2012), increasing amount of DMSO made the plasma membrane more permeable, thus the penetration of thaspine could be easier and the effects of thaspine on ATP-evoked calcium response could be observed quicker. Figure 3.44 shows the inhibition observed at different percentages of DMSO. It could be clearly seen that the amount of inhibition increased as DMSO percentage increased. However, the data obtained was not substantial to draw a conclusive deduction if thaspine acted by crossing the plasma membrane and sequentially causing loss of calcium response.
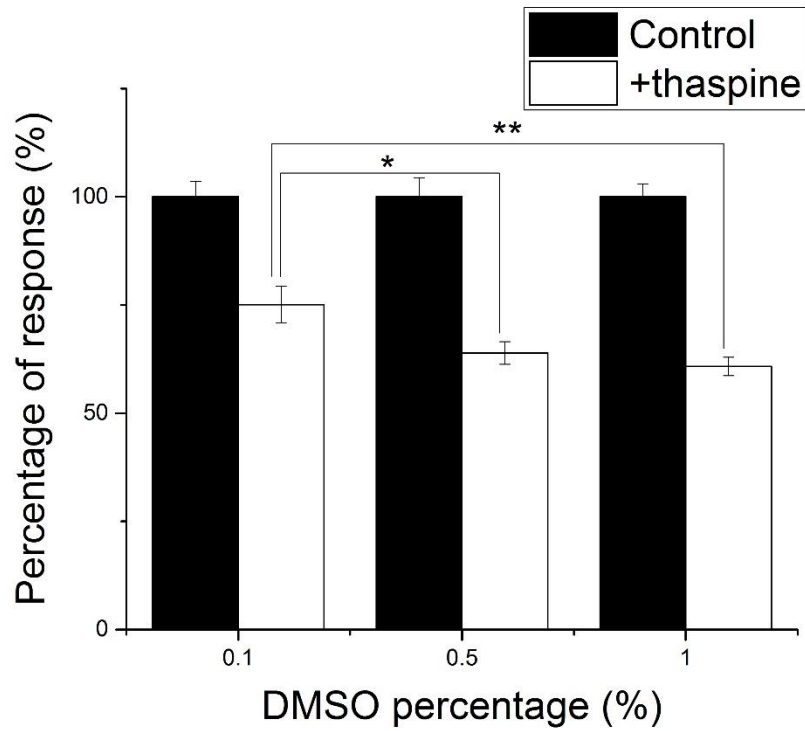
Figure 3.44 Effects of thaspine in different percentages of DMSO on ATP-evoked concentration-response.

The figure shows the effects of preincubation of 10 µM thaspine for 10 minutes on ATP-evoked response when thaspine was dissolved in different concentrations of DMSO prior to its treatment on cells. The amount of inhibition proportionally increased with DMSO percentage increment. The responses were normalised to control response for each condition. Asterisk denotes p-value: $* = < 0.05$, $** = < 0.01$, $*** = < 0.001$. ($n = 3$)

3.4 Discussion

3.4.1 Identification of thaspine as a P2X$_4$ inhibitor by high throughput screening

The process of identification of thaspine began with the establishment of the human P2X$_4$ overexpressing cells using astrocytoma. After its characterisation, high throughput screening was carried out using the overexpressing cells and hit compounds were further explored to finally choose one final compound as a lead, i.e., thaspine. Thaspine was further investigated in several experiments to elaborate more on its properties.

3.4.1.1 Transfection of human P2X$_4$

The human P2X$_4$ DNA was initially engineered into vector pIRESpuro3 and transfected using Fugene HD transfecting agent into astrocytoma cells. The bicistronic vector was a good vector because it could express two genes simultaneously, i.e., P2X$_4$ and puromycin resistant genes. The latter gene was very useful since it could be used to select cells that highly expressed P2X$_4$ using puromycin and maintain high expression of P2X$_4$ receptors. However, the transfection technique failed to establish a stable overexpressing cell line. One successful transfection out of several trials suggested that the transfection technique was not efficient as puromycin treatment caused the death of transfected cells.

However, the viral transfection technique employed later showed success using pLVX-IRES-mCherry vector. Instead of carrying antibiotic resistance gene, the vector co-expressed mCherry fluorescent protein which was used as a marker for selection using BD FACSAria III Sorter. Throughout this study, the cells were constantly monitored to avoid over-confluency because the cells tended to switch off the expression of P2X$_4$ under stress, as evidenced by reduced magnitude of calcium response and mCherry fluorescence. In addition, only cells passaged up to five times were used in this study to maintain high expression. Overall, these overexpressing cells — containing P2X$_4$ DNA engineered into pLVX-IRES-mCherry and virally transfected — were a good model for high throughput screening. The high response

elicited by the cells (maximal response about 1.0 – 1.3 F ratio) made it more conducive for high throughput screening because the inhibition could easily be seen.

3.4.1.2 Identification of thaspine through high throughput screening

High throughput screening performed in this study has successfully narrowed 1,710 compounds from NCI down to thaspine, which was found to be a potent inhibitor of $P2X_4$ receptor. The method of screening by measuring calcium influx into the cells based on fluorescence was a good method for high throughput screening to discover $P2X_4$ modulators. A handful of studies used the cytosolic calcium measurement as an indicator of $P2X_4$ activity (Ase et al., 2015; Balazs et al., 2013; Hernandez-Olmos et al., 2012; Matsumura et al., 2016). When $P2X_4$ receptors were activated by ATP, calcium entered the cells which would then bind to Fura-2 that was subsequently excited and emitted light for detection. This directly gave a reading on the amount of cytosolic calcium, representing the activation of $P2X_4$ receptors. Excitation of Fura-2 at two wavelengths, i.e., 340 and 380 nm, was a great advantage of this dye because resulting ratiometric reading cancelled out confounding variables such as cell thickness, uneven dye loading, and photobleaching (Tsien & Poenie, 1986). Fura-2 also accurately measured calcium in the cytosol and did not take into account calcium that resided in intracellular stores such as nucleus and endoplasmic reticulum (Williams et al., 1985). Thus, it was a robust dye to detect influx of calcium into the cytosol in response to activation of $P2X_4$ receptor by ATP. It is also worth mentioning that, to date, this was the first study that involved high throughput screening of a library of natural compounds for $P2X_4$ receptor modulators.

In the high throughput screening, two filters were applied to exclude false positives. The criteria for the first filter was that the screened compounds must have potentiated at least 75 % response or inhibited at least 60 % of the vehicle control responses. The criteria for the second filter was that the compounds must not have modulated the baseline of F ratio reading by ±0.25 F ratio after compound addition. Based on the screening of 1,710 compounds, a total of 87 compounds were identified to modulate ATP-evoked responses after primary filter. Thirty-one of them potentiated and 56 compounds inhibited the response. Referring to Figure 3.19, the response of most tested compounds was seen to fluctuate around control response (100 %). Seeing a

large portion of responses were confined to one region, i.e., between 80 and 150 % response, it was suggested that the modulation within that region was a result of variability, due to various reasons including inadequate technical repeat, solubility of compounds, pipetting error, and uneven cell density. Therefore, the exclusion boundaries were set outside of the region to identify potential potentiators and blockers.

Next, the observation on the Flexstation 3 data revealed that the addition of some compounds into the buffer distorted the Fura-2 fluorescence baseline signal and loading value. There was a trend observed in which when a compound caused a peak on the baseline and uncommonly high value of Fura-2 loading after addition of a compound, it would appear to potentiate the subsequent ATP-evoked response. Similarly, when a compound caused a sharp decline on the baseline and unusually low value of Fura-2 loading, the ATP-evoked response afterwards would be reduced. For example, compound NSC193043 caused a large peak in the baseline signal (8.3 F ratio, $n = 1$) and it potentiated ATP-evoked response by 87 %.

The potentiation observed might be a result of auto-fluorescence of the compound that gave rise to the response which was a common disadvantage in fluorescence-based assay, as reported by Pope et al. (1999). Another explanation is that, maybe the compounds caused the increased permeability of plasma membrane which allowed calcium influx. Another deduction was that such compounds might lyse the cells that in turn released Fura-2 into extracellular environment that was highly concentrated with calcium. Another reason was that the compounds might have activated other calcium transporting signalling which resulted in calcium influx. On the other hand, dips observed on the baseline after addition of some compounds might be a result of quenching the fluorescence of Fura-2 or could also be a result of auto-fluorescence that interfered with emission light by Fura-2. While these deductions were made to explain the situation, there might be many other reasons that could have caused this discrepancy. Therefore, a second inclusion criterion was applied to reduce the amount of false positive results, which resulted in the recognition of eight positive modulator and six inhibitor hits, and subsequently NSC17055 was chosen as the lead compound.

However, further investigation revealed that the NSC17055 was also a false positive. One obvious indication was that one of its analogues (STK331042) did not show any fluorescence reading in an inhibition screening experiment whereas this was not observed in other compounds. Upon studying the structure activity relationship between NSC17055 and its analogues towards the P2X$_4$ activity, it was found that there was a structural similarity in all compounds. All the "inhibiting" analogues contained a coumarin backbone and a polar functional group at carbon number 7 (R group, refer to Figure 3.45). Based on the tested analogues, only compounds with either acetate (7-acetoxy) or hydroxyl (7-hydroxyl) at R position were found to "inhibit" P2X$_4$ activity. Substituting R group with methoxy ($-CH_3$) or hydrogen completely eradicated the "inhibitory" characteristic. Findings by Sherman and Robins (1968) stated that the backbone of the compound, 7-hydroxycoumarin was a fluorescent molecule. Mostovnikov et al. (1977) also described the auto-fluorescence property of coumarin and its derivatives, particularly 7-hydroxycoumarin and 7-acetoxycoumarin, which confirmed the findings in the present study. Their further investigation revealed that the excitation wavelength of the studied compounds overlapped with the excitation wavelength of Fura-2 but their emission wavelengths were different. Thus, it was postulated that NSC17055 and its analogues absorbed the excitation light and therefore reduced the excitation and emission of Fura-2.
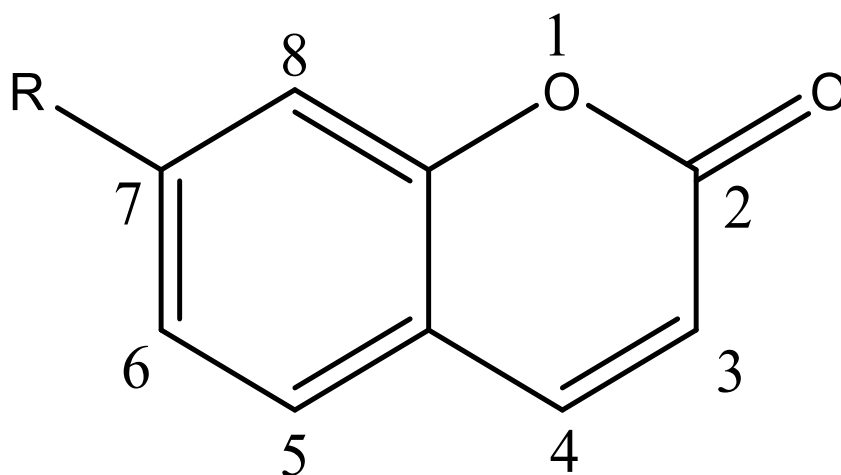
Figure 3.45 Chemical structure of coumarin

The chemical structure above is the backbone of NSC17055 and its analogues. The numbering was based on IUPAC numbering. The differences were some compounds had an additional functional group at carbon number 3 which did not affect the auto-fluorescence characteristic. The vital functional group that affected auto-fluorescence was at carbon number 7, labelled as R. Polar functional group such as acetoxy and hydroxyl displayed auto-fluorescence characteristic while non-polar like methoxy did not. Carbonyl group at carbon number 2 was also crucial as when one compound that had carbonyl group at carbon number 4 instead at number 2, lost the auto-fluorescence property.

3.4.1.3 Verification of high throughput screening results

To further discount false positives, an experiment using ionomycin and carbachol was employed. Ionomycin was reported as an ionophore that mobilises calcium through different pathways. It was suggested to translocate calcium across the plasma membrane (Liu & Hermann, 1978; Pressman & Fahim, 1982), to activate the native calcium channels that allow calcium influx, and to cause calcium release from intracellular store via phospholipase (Dedkova et al., 2000; Morgan & Jacob, 1994). Meanwhile, carbachol was reported to activate muscarinic acetylcholine receptors that mediate extracellular calcium influx through voltage-dependent calcium channels and also calcium release from intracellular stores (Blackwood & Bolton, 1993). Together, both ionomycin and carbachol action are deductively independent of $P2X_4$ activation and therefore, it can be inferred that any compounds that cause modulation on ionomycin- or carbachol-evoked responses might do so via different pathways and not by directly inactivating $P2X_4$.

The outcomes of the experiment suggested that five of the six potential inhibitor hits significantly decreased both ionomycin- and carbachol-evoked responses including NSC17055. The magnitude of inhibition was also similar between ionomycin- and carbachol-evoked responses of each compound. Those compounds either acted on different pathways that affected calcium regulation intracellularly or interfered with Fura-2 fluorescence. For example, the backbone structure of NSC50688 was 2-naphtol which was reported to have an auto-fluorescence characteristic (Boyer et al., 1985; Wu & Hurtubise, 1993). This has left one compound that did not have a significant effect on the ionomycin- and carbachol-evoked responses, which was thaspine.

Since the screening was performed once in triplicate, it was anticipated that the variabilities present in data would create false positives. Apart from that, it was also acknowledged that another caveat of this fluorescence-based screening method was that there would also be false negative results of which the exclusion criteria might have excluded the true potential modulators. Thus, fluorescence-based assay could be a good tool for high throughput screening if combined with additional tests to control the experiment, such as increasing technical repeats, applying strict cut off points, measuring baseline alteration after compound addition, observing Fura-2 loading

values after compound addition, and ionomycin and carbachol tests. It is also worth noting that the use of astrocytoma cells in this screening had advantage because the data obtained indicated astrocytoma cells had no endogenous ATP response up to 600 µM, which was in parallel with Ballini et al. (2011). Therefore, the measured calcium response following ATP application on the human $P2X_4$ overexpressing cells was exclusively due to the activation of $P2X_4$ receptor alone.

3.4.1.4 Thaspine characterisation

The screening has successfully identified thaspine as an inhibitor of human $P2X_4$ receptor. Thaspine is an alkaloid extracted from the South American tree, *Croton lechleri*. It was reported to have anticancer activity by causing apoptosis on human colon carcinoma cell line. At a molecular level, it inhibited topoisomerase which are involved in cleavage and resealing of DNA strands during replication process and that results in apoptosis of cancerous cells (Castelli et al., 2013; Fayad et al., 2009). Apart from that, it was also shown to have an anti-inflammatory activity (Perdue et al., 1979). To date, it has not been reported in literatures other than cancer- and inflammation-related studies. Following the identification, several characterisation experiments were carried out to understand its potency, mode of its inhibition, selectivity, reversibility, and mechanism of action.

3.4.1.4.1 Thaspine inhibition concentration-response

From the obtained data and analysis, it was shown that thaspine had an IC_{50} value of 3.81 ± 0.2 µM at human $P2X_4$ and 3.53 ± 0.26 µM at mouse $P2X_4$. The shape of curves was also the same, suggesting that they had the same threshold concentration for thaspine to start taking effect. At 30 µM of thaspine concentration, the responses were completely abolished. Since human and mouse $P2X_4$ share 87 % similarity in their amino acid sequence, it was predicted that thaspine would have similar potency at these two receptors. Tian et al. (2014) and Hernandez-Olmos et al. (2012) also observed the same pattern when their novel compounds acted on both human and mouse $P2X_4$.

To exclude the possibility of thaspine action was cell-dependent, thaspine was then tested on human $P2X_4$ which was overexpressed in different cell type, HEK293F. Since HEK293F also carries the endogenous P2Y receptors (Gerevich et al., 2007; Schachter et al., 1997), CTP — which does not activate P2Y — was used as the agonist. Thaspine's potency at human $P2X_4$ receptor in this cell line was comparable to astrocytoma cells, with an IC_{50} value of $3.99 \pm 1.0\,\mu M$, suggesting that thaspine was active at inhibiting human $P2X_4$ regardless of the cell system used. The use of CTP instead of ATP on this cell system also indicated that the effects of thaspine were independent of agonist. Further comparison analysis of representative traces of ATP-evoked response with and without thaspine (Figure 3.27) revealed that thaspine only affected magnitude of peak response, but not decay kinetics.

3.4.1.4.2 Mode of inhibition

In an experiment to determine thaspine mode of inhibition, the highest concentration of ATP used ($100\,\mu M$) failed to overcome thaspine inhibition and produce calcium response as high as the vehicle control, in addition to unaltered values of EC_{50} ($0.44 \pm 0.1\,\mu M$ and $0.48 \pm 0.2\,\mu M$ for vehicle control and thaspine-treated cells, respectively). Together, these evidences were in line with common characteristics of a noncompetitive antagonism, as explained by Hollinger (2007), who stated that such noncompetitive antagonism can be a result of either two occurrences: 1) compound binding to orthosteric site irreversibly or pseudo irreversibly (a very small dissociation constant) which disallows the binding of agonists; or 2) compound binding to allosteric site which then may alter the binding motif of orthosteric site for agonists. But the latter mode can be excluded by the fact that allosteric noncompetitive inhibitor could totally diminish the agonist response. And this was the case based on the concentration-response curve, where thaspine totally abolished the ATP-evoked response, indicating that it was an allosteric inhibitor.

3.4.1.4.3 Reversibility of thaspine

Thaspine was found to be a noncompetitive inhibitor since the increasing amount of agonist could not surmount thaspine inhibition. Noncompetitive inhibitors are mostly irreversible due to their covalent binding with receptors (Foreman & Johansen, 2003;

Katzung et al., 2012). Washing the cells with thaspine-free buffer was expected displace thaspine from its binding, and the change in response to the agonist application could have been observed. However, the data from reversibility experiment showed that the second stimulation by ATP could not restore the response as high as the vehicle control. The results suggested that thaspine was not displaced by washing and thus, remained the binding and inhibited the receptors.

3.4.1.4.4 Thaspine inhibition was slow-acting

Next, experimental data demonstrated that the action of thaspine was slow-acting. The data showed that pre-incubation of thaspine prior to ATP stimulation for 5 minutes did not cause a significant reduction in ATP-evoked response. Longer pre-incubation period progressively and significantly decreased the response. The first significant inhibition was observed after thaspine pre-incubation for 10 minutes, relative to the vehicle control. As the pre-incubation period increased, the inhibition became stronger with 40 minutes pre-incubation being the most optimum period for maximum inhibition. Its slow-acting effect might suggest two hypotheses pertaining to its mechanism of action: 1) thaspine did not directly affect $P2X_4$, but rather caused the internalisation of $P2X_4$ receptors. As previously described, $P2X_4$ receptors are continuously cycled in and out between the plasma membrane and lysosomes and late endosomes (Bobanovic et al. 2002), so it could be that thaspine inhibited the reinsertion of $P2X_4$ into the plasma membrane or promoted the internalisation of $P2X_4$, or both, and consequently reduced the number of activated $P2X_4$ receptor, calcium influx, and eventually fluorescence reading; or 2) thaspine diffused through the plasma membrane. Having an XLogP3 value of 2.8 (PubChem database), thaspine is relatively hydrophobic and that might help it diffuse through hydrophobic tail of the phospholipid bilayer. Once inside the cells, it might act on $P2X_4$ intracellular epitope or interfere with other calcium intracellular signalling pathways.

3.4.1.4.5 Mechanism of action

To determine its mechanism of action, the two hypotheses were tested. The first hypothesis was tested by quantitating the number of $P2X_4$ receptors present on the plasma membrane in response to treatment of thaspine or vehicle control for 30 minutes. This was achieved by labelling the extracellular epitope of $P2X_4$ receptor with $P2X_4$ antibody which was then labelled with AF488-conjugated secondary antibody. The fluorescence of AF488 was subsequently detected using flow cytometry technique. The results suggested that pre-incubation of thaspine did not markedly reduce the cell surface expression of $P2X_4$ receptors compared to the vehicle control. Nevertheless, it was argued that the result might be partly due to the lengthy procedure of antibody labelling which might cause the re-emergence of $P2X_4$ receptors on the plasma membrane. The data from Figure 3.32 and Figure 3.43, however, suggested that thaspine inhibition was irreversible. Therefore, the data together suggested that thaspine might not cause the internalisation of $P2X_4$ receptors though more experiments are required to come to a solid conclusion.

In regards to the second hypothesis, Williams and Barry (2012) mentioned that DMSO could enhance the drug penetration through the plasma membrane by decreasing the barrier resistance. Therefore, to test the second hypothesis, different percentages of DMSO was used to dissolve thaspine to reflect thaspine penetration level and thaspine was pre-incubated for only 10 minutes. Theoretically, a higher DMSO percentage would increase magnitude of inhibition since more thaspine could penetrate the plasma membrane in a limited time. Based on analysis, it showed that it was the case. The inhibition with 0.5 and 1 % DMSO was significantly higher than 0.1 % which was the amount of DMSO used in any thaspine experiment in this study. However, it could also be argued that the increase in inhibition along with the increase in DMSO percentage might be due to thaspine being more soluble in higher DMSO percentage and thus, the compound delivery to receptors was more efficient. Therefore, more experiments should be employed to reach a conclusive remark. In short, the results obtained were incomplete to explain the mechanism of action for thaspine.

3.4.1.4.6 Selectivity study

Meanwhile, the selectivity study revealed that 10 µM of thaspine was $P2X_4$-selective versus $P2X_2$, $P2X_7$, and heteromer $P2X_{2/3}$. Meanwhile, at $P2Y_2$ and $P2Y_6$, thaspine was inactive at concentrations of 10 µM and 30 µM, respectively but it abolished the response at concentrations above those. The concentration-independent inhibition of thaspine at the P2Y receptors might be due to thaspine interfere with later stages of P2Y signalling pathways.

3.4.1.4.7 Effect of thaspine on BV2 cells

Thaspine was also tested on primary cell model, BV2 cell (murine microglial cell line) which are known to express metabotropic P2Y and ionotropic P2X receptors (Ferrari et al., 1996; Haas et al., 1996; Walz et al., 1993). The response elicited by ATP stimulation in this experiment was a collective contribution of those receptors. By comparing the representative traces of quiescent and LPS-activated cells (Figure 3.40 and 3.41), it could clearly be seen that the magnitudes of potentiation by IVM between the two cell states were significantly different ($p < 0.05$, $n = 6$). This was because LPS induced inflammatory response and in LPS-activated cells, the expression of $P2X_4$ receptor was upregulated (Raouf et al., 2007). This in turn caused more $P2X_4$ receptors available on cell surface that could be activated by ATP. Being a selective $P2X_4$ positive allosteric modulator, IVM therefore could potentiate more $P2X_4$ receptors that in turn gave higher rise in the potentiation in the LPS-activated cells.

In terms of inhibition, PSB12062 (a known $P2X_4$ inhibitor) did not affect the ATP-evoked response in both quiescent and LPS-activated cells. This could be that the response recorded was largely due to purinergic receptors other than $P2X_4$ receptor. But when PSB12062 was co-treated with IVM, the inhibitor significantly suppressed the ATP-evoked response which suggested that IVM potentiated $P2X_4$ receptors that were subsequently inhibited by PSB12062. Meanwhile, thaspine did not affect the ATP- response of LPS-activated cells but interestingly potentiated the response of quiescent cells. It was likely that thaspine potentiated other purinergic receptors in the quiescent cells. On the other hand, when thaspine was co-treated with IVM, the inhibition in activated cells was larger than quiescent cells. This could be explained by

the fact that there were more $P2X_4$ receptors in the activated cells than quiescent cells, hence the inhibition became larger.

CHAPTER 4

STRUCTURE ACTIVITY RELATIONSHIP STUDY OF 5-BDBD AND P2X$_4$ RECEPTOR

4.1   Introduction

In 2004, Fischer et al. discovered a novel compound, known as 5-BDBD, that potently inhibited P2X$_4$ receptor heterologously expressed in Chinese hamster ovary cells. The group claimed that 5-BDBD has the potential to treat arteriosclerosis and restenosis in human and animals via the blockade of P2X$_4$ receptor. However, the reports were in the form of a commercial patent and there were no other elaborative reports on the characterisation of the compound. A decade later, Balazs and co-researchers (2013) made an extensive study on the compound as well as a known P2X inhibitor, TNP-ATP, which is less sensitive at P2X$_4$ receptor than P2X$_1$ and P2X$_3$ (Jarvis & Khakh, 2009). They studied the inhibitory effects of both antagonists in two ways, i.e., by measuring intracellular Ca^{2+} signals and whole cell ion currents in P2X$_4$ overexpressing HEK293 cells. They found that 5-BDBD and TNP-ATP inhibited the P2X$_4$-mediated Ca^{2+} influx in a concentration-dependent manner in both methods and their IC$_{50}$ values were 1.2 µM and 1.5 µM, respectively. In addition, their data showed that 5-BDBD blocked P2X$_4$ competitively based on the increased ATP EC$_{50}$ values when the cells were treated with 2 µM and 20 µM of 5-BDBD. On the other hand, in a more recent study, Abdelrahman et al. (2017) reported that the inhibition was noncompetitive which indicated that 5-BDBD bound to an allosteric site on the receptor. The proposed mode of action was determined using a radiolabelled ATP analogue, which was not being displaced by the increasing concentration of 5-BDBD.

The lack of information and discrepancy about 5-BDBD mode of inhibition highlighted a gap that needed to be filled. Ten compounds were synthesised in laboratory and eight compounds were purchased commercially. The list of compounds used in this study is tabulated in Table 2.5 and 2.6. The analogues manipulated three substitution sites, numbered from 1 to 3 to assist explanation (as shown in Figure 4.1).

The basis on the selection of substitution sites were according to the original patent by Fischer et al. (2004) who described that substitutions at either site 1 and 3 produced similar magnitude of inhibition for P2X$_4$ receptor. Firstly, the sites were substituted with halogens other than bromine to see if the size of halogen plays any role in the inhibition potency. Secondly, it has been widely reported that trifluoromethyl can enhance the activity of a molecule. The history of the advantages of fluorine-containing compounds was first reported by Lehmann (1928) (as reviewed by Yale (1959)) who found that benzotrifluoride positively affected the central nervous system of frogs. Later, the success of molecules containing trifluoromethyl group was reported in numerous articles which were reviewed by Yale (1959). Thus, it was decided to substitute site 1 and 3 with trifluoromethyl group to see if the substitutions can also enhance the inhibition. Thirdly, it was also interesting to see if a simultaneous halogen substitution at site 1 and 3 will affect the inhibition potency. Lastly, apart from the synthesis of modified compounds, it was also decided to look at the readily available analogues of 5-BDBD. The search for the analogues were done via MolPort web-based server, which was set up to show similar compounds with 5-BDBD by 0.8 similarity based on the Tanimoto index.
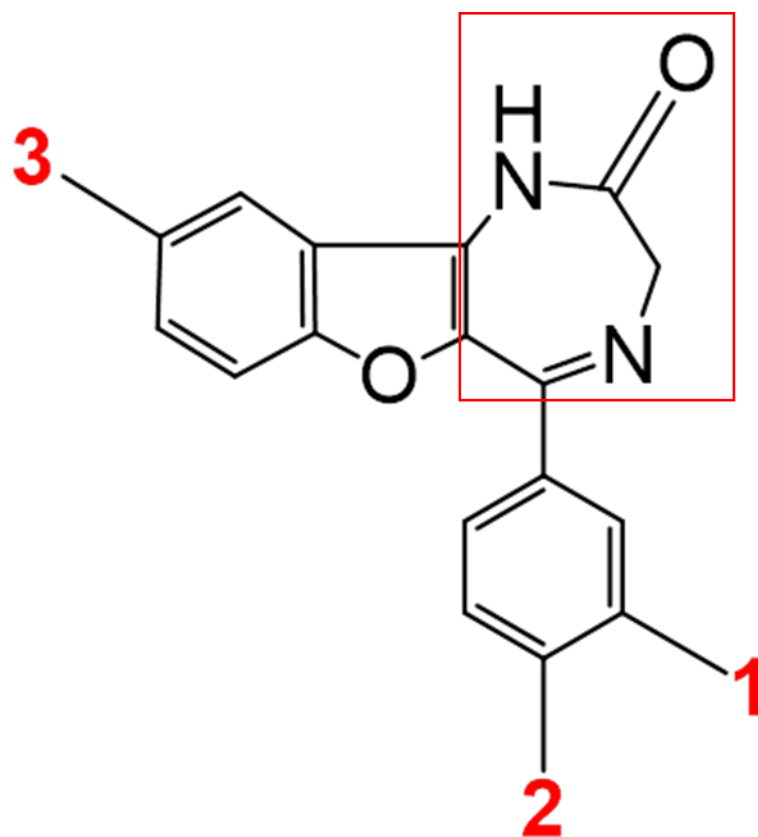
Figure 4.1 Sites of chemical modification of 5-BDBD backbone

The chemical structure in the figure shows the backbone structure of 5-BDBD. Three sites were manipulated to study the relationship between P2X$_4$ receptor and 5-BDBD. Substitution site 1 is meta-positioned at phenyl, substitution site 2 is para-positioned at phenyl and substitution 3 is at carbon number 9 of benzofurodiazepinone. If there is no substitution, it means that the substitution sites are filled with hydrogens. The red box indicates the diazepinone, a seven-membered heterocyclic compound with two nitrogen atoms and a ketone functional group (R – O – R) attached to the ring, which was absent in one of the purchased analogues (STK021512).

To investigate the structure–activity relationship between 5-BDBD and P2X$_4$ receptor, pharmacological and in silico investigations were employed. In terms of pharmacological investigation, the potency and mode of action of compounds were determined to see if structural variation caused the significant effect on their potency and mode of action, relative to 5-BDBD. These experiments were performed using the same protocol as in the previous chapter. To study the binding at structural level, 5-BDBD and its analogues were docked virtually (experiment performed by Dr Marco Cominetti). This technique has become feasible with the findings of Hattori and Gouaux (2012), where crystal structures of zfP2X$_4$ in closed (PDB ID: 4DW0) and open state ATP-bound (PDB ID: 4DW1) state were solved. The protein sequence similarity between human and zebrafish is 67 %, based on the comparison between accession number AAF06661.1 (human, from NCBI database) and 4DW0_A (zebrafish, from PDB).

The crystal structure of the closed, resting state P2X$_4$ (4DW0) was used as a template to simulate the binding of 5-BDBD into its binding pocket (homology modelling to build human P2X$_4$ was done by Associate Professor Dr Ralf Schmid). This was based on pharmacological protocol conducted in this study where 5-BDBD was pre-incubated for 30 minutes prior to ATP stimulation, which suggested 5-BDBD could bind to the closed state P2X$_4$ and block the stimulation by ATP. Although there were concerns regarding the crystal structure because of truncation of both termini, it was shown that it only affected the gating mechanism and pore opening but not the binding itself (Habermacher et al., 2015; Mansoor et al., 2016). Since this simulation only involved the docking between the compounds at orthosteric site, so the closed, resting state crystal structure was used. The experiment was carried out to study the possible docking poses that can explain the position of 5-BDBD in the pocket, and recognise important amino acids on P2X$_4$ receptor and functional groups on 5-BDBD that play a role in binding.

4.2 Aims

The aim of this study was to pharmacologically investigate the structure activity relationship between human P2X$_4$ and 5-BDBD and its analogues, identify important

functional groups for antagonistic action, and predict the binding modalities using molecular modelling.

4.3 Results

4.3.1 Pharmacological characterisation of 5-BDBD

Before investigating the effects of altering 5-BDBD structure, 5-BDBD was first investigated to compare its characteristics with the altered compounds. The potency and mode of inhibition of 5-BDBD were first determined. Figure 4.2 displays the inhibition concentration-response curve for 5-BDBD. Based on three experiment repeats on the human P2X$_4$ overexpressing cells, the calculated IC$_{50}$ value was $1.6 \pm 0.63\,\mu M$ ($n = 3$) which was close to the reported value of $1.2\,\mu M$ (Balazs et al., 2013). The peak response started to decrease when $0.3\,\mu M$ of 5-BDBD was applied and reached a plateau at $10\,\mu M$. The strongest inhibition was observed at $10\,\mu M$, which was $54.6 \pm 10.8\,\%$ relative to the peak response of control.

Figure 4.3 shows the ATP concentration-response with and without 5-BDBD. In the presence of 5-BDBD, the calcium response reached the same maximal magnitude as without 5-BDBD, but at a slower rate, which shifted the calcium response curve to the right. This also made the EC$_{50}$ value of ATP for the treated cells significantly higher than the untreated ($1.9 \pm 0.10\,\mu M$ versus $0.6 \pm 0.08\,\mu M$, respectively ($p < 0.05$, $n = 4$). Taken together, these suggested that the mode of inhibition of 5-BDBD was competitive, which was in agreement with Balazs et al. (2013).
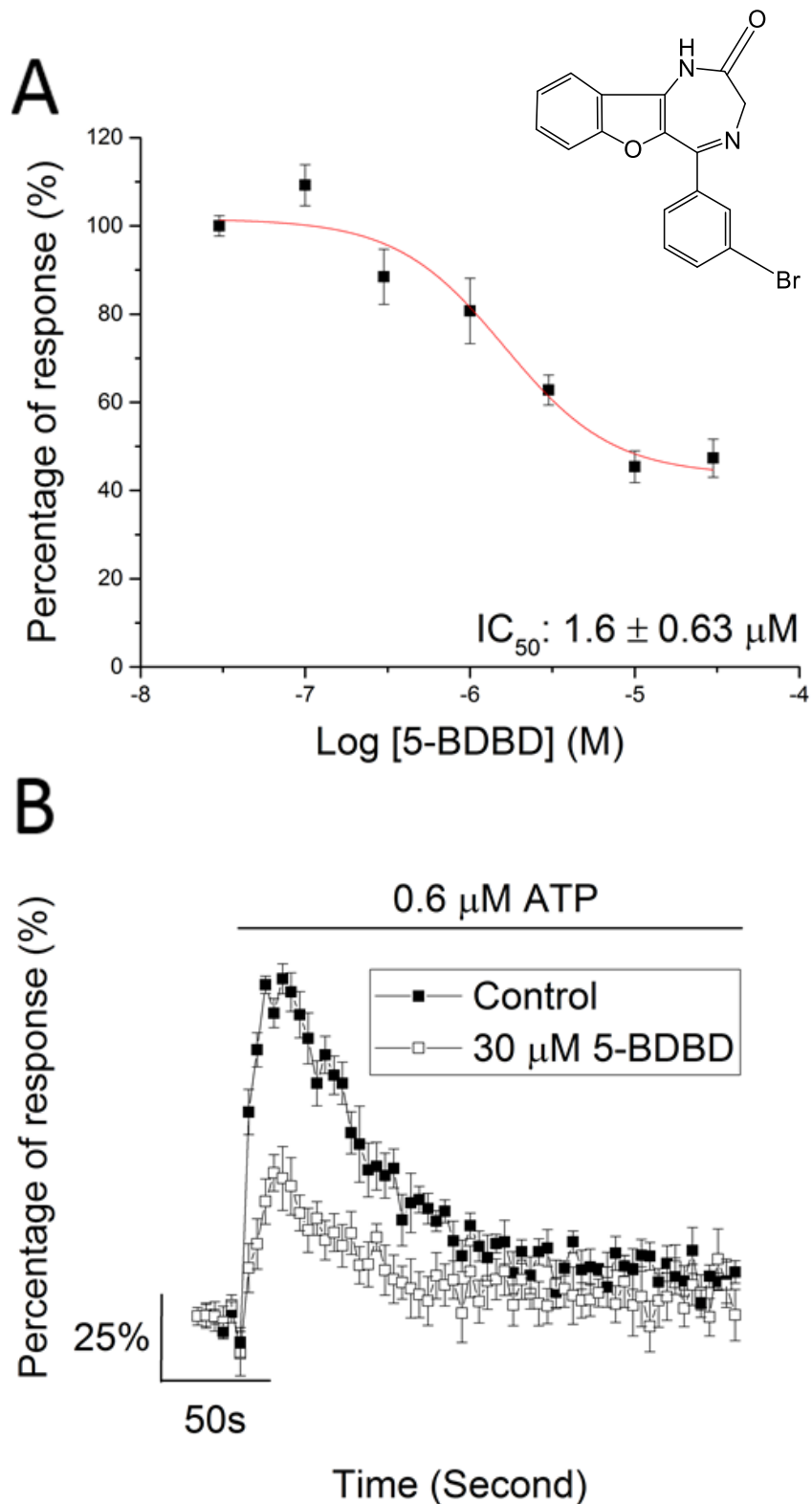
Figure 4.2 Inhibition concentration-response for 5-BDBD at human P2X$_4$ receptor.

Panel A shows the inhibition concentration-response curve for 5-BDBD (0.03 – 30 µM) when the human P2X$_4$ overexpressing cells were stimulated with 0.6 µM of ATP. Panel B shows the representative traces in the absence and presence of 30 µM of 5-BDBD dissolved in 1 % DMSO. All responses were normalised to mean peak response of vehicle response. The inset shows the chemical structure of 5-BDBD. ($n = 3$)
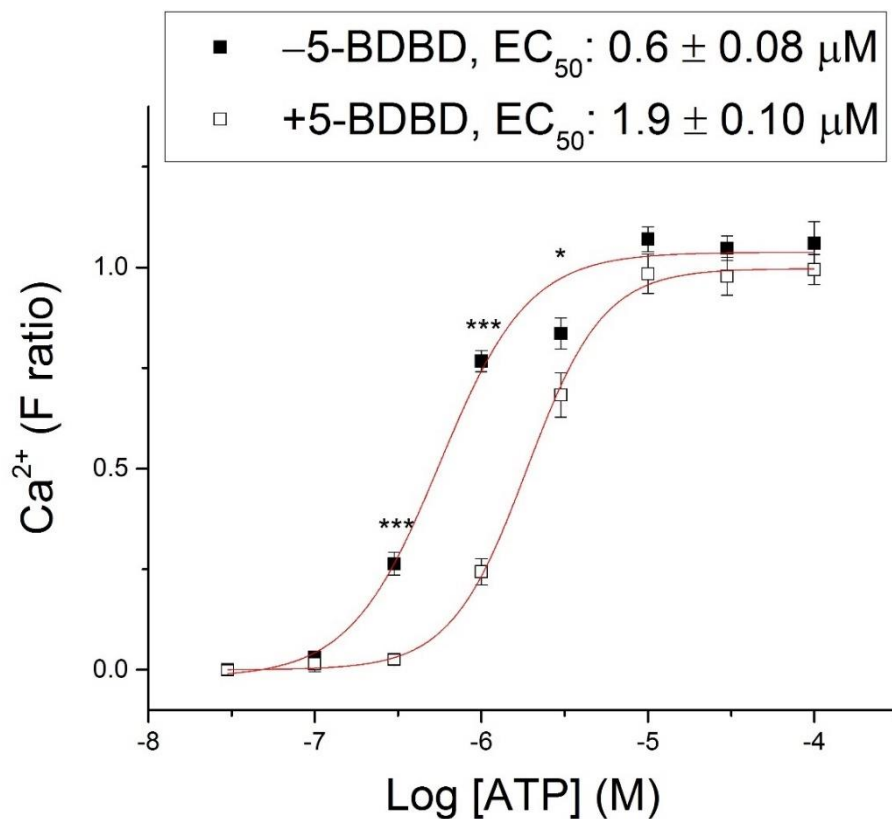
Figure 4.3 ATP concentration-response in the absence and presence of 5-BDBD. The plots show the ATP concentration-response curves of untreated (close square) and 5-BDBD-treated (open square) human P2X$_4$ overexpressing cells. The concentrations used were 0.03 to 100 µM for ATP and 1.6 µM for 5-BDBD. The difference between each data point was statistically calculated. The responses from both cell conditions were significantly different at 0.3, 1, and 3 µM of ATP before both equalled at 10 µM of ATP. The difference between both EC$_{50}$ values was also significant ($p < 0.05$). The right shift of ATP concentration-response curve and significant increase in EC$_{50}$ of ATP for treated cells compared to the vehicle control indicated a competitive mode of antagonism. Asterisk denotes p-value: * = < 0.05, ** = < 0.01, *** = < 0.001. ($n = 4$)

4.3.2 Potency determination of 5-BDBD analogues

To further investigate the effects of manipulating substitution sites on the potency of 5-BDBD analogues, their IC_{50} values were determined by establishing the inhibition concentration-response curves. Varying concentrations of compound were used: 0.03, 0.1, 0.3, 1, 3, 10, and 30 µM, to plot the inhibition concentration-response curves while ATP concentration used was 0.6 µM, corresponded to ATP EC_{50} value. The curves were plotted using the values of mean peak response of each compound concentration, which were normalised to mean peak response of vehicle control.

4.3.2.1 Halogen substitution at site 1 or 3

To investigate the effect of substituting site 1 or 3 with other halogens (5-BDBD has bromine at site 1), chlorine and fluorine were chosen. Figure 4.4 presents the inhibition concentration-response curve for STK731427 and its representative traces of responses. In terms of chemical structure, this compound had its substitution site 3 replaced with bromine. Calculated IC_{50} value was 1.0 ± 0.43 µM, not significantly different ($p > 0.05$, $n = 3$) compared to 5-BDBD. However, the maximum inhibition recorded at 30 µM was 47.1 ± 14.4 % which was significantly lower than 5-BDBD by 8.9 % ($p < 0.05$, $n = 3$). The first inhibition in peak response was noted when the cells were treated with 0.3 µM compound and the inhibition plateaued at 10 µM of STK731427.

Figure 4.5 shows the inhibition concentration-response curve for IA1 and its representative trace of response in the absence and presence of 30 µM of IA1. This compound had its substitution site 1 substituted with chlorine. The inhibition was first recorded at 0.1 µM compound, exponentially increased at higher concentrations, and plateaued at 10 µM. From the curve, the calculated IC_{50} value was 2.3 ± 0.28 µM, not significantly different ($p > 0.05$, $n = 3$) from 5-BDBD. The maximum inhibition measured was 55.3 ± 3.8 % when 30 µM of compound was applied, which was similar to 5-BDBD maximum inhibition ($p > 0.05$, $n = 3$).

Next, Figure 4.6 shows the inhibition concentration-response curve for IA9 and its representative trace of response. IA9 had a chlorine substitution at position 3. The IC_{50} value obtained from the curve was 1.1 ± 0.65 µM, not significantly different ($p > 0.05$, $n = 3$) from that of 5-BDBD. The strongest inhibition observed at the highest concentration of IA9 (30 µM) which was not significantly different from 5-BDBD (72.9 ± 6.2 %, $p > 0.05$, $n = 3$).

Meanwhile, Figure 4.7 shows the inhibition concentration-response curve for IA6 and its representative trace when 30 µM of IA6 was added. Structurally, site 3 of this compound was substituted with fluorine. The compound started to inhibit at 0.1 µM and it progressively reduced the response until it reached its maximum inhibition at 3 µM. The calculated IC_{50} value was 1.2 ± 0.18 µM and the maximal inhibition recorded was 55.0 ± 2.9 % when the cells were treated with 30 µM of IA6, which were both not significantly different ($p > 0.05$, $n = 4$) from that of 5-BDBD.

Lastly, Figure 4.8 shows the inhibition concentration-response curve for IA11 and its representative trace of response from treated and untreated cells. Structurally, IA11 had its position 1 substituted with fluorine. From the curve, the inhibition was only observed when the cells were treated with 3 µM and it plateaued at 10 µM. The maximum inhibition was recorded at 30 µM which was 51.9 ± 2.6 %, not significantly different ($p > 0.05$, $n = 3$) from 5-BDBD. On the other hand, the IC_{50} value was significantly increased compared to 5-BDBD, 4.5 ± 0.63 µM ($p < 0.05$, $n = 3$).
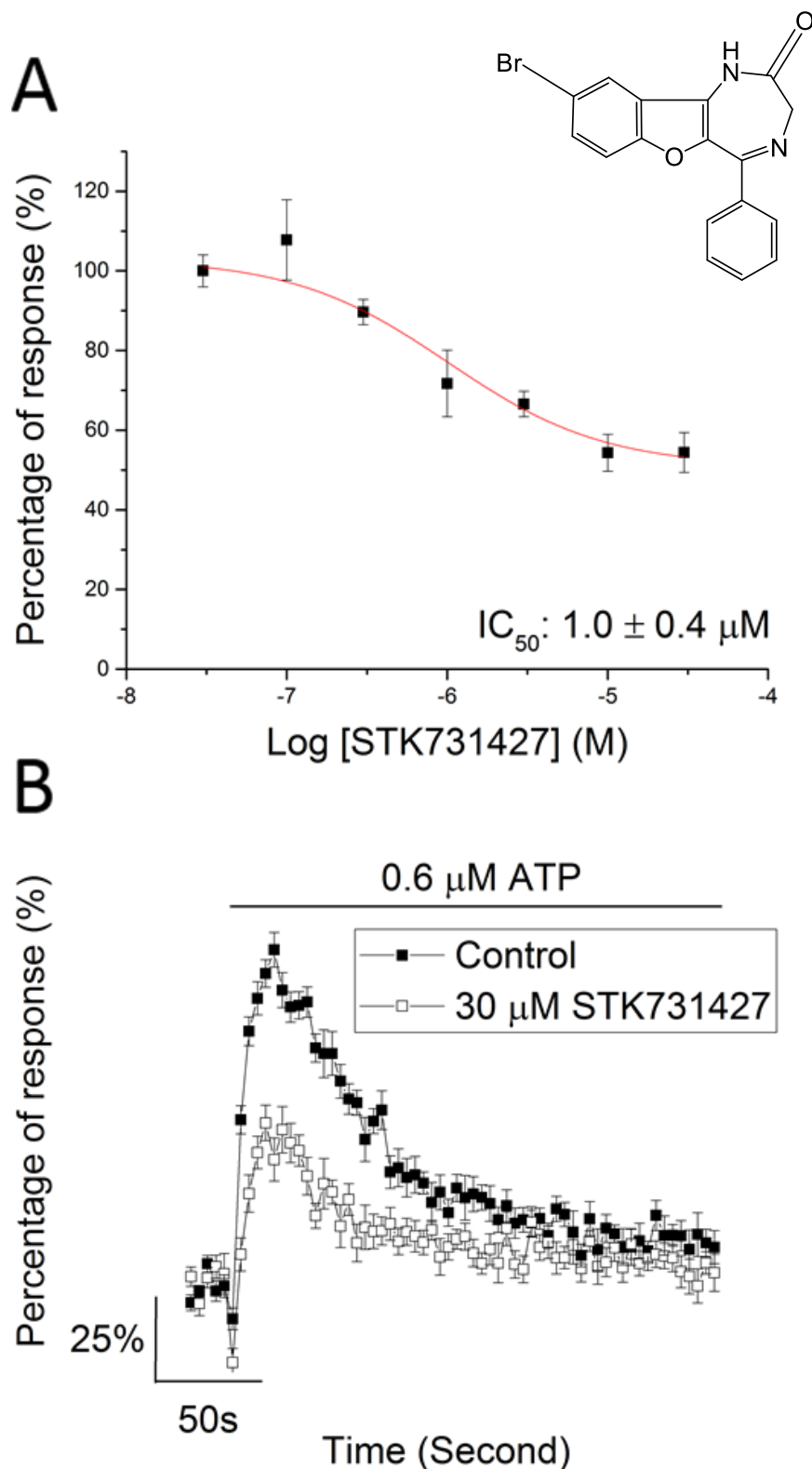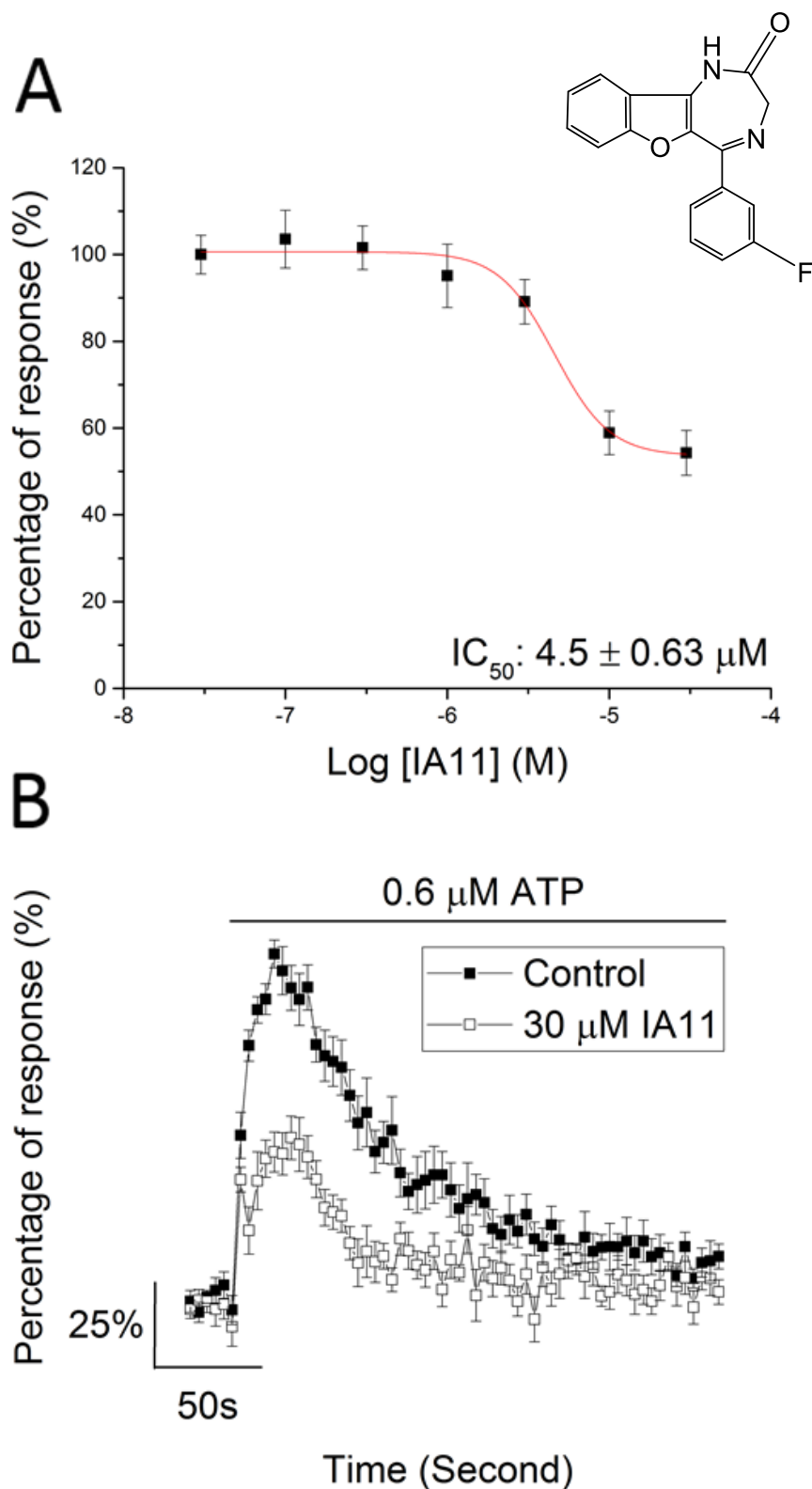
Figure 4.4 Inhibition concentration-response for STK731427 at human P2X$_4$ receptor.

Panel A shows the inhibition concentration-response curve for STK731427 (0.03 – 30 µM) when the human P2X$_4$ overexpressing cells were stimulated with 0.6 µM of ATP. Panel B shows its representative traces in the absence and presence of 30 µM of IA1 dissolved in 1 % DMSO. All responses were normalised to mean peak response of vehicle control. The inset shows the chemical structure of STK731427. ($n = 3$)
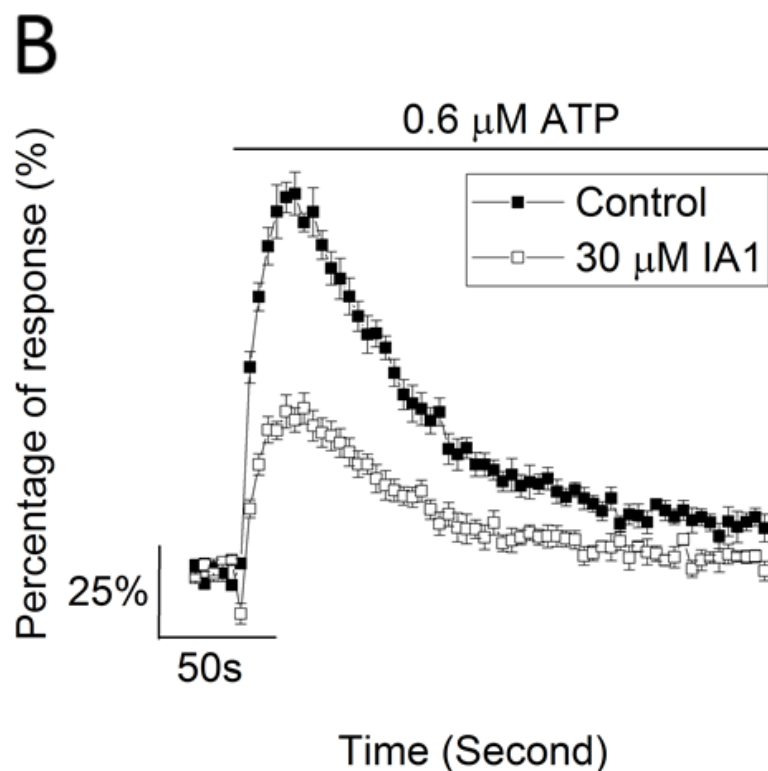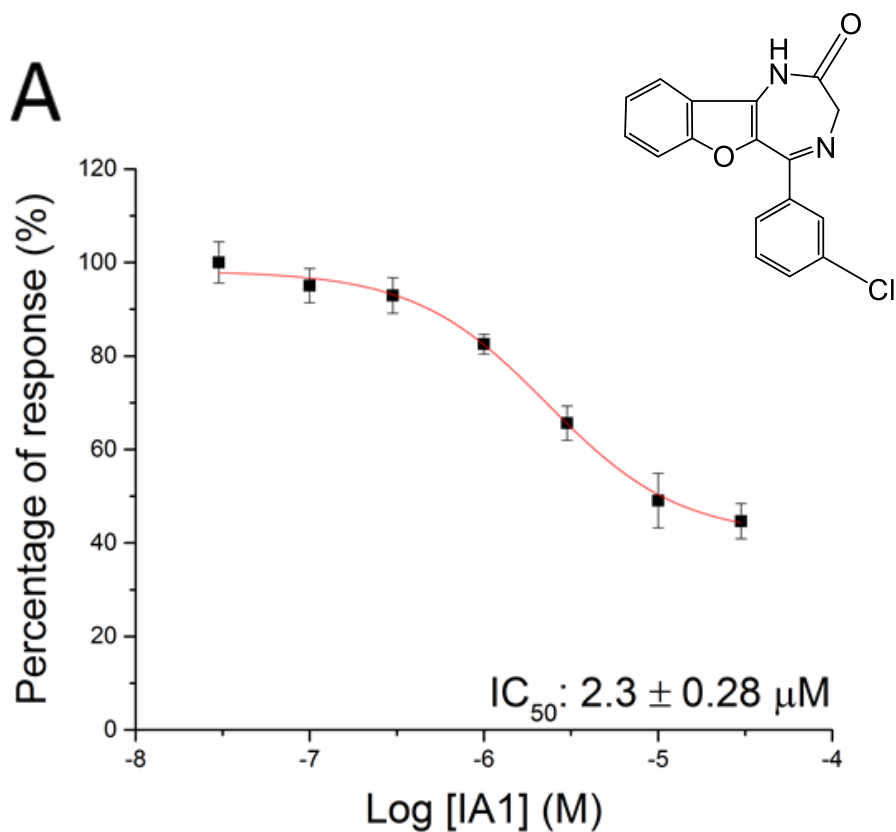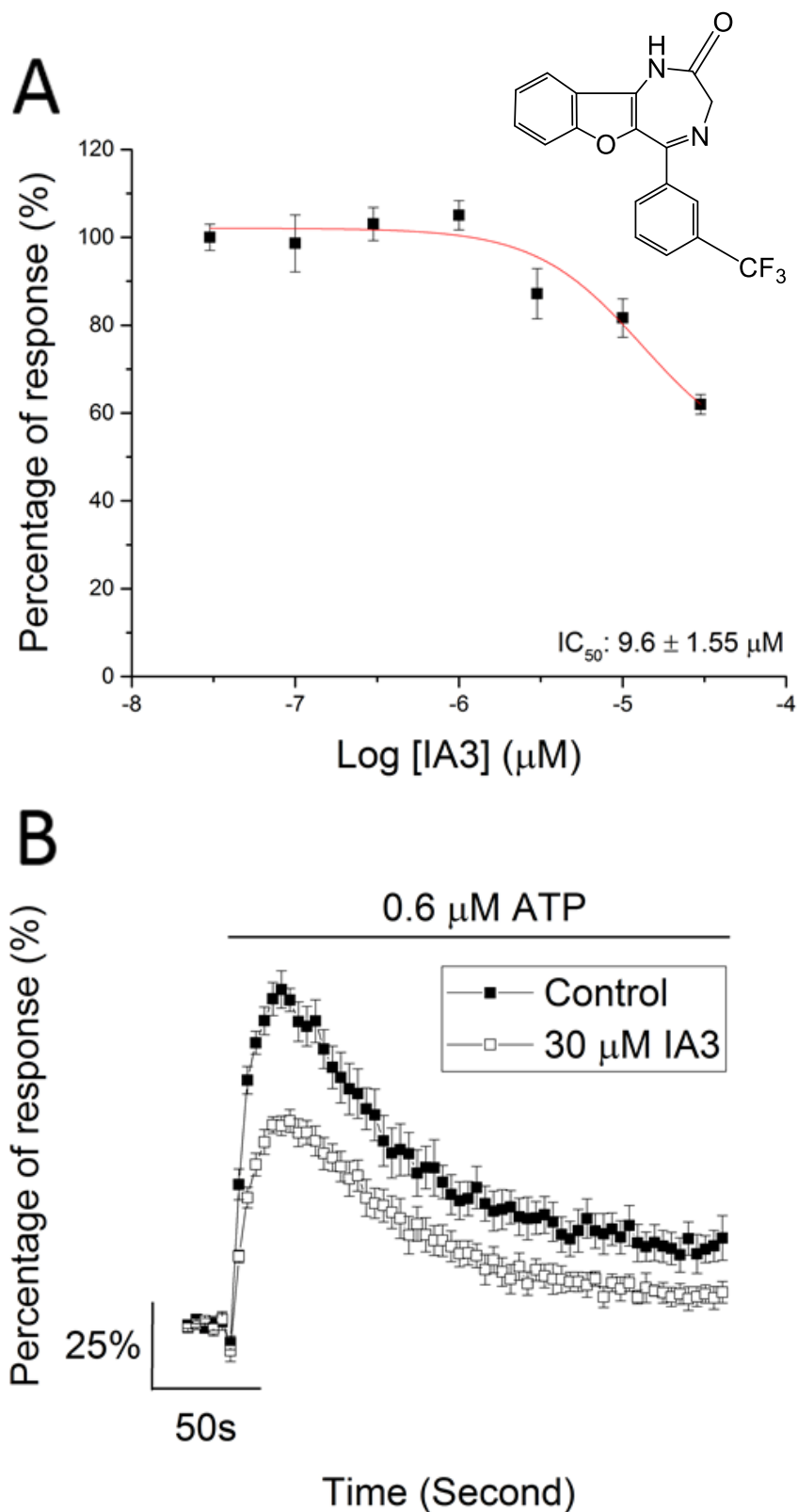
Figure 4.5 Inhibition concentration-response for IA1 at human P2X$_4$ receptor.
Panel A shows the inhibition concentration-response curve for IA1 (0.03 – 30 µM) when the human P2X$_4$ overexpressing cells were stimulated with 0.6 µM of ATP. Panel B shows its representative traces in the absence and presence of 30 µM of IA1 dissolved in 1 % DMSO. All responses were normalised to mean peak response of vehicle control. The inset shows the chemical structure of IA1. ($n = 3$)
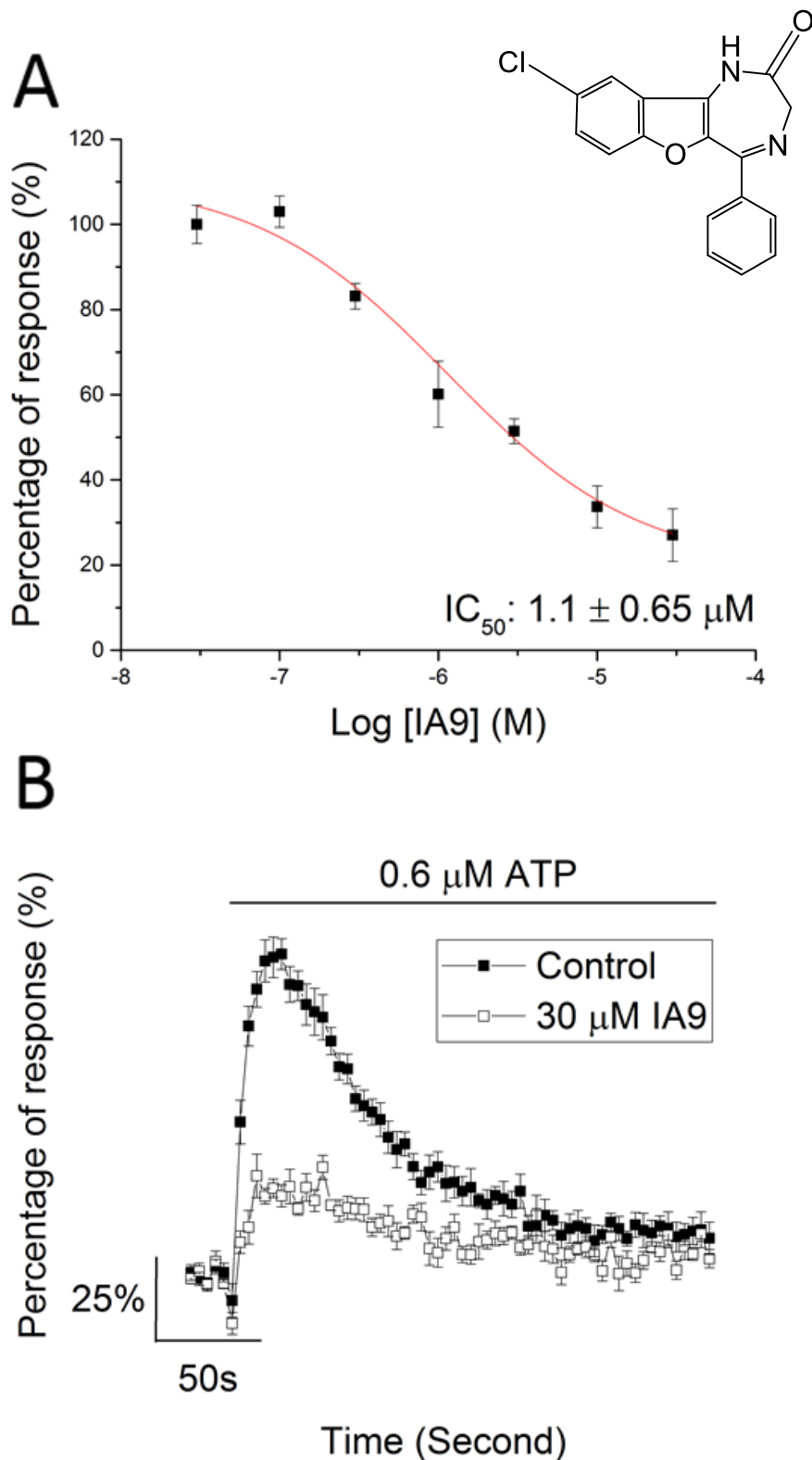
Figure 4.6 Inhibition concentration-response for IA9 at human P2X$_4$ receptor.
Panel A shows the inhibition concentration-response curve for IA9 (0.03 – 30 µM)
when the human P2X$_4$ overexpressing cells were stimulated with 0.6 µM of ATP.
Panel B shows its representative traces in the absence and presence of 30 µM of IA1
dissolved in 1 % DMSO. All responses were normalised to mean peak response of
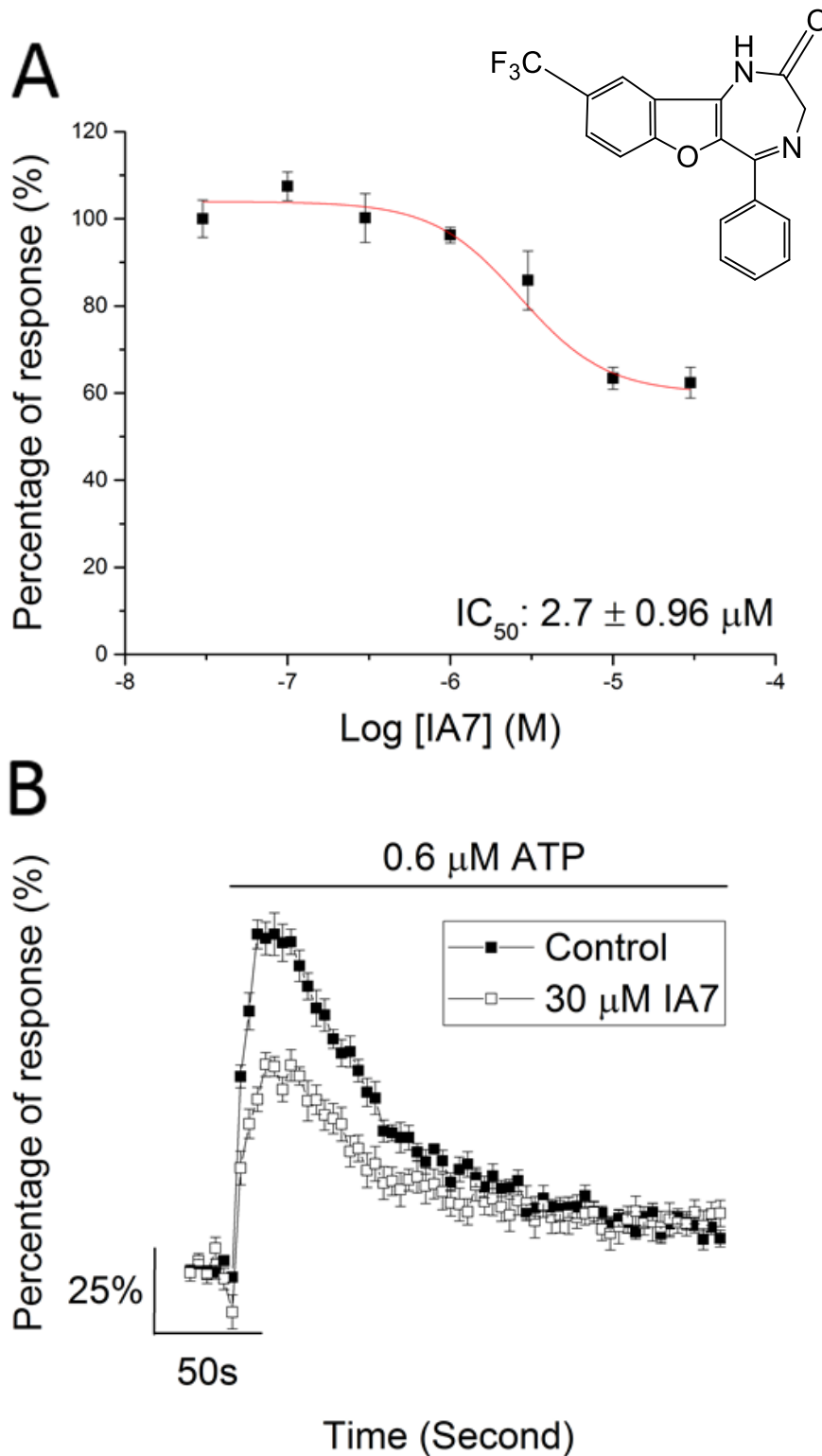vehicle control. The inset shows the chemical structure of IA9. ($n = 3$)
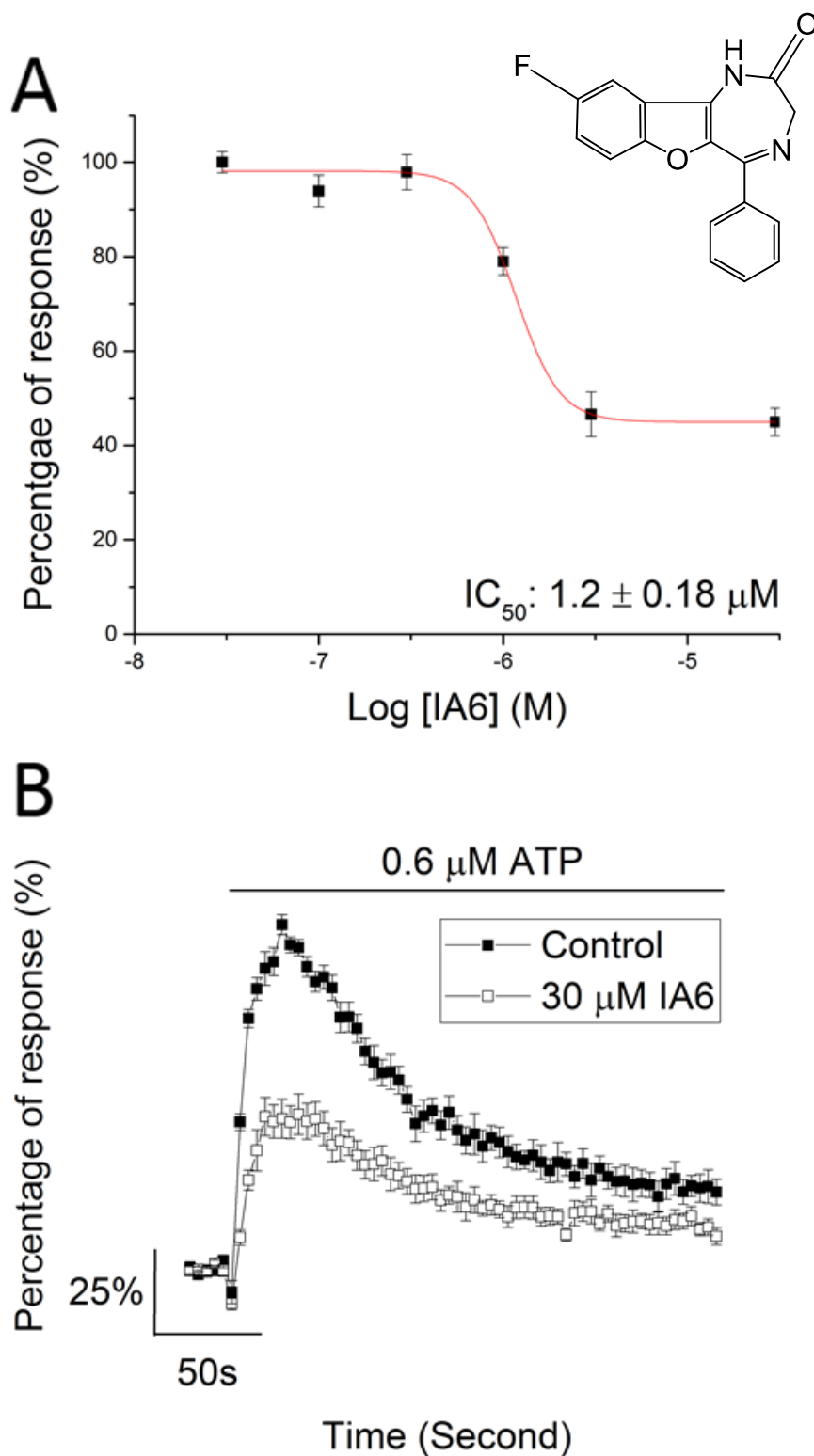
Figure 4.7 Inhibition concentration-response for IA6 at human P2X₄ receptor.
Panel A shows the inhibition concentration-response curve for IA6 (0.03 – 30 μM)
when the human P2X₄ overexpressing cells were stimulated with 0.6 μM of ATP.
Panel B shows its representative traces in the absence and presence of 30 μM of IA1
dissolved in 1 % DMSO. All responses were normalised to mean peak response of
vehicle control. The inset shows the chemical structure of IA6. ($n = 4$)

Figure 4.8 Inhibition concentration-response for IA11 at human P2X$_4$ receptor.
Panel A shows the inhibition concentration-response curve for IA11 (0.03 – 30 μM)
when the human P2X$_4$ overexpressing cells were stimulated with 0.6 μM of ATP.
Panel B shows its representative traces in the absence and presence of 30 μM of IA1
dissolved in 1 % DMSO. All responses were normalised to mean peak response of
vehicle control. The inset shows the chemical structure of IA11. (n = 3)

4.3.2.2 Substitution with trifluoromethyl at site 1 or 3

Figure 4.9 illustrates the activity of IA3. In terms of chemical structure, its substitution site 1 was replaced with trifluoromethyl. This compound was significantly less potent than 5-BDBD as the inhibition concentration-response curve showed that its IC_{50} value was significantly higher than 5-BDBD, 9.6 ± 1.55 µM ($p < 0.05$, $n = 3$). The first significant inhibition ($p < 0.01$, $n = 3$) was observed when 10 µM of IA3 was applied and 30 µM of IA3 only inhibited to 38.0 ± 2.2 % of control, significantly lower than 5-BDBD ($p < 0.01$, $n = 3$).

Next, the inhibition concentration-response of IA7 is shown in Figure 4.10 together with its representative traces in the absence and presence of 30 µM of IA7. Structurally, IA7 was similar with IA3 in terms of substituent but IA7 had its position 3 substituted with trifluoromethyl. Similar to IA3, the first significant inhibition was observed when the cells were treated with 10 µM of IA7 and at 30 µM, IA7 produced similar magnitude of inhibition (37.6 ± 3.5 %) which was significantly lower ($p < 0.05$, $n = 3$) than 5-BDBD. The calculated IC_{50} value was 2.7 ± 0.96 µM, not significantly different ($p > 0.05$, $n = 3$) than that of 5-BDBD.
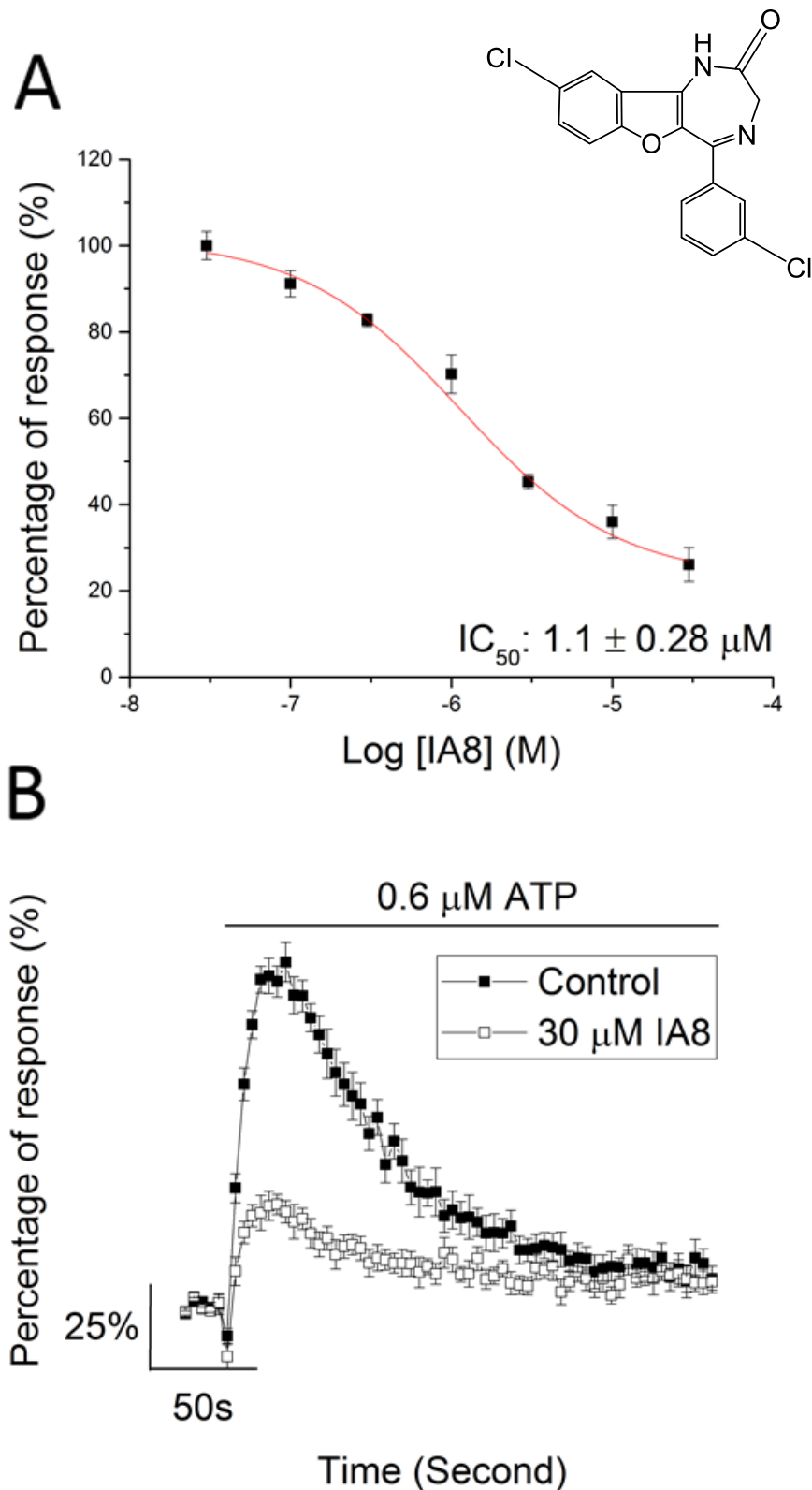
Figure 4.9 Inhibition concentration-response for IA3 at human P2X₄ receptor.
Panel A shows the inhibition concentration-response curve for IA3 (0.03 – 30 µM)
when the human P2X₄ overexpressing cells were stimulated with 0.6 µM of ATP.
Panel B shows its representative traces in the absence and presence of 30 µM of IA1
dissolved in 1 % DMSO. All responses were normalised to mean peak response of
vehicle control. The inset shows the chemical structure of IA3. ($n = 3$)

Figure 4.10 Inhibition concentration-response for IA7 at human P2X₄ receptor. Panel A shows the inhibition concentration-response curve for IA7 (0.03 – 30 µM) when the human P2X₄ overexpressing cells were stimulated with 0.6 µM of ATP. Panel B shows its representative traces in the absence and presence of 30 µM of IA1 dissolved in 1 % DMSO. All responses were normalised to mean peak response of vehicle control. The inset shows the chemical structure of IA7. (*n* = 3)

4.3.2.3   Multiple substitutions at site 1 and 3

Since Fischer et al. (2004) suggested that substitution at either site 1 or 3 could inhibit the activity of P2X$_4$ receptors, it was interesting to see if substitutions at both positions would affect the inhibitory action. Each analogue had the same constituent at both sites, either fluorine, chlorine, bromine, or trifluoromethyl.

In terms of chemical structure, IA8 had site 1 and 3 substituted with chlorine. Its inhibition concentration-response curve and representative trace of responses at 30 μM are shown in Figure 4.11. Based on the inhibition concentration-response curve, the calculated IC$_{50}$ value was 1.1 μM ± 0.28 μM, not significantly different ($p > 0.05$, $n = 3$) from that of 5-BDBD. The maximum peak inhibition response was 73.9 ± 3.9 %, significantly higher ($p < 0.05$, $n = 3$) than 5-BDBD.

However, for compound IA2, IA4, and IA10 which had bromine, trifluoromethyl, and fluorine substitution respectively; the modification of these analogues greatly reduced the potency compared to 5-BDBD. For IA2, the first significant inhibition was observed after 0.3 μM of IA2 treatment (10.6 ± 3.3 % inhibition, $p < 0.01$, $n = 3$) and the inhibition magnitude remained unchanged at higher concentrations of IA2 (Figure 4.12). The strongest inhibition was also significantly lower than 5-BDBD ($p < 0.01$, $n = 3$). While for IA4 (Figure 4.13) and IA10 (Figure 4.14), no inhibition was observed except at 30 μM of compound treatment, which resulted in 13.8 ± 4.8 % and 29.5 ± 4.5 % inhibition, respectively. Both were significantly lower than 5-BDBD ($p < 0.001$, $n = 3$ and $p < 0.01$, $n = 3$, respectively).

Figure 4.11 Inhibition concentration-response for IA8 at human P2X₄ receptor.
Panel A shows the inhibition concentration-response curve for IA8 (0.03 – 30 µM)
when the human P2X4 overexpressing cells were stimulated with 0.6 µM of ATP.
Panel B shows its representative traces in the absence and presence of 30 µM of IA1
dissolved in 1 % DMSO. All responses were normalised to mean peak response of
vehicle control. The inset shows the chemical structure of IA8. ($n = 3$)
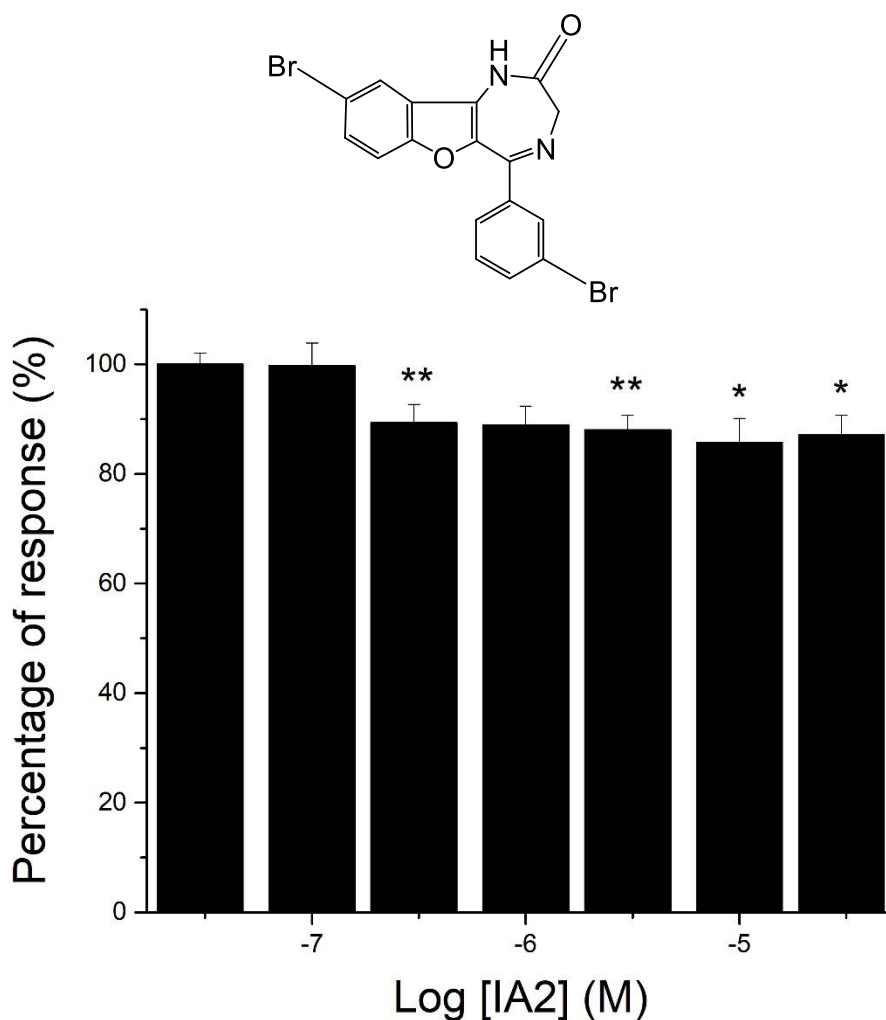
Figure 4.12 Effect of IA2 treatment on ATP-evoked response of the human P2X$_4$ overexpressing cells

The bar chart illustrates the effects of different concentrations of IA2 ($0.3 - 30\ \mu M$) treatment on ATP-evoked response of the human P2X$_4$ overexpressing cells. The concentration of ATP used was $0.6\ \mu M$. All responses were normalised to mean peak response of vehicle control. The top panel shows the chemical structure of IA2. Asterisk denotes p-value: $* = < 0.05$, $** = < 0.01$, $*** = < 0.001$. ($n = 3$)
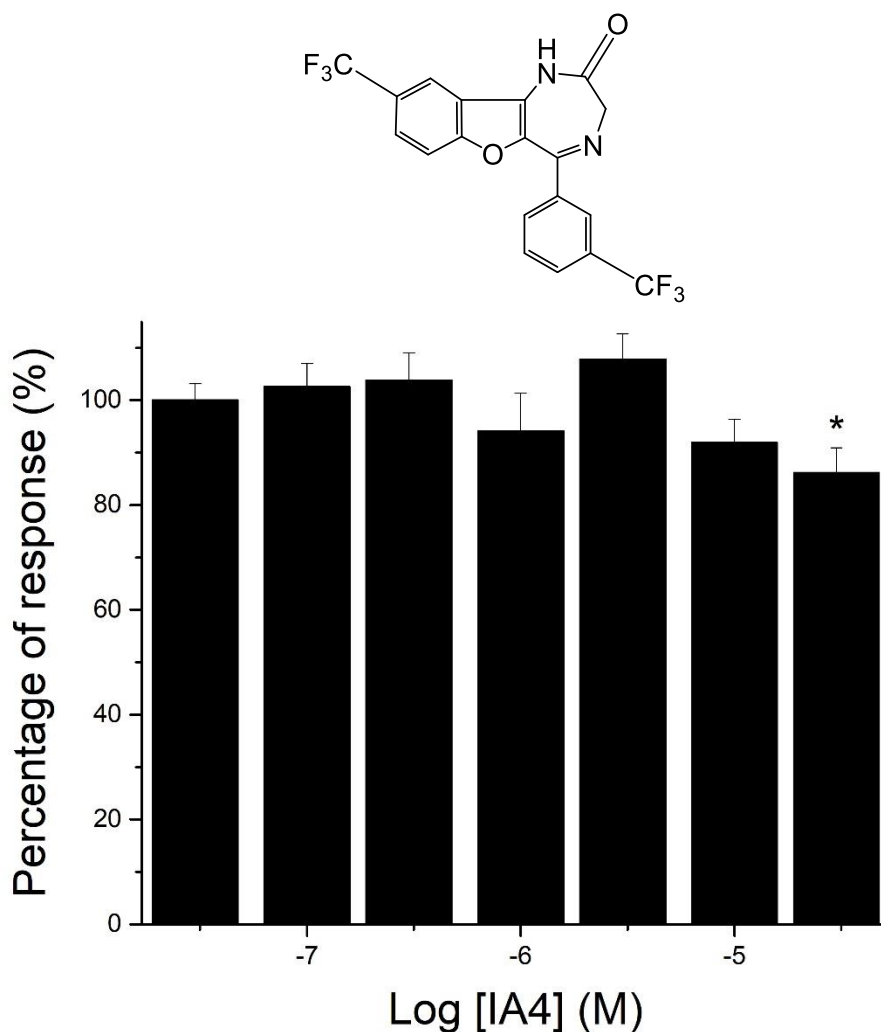
Figure 4.13 Effect of IA4 treatment on ATP-evoked response of the human P2X$_4$ overexpressing cells

The bar chart illustrates the effects of different concentrations of IA4 (0.3 – 30 µM) treatment on ATP-evoked response of the human P2X$_4$ overexpressing cells. The concentration of ATP used was 0.6 µM. All responses were normalised to mean peak response of vehicle control. The top panel shows the chemical structure of IA4. Asterisk denotes *p*-value: * = < 0.05, ** = < 0.01, *** = < 0.001. (*n* = 3)
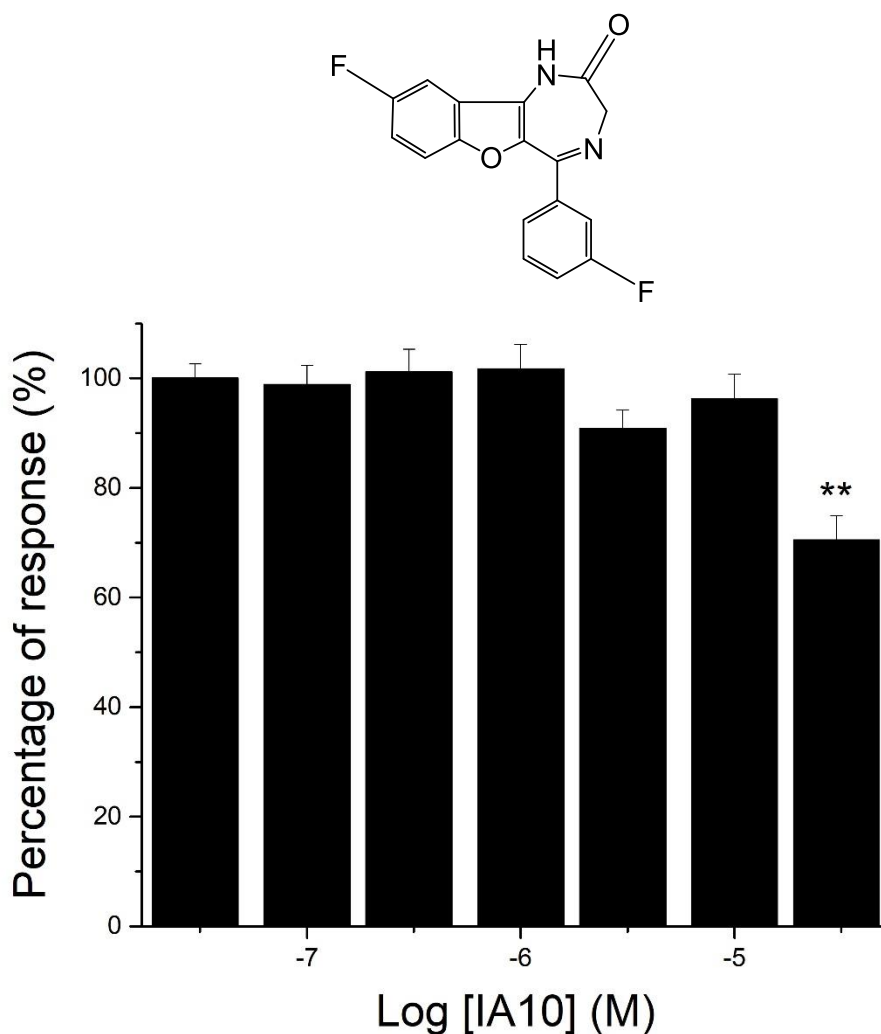
Figure 4.14 Effect of IA10 treatment on ATP-evoked response of the human P2X$_4$ overexpressing cells.

The bar chart illustrates the effects of different concentrations of IA10 (0.3 – 30 µM) treatment on ATP-evoked response of the human P2X$_4$ overexpressing cells. The concentration of ATP used was 0.6 µM. All responses were normalised to mean peak response of vehicle control. The top panel shows the chemical structure of IA10. Asterisk denotes *p*-value: * = < 0.05, ** = < 0.01, *** = < 0.001. (*n* = 3)

4.3.2.4 Commercially available analogues

Apart from that, the commercially available analogues were also investigated. Some of the purchased compounds allowed the investigation on the effect of site 2 substitution. First, Figure 4.15 shows the inhibition concentration-response of STK045532 and its representative traces of response with and without 30 µM of compound. Structurally, this compound did not have any substitutions at all sites. A significant inhibition was first observed with 0.3 µM of STK045532 treatment (13.5 ± 3.3 % inhibition, $p < 0.05$, $n = 3$) and it exponentially amplified at higher concentrations before reaching a plateau at 10 µM. The calculated IC_{50} value was 1.9 ± 0.31 µM, insignificantly different to 5-BDBD IC_{50} value ($p > 0.05$, $n = 3$). The highest blockade of 74.5 ± 7.7 % was recorded when 30 µM compound was applied, which was significantly higher compared to 5-BDBD ($p < 0.05$, $n = 3$).

Figure 4.16 shows the inhibition concentration-response curve for STK864662 with its representative traces of responses on the lower panel. Structurally, STK864662 had its site 3 substituted with methoxy group. The first significant inhibition was observed from 3 µM of compound treatment ($p < 0.05$, n = 3). Based on the curve, the calculated IC_{50} value was 4.8 ± 0.82 µM which was significantly higher ($p < 0.05$, $n = 3$) than 5-BDBD, indicating that chemical variation on this compound reduced its potency for inhibiting P2X$_4$. The maximum inhibition observed was 53.8 ± 11.5 %, which was not significantly different ($p > 0.05$, $n = 3$) compared to 5-BDBD.

Meanwhile, five of the tested compounds were found to cause no or minimal inhibition of calcium response. STK021512 and STK775918 did not significantly (both $p > 0.05$, $n = 3$) alter the peak calcium response regardless of the concentrations used (Figure 4.17 and 4.18, respectively). Structurally, STK021512 had a major difference compared to other analogues tested in this study where it lacked the benzodiazepinone while STK775918 had its site 2 substituted with bromine.

STK027946 only caused the significant inhibition of calcium response when 10 µM (9.5 ± 2.5 % inhibition) and 30 µM (12.0 ± 3.6 % inhibition) of compound were applied ($p < 0.01$ and $p < 0.05$, respectively, $n = 3$). This compound had methyl group at its site 2 (Figure 4.19). Meanwhile, STK079751 (Figure 4.20) and STK747973 (Figure

4.21) only caused significant inhibition after treatment with 30 µM of compound (19.1 $\pm$ 4.0 % and 25.2 $\pm$ 5.6 % inhibition, respectively; both $p < 0.01$, $n = 3$). Both STK079751 and STK747973 had their site 2 substituted with chlorine and fluorine, respectively.
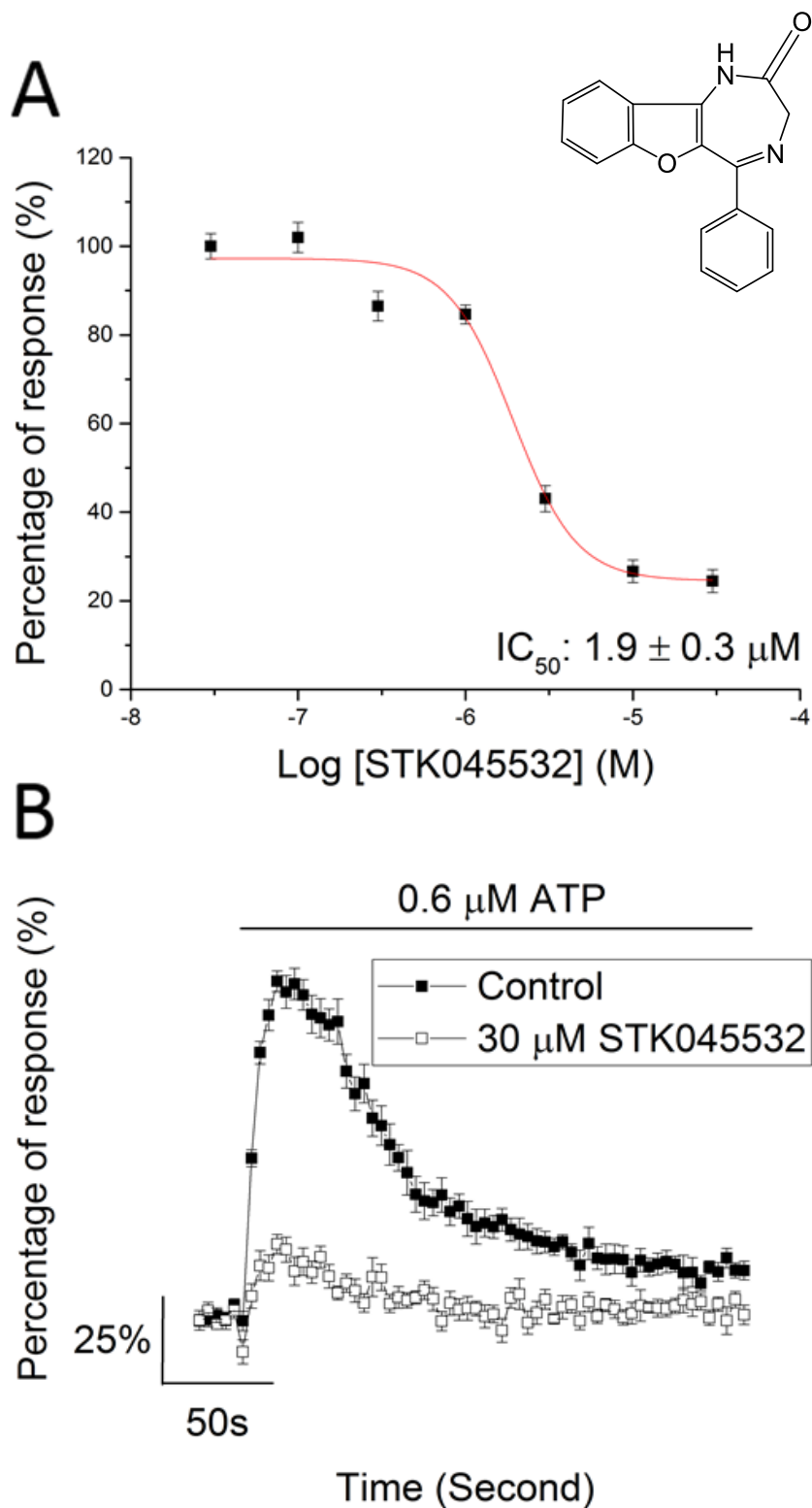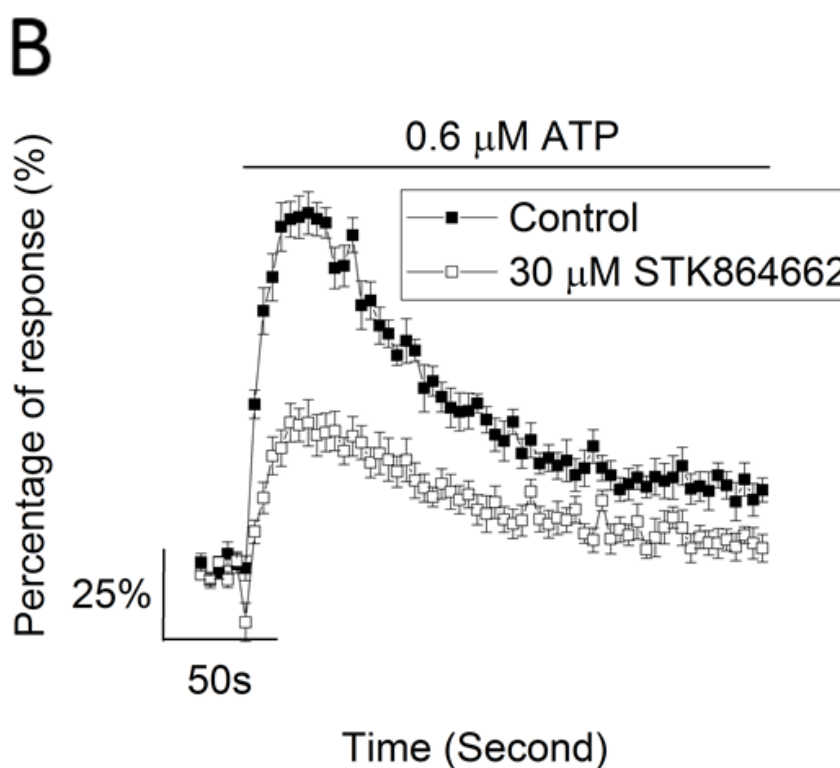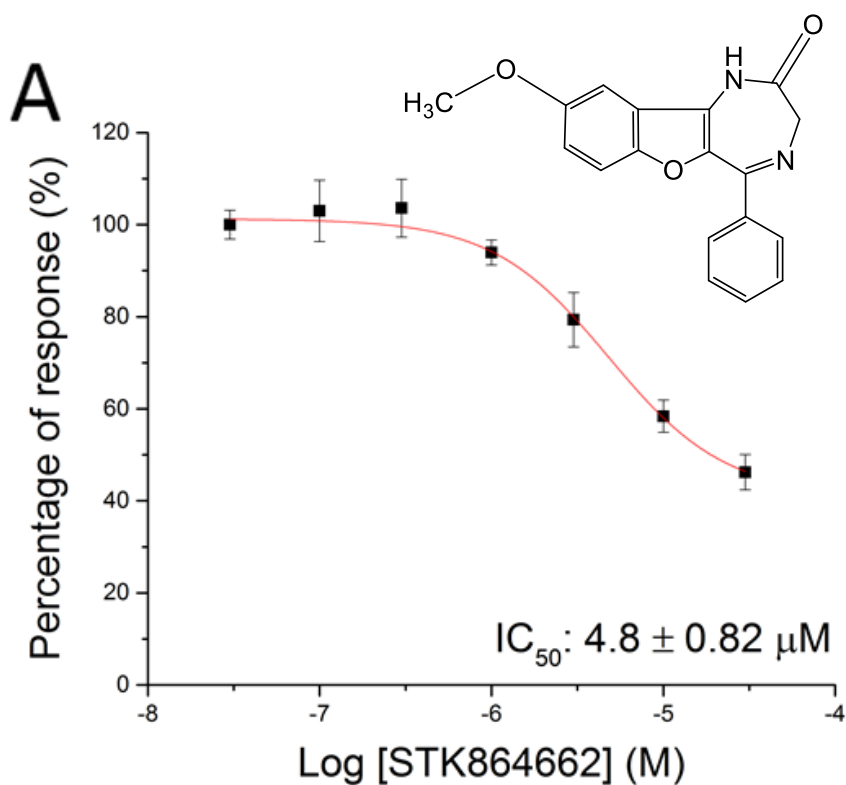
Figure 4.15 Inhibition concentration-response for STK045532 at human P2X₄ receptor.

Panel A shows the inhibition concentration-response curve for STK045532 (0.3 – 30 µM) when the human P2X₄ overexpressing cells were stimulated with 0.6 µM of ATP. Panel B shows its representative traces in the absence and presence of 30 µM of IA1 dissolved in 1 % DMSO. All responses were normalised to mean peak response of vehicle control. The inset shows the chemical structure of STK045532. ($n = 3$)

Figure 4.16 Inhibition concentration-response for STK864662 at human P2X$_4$ receptor.

Panel A shows the inhibition concentration-response curve for STK864662 (0.3 – 30 µM) when the human P2X$_4$ overexpressing cells were stimulated with 0.6 µM ATP. Panel B shows its representative traces in the absence and presence of 30 µM of IA1 dissolved in 1 % DMSO. All responses were normalised to mean peak response of vehicle control. The inset shows the chemical structure of STK864662. ($n = 3$)
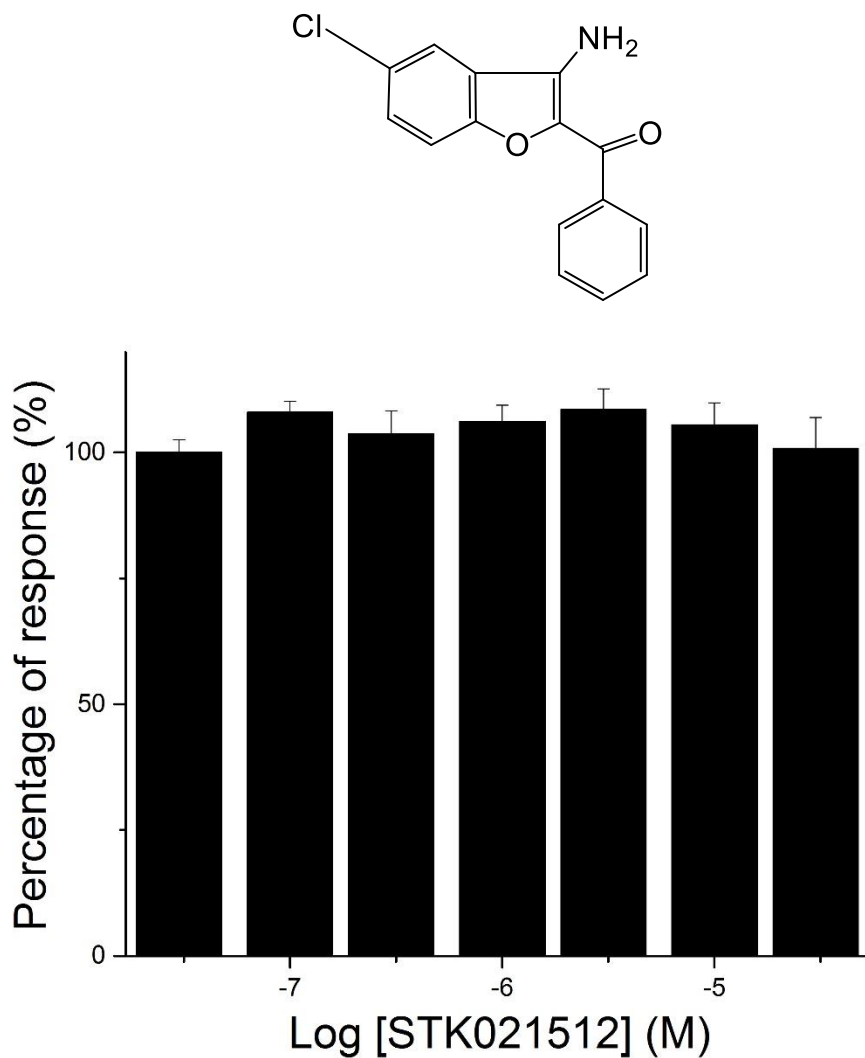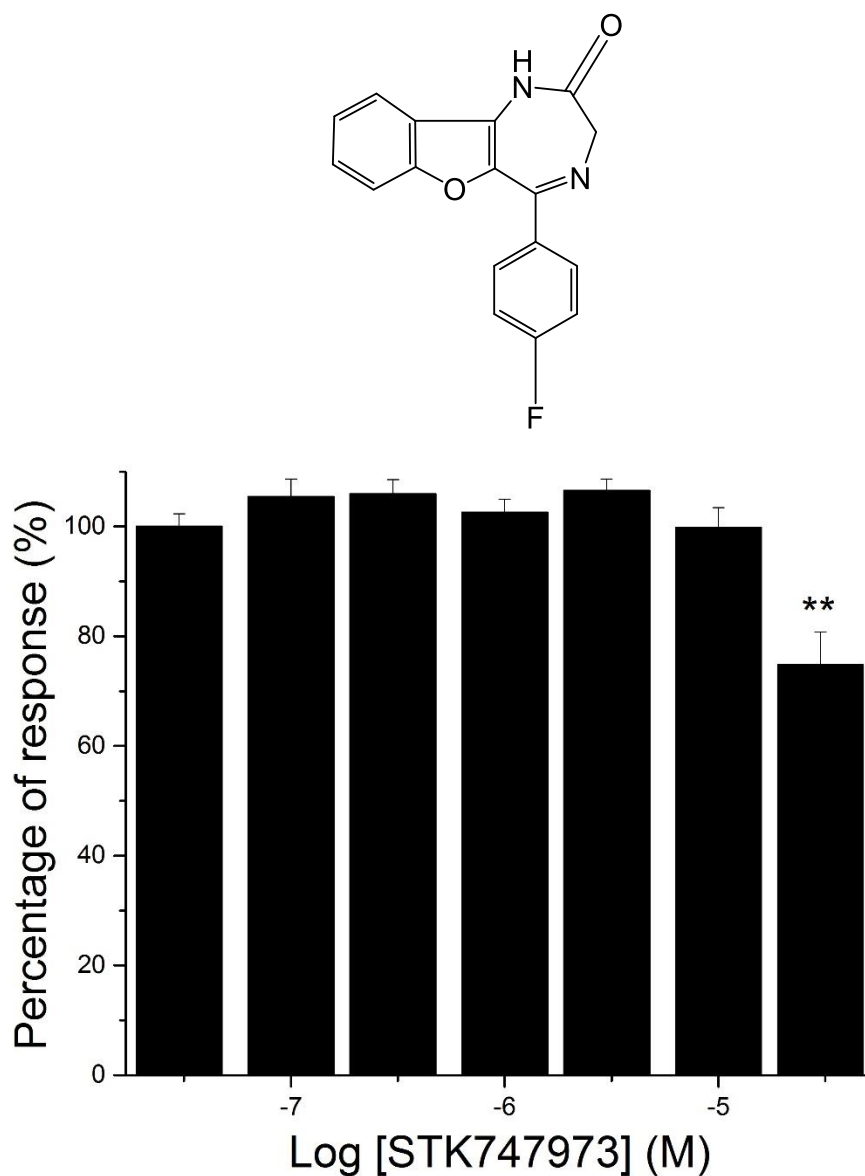
Figure 4.17 Effect of STK021512 treatment on ATP-evoked response of the human P2X$_4$ overexpressing cells.

The bar chart illustrates the effects of different concentrations of STK021512 (0.3 – 30 µM) on ATP-evoked response of the human P2X$_4$ overexpressing cells. The concentration of ATP used was 0.6 µM. All responses were normalised to mean peak response of vehicle control. The top panel shows the chemical structure of STK021512. Asterisk denotes p-value: * = < 0.05, ** = < 0.01, *** = < 0.001. (n = 3)
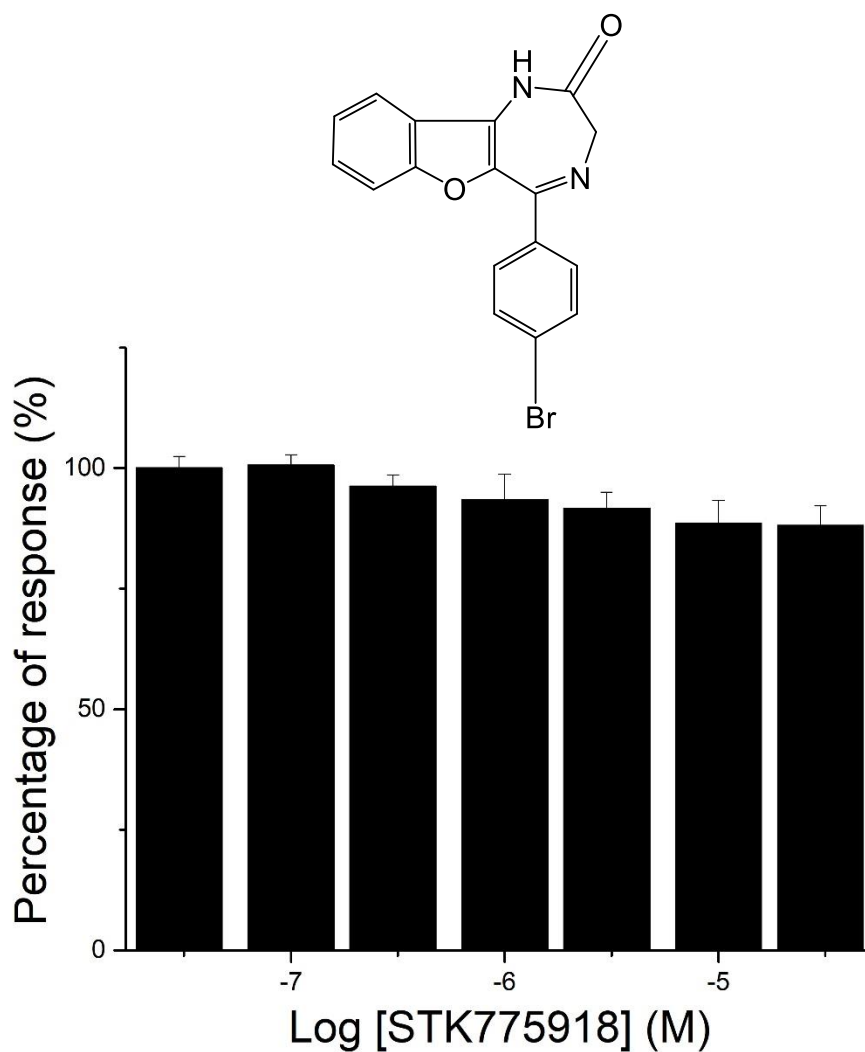
Figure 4.18 Effect of STK775918 treatment on ATP-evoked response of the human P2X$_4$ overexpressing cells.

The bar chart illustrates the effects of different concentrations of STK775918 (0.3 – 30 µM) treatment on ATP-evoked response of the human P2X$_4$ overexpressing cells. The concentration of ATP used was 0.6 µM. All responses were normalised to mean peak response of vehicle control. The top panel shows the chemical structure of STK775918. Asterisk denotes *p*-value: $* = < 0.05$, $** = < 0.01$, $*** = < 0.001$. ($n = 3$)
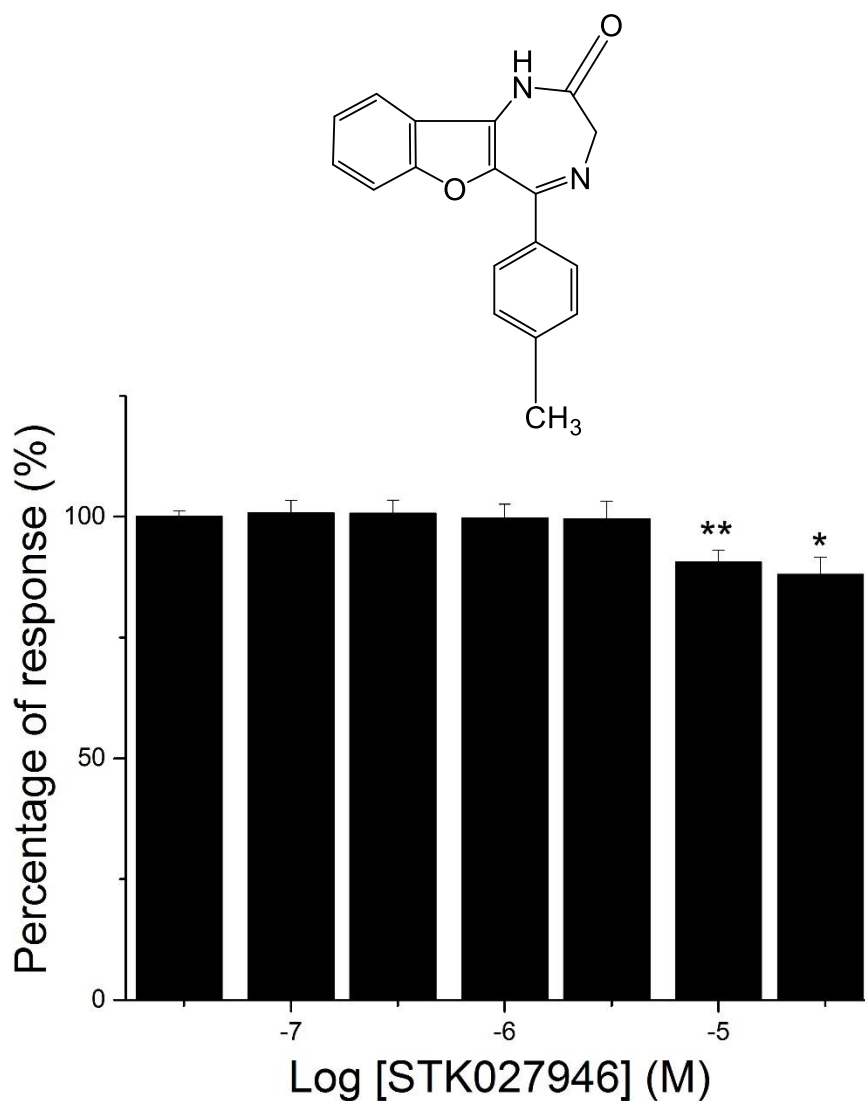
Figure 4.19 Effect of STK027946 treatment on ATP-evoked response of the human P2X$_4$ overexpressing cells.

The bar chart illustrates the effects of different concentrations of STK027946 (0.3 – 30 µM) treatment on ATP-evoked response of the human P2X$_4$ overexpressing cells. The concentration of ATP used was 0.6 µM. All responses were normalised to mean peak response of vehicle control. The top panel shows the chemical structure of STK027946. Asterisk denotes p-value: * = < 0.05, ** = < 0.01, *** = < 0.001. (n = 3)
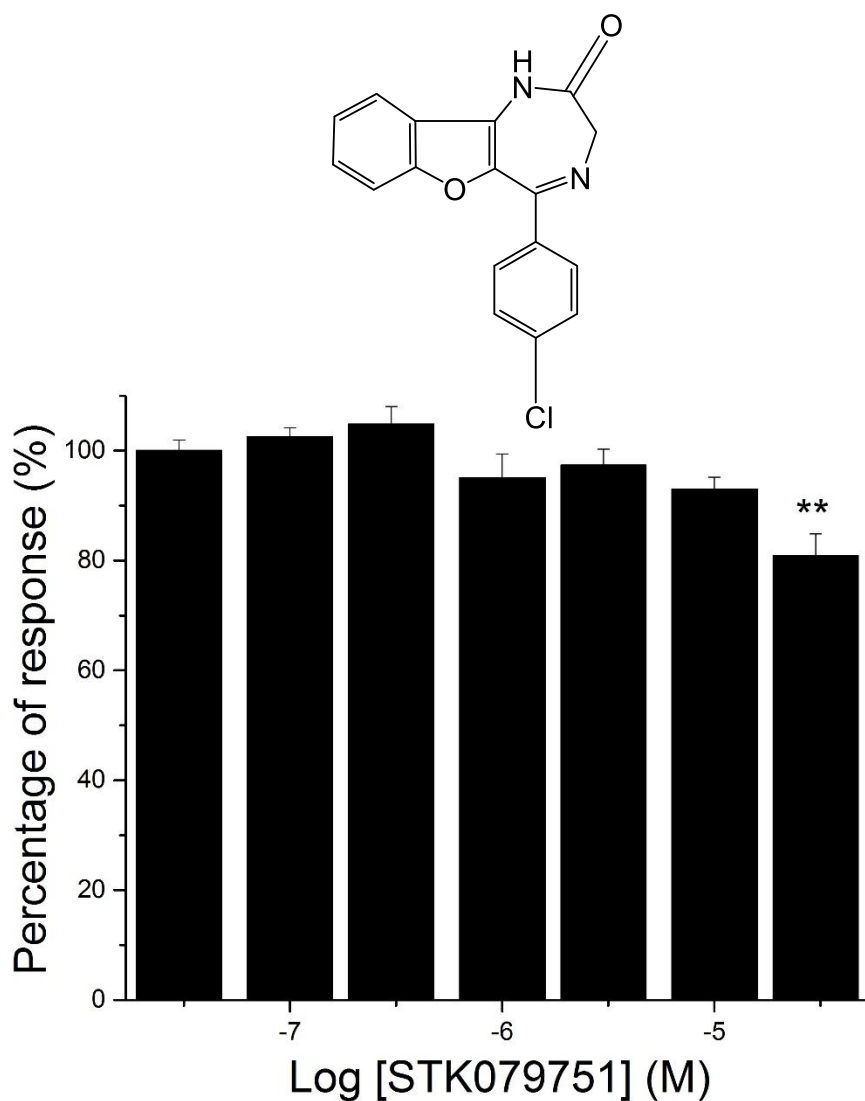
Figure 4.20 Effect of STK079751 treatment on ATP-evoked response of the human P2X$_4$ overexpressing cells.

The bar chart illustrates the effects of different concentrations of STK079751 (0.3 – 30 µM) treatment on ATP-evoked response of the human P2X$_4$ overexpressing cells. The concentration of ATP used was 0.6 µM. All responses were normalised to mean peak response of vehicle control. The top panel shows the chemical structure of STK079751. Asterisk denotes p-value: * = < 0.05, ** = < 0.01, *** = < 0.001. ($n = 3$)

Figure 4.21 Effect of STK747973 treatment on ATP-evoked response of the human P2X4 overexpressing cells.

The bar chart illustrates the effects of different concentrations of STK747973 (0.3 – 30 μM) treatment on ATP-evoked response of the human P2X4 overexpressing cells. The concentration of ATP used was 0.6 μM. All responses were normalised to mean peak response of vehicle control. The top panel shows the chemical structure of STK747973. Asterisk denotes *p*-value: * = <0.05, ** = < 0.01, *** = < 0.001. (*n* = 3)

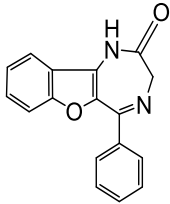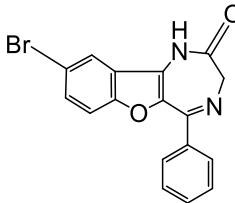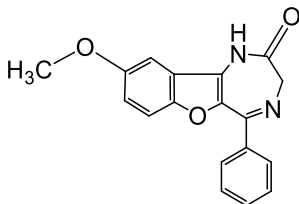### 4.3.3 Determining the mode of inhibition of inhibiting compounds

Next, to further study the relationship between 5-BDBD and P2X$_4$ receptor, an experiment was designed to determine the mode of inhibition. The mode of inhibition was determined by looking at the ATP concentration-response curves in the absence and presence of IC$_{50}$ concentrations of each compound. Generally, there are two indications to determine a competitive inhibition. Firstly, the response in the presence of compound should reach the same peak response as the vehicle control when the concentration of agonist is increased and secondly, the curve of response for treated cells should shift to the right of curve for untreated cells which results in higher EC$_{50}$ value for treated cells than untreated cells. If the curves fulfil those two requirements, it could be deduced that a compound is a competitive inhibitor (Balazs et al., 2013). Whereas, if a compound is not competitive, the maximum peak response of treated cells could not reach the same magnitude as the untreated cells, even though high concentration of agonist was used.

Since the inhibiting analogues were not vastly different from 5-BDBD, i.e., only variations at site 1 and 3, it was hypothesised that they would show competitive inhibition like 5-BDBD and this was later confirmed with the experiments. The characteristics shown by STK045532, STK731427, STK864662, IA1, IA6, IA7, IA8, IA9, and IA11 indicated that they inhibited P2X$_4$ receptor competitively. The response curves for all compounds shifted to the right that subsequently yielded higher values of ATP EC$_{50}$ compared to the untreated cells. All compounds produced the same maximum magnitude of calcium response between treated and untreated cells. An example for the plots is shown in Figure 4.22 which represents STK045532 while the rests can be found in Appendix V – XII. The summary of all results for this chapter is shown in Table 4.1.
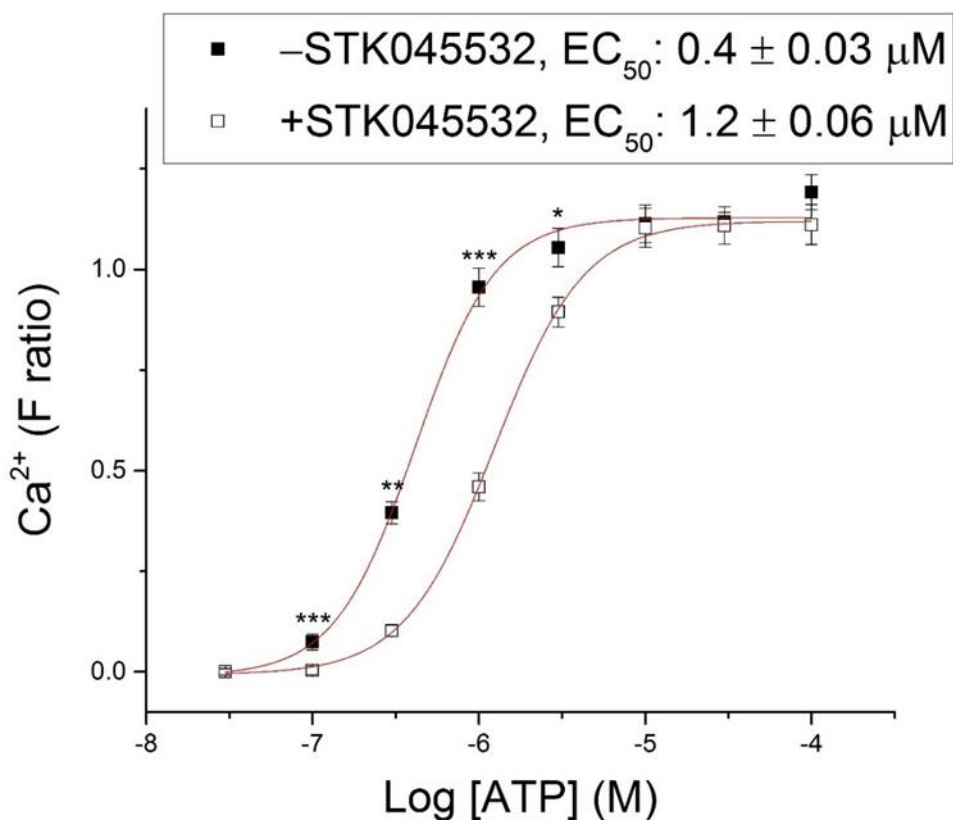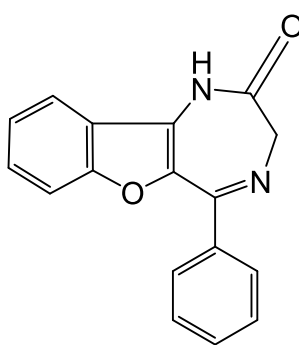
Figure 4.22 ATP concentration-response in the absence and presence of STK045532.

The plots show the ATP concentration-response in the presence (open square) and absence (close square) of 1.9 µM of STK045532. The EC_{50} value in the presence of STK045532 was significantly higher than that with the compound ($p < 0.001$). The difference between each data point was statistically calculated and marked with asterisk to indicate the level of difference. The right shift of treated cells curve compared to the vehicle control together with significant increase in EC_{50} value indicated the competitive mode of antagonism. The top panel shows the chemical structure of STK045532. Asterisk denotes p-value: $* = < 0.05$, $** = < 0.01$, $*** = < 0.001$. ($n = 3$)

Table 4.1 Summary of active compounds.
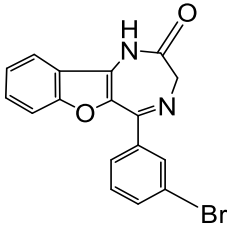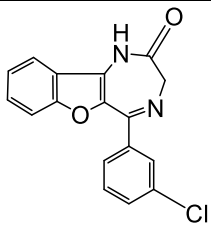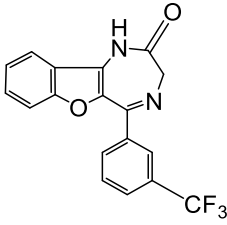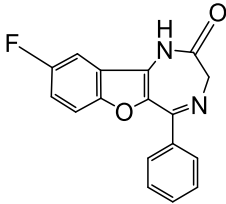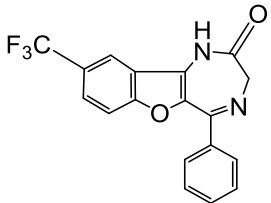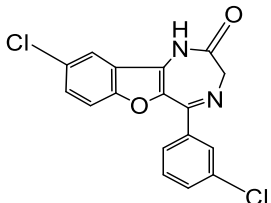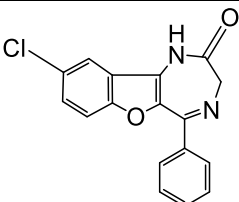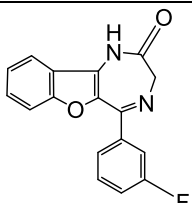
Compound	Structure	IC$_{50}$ (µM)/ (p value)*	Average maximum inhibition (%)/ (p-value)*	Type of inhibition (p-value)**
5-BDBD		1.6 ± 0.63	56.8	Competitive ($p < 0.05$)
STK045532		1.9 ± 0.31 (n.s.)	74.5 ($p < 0.05$)	Competitive ($p < 0.001$)
STK731427		1.0 ± 0.43 (n.s.)	47.9 ($p < 0.05$)	Competitive ($p < 0.05$)
STK864662		4.8 ± 0.82 ($p < 0.05$)	53.8 (n.s.)	Competitive ($p < 0.05$)
IA1		2.3 ± 0.28 (n.s.)	55.4 (n.s.)	Competitive ($p < 0.01$)
IA3		9.6 ± 1.55 ($p < 0.05$)	32.0 ($p < 0.01$)	n.d.

Table 4.1 cont.: Summary of active compounds.

IA6		1.2 ± 0.18 (n.s.)	58.6 (n.s.)	Competitive ($p < 0.05$)
IA7		2.7 ± 0.96 (n.s.)	37.6 ($p < 0.05$)	Competitive ($p < 0.05$)
IA8		1.1 ± 0.28 (n.s.)	73.9 ($p < 0.05$)	Competitive ($p < 0.05$)
IA9		1.1 ± 0.65 (n.s.)	72.9 (n.s.)	Competitive ($p < 0.01$)
IA11		4.5 ± 0.63 ($p < 0.05$)	51.9 (n.s.)	Competitive ($p < 0.05$)

*p-value is the statistical comparison between respected compound and 5-BDBD.

** Statistical difference between EC_{50} values from treated and untreated cells.

n.s. = no significant difference

n.d. = not determined

4.3.4 Generating a hypothesis of the human P2X$_4$-5-BDBD binding site using molecular docking approaches

Docking simulations between 5-BDBD and its analogues were employed to predict the binding pose and orientation for understanding the observed pharmacological results. Generally, docking can be performed in two ways, which are blind and targeted docking. Blind docking refers to a docking simulation that does not define a fixed binding site which is commonly practised to identify a possible binding site for small molecules. Targeted docking is a docking simulation that has a predefined binding site and this type of docking is usual in lead optimisation and hit identification through virtual screening (Ghersi & Sanchez, 2009).

In this study, targeted docking was employed since the data showed that 5-BDBD and its analogues competitively inhibited P2X$_4$ likely by binding to the ATP binding site which was already identified through zfP2X$_4$ crystal structure (Hattori & Gouaux, 2012). Based on the human P2X$_4$ model generated, it was observed that the conformation of three ATP binding sites at P2X$_4$ receptors were slightly different, therefore the compounds were docked at each site to increase the sampling. Based on the docking results, the inhibiting compounds (i.e., 5-BDBD, STK045532, STK747973, STK864662, IA1, IA3, IA6, IA7, IA8, IA9, and IA11) shared a preferential pose, repeated across each binding site. The compounds took advantage of a deeper hydrophobic region of the binding pocket to accomodate protruding phenyl or halo-phenyl moieties, while ATP bound at a more superficial region than 5-BDBD and its analogues (Figure 4.23).

Detailed analysis of the docking pose (Figure 4.24) revealed that the hydrophobic part of the binding site was the main region involved in the binding with 5-BDBD (and its active analogues). The residues that encapsulated the binding site were Phe294 and Arg295 at one subunit as well as Thr66, Lys67, Val86, Val90, and Ala93 at the neighbouring subunit. Interestingly, 5-BDBD and ATP shared two residues for binding, Arg295 and Lys67 (Hattori & Gouaux, 2012). Possibly, the residue that played a major role in 5-BDBD (and inhibiting analogues) binding was Arg295. The residue was important in the binding because it could establish one or two hydrogen

bonds with the carbonyl group of diazepinone on 5-BDBD (number of hydrogen bonds varied with different conformations).

In the absence of inhibitor, binding of ATP induced a conformational change, and the side chain of Lys67 covered the hydrophobic pocket, which made the binding site inaccessible for 5-BDBD. However, in the absence of ATP, the binding site was open and thus 5-BDBD could access the pocket for binding.
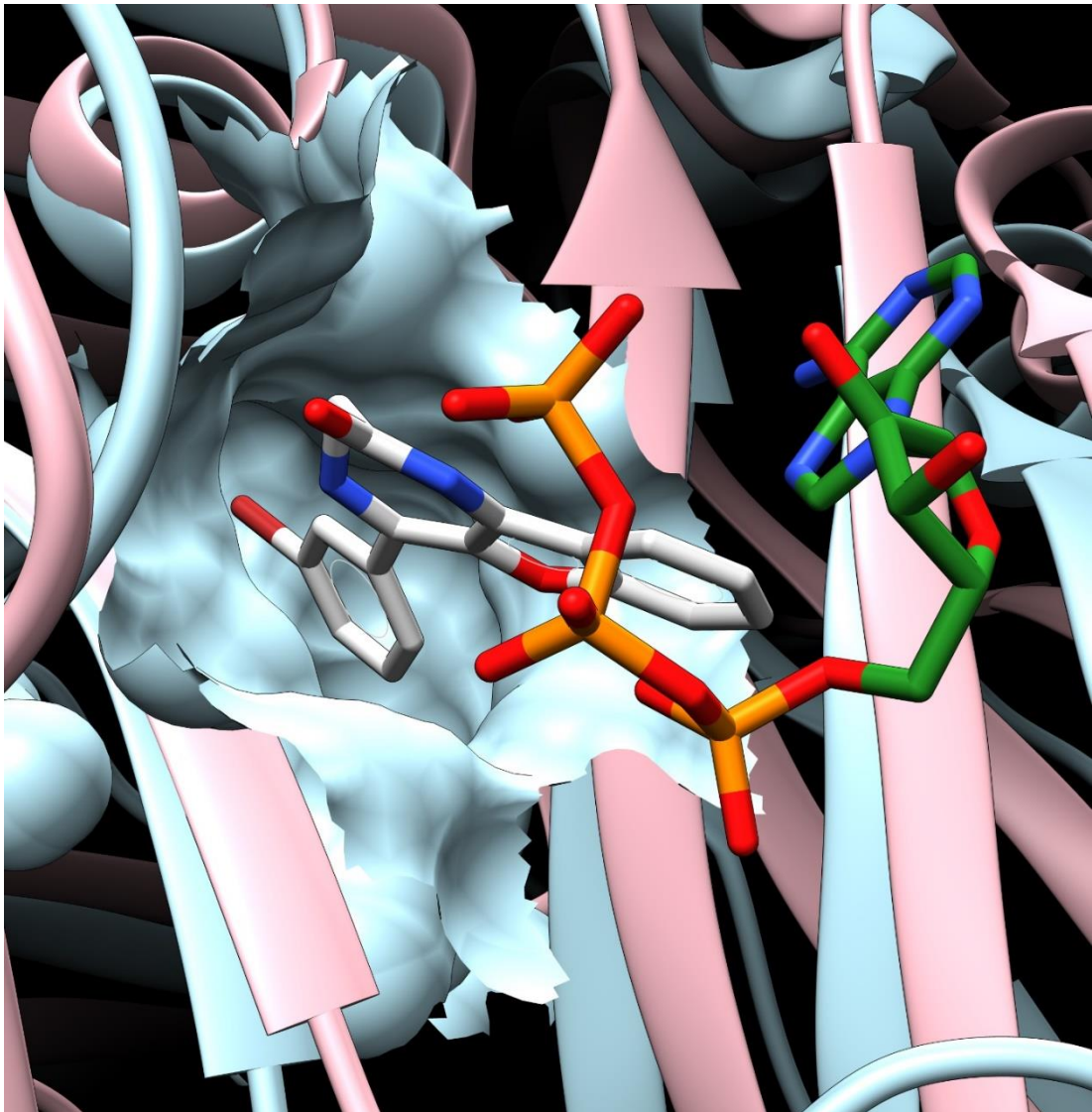
Figure 4.23 Docking poses of 5-BDBD and ATP in P2X₄ binding site.

The figure shows the binding of both 5-BDBD and ATP. The docking poses of 5-BDBD and ATP in the P2X$_4$ pocket are represented by grey stick and green/orange stick, respectively. As seen in the figure, 5-BDBD went deeper into the pocket relative to ATP. The deeper pocket was benefited by the protruding bromophenyl. The pink ribbon is P2X$_4$ receptor in its open, ATP-bound state while the blue ribbon is P2X$_4$ receptor in its closed state, which were overlaid on top of each other. Heteroatoms were coloured red for oxygen, orange for phosphate, blue for nitrogen, and dark red for bromine.
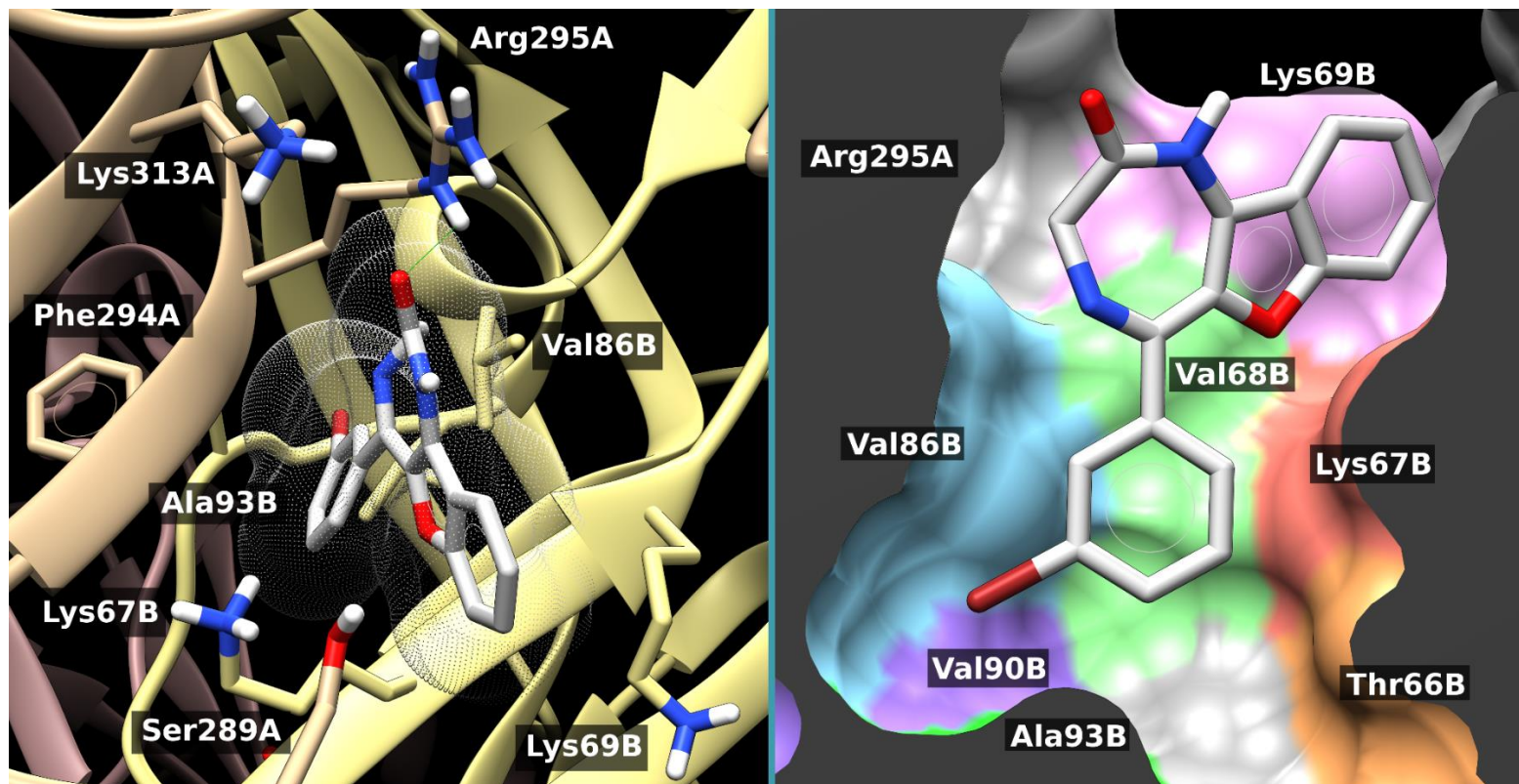
Figure 4.24 Docking poses between 5-BDBD and human P2X$_4$ homology model.

Left panel: 5-BDBD is represented with white stick, in the middle of the figure. Pink ribbon represents one subunit of P2X$_4$ receptor (coded as A) and yellow ribbon represents the neighbouring subunit (coded as B). The figure displays four important residues for binding at chain A and three residues at chain B. The translucent mesh represents the space that 5-BDBD filled in the binding pocket. Right panel: Different viewing angle of docking pose. In the figure, Ala93B was close to para-position (substitution site 2) of phenyl. Thus, any para substitution would cause the compounds to lose its inhibitory properties as substituted atom would clash with Ala93B and prevent the fitting of compound in the binding pocket. Heteroatoms were coloured red for oxygen, blue for nitrogen, and dark red for bromine.

4.4   Discussion

4.4.1   Structure activity relationship study of 5-BDBD and P2X$_4$

5-BDBD has been widely used in studies involving P2X$_4$ receptor over the past decade despite the limited information until it was recently characterised pharmacologically (Balazs et al., 2013). This situation drives the curiosity to unveil more information about this compound to better enhance the understanding of its application in P2X$_4$ research field. Thus, this part of study focused on the structure activity relationship between 5-BDBD and P2X$_4$ receptor. Firstly, several analogues of 5-BDBD were synthesised, purchased, and tested for their potency and secondly, the mode of action of each inhibiting analogue was determined. The interaction of the analogues with P2X$_4$ receptor was subsequently simulated in virtual docking to further understand the experimental data. The 5-BDBD analogues differed in terms of three substitution sites which has been shown in Figure 4.1. This will be used to effectively explain the relationship between 5-BDBD and P2X$_4$.

4.4.1.1   Substitution at position 1

Based on pharmacological data, all compounds that were substituted with either chlorine (IA1), trifluoromethane (IA3), and fluorine (IA11) at position 1 showed the inhibitory properties. IA1 yielded similar IC$_{50}$ value as 5-BDBD but IA3 and IA11 showed significantly higher IC$_{50}$ values than 5-BDBD. In terms of the magnitude of maximum inhibition, both IA1 and IA11 produced similar magnitude with 5-BDBD whereas the IA3's maximum inhibition was lower. The virtual docking showed that the docking poses of all three compounds were consistent with the docking poses of 5-BDBD.

However, the reduced potency of IA3 and IA11 might be explained with the effect of fluorine substitution. Whilst fluorine substitution in drug development has been extensively claimed for better biological activity, chemical or metabolic stabilities, and bioavailability in various classes of drugs including anti-cancer (Böhm et al., 2004; Hagmann, 2008; Isanbor & O'Hagan, 2006; Shah & Westwell, 2007), this was not the

case in this study. The fluorine substitution has significantly reduced the potency relative to 5-BDBD, which may be due to the increased lipophilicity and adjustments of pharmacokinetic properties that result in changes of primary pharmacology (Gillis et al., 2015). Overall, the substitution at position 1 was tolerated but fluorine-containing analogues were observed to have reduced potency.

4.4.1.2 Substitution at position 3

Experimental data indicated that the compounds with their position 3 substituted with halogens, i.e., fluorine (IA6), chlorine (IA9), bromine (STK731427), and trifluoromethane (IA7), still showed inhibitory properties comparable to 5-BDBD potency. They did not markedly change the potency of compounds relative to 5-BDBD since their IC_{50} values were not significantly different. In agreement with pharmacological data, the in silico experiment showed that the substituent at site 3 pointed away from the binding site and no evidence showed that those substituents took part in the binding.

Substitution with methoxy (STK864662) however, significantly decreased its potency relative to 5-BDBD. The relatively long chain of methoxy compared to the other four analogues might create a steric clash with other residues that subsequently make the binding less favourable. Hence, site 3 substitution with halogens and trifluoromethane was tolerated but not with a longer chain substituent such as methoxy.

4.4.1.3 Substitution at position 1 and 3

Among the analogues, four of them had both of their position 1 and 3 substituted with halogens; IA2 (both substituted with bromine), IA4 (trifluoromethane), IA8 (chlorine), and IA10 (fluorine). IA2, IA4, and IA10 lost their inhibitory properties while IA8 still blocked $P2X_4$ activity with a significantly higher maximum inhibition compared to 5-BDBD. From a modelling perspective, the presence of two substituents bulkier than chlorine appeared to be excessive compared to the available space within the binding pocket, thus only IA8 was tolerated but not others. However, IA10 had two smaller substituents (fluorine) than chlorine but it was not active at antagonising $P2X_4$ receptor activity. This data, nevertheless, was parallel with the data for IA11 (site 1 substituted

with fluorine) which also lost its inhibitory properties. This meant that fluorine substitution at site 1 caused the loss of inhibition.

4.4.1.4 Commercially available analogues

4.4.1.4.1 Substitution at position 2

Pharmacological data demonstrated that any substitution at position 2 greatly compromised the efficacy of molecules to inhibit P2X$_4$ activity. STK747973, STK079751, STK027946, and STK775918 were substituted with fluorine, chlorine, methyl, and bromine, respectively (in order of increasing substituent size). STK775918 which had the biggest substituent did not exhibit inhibition on the calcium response while the other three showed minimal inhibition relative to 5-BDBD when maximum concentration of compound was used (30 µM). The maximum inhibition recorded was 25.2 ± 5.6 %, 19.1 ± 4.0 % and 9.5 ± 2.5 % for compound STK747973, STK079751, and STK027946, respectively.

As observed in the docking of 5-BDBD (Figure 4.24), substitution site 2 was in close contact with Ala93 of the receptor. The substitution of hydrogen with a bulkier substituent than hydrogen would produce a steric clash, thus impeding efficient binding. Combining the results from pharmacological and computational simulation data, a likely explanation was that when the substituent became bigger, the molecule was offset from its ideal position within the binding site. In short, it was concluded that any substitution at position 2 was non-tolerable.

4.4.1.4.2 No substitution at any site

Apart from those three substitution sites discussed above, there was one compound that did not have any substitutions at any of the three positions (only hydrogens), which was STK045532. Surprisingly, this compound exhibited a good inhibition, like that of 5-BDBD and moreover significantly increased the maximum inhibition. Docking data showed this compound could bind at the orthosteric site of P2X$_4$, in a similar conformation to those described previously. It is worth noting that there was a

hydrophobic interaction between the phenylic region of 5-BDBD and deeper pocket of orthosteric binding site.

Taking the results from pharmacological and computational approaches, it can be deduced that the hydrophobic phenyl group was already sufficient for binding and that by substituting site 1 with halogen which made it more hydrophobic (e.g. as a comparison, XLogP3 value of 5-BDBD is 3.8 while 3.1 for STK045532, source: PubChem database) did not significantly enhance the potency (considering hydrophobic interaction would be stronger). It is likely that this interaction was not the most important interaction involved in binding or hydrophobicity difference has no significant impact on the binding potency. Meanwhile, the site 3 substitution was shown earlier to not involve in the binding interaction. Together, this showed that any substitution at either position 1 or 3 was not crucial for inhibitory action and potency.

4.4.1.4.3 Compound that lacked diazepinone

Compound STK021512 had a quite different backbone compared to 5-BDBD. It lacked the diazepinone ring that held the carbonyl group which was shown to form hydrogen bonds with Arg295 in virtual docking between the active compounds and human P2X$_4$ receptor model. Based on the pharmacological data, this compound did not inhibit the response which suggested that there was no binding between the compound and P2X$_4$ receptor. This data underlined that the diazepinone ring was essential for binding since the carbonyl group can form a hydrogen bond with Arg295.

4.4.2 Mode of action

The experimental data showed that all inhibiting compounds blocked the P2X$_4$ receptor competitively, just like 5-BDBD. The inhibition of all compounds was surmounted by high concentration of ATP, around 3 – 10 µM. In addition, the concentration-response curves of all compounds were shifted to the right of untreated cells, indicating that more ATP was required to overcome the inhibition; a classical indication of competitive antagonism. The unchanged mode of action across all compounds was also reflected in virtual docking where all active compounds docked into P2X$_4$ binding pocket in the same way as 5-BDBD. Ample space around

substitution site 1 (refer to Figure 4.24) allowed substitution with halogens and trifluoromethane (although fluorine and trifluoromethane substitution relatively reduced the potency, likely because of pharmacokinetic changes). Meanwhile, substitution at position 3 was robust because the substituent faced outside of the binding pocket.

In contrast with this finding, Abdelrahman et al. (2017) documented a different mode of action for 5-BDBD. Instead of competitive inhibition, their data indicated that 5-BDBD was an allosteric antagonist. This contradicting finding might be due to different experiment settings used. In this study, the experiment setting was that the cells that were pre-incubated with 5-BDBD for 30 minutes and then stimulated with different ATP concentrations to displace 5-BDBD. However, the study by Abdelrahman et al. (2017) was performed in the other way around. Radiolabelled [^{35}S]ATPγS was firstly pre-incubated for a period and then different concentrations of 5-BDBD were applied to displace [^{35}S]ATPγS. Based on the docking data from this study, the binding of ATP induced conformational change that caused the side chain of Lys67 to cover the hydrophobic pocket, which denied the entrance of 5-BDBD into the deeper pocket of orthosteric site. Therefore, that might explain the inability of 5-BDBD to displace [^{35}S]ATPγS even at high concentration because the entrance for 5-BDBD was totally blocked as [^{35}S]ATPγS remained at the binding pocket.

CHAPTER 5

CONCLUSIONS

5.1 Identification of thaspine as a P2X$_4$ inhibitor through high throughput screening

5.1.1 Conclusion

In summary, the human P2X$_4$ and P2X$_7$, and mouse P2X$_4$ DNAs were successfully inserted into pLVX-IRES-mCherry vector and transformed into *E. coli*, and DNA sequencing confirmed that there was no mutation occurred. The recombinant DNAs were then successfully transfected into human astrocytoma cells which then overexpressed the respective P2X receptors, as confirmed by calcium response and fluorescence microscopy. All overexpressing cells were characterised as the preparation for them to be used in the next phase of this study; the high throughput screening.

Throughout the screening, eight positive modulator and six inhibitor hits were identified to show the potential modulations on calcium response of the human P2X$_4$ overexpressing cells. Further investigation led to the identification of thaspine as the most potent inhibitor among the hits. Thaspine was further characterised using the human P2X$_4$ and other P2 overexpressing cells. It was found that thaspine blocks the human P2X$_4$ receptor noncompetitively with an IC$_{50}$ value of 3.81 ± 0.2 µM and it is also equipotent at the mouse P2X$_4$ receptor (3.53 ± 0.26 µM). It is an irreversible and slow-acting compound with maximum inhibition observed after $30 - 40$ minutes of pre-incubation. It also actively inhibits CTP-evoked response of the human P2X$_4$ receptor in a different host cells (HEK293) with a similar IC$_{50}$ value of 3.99 ± 1.0 µM, which indicated that the inhibitory activity of thaspine is independent of the type of host cells or nucleotides used.

Other than that, it is not active at human $P2X_2$, $P2X_{2/3}$, $P2X_7$, and $P2Y_6$ at ~3-fold IC_{50} concentration while at $P2Y_2$, it is not active below 10 µM. The testing on BV2 cells showed that its inhibitory effect is prominent on IVM-potentiated response in both quiescent and LPS-activated cells, as also observed for PSB12062-treated cells. However, it slightly potentiates the response in quiescent cells when activated by ATP but has no effect in the LPS-activated cells. In terms of mechanism of action, the current data suggested that it does not act by internalising the $P2X_4$ receptors but might diffuse through the plasma membrane and acts internally. However, the data are yet to be conclusive to support this theory.

Compared to previously reported $P2X_4$ antagonists — paroxetine (IC_{50} = 1.87 µM), N,N-diisopropyl-5H-dibenz[b,f]azepine-5-carboxamide (IC_{50} = 3.44 µM), PSB12054 (IC_{50} = 0.19 µM), PSB12062 (IC_{50} = 0.9 µM), TNP-ATP (IC_{50} = 15.0 µM), 5-BDBD (IC_{50} = 0.5 µM), BX430 (IC_{50} = 0.54 µM), NP-1815-PX (IC_{50} = 0.26 µM), and duloxetine (IC_{50} = 1.59 µM) (Ase et al., 2015; Fischer et al., 2004; Gum et al., 2012; Hernandez-Olmos et al., 2012; Matsumura et al., 2016; Nagata et al., 2009; Tian et al., 2014; Yamashita et al., 2016) — thaspine was less potent except the TNP-ATP. However, it has been demonstrated that it was equipotent at both human and mouse $P2X_4$, unlike the PSB12054 and BX430 which were respectively less active and unresponsive at mouse $P2X_4$. It also selectively inhibited the $P2X_4$ compared to $P2X_2$, $P2X_{2/3}$, and $P2X_7$ and was selective at $P2Y_2$ and $P2Y_6$ at concentrations of lower than 10 and 30 µM, respectively.

5.1.2 Future direction

Thaspine is a novel potential compound that can be developed as an inhibitor for $P2X_4$ receptor or as a template to design a more potent compound. Yet, there are more experiments needed to be done to further characterise the compound. One of them is that thaspine should be tested in electrophysiology experiments to directly measure the $P2X_4$ cation current in the cells. It is hoped that the electrophysiology experiment can give direct evidence of the inhibitory properties of thaspine at $P2X_4$ receptor.

Besides, as the data suggested that thaspine does not act by internalising $P2X_4$ receptors, this can be further tested by biotinylation of surface receptors, and analysed

by SDS-PAGE and immunoblotting to quantitate the membrane-bound $P2X_4$ receptors in the presence and absence of thaspine pre-incubation. Whereas, for the second theory on the mechanism of action is thaspine acts on an internal epitope of P2X4, it can be verified using the electrophysiology experiment in an inside-out configuration or adding thaspine into internal solution in a whole-cell configuration. If thaspine acts from the cytosolic environment, the application of thaspine directly into the cytosol may exhibit a relatively faster inhibition (than observed in calcium assay) on cation current.

In addition, this present investigation was not carried out on primary cells. It would be better if it is tested on primary cells such as microglial cells or macrophage that are reported to abundantly contain $P2X_4$ receptors. Data acquired from such experiments would reflect a more accurate prediction for the in vivo data.

5.2   Structure activity relationship study of 5-BDBD and $P2X_4$ receptor

5.2.1   Conclusion

So far, this is the first study that explored the structure activity relationship of 5-BDBD and $P2X_4$ receptor. In this part of study, a few novel findings were discovered. The first one was the substitution at either site 1 or 3 was tolerated. This was supported by molecular modelling, which identified a cavity able to accommodate a range of substituents. On the other hand, substitution at position 2 seriously impaired the ability of a compound inhibition because of clashing with Ala93 on the receptor that prevented the effective binding. On top of that, a compound without any substitutions at the considered positions was equipotent with 5-BDBD, indicating that the substitutions were not necessary for the inhibitory property. The carbonyl group at benzodiazepinone of 5-BDBD and Arg295 of receptor were the crucial elements of compound and receptor, respectively, for binding to occur. Apart from that, both pharmacological and virtual docking data led to a conclusion that 5-BDBD was a competitive inhibitor and the contradicting discoveries with previous report were a consequence of different experiment settings.

5.2.2 Future direction

There are many experiments and analyses that can be done to explore 5-BDBD further but only experiments that are most related to this present study will be discussed. The mode of action of 5-BDBD can be further verified using two methods. One of them is Schild analysis which is a technique of measuring response in the presence of few concentrations of 5-BDBD, stimulated by extensive concentrations of ATP to surmount the inhibition. If responses for all 5-BDBD concentrations can reach the same maximum magnitude and there is a clear right-shift of sigmoidal curves compared to untreated cells, as well as significant change in EC_{50} value, it can be deduced that it is a competitive blocker. However, due to time constraint, this analysis was not performed.

Another method to verify the finding is the mutagenesis of P2X$_4$ receptor. Based on the docking data, Arg295 is critical for the binding of 5-BDBD and P2X$_4$. Thus, by mutating Arg295, it is hypothesised that 5-BDBD cannot bind to the binding site and hence, lose its inhibitory property. However, there is also a chance that by mutating the residue, it will also impair the binding of ATP as Arg295 is one of six key residues that form hydrogen bond with ATP to form the binding. In that case, it is impossible to measure the ATP-evoked response because ATP unable to bind with P2X$_4$. Having said that, there are also five other residues that might salvage the loss of Arg295 and establish the ATP binding conformation.

Zemkova et al. (2007) did a mutation study on P2X$_4$ and reported that the mutation of Arg295 into alanine or lysine severely impaired the sensitivity of mutants towards ATP. Nevertheless, they found that the loss of sensitivity could be rescued by IVM pre-treatment and ATP-evoked response was restored, with EC_{50} values of 267 ± 41 µM for R295A and 57 ± 12 µM for R295K. Therefore, mutagenesis study of 5-BDBD could involve the mutation of Arg295 with lysine and pre-treating cells with IVM and 5-BDBD as well as proper controls, to observe the effect of 5-BDBD on the mutants. If there is no inhibition observed on the IVM-potentiated response, it may indicate that Arg295 is the key player for binding and that 5-BDBD is a true competitive inhibitor. That is because 5-BDBD is hypothesised to bind at orthosteric site and if it loses its ability to bind when the key residue is mutated, it means that Arg295 is important for

binding to occur. Another way to determine the binding is by employing the saturation transfer difference nuclear magnetic resonance (STD-NMR). The tool can give information on the binding occurs between a ligand and protein by looking at the spectrum difference between the unbound and protein-bound ligand (Viegas et al., 2011). Hence, the possibility of 5-BDBD binding with $P2X_4$ mutants can be determined without the need to measure the ATP-evoked response.
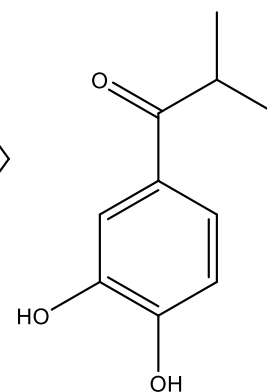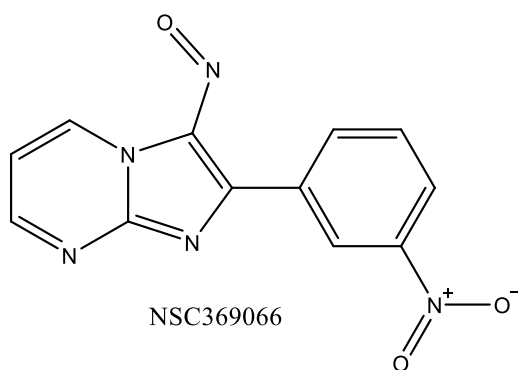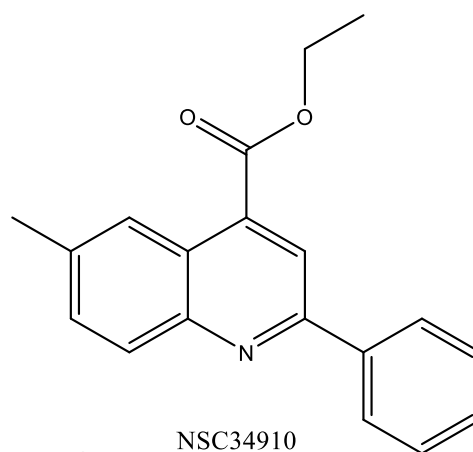
APPENDICES
Appendix I
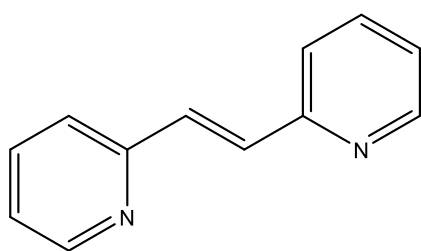
NSC9489
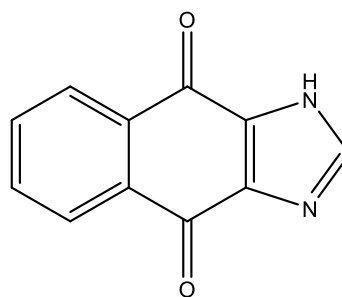
NSC14771

NSC27389

NSC369066

NSC34910
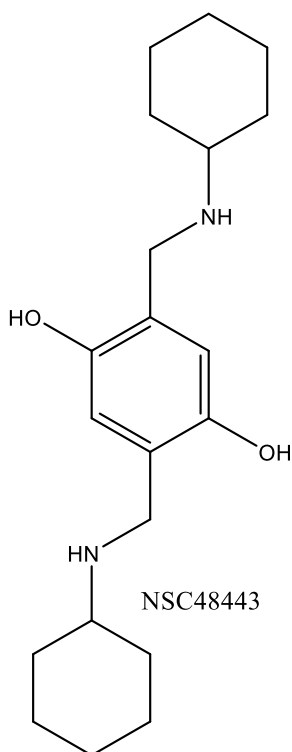
NSC48443
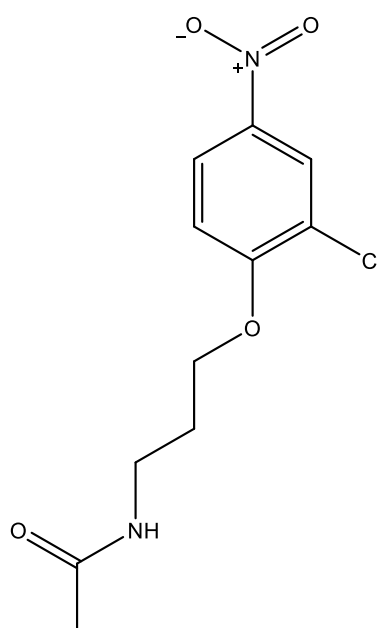
NSC211336
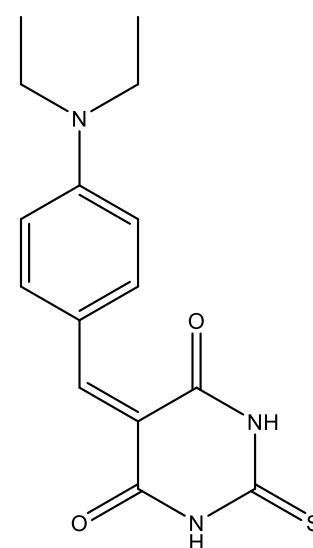
NSC90749

Chemical structures of potential positive modulators.
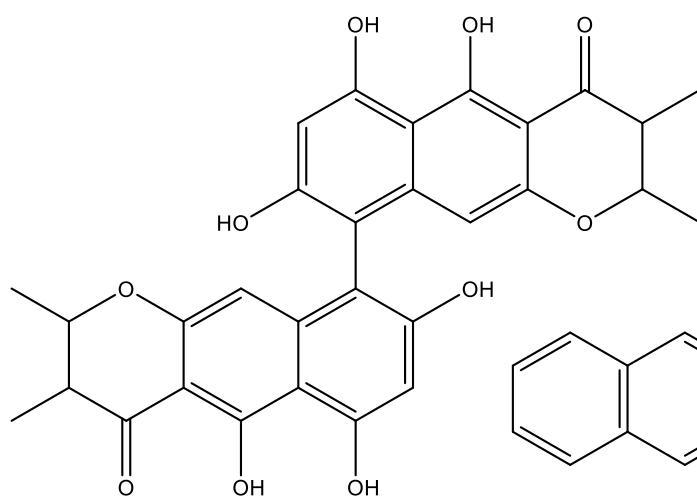
NSC345647
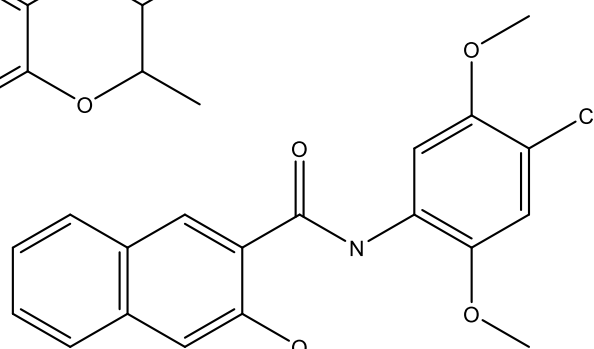
NSC50688
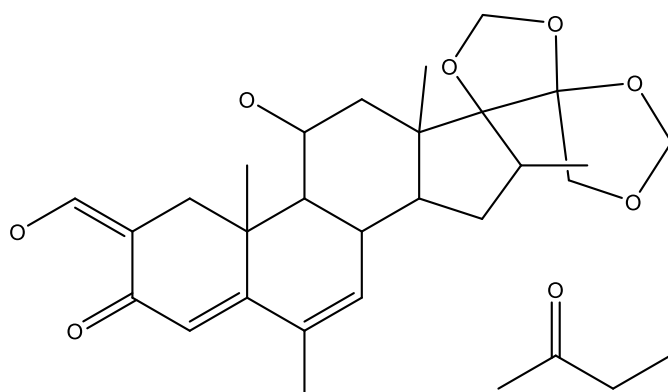
NSC116339
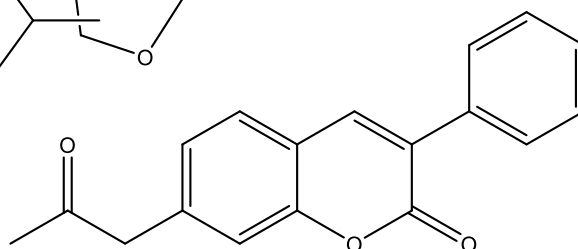
NSC17055
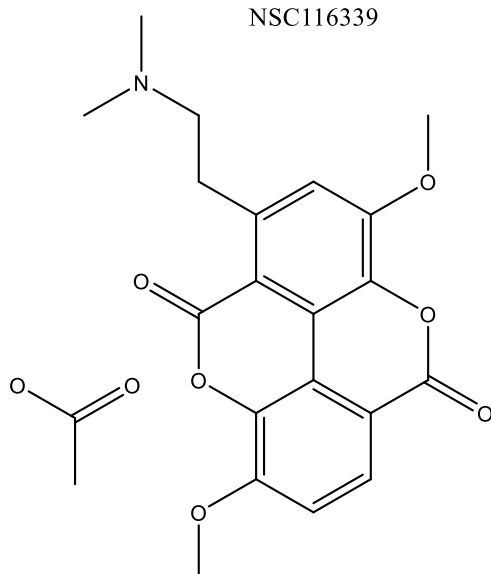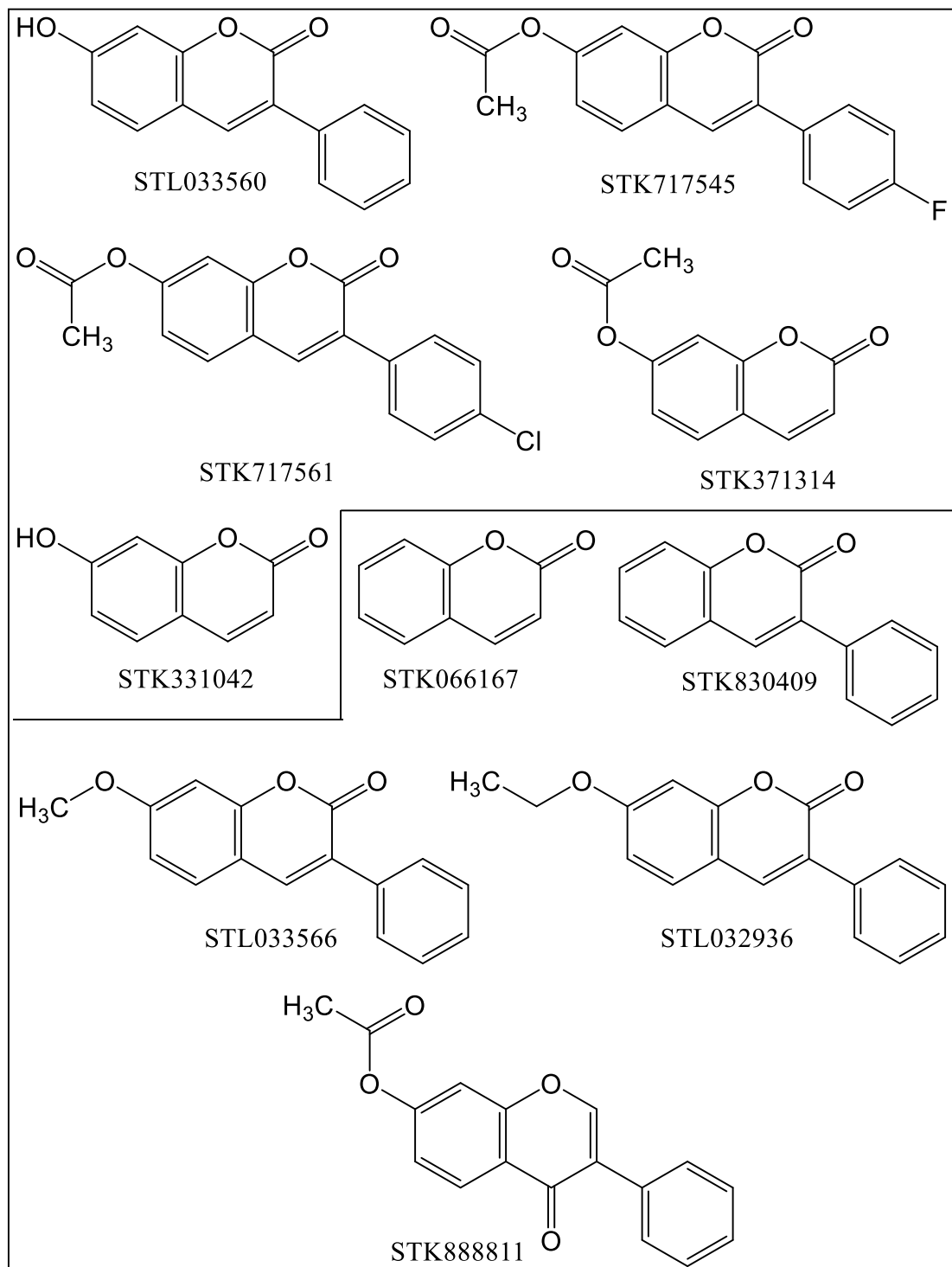
Thaspine
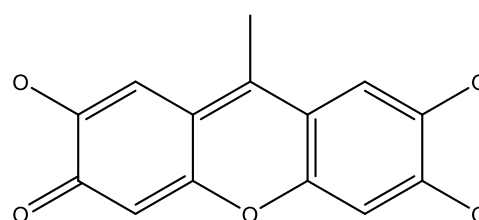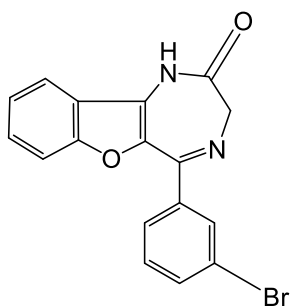
NSC5426

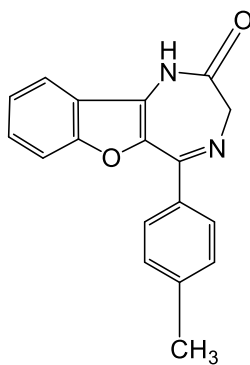**Chemical structures of potential antagonists.**

Chemical structures of NSC17055 analogues.

The upper part are the compounds that reduced ATP-evoked response and the lower part did not have effect on the response.
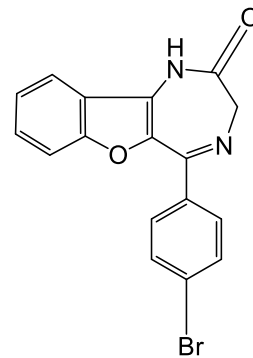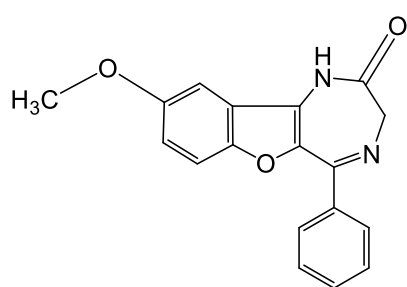
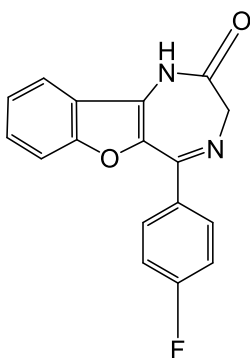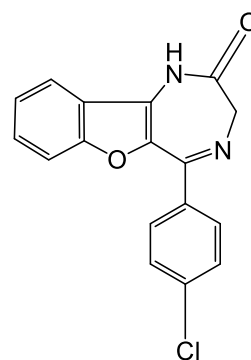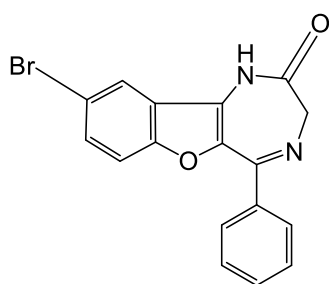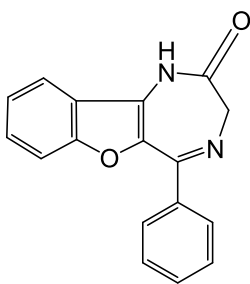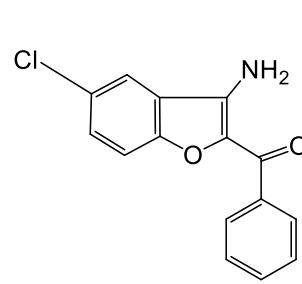**Chemical structures of 5-BDBD and commercial analogues.**
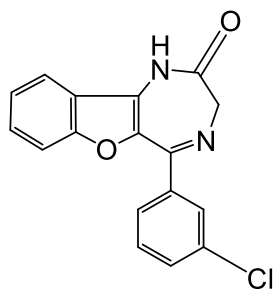
IA1
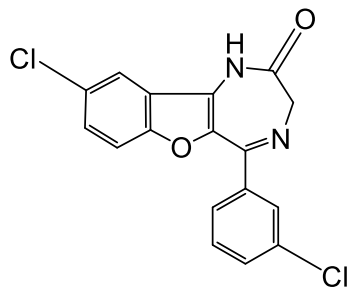
IA8
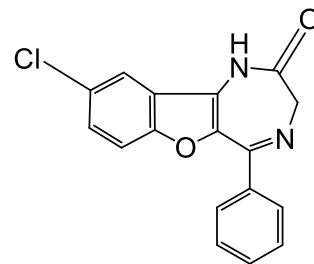
IA9
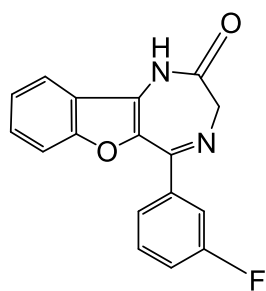
IA11
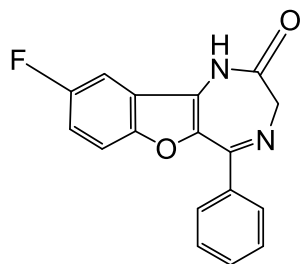
IA6
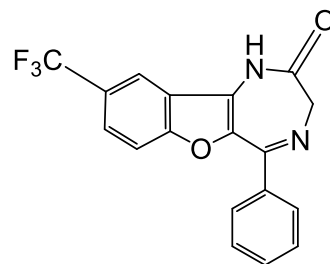
IA7
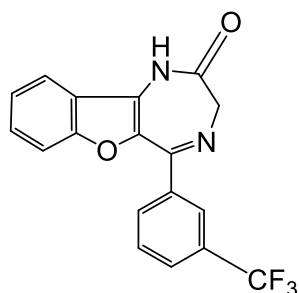
IA3
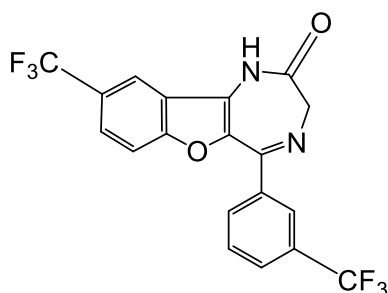
IA4
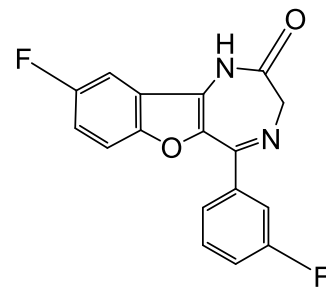
IA10
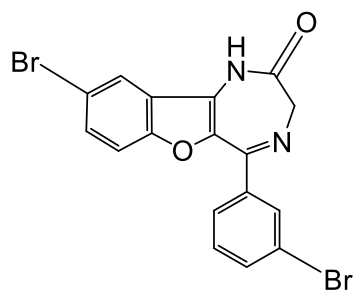
IA2

Chemical structures of synthesised 5-BDBD analogues.
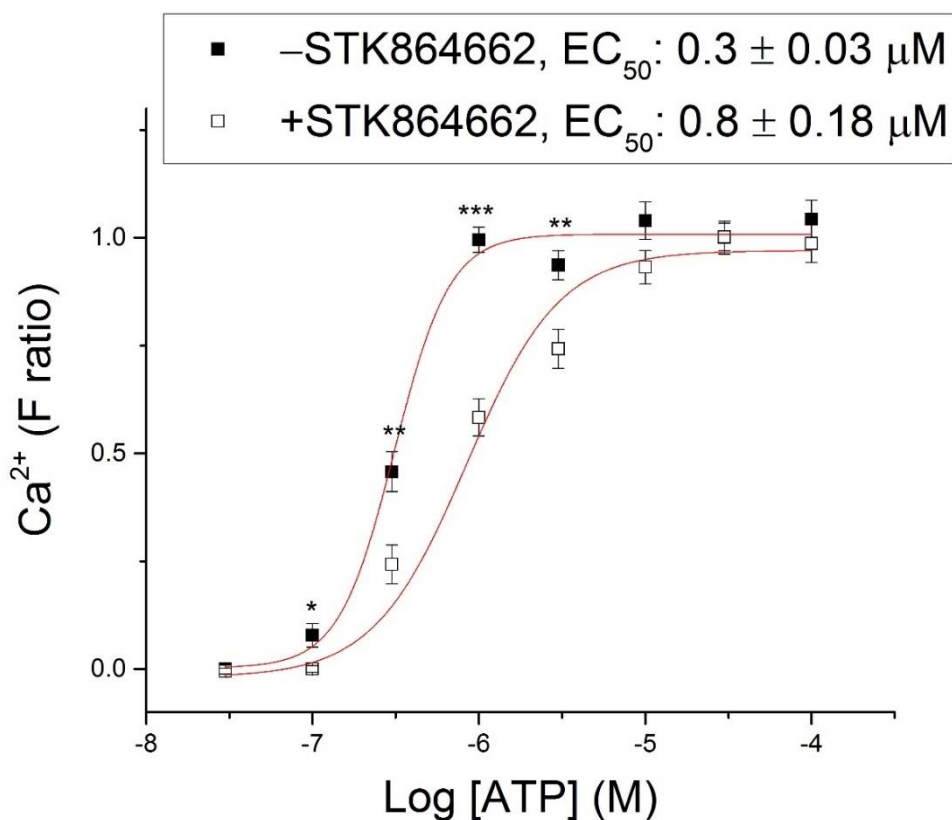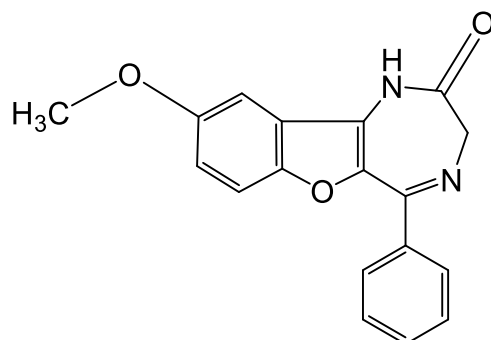
ATP concentration-response in the absence and presence of STK864662.
The plots show ATP concentration-response in the presence (open square) and absence (close square) of 4.8 μM of STK864662. EC_{50} value in the presence of STK864662 was significantly higher than that with the compound ($p<0.05$). The difference between each data point was statistically calculated and marked with asterisk to indicate level of difference. The right shift of treated cells curve compared to vehicle together with significant increase in EC_{50} value indicated competitive mode of antagonism. The top panel shows the chemical structure of STK864662. Asterisk denotes p value; * - <0.05, ** - <0.01, *** - <0.001. (n=4)

ATP concentration-response in the absence and presence of STK731427.
The plots show ATP concentration-response in the presence (open square) and absence (close square) of 1.0 µM of STK731427. EC_{50} value in the presence of STK731427 was significantly higher than that with the compound (p<0.05). The difference between each data point was statistically calculated and marked with asterisk to indicate level of difference. The right shift of treated cells curve compared to vehicle together with significant increase in EC_{50} value indicated competitive mode of antagonism. The top panel shows the chemical structure of STK731427. Asterisk denotes p value; * - <0.05, ** - <0.01, *** - <0.001. (n=3)

ATP concentration-response in the absence and presence of IA1.
The plots show ATP concentration-response in the presence (open square) and absence (close square) of 2.3 µM of IA1. EC_{50} value in the presence of IA1 was significantly higher than that with the compound ($p<0.01$). The difference between each data point was statistically calculated and marked with asterisk to indicate level of difference. The right shift of treated cells curve compared to vehicle together with significant increase in EC_{50} value indicated competitive mode of antagonism. The top panel shows the chemical structure of IA1. Asterisk denotes p value; * - <0.05, ** - <0.01, *** - <0.001. (n=3)

ATP concentration-response in the absence and presence of IA6.
The plots show ATP concentration-response in the presence (open square) and absence (close square) of 1.2 μM of IA6. EC_{50} value in the presence of IA6 was significantly higher than that with the compound ($p < 0.05$). The difference between each data point was statistically calculated and marked with asterisk to indicate level of difference. The right shift of treated cells curve compared to vehicle together with significant increase in EC_{50} value indicated competitive mode of antagonism. The top panel shows the chemical structure of IA6. Asterisk denotes p value; * - <0.05, ** - <0.01, *** - <0.001. (n=4)
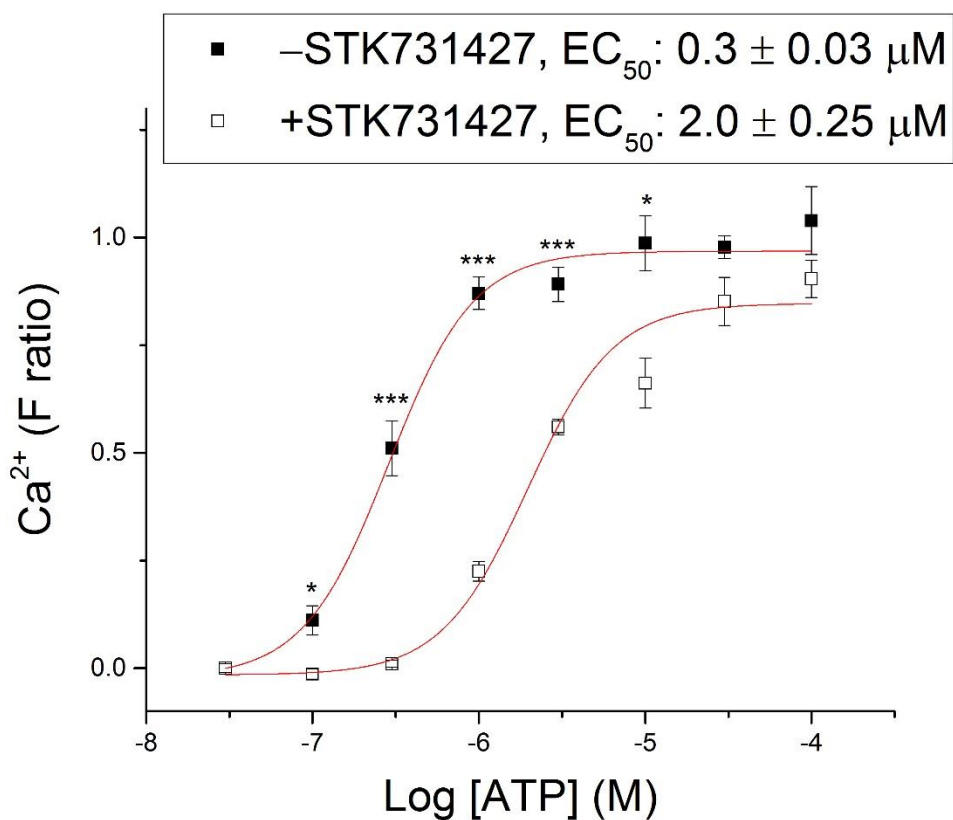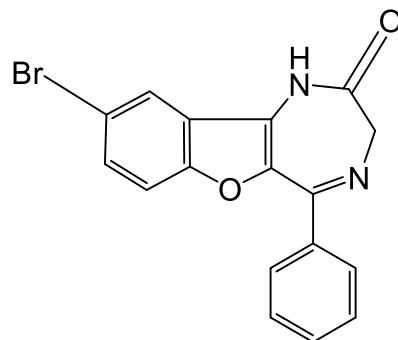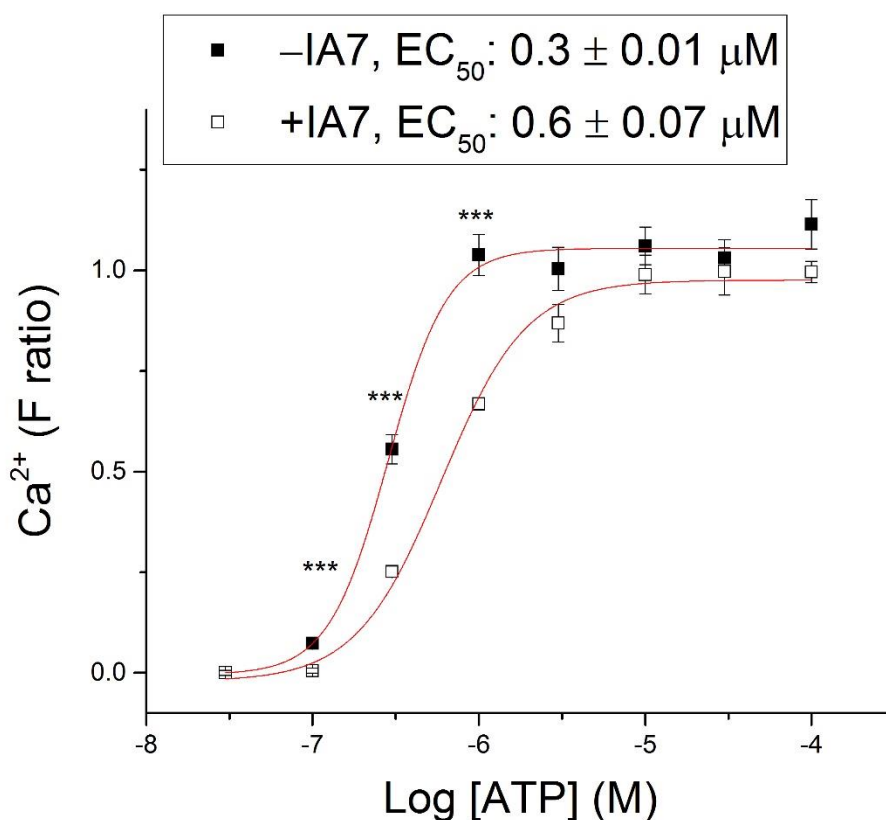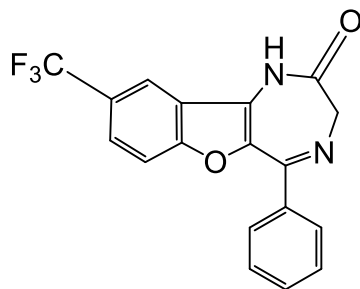
ATP concentration-response in the absence and presence of IA7.
The plots show ATP concentration-response in the presence (open square) and absence (close square) of 2.7 μM of IA7. EC_{50} value in the presence of IA7 was significantly higher than that with the compound ($p<0.05$). The difference between each data point was statistically calculated and marked with asterisk to indicate level of difference. The right shift of treated cells curve compared to vehicle together with significant increase in EC_{50} value indicated competitive mode of antagonism. The top panel shows the chemical structure of IA7. Asterisk denotes p value; * - <0.05, ** - <0.01, *** - <0.001. (n=4)
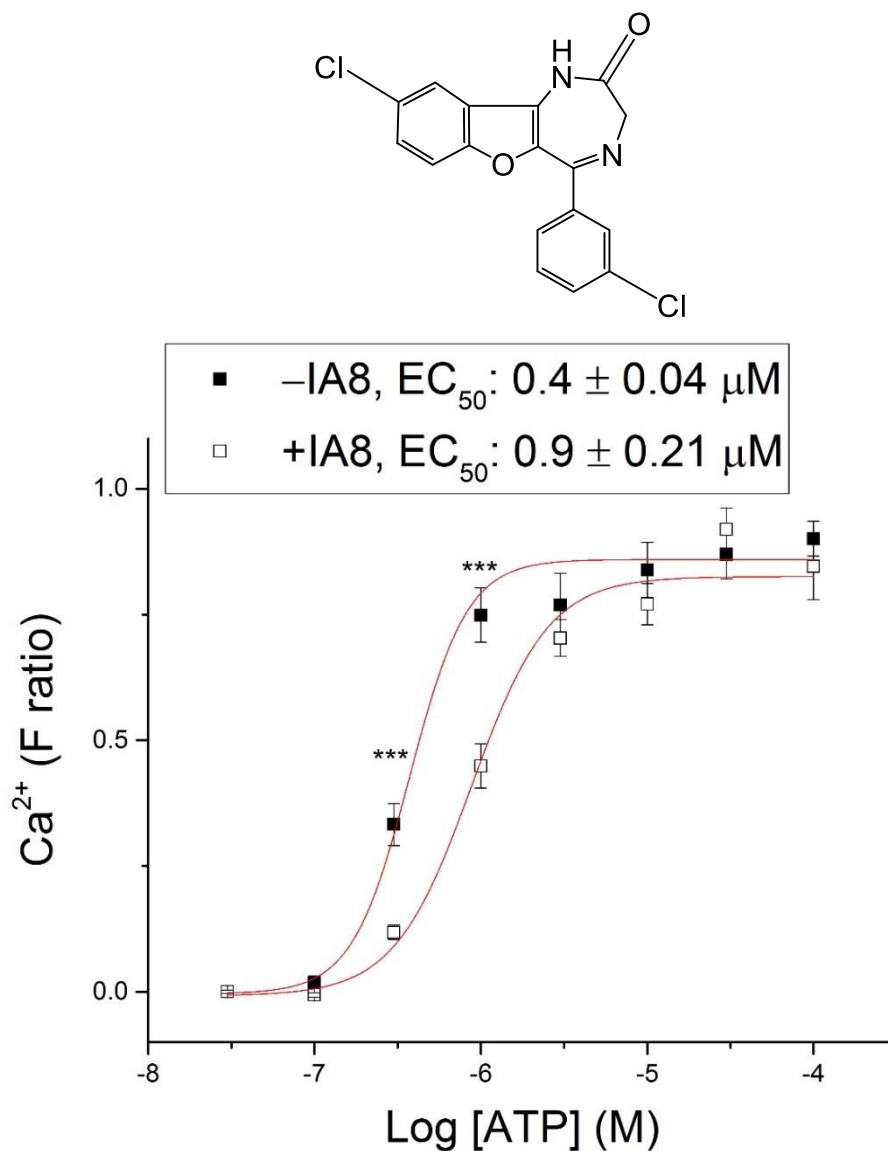
ATP concentration-response in the absence and presence of IA8.
The plots show ATP concentration-response in the presence (open square) and absence (close square) of 1.1 µM of IA8. EC_{50} value in the presence of IA8 was significantly higher than that with the compound ($p<0.05$). The difference between each data point was statistically calculated and marked with asterisk to indicate level of difference. The right shift of treated cells curve compared to vehicle together with significant increase in EC_{50} value indicated competitive mode of antagonism. The top panel shows the chemical structure of IA8. Asterisk denotes p value; * - <0.05, ** - <0.01, *** - <0.001. (n=4)
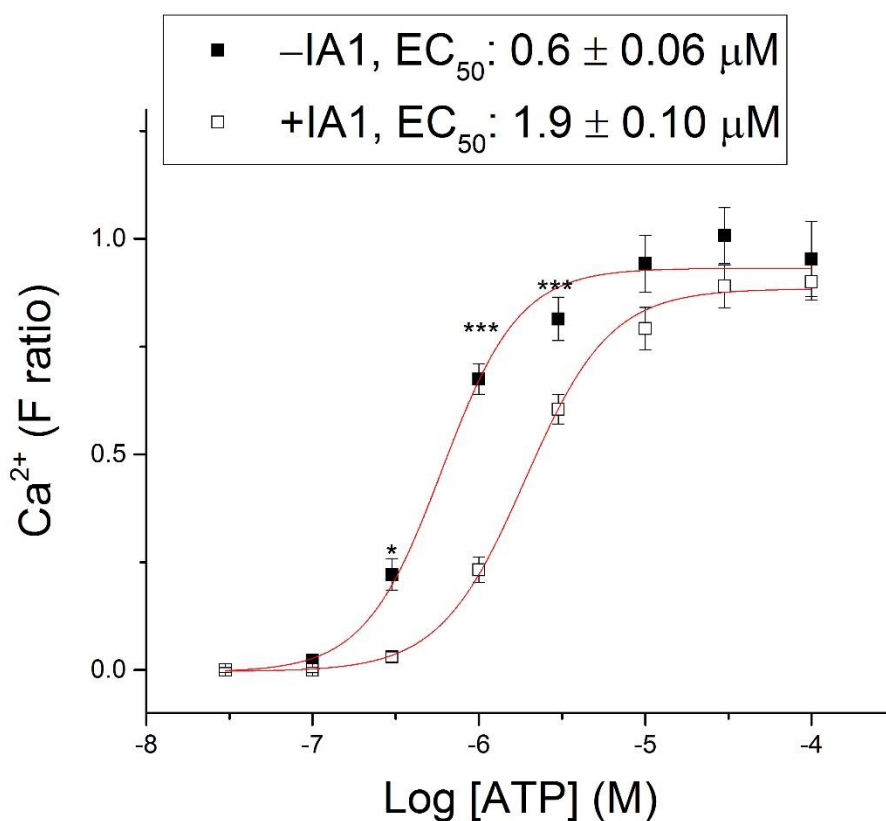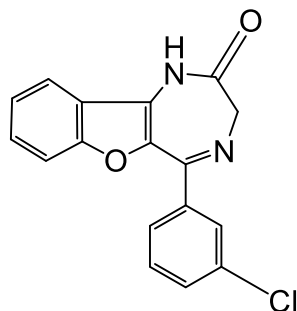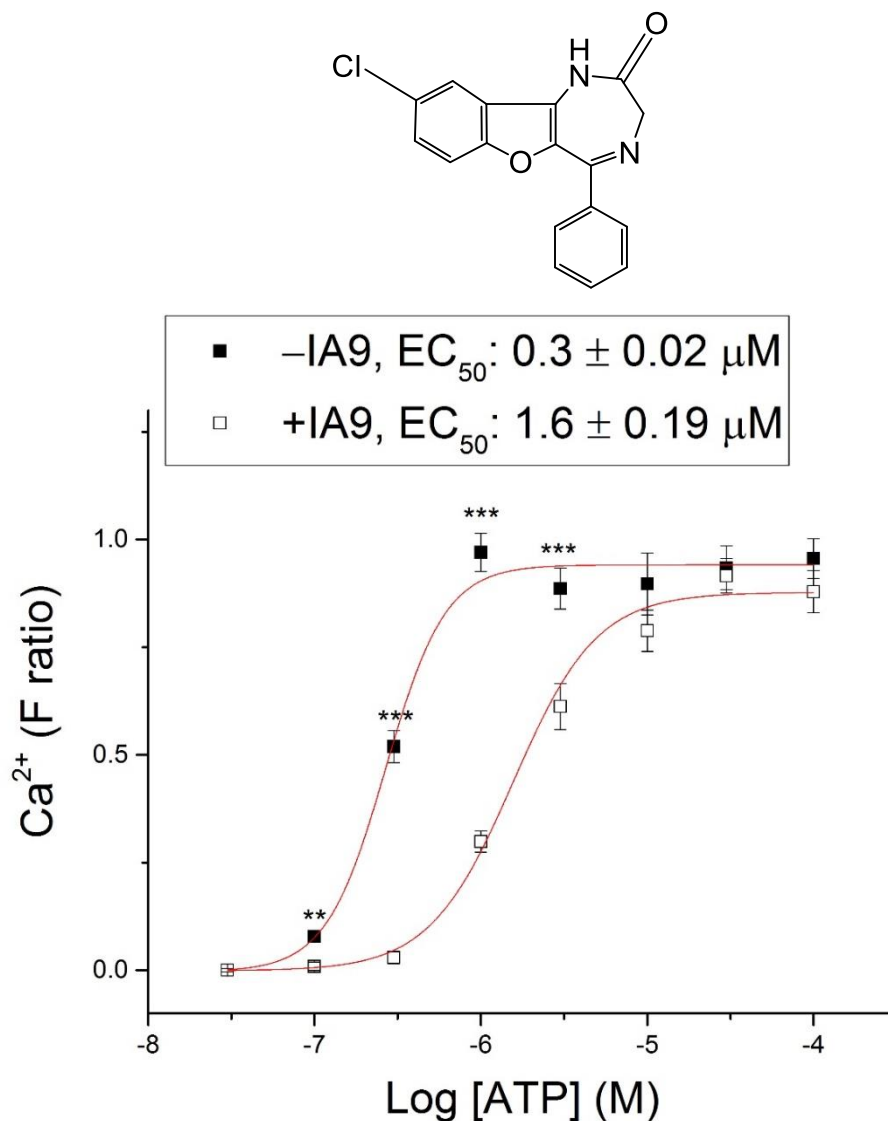
ATP concentration-response in the absence and presence of IA9.
The plots show ATP concentration-response in the presence (open square) and absence (close square) of 1.1 µM of IA9. EC_{50} value in the presence of IA9 was significantly higher than that with the compound ($p<0.01$). The difference between each data point was statistically calculated and marked with asterisk to indicate level of difference. The right shift of treated cells curve compared to vehicle together with significant increase in EC_{50} value indicated competitive mode of antagonism. The top panel shows the chemical structure of IA9. Asterisk denotes p value; * - <0.05, ** - <0.01, *** - <0.001. (n=4)
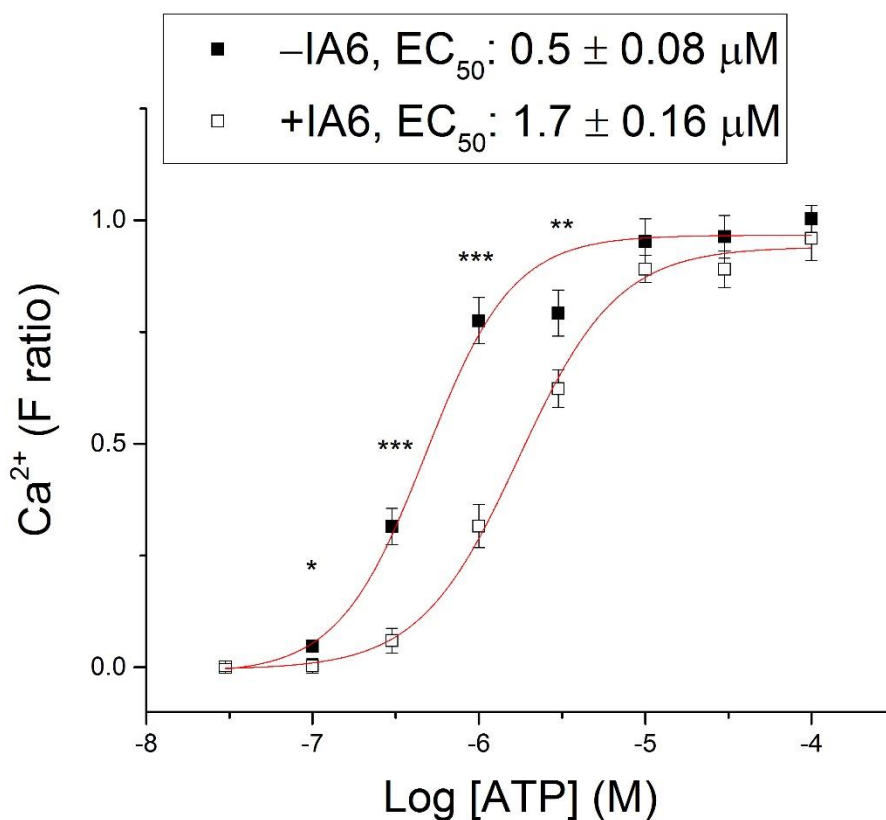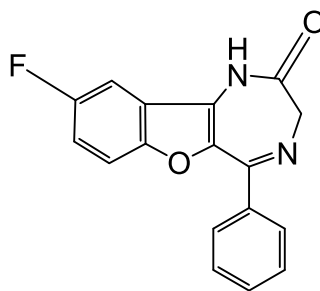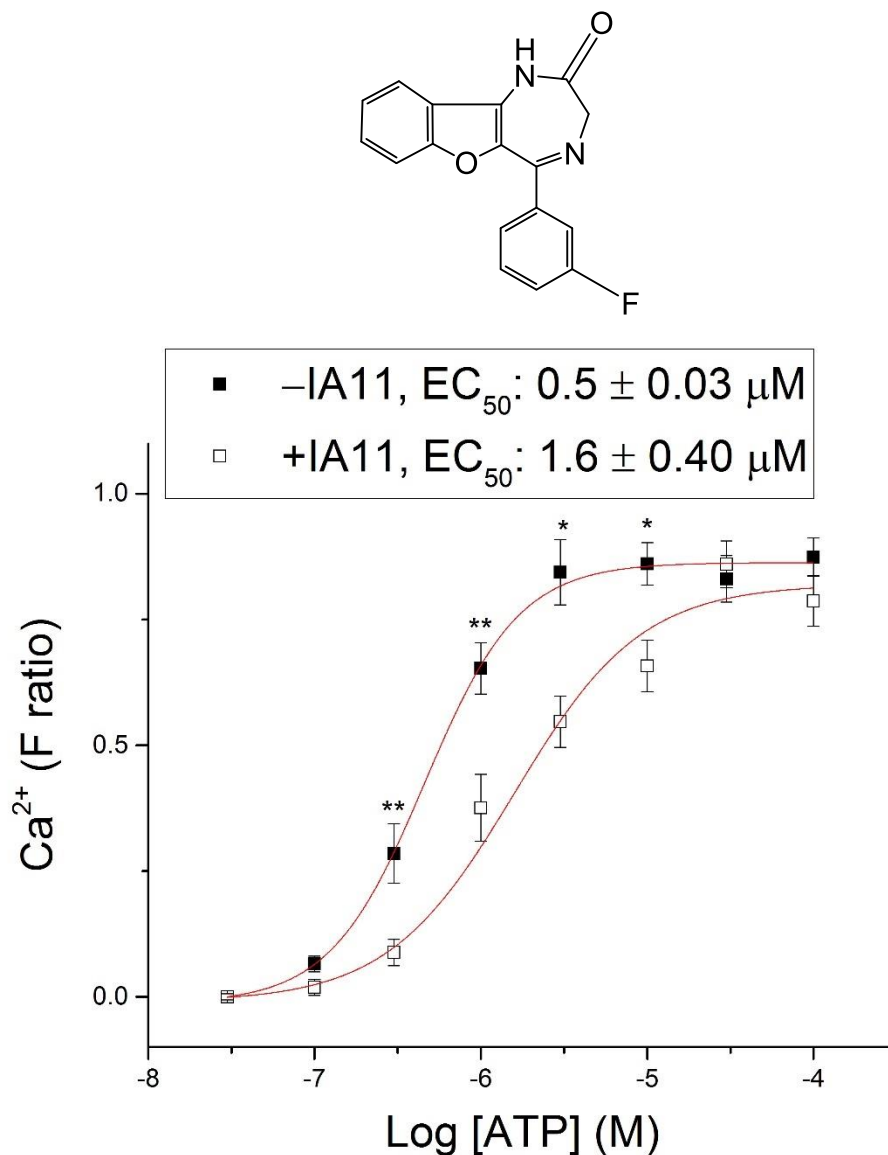
ATP concentration-response in the absence and presence of IA11.
The plots show ATP concentration-response in the presence (open square) and absence (close square) of 4.5 µM of IA11. EC_{50} value in the presence of IA11 was significantly higher than that with the compound ($p<0.05$). The difference between each data point was statistically calculated and marked with asterisk to indicate level of difference. The right shift of treated cells curve compared to vehicle together with significant increase in EC_{50} value indicated competitive mode of antagonism. The top panel shows the chemical structure of IA11. Asterisk denotes p value; * - <0.05, ** - <0.01, *** - <0.001. (n=4)

BIBLIOGRAPHY

Abbracchio, M. P., Boeynaems, J.-M., Barnard, E. A., Boyer, J. L., Kennedy, C., Miras-Portugal, M. T., King, B. F., Gachet, C., Jacobson, K. A., Weisman, G. A., & Burnstock, G. (2003). Characterization of the UDP-glucose receptor (renamed here the $P2Y_{14}$ receptor) adds diversity to the P2Y receptor family. *Trends in Pharmacological Sciences, 24*(2), 52-55.

Abbracchio, M. P., Burnstock, G., Boeynaems, J.-M., Barnard, E. A., Boyer, J. L., Kennedy, C., Knight, G. E., Fumagalli, M., Gachet, C., Jacobson, K. A., & Weisman, G. A. (2006). International Union of Pharmacology LVIII: Update on the P2Y G Protein-Coupled Nucleotide Receptors: From Molecular Mechanisms and Pathophysiology to Therapy. *Pharmacological Reviews, 58*(3), 281-341.

Abbracchio, M. P., Burnstock, G., Verkhratsky, A., & Zimmermann, H. (2009). Purinergic signalling in the nervous system: an overview. *Trends in Neurosciences, 32*(1), 19-29.

Abdelrahman, A., Namasivayam, V., Hinz, S., Schiedel, A. C., Köse, M., Burton, M., El-Tayeb, A., Gillard, M., Bajorath, J., de Ryck, M., & Müller, C. E. (2017). Characterization of $P2X_4$ receptor agonists and antagonists by calcium influx and radioligand binding studies. *Biochemical Pharmacology, 125*, 41-54.

Acuña-Castillo, C., Morales, B., & Huidobro-Toro, J. P. (2000). Zinc and Copper Modulate Differentially the P2X4 Receptor. *Journal of Neurochemistry, 74*(4), 1529-1537.

Altschul, S. F., Madden, T. L., Schäffer, A. A., Zhang, J., Zhang, Z., Miller, W., & Lipman, D. J. (1997). Gapped BLAST and PSI-BLAST: a new generation of protein database search programs. *Nucleic Acids Research, 25*(17), 3389-3402.

Altschul, S. F., Wootton, J. C., Gertz, E. M., Agarwala, R., Morgulis, A., Schäffer, A. A., & Yu, Y.-K. (2005). Protein Database Searches Using Compositionally Adjusted Substitution Matrices. *The FEBS journal, 272*(20), 5101-5109.

Asatryan, L., Popova, M., Perkins, D., Trudell, J. R., Alkana, R. L., & Davies, D. L. (2010). Ivermectin Antagonizes Ethanol Inhibition in Purinergic $P2X_4$ Receptors. *Journal of Pharmacology and Experimental Therapeutics, 334*(3), 720-728.

Ase, A. R., Honson, N. S., Zaghdane, H., Pfeifer, T. A., & Séguéla, P. (2015). Identification and Characterization of a Selective Allosteric Antagonist of Human $P2X_4$ Receptor Channels. *Mol Pharmacol, 87*(4), 606-616.

Balazs, B., Danko, T., Kovacs, G., Koles, L., Hediger, M. A., & Zsembery, A. (2013). Investigation of the Inhibitory Effects of the Benzodiazepine Derivative, 5-BDBD on P2X(4) Purinergic Receptors by two Complementary Methods. *Cellular Physiology and Biochemistry, 32*(1), 11-24.

Balboa, M. a. A., Balsinde, J., Johnson, C. A., & Dennis, E. A. (1999). Regulation of Arachidonic Acid Mobilization in Lipopolysaccharide-activated P388D1 Macrophages by Adenosine Triphosphate. *Journal of Biological Chemistry, 274*(51), 36764-36768.

Ballini, E., Virginio, C., Medhurst, S. J., Summerfield, S. G., Aldegheri, L., Buson, A., Carignani, C., Chen, Y. H., Giacometti, A., Lago, I., Powell, A. J., & Jarolimek, W. (2011). Characterization of three diaminopyrimidines as potent and selective antagonists of $P2X_3$ and $P2X_{2/3}$ receptors with in vivo efficacy in a pain model. *British Journal of Pharmacology, 163*(6), 1315-1325.

Baxter, A. W., Choi, S. J., Sim, J. A., & North, R. A. (2011). Role of $P2X_4$ receptors in synaptic strengthening in mouse CA1 hippocampal neurons. *European Journal of Neuroscience, 34*(2), 213-220.

Bean, B. P. (1990). ATP-activated channels in rat and bullfrog sensory neurons: concentration dependence and kinetics. *Journal of Neuroscience, 10*(1), 1-10.

Beggs, S., & Salter, M. W. (2010). Microglia-neuronal signalling in neuropathic pain hypersensitivity 2.0. *Current Opinion in Neurobiology, 20*(4), 474-480.

Bianchi, B. R., Lynch, K. J., Touma, E., Niforatos, W., Burgard, E. C., Alexander, K. M., Park, H. S., Yu, H., Metzger, R., Kowaluk, E., Jarvis, M. F., & van Biesen, T. (1999). Pharmacological characterization of recombinant human and rat P2X receptor subtypes. *European Journal of Pharmacology, 376*(1–2), 127-138.

Biber, K., & Boddeke, E. (2014). Neuronal CC chemokines: the distinct roles of CCL21 and CCL2 in neuropathic pain. *Frontiers in Cellular Neuroscience, 8*, 210.

Biber, K., Tsuda, M., Tozaki-Saitoh, H., Tsukamoto, K., Toyomitsu, E., Masuda, T., Boddeke, H., & Inoue, K. (2011). Neuronal CCL21 up-Regulates Microglia $P2X_4$ Expression and Initiates Neuropathic Pain Development. *Glia, 59*, S100-S100.

Bjelobaba, I., Janjic, M. M., & Stojilkovic, S. S. (2015). Purinergic Signaling Pathways in Endocrine System. *Autonomic Neuroscience : Basic & Clinical, 191*, 102-116.

Blackwood, A. M., & Bolton, T. B. (1993). Mechanism of carbachol-evoked contractions of guinea-pig ileal smooth muscle close to freezing point. *British Journal of Pharmacology, 109*(4), 1029-1037.

Bo, X., Zhang, Y., Nassar, M., Burnstock, G., & Schoepfer, R. (1995). A P2X purinoceptor cDNA conferring a novel pharmacological profile. *FEBS Letters, 375*(1-2), 129-133.

Bobanovic, L. K., Royle, S. J., & Murrell-Lagnado, R. D. (2002). P2X Receptor Trafficking in Neurons Is Subunit Specific. *The Journal of Neuroscience, 22*(12), 4814-4824.

Böhm, H.-J., Banner, D., Bendels, S., Kansy, M., Kuhn, B., Müller, K., Obst-Sander, U., & Stahl, M. (2004). Fluorine in Medicinal Chemistry. *Chembiochem, 5*(5), 637-643.

Boumechache, M., Masin, M., Edwardson, J. M., Górecki, D. C., & Murrell-Lagnado, R. (2009). Analysis of Assembly and Trafficking of Native P2X4 and P2X7 Receptor Complexes in Rodent Immune Cells. *Journal of Biological Chemistry, 284*(20), 13446-13454.

Boyer, R., Deckey, G., Marzzacco, C., Mulvaney, M., Schwab, C., & Halpern, A. M. (1985). The photophysical properties of 2-naphthol: A physical chemistry experiment. *Journal of Chemical Education, 62*(7), 630.

Bridges, T. M., & Lindsley, C. W. (2008). G-Protein-Coupled Receptors: From Classical Modes of Modulation to Allosteric Mechanisms. *ACS Chemical Biology, 3*(9), 530-541.

Burnstock, G. (1971). Neural nomenclature. *Nature, 229*(5282), 282-283.

Burnstock, G. (1998). History of Extracellular Nucleotides and Their Receptors. In J. T. Turner, G. A. Weisman & J. S. Fedan (Eds.), *The P2 Nucleotide Receptors* (pp. 3-40). Totowa, NJ: Humana Press.

Burnstock, G. (2004). Introduction: P2 Receptors. *Current Topics in Medicinal Chemistry, 4*, 793-803.

Burnstock, G. (2006). Purinergic signalling. *British Journal of Pharmacology, 147*(S1), S172-S181.

Burnstock, G. (2007). Purine and pyrimidine receptors. *Cellular and Molecular Life Sciences, 64*(12), 1471.

Burnstock, G., & Kennedy, C. (1985). Is there a basis for distinguishing two types of P2-purinoceptor? *General Pharmacology: The Vascular System, 16*(5), 433-440.

Burnstock, G., & WIlliams, M. (2000). P2 Purinergic Receptors: Modulation of Cell Function and Therapeutic Potential. *Journal of Pharmacology and Exparimental Therapeutics, 295*(3), 862-869.

Campbell, I. D., & Humphries, M. J. (2011). Integrin structure, activation, and interactions. *Cold Spring Harbor Perspectives in Biology, 3*(3), a004994.

Campwala, H. (2015). *Investigating the role of the CCL2/CCR2 axis in monocytes and its modulation by extracellular nucleotides.* (Doctor of Philosophy), University of East Anglia, Norwich, United Kingdom.

Caridha, D., Yourick, D., Cabezas, M., Wolf, L., Hudson, T. H., & Dow, G. S. (2008). Mefloquine-Induced Disruption of Calcium Homeostasis in Mammalian Cells Is Similar to That Induced by Ionomycin. *Antimicrobial Agents and Chemotherapy, 52*(2), 684-693.

Castelli, S., Katkar, P., Vassallo, O., Falconi, M., Linder, S., & Desideri, A. (2013). A Natural Anticancer Agent Thaspine Targets Human Topoisomerase IB. *Anti-Cancer Agents in Medicinal Chemistry, 13*(2), 356-363.

Chen, Y., Corriden, R., Inoue, Y., Yip, L., Hashiguchi, N., Zinkernagel, A., Nizet, V., Insel, P. A., & Junger, W. G. (2006). ATP Release Guides Neutrophil Chemotaxis via $P2Y_2$ and A_3 Receptors. *Science, 314*(5806), 1792-1795.

Chough, S. P., Goldenring, J. R., Hurst, R. D., Ballantyne, G. H., & Modlin, I. M. (1993). Calcium modulation of the effects of serotonin, carbachol, and histamine on rabbit ileal ion transport. *The Yale Journal of Biology and Medicine, 66*(6), 525-540.

Clarke, C. E., Benham, C. D., Bridges, A., George, A. R., & Meadows, H. J. (2000). Mutation of histidine 286 of the human P2X4 purinoceptor removes extracellular pH sensitivity. *The Journal of Physiology, 523*(3), 697-703.

Coddou, C., Yan, Z., Obsil, T., Huidobro-Toro, J. P., & Stojilkovic, S. S. (2011). Activation and Regulation of Purinergic P2X Receptor Channels. *Pharmacological Reviews, 63*(3), 641-683.

Communi, D., Gonzalez, N. S., Detheux, M., Brézillon, S., Lannoy, V., Parmentier, M., & Boeynaems, J.-M. (2001). Identification of a Novel Human ADP Receptor Coupled to Gi. *Journal of Biological Chemistry, 276*(44), 41479-41485.

Communi, D., Parmentier, M., & Boeynaems, J.-M. (1996). Cloning, Functional Expression and Tissue Distribution of the Human P2Y6Receptor. *Biochemical and Biophysical Research Communications, 222*(2), 303-308.

Coull, J. A. M., Beggs, S., Boudreau, D., Boivin, D., Tsuda, M., Inoue, K., Gravel, C., Salter, M. W., & De Koninck, Y. (2005). BDNF from microglia causes the shift in neuronal anion gradient underlying neuropathic pain. *Nature, 438*(7070), 1017-1021.

Davis, H. E., Morgan, J. R., & Yarmush, M. L. (2002). Polybrene increases retrovirus gene transfer efficiency by enhancing receptor-independent virus adsorption on target cell membranes. *Biophysical Chemistry, 97*(2), 159-172.

Dedkova, E. N., Sigova, A. A., & Zinchenko, V. P. (2000). Mechanism of action of calcium ionophores on intact cells: ionophore-resistant cells. *Membrane & Cell Biology, 13*(3), 357-368.

Donnelly-Roberts, D., McGaraughty, S., Shieh, C. C., Honore, P., & Jarvis, M. F. (2008). Painful purinergic receptors. *Journal of Pharmacology and Experimental Therapeutics, 324*(2), 409-415.

Drury, A. N., & Szent-Györgyi, A. (1929). The physiological activity of adenine compounds with especial reference to their action upon the mammalian heart. *The Journal of Physiology, 68*(3), 213-237.

Emmelin, N., & Feldberg, W. (1948). Systemic Effects of Adenosine Triphosphate. *British Journal of Pharmacology and Chemotherapy, 3*(4), 273-284.

Fayad, W., Fryknäs, M., Brnjic, S., Olofsson, M. H., Larsson, R., & Linder, S. (2009). Identification of a Novel Topoisomerase Inhibitor Effective in Cells Overexpressing Drug Efflux Transporters. *Plos One, 4*(10), e7238.

Feng, J., Shi, W., Zhang, S., & Zhang, Y. (2015). Identification of new compounds with high activity against stationary phase Borrelia burgdorferi from the NCI compound collection. *Emerging Microbes & Infections, 4*, e31.

Ferrari, D., Villalba, M., Chiozzi, P., Falzoni, S., Ricciardi-Castagnoli, P., & Di Virgilio, F. (1996). Mouse microglial cells express a plasma membrane pore gated by extracellular ATP. *The Journal of Immunology, 156*(4), 1531-1539.

Fischer, R., Kalthof, B., Rank, E., Stelte-Ludwig, B., and Wuttke, M. (2004). *Preparation of benzofuro-1,4-diazepin-2-ones as P2X4 receptor antagonists for the treatment of arteriosclerosis and restenosis*. DE 10312969A1. 1–14.

Foreman, J. C., & Johansen, T. (2003). *Textbook of Receptor Pharmacology* (2 ed.). Boca Raton, Fla: CRC Press.

Franklin, K. M., Asatryan, L., Jakowec, M. W., Trudell, J. R., Bell, R. L., & Davies, D. L. (2014). P2X4 receptors (P2X4Rs) represent a novel target for the development of drugs to prevent and/or treat alcohol use disorders. *Frontiers in Neuroscience, 8*, 176.

Franklin, K. M., Hauser, S. R., Lasek, A. W., Bell, R. L., & McBride, W. J. (2015). Involvement of Purinergic P2X4 Receptors in Alcohol Intake of High-Alcohol-Drinking (HAD) Rats. *Alcoholism: Clinical and Experimental Research, 39*(10), 2022-2031.

Garcia-Guzman, M., Soto, F., Gomez-Hernandez, J. M., Lund, P.-E., & Stühmer, W. (1997). Characterization of Recombinant Human P2X$_4$ Receptor Reveals Pharmacological Differences to the Rat Homologue. *Molecular Pharmacology, 51*(1), 109-118.

Gendron, F. P., Chalimoniuk, M., Strosznajder, J., Shen, S., González, F. A., Weisman, G. A., & Sun, G. Y. (2003). P2X$_7$ nucleotide receptor activation enhances IFNγ-induced type II nitric oxide synthase activity in BV-2 microglial cells. *Journal of Neurochemistry, 87*(2), 344-352.

Gerevich, Z., Zadori, Z., Müller, C., Wirkner, K., Schröder, W., Rubini, P., & Illes, P. (2007). Metabotropic P2Y receptors inhibit P2X3 receptor-channels via G protein-dependent facilitation of their desensitization. *British Journal of Pharmacology, 151*(2), 226-236.

Ghersi, D., & Sanchez, R. (2009). Improving accuracy and efficiency of blind protein-ligand docking by focusing on predicted binding sites. *Proteins: Structure, Function, and Bioinformatics, 74*(2), 417-424.

Gillis, E. P., Eastman, K. J., Hill, M. D., Donnelly, D. J., & Meanwell, N. A. (2015). Applications of Fluorine in Medicinal Chemistry. *Journal of Medicinal Chemistry, 58*(21), 8315-8359.

Grynkiewicz, G., Poenie, M., & Tsien, R. Y. (1985). A new generation of Ca2+ indicators with greatly improved fluorescence properties. *Journal of Biological Chemistry, 260*(6), 3440-3450.

Gu, B. J., Baird, P. N., Vessey, K. A., Skarratt, K. K., Fletcher, E. L., Fuller, S. J., Richardson, A. J., Guymer, R. H., & Wiley, J. S. (2013). A rare functional haplotype of the P2RX4 and P2RX7 genes leads to loss of innate phagocytosis and confers increased risk of age-related macular degeneration. *The FASEB Journal, 27*(4), 1479-1487.

Gum, R., Wakefield, B., & Jarvis, M. (2012). P2X receptor antagonists for pain management: examination of binding and physicochemical properties. *Purinergic Signalling, 8*(1), 41-56.

Haas, S., Brockhaus, J., Verkhratsky, A., & Kettenmann, H. (1996). ATP-induced membrane currents in ameboid microglia acutely isolated from mouse brain slices. *Neuroscience, 75*(1), 257-261.

Habermacher, C., Martz, A., Calimet, N., Lemoine, D., Peverini, L., Specht, A., Cecchini, M., & Grutter, T. (2016). Photo-switchable tweezers illuminate pore-opening motions of an ATP-gated P2X ion channel. *eLife, 5*, e11050.

Hagmann, W. K. (2008). The Many Roles for Fluorine in Medicinal Chemistry. *Journal of Medicinal Chemistry, 51*(15), 4359-4369.

Harhun, M. I., Povstyan, O. V., Albert, A. P., & Nichols, C. M. (2014). ATP-Evoked Sustained Vasoconstrictions Mediated by Heteromeric $P2X_{1/4}$ Receptors in Cerebral Arteries. *Stroke, 45*(8), 2444-2450.

Hattori, M., & Gouaux, E. (2012). Molecular mechanism of ATP binding and ion channel activation in P2X receptors. *Nature, 485*(7397), 207-212.

Hechler, B., Léon, C., Vial, C., Vigne, P., Frelin, C., Cazenave, J.-P., & Gachet, C. (1998). The $P2Y_1$ Receptor Is Necessary for Adenosine 5′-Diphosphate–Induced Platelet Aggregation. *Blood, 92*(1), 152-159.

Henn, A., Lund, S., Hedtjarn, M., Schrattenholz, A., Porzgen, P., & Leist, M. (2009). The suitability of BV2 cells as alternative model system for primary microglia cultures or for animal experiments examining brain inflammation. *Alternatives to Animal Experimentation, 26*(2), 83-94.

Hernandez-Olmos, V., Abdelrahman, A., El-Tayeb, A., Freudendahl, D., Weinhausen, S., & Muller, C. E. (2012). N-Substituted Phenoxazine and Acridone Derivatives: Structure-Activity Relationships of Potent P2X$_4$ Receptor Antagonists. *Journal of Medicinal Chemistry, 55*(22), 9576-9588.

Heymann, G., Dai, J., Li, M., Silberberg, S. D., Zhou, H. X., & Swartz, K. J. (2013). Inter- and intrasubunit interactions between transmembrane helices in the open state of P2X receptor channels. *Proceedings of the National Academy of Sciences of the United States of America, 110*(42), e4045-4054.

Hirst, R. A., Harrison, C., Hirota, K., & Lambert, D. G. (1999). Measurement of [Ca2+]i in Whole Cell Suspensions Using Fura-2. In D. G. Lambert (Ed.), *Calcium Signaling Protocols* (pp. 31-39). Totowa, NJ: Humana Press.

Hollinger, M. A. (2007). *Introduction to Pharmacology* (Third ed.). USA: CRC Press.

Hollopeter, G., Jantzen, H.-M., Vincent, D., Li, G., England, L., Ramakrishnan, V., Yang, R.-B., Nurden, P., Nurden, A., Julius, D., & Conley, P. B. (2001). Identification of the platelet ADP receptor targeted by antithrombotic drugs. *Nature, 409*(6817), 202-207.

Hu, B., Mei, Q.-B., Yao, X.-J., Smith, E., Barry, W. H., & Liang, B. T. (2001). A novel contractile phenotype with cardiac transgenic expression of the human P2X$_4$ receptor. *The FASEB Journal, 15*(14), 2739-2741.

Hung, S. C., Choi, C. H., Said-Sadier, N., Johnson, L., Atanasova, K. R., Sellami, H., Yilmaz, O., & Ojcius, D. M. (2013). P2X$_4$ assembles with P2X$_7$ and pannexin-1 in gingival epithelial cells and modulates ATP-induced reactive oxygen species production and inflammasome activation. *Plos One, 8*(7), e70210.

Huynh, N., Arabian, N., Naito, A., Louie, S., Jakowec, M. W., Asatryan, L., & Davies, D. L. (2017). Preclinical development of moxidectin as a novel therapeutic for alcohol use disorder. *Neuropharmacology, 113*, 60-70.

Isanbor, C., & O'Hagan, D. (2006). Fluorine in medicinal chemistry: A review of anti-cancer agents. *Journal of Fluorine Chemistry, 127*(3), 303-319.

Jaakola, V. P., Griffith, M. T., Hanson, M. A., Cherezov, V., Chien, E. Y., Lane, J. R., Ijzerman, A. P., & Stevens, R. C. (2008). The 2.6 angstrom crystal structure of a human A2A adenosine receptor bound to an antagonist. *Science, 322*(5905), 1211-1217.

Jacobson, K. A., & Müller, C. E. (2016). Medicinal chemistry of adenosine, P2Y and P2X receptors. *Neuropharmacology, 104*, 31-49.

Jarvis, M. F., & Khakh, B. S. (2009). ATP-gated P2X cation-channels. *Neuropharmacology, 56*(1), 208-215.

Jelínkova, I., Vávra, V., Jindrichova, M., Obsil, T., Zemkova, H. W., Zemkova, H., & Stojilkovic, S. S. (2008). Identification of P2X$_4$ receptor transmembrane residues contributing to channel gating and interaction with ivermectin. *Pflügers Archiv - European Journal of Physiology, 456*(5), 939-950.

Jelínková, I., Yan, Z., Liang, Z., Moonat, S., Teisinger, J., Stojilkovic, S. S., & Zemková, H. (2006). Identification of P2X$_4$ receptor-specific residues contributing to the ivermectin effects on channel deactivation. *Biochemical and Biophysical Research Communications, 349*(2), 619-625.

Ji, R.-R., Baba, H., Brenner, G. J., & Woolf, C. J. (1999). Nociceptive-specific activation of ERK in spinal neurons contributes to pain hypersensitivity. *Nature Neuroscience, 2*(12), 1114-1119.

Jo, Y.-H., Donier, E., Martinez, A., Garret, M., Toulmé, E., & Boué-Grabot, E. (2011). Cross-talk between P2X$_4$ and γ-Aminobutyric Acid, Type A Receptors Determines Synaptic Efficacy at a Central Synapse. *Journal of Biological Chemistry, 286*(22), 19993-20004.

Jones, C. A., Chessell, I. P., Simon, J., Barnard, E. A., Miller, K. J., Michel, A. D., & Humphrey, P. P. A. (2000). Functional characterization of the P2X$_4$ receptor orthologues. *British Journal of Pharmacology, 129*(2), 388-394.

Kaczmarek-Hájek, K., Lörinczi, É., Hausmann, R., & Nicke, A. (2012). Molecular and functional properties of P2X receptors—recent progress and persisting challenges. *Purinergic Signalling, 8*(3), 375-417.

Katsura, H., Obata, K., Mizushima, T., Sakurai, J., Kobayashi, K., Yamanaka, H., Dai, Y., Fukuoka, T., Sakagami, M., & Noguchi, K. (2006). Activation of Src-family kinases in spinal microglia contributes to mechanical hypersensitivity after nerve injury. *Journal of Neuroscience, 26*(34), 8680-8690.

Katzung, B. G., Masters, S. B., & Trevor, A. J. (2012). *Basic & Clinical Pharmacology* (12 ed.). New York: McGraw-Hill Medical.

Kawate, T., Michel, J. C., Birdsong, W. T., & Gouaux, E. (2009). Crystal structure of the ATP-gated P2X$_4$ ion channel in the closed state. *Nature, 460*(7255), 592-598.

Khakh, B. S., Proctor, W. R., Dunwiddie, T. V., Labarca, C., & Lester, H. A. (1999). Allosteric Control of Gating and Kinetics at P2X$_4$ Receptor Channels. *The Journal of Neuroscience, 19*(17), 7289-7299.

Khoja, S., Shah, V., Garcia, D., Asatryan, L., Jakowec, M. W., & Davies, D. L. (2016). Role of purinergic P2X$_4$ receptors in regulating striatal dopamine homeostasis and dependent behaviors. *Journal of Neurochemistry, 139*(1), 134-148.

Kim, D., Kim, M. A., Cho, I. H., Kim, M. S., Lee, S., Jo, E. K., Choi, S. Y., Park, K., Kim, J. S., Akira, S., Na, H. S., Oh, S. B., & Lee, S. J. (2007). A critical role of toll-like receptor 2 in nerve injury-induced spinal cord glial cell activation and pain hypersensitivity. *Journal of Biological Chemistry, 282*(20), 14975-14983.

Kim, T. K., & Eberwine, J. H. (2010). Mammalian cell transfection: the present and the future. *Analytical and Bioanalytical Chemistry, 397*(8), 3173-3178.

Kimpel, M. W., Strother, W. N., McClintick, J. N., Carr, L. G., Liang, T., Edenberg, H. J., & McBride, W. J. (2007). Functional gene expression differences between inbred alcohol-preferring and –non-preferring rats in five brain regions. *Alcohol, 41*(2), 95-132.

Klämbt, V., Wohlfeil, S. A., Schwab, L., Hülsdünker, J., Ayata, K., Apostolova, P., Schmitt-Graeff, A., Dierbach, H., Prinz, G., Follo, M., Prinz, M., Idzko, M., & Zeiser, R. (2015). A Novel Function for P2Y$_2$ in Myeloid Recipient–Derived Cells during Graft-versus-Host Disease. *The Journal of Immunology, 195*(12), 5795-5804.

Koebel, M. R., Schmadeke, G., Posner, R. G., & Sirimulla, S. (2016). AutoDock VinaXB: implementation of XBSF, new empirical halogen bond scoring function, into AutoDock Vina. *Journal of Cheminformatics, 8*(1), 27.

Kong, S. K., & Lee, C. Y. (1995). The use of fura 2 for measurement of free calcium concentration. *Biochemical Education, 23*(2), 97-98.

Koshimizu, T.-a., Koshimizu, M., & Stojilkovic, S. S. (1999). Contributions of the C-terminal Domain to the Control of P2X Receptor Desensitization. *Journal of Biological Chemistry, 274*(53), 37651-37657.

Krause, R. M., Buisson, B., Bertrand, S., Corringer, P.-J., Galzi, J.-L., Changeux, J.-P., & Bertrand, D. (1998). Ivermectin: A Positive Allosteric Effector of the α7 Neuronal Nicotinic Acetylcholine Receptor. *Molecular Pharmacology, 53*(2), 283-294.

Kru˚šek, J., & Zemkova´, H. (1994). Effect of ivermectin on γ-aminobutyric acid-induced chloride currents in mouse hippocampal embryonic neurones. *European Journal of Pharmacology, 259*(2), 121-128.

Kwon, H. J. (2012). Extracellular ATP signaling via P2X$_4$ receptor and cAMP/PKA signaling mediate ATP oscillations essential for prechondrogenic condensation. *Journal of Endocrinology, 214*(3), 337-348.

Le, K. T., Babinski, K., & Seguela, P. (1998). Central P2X4 and P2X6 channel subunits coassemble into a novel heteromeric ATP receptor. *Journal of Neuroscience, 18*(18), 7152-7159.

Lehmann, F. (1928). Chemical constitution and activity. Aromatic fluorine compounds. *Archiv für experimentelle Pathologie und Pharmakologie, 130*(1), 250-255.

Lewis, C., Neidhart, S., Holy, C., North, R. A., Buell, G., & Surprenant, A. (1995). Coexpression of P2X2 and P2X3 receptor subunits can account for ATP-gated currents in sensory neurons. *Nature, 377*(6548), 432-435.

Li, C., Aguayo, L., Peoples, R. W., & Weight, F. F. (1993). Ethanol inhibits a neuronal ATP-gated ion channel. *Molecular Pharmacology, 44*(4), 871-875.

Li, C., Peoples, R. W., & Weight, F. F. (1998). Ethanol-induced inhibition of a neuronal P2X purinoceptor by an allosteric mechanism. *British Journal of Pharmacology, 123*(1), 1-3.

Li, C., Xu, L., Wolan, D. W., Wilson, I. A., & Olson, A. J. (2004). Virtual Screening of Human 5-Aminoimidazole-4-carboxamide Ribonucleotide Transformylase against the NCI Diversity Set by Use of AutoDock to Identify Novel Nonfolate Inhibitors. *Journal of Medicinal Chemistry, 47*(27), 6681-6690.

Li, F., Wang, L., Li, J. W., Gong, M., He, L., Feng, R., Dai, Z., & Li, S. Q. (2011). Hypoxia induced amoeboid microglial cell activation in postnatal rat brain is mediated by ATP receptor P2X4. *BMC Neuroscience, 12*.

Li, J., & Fountain, S. J. (2012). Fluvastatin suppresses native and recombinant human P2X(4) receptor function. *Purinergic Signalling, 8*(2), 311-316.

Lim, H., Gwon, M., & Lee, S. J. (2016). Toll-like receptor 2 signaling induces interferon regulatory factor 8 expression in spinal cord microglia after peripheral nerve injury. *Itch & Pain, 3*(e1457), 1-7.

Lim, H., Kim, D., & Lee, S. J. (2013). Toll-like Receptor 2 Mediates Peripheral Nerve Injury-induced NADPH Oxidase 2 Expression in Spinal Cord Microglia. *Journal of Biological Chemistry, 288*(11), 7572-7579.

Lipinski, C. A., Lombardo, F., Dominy, B. W., & Feeney, P. J. (1997). Experimental and computational approaches to estimate solubility and permeability in drug discovery and development settings. *Advanced Drug Delivery Reviews, 23*(1), 3-25.

Liu, C., & Hermann, T. E. (1978). Characterization of ionomycin as a calcium ionophore. *Journal of Biological Chemistry, 253*(17), 5892-5894.

Mansoor, S. E., Lü, W., Oosterheert, W., Shekhar, M., Tajkhorshid, E., & Gouaux, E. (2016). X-ray structures define human P2X3 receptor gating cycle and antagonist action. *Nature, 538*, 66-71.

Marquez-Klaka, B., Rettinger, J., Bhargava, Y., Eisele, T., & Nicke, A. (2007). Identification of an Intersubunit Cross-Link between Substituted Cysteine

Residues Located in the Putative ATP Binding Site of the P2X$_1$ Receptor. *The Journal of Neuroscience, 27*(6), 1456-1466.

Masuda, T., Iwamoto, S., Yoshinaga, R., Tozaki-Saitoh, H., Nishiyama, A., Mak, T. W., Tamura, T., Tsuda, M., & Inoue, K. (2014). Transcription factor IRF5 drives P2X$_4$R+-reactive microglia gating neuropathic pain. *Nature Communications, 5*, 3771.

Masuda, T., Tsuda, M., Yoshinaga, R., Tozaki-Saitoh, H., Ozato, K., Tamura, T., & Inoue, K. (2012). IRF8 Is a Critical Transcription Factor for Transforming Microglia into a Reactive Phenotype. *Cell Reports, 1*(4), 334-340.

Matsumura, Y., Yamashita, T., Sasaki, A., Nakata, E., Kohno, K., Masuda, T., Tozaki-Saitoh, H., Imai, T., Kuraishi, Y., Tsuda, M., & Inoue, K. (2016). A novel P2X$_4$ receptor-selective antagonist produces anti-allodynic effect in a mouse model of herpetic pain. *Scientific Reports, 6*, 32461.

Miklavc, P., Thompson, K., & Frick, M. (2013). A new role for P2X$_4$ receptors as modulators of lung surfactant secretion. *Frontiers in Cellular Neuroscience, 7*(171).

Morgan, A. J., & Jacob, R. (1994). Ionomycin enhances Ca^{2+} influx by stimulating store-regulated cation entry and not by a direct action at the plasma membrane. *Biochemical Journal, 300*(3), 665-672.

Morris, G. M., Huey, R., Lindstrom, W., Sanner, M. F., Belew, R. K., Goodsell, D. S., & Olson, A. J. (2009). AutoDock4 and AutoDockTools4: Automated docking with selective receptor flexibility. *Journal of Computational Chemistry, 30*(16), 2785-2791.

Mostovnikov, V. A., Rubinov, A. N., Anufrik, S. S., Ginevich, G. R., Nikitchenko, V. M., & Vodotyka, G. S. (1977). Effect of the molecular structure of coumarin derivatives on the spectral-luminescent and generating properties of their solutions. *Journal of Applied Spectroscopy, 27*(1), 866-871.

Müller, M. S., Obel, L. F., Waagepetersen, H. S., Schousboe, A., & Bak, L. K. (2013). Complex Actions of Ionomycin in Cultured Cerebellar Astrocytes Affecting Both Calcium-Induced Calcium Release and Store-Operated Calcium Entry. *Neurochemical Research, 38*(6), 1260-1265.

Murphy, K.L., Bethea, J.R., & Fischer, R. (2017). *Multiple Sclerosis: Perspectives in Treatment and Pathogenesis*. Australia: Codon Publications.

Nagaoka, M., Nara, M., Tamada, T., Kume, H., Oguma, T., Kikuchi, T., Zaini, J., Moriya, T., Ichinose, M., Tamura, G., & Hattori, T. (2009). Regulation of adenosine 5′-triphosphate (ATP)-gated P2X$_4$ receptors on tracheal smooth muscle cells. *Respiratory Physiology & Neurobiology, 166*(1), 61-67.

Nagata, K., Imai, T., Yamashita, T., Tsuda, M., Tozaki-Saitoh, H., & Inoue, K. (2009). Antidepressants inhibit P2X$_4$ receptor function: A possible involvement in neuropathic pain relief. *Molecular Pain, 5*.

National Cancer Institute Development Therapeutics Program. (2016, 26/8/16). Retrieved 27/09, 2016, from https://dtp.cancer.gov/organization/dscb/obtaining/available_plates.htm

National Institute of Health. (no date). *Basic Local Alignment Search.* Retrieved 15 October, 2016, from https://blast.ncbi.nlm.nih.gov/Blast.cgi

NCI. (2015, November 10, 2015). Obtaining Vialed and Plated Compounds. Retrieved February 17, 2017, 2017, from https://dtp.cancer.gov/organization/dscb/obtaining/default.htm

NCI. (2016, August 26, 2016). Available Plates. Retrieved February 17, 2017, 2017, from https://dtp.cancer.gov/organization/dscb/obtaining/available_plates.htm

NCI. (no date-a). NCI Overview. Retrieved February 17, 2017, 2017, from https://www.cancer.gov/about-nci/overview

NCI. (no date-b). Welcome to the Developmental Therapeutics Program. Retrieved February 17, 2017, 2017, from https://dtp.cancer.gov/

Nicke, A., Kerschensteiner, D., & Soto, F. (2005). Biochemical and functional evidence for heteromeric assembly of P2X1 and P2X4 subunits. *Journal of Neurochemistry, 92*(4), 925-933.

Norenberg, W., Sobottka, H., Hempel, C., Plotz, T., Fischer, W., Schmalzing, G., & Schaefer, M. (2012). Positive allosteric modulation by ivermectin of human but not murine P2X$_7$ receptors. *British Journal of Pharmacology, 167*(1), 48-66.

North, R. A. (2002). Molecular physiology of P2X receptors. *Physiological Reviews, 82*, 1013-1067.

Ohsawa, K., Irino, Y., Nakamura, Y., Akazawa, C., Inoue, K., & Kohsaka, S. (2007). Involvement of P2X$_4$ and P2Y$_{12}$ receptors in ATP-induced microglial chemotaxis. *Glia, 55*(6), 604-616.

Ostrovskaya, O., Asatryan, L., Wyatt, L., Popova, M., Li, K., Peoples, R. W., Alkana, R. L., & Davies, D. L. (2011). Ethanol Is a Fast Channel Inhibitor of P2X$_4$ Receptors. *Journal of Pharmacology and Experimental Therapeutics, 337*(1), 171-179.

Paredes, R. M., Etzler, J. C., Watts, L. T., Zheng, W., & Lechleiter, J. D. (2008). Chemical calcium indicators. *Methods, 46*(3), 143-151.

Perdue, G. P., Blomster, R. N., Blake, D. A., & Farnsworth, N. R. (1979). South American Plants II: Taspine Isolation and Anti-Inflammatory Activity. *Journal of Pharmaceutical Sciences, 68*(1), 124-126.

Pettersen, E. F., Goddard, T. D., Huang, C. C., Couch, G. S., Greenblatt, D. M., Meng, E. C., & Ferrin, T. E. (2004). UCSF Chimera—A visualization system for exploratory research and analysis. *Journal of Computational Chemistry, 25*(13), 1605-1612.

Pontén, J. A. N., & Macintyre, E. H. (1968). Long term culture of normal and neoplastic human glia. *Acta Pathologica Microbiologica Scandinavica, 74*(4), 465-486.

Pope, A. J., Haupts, U. M., & Moore, K. J. (1999). Homogeneous fluorescence readouts for miniaturized high-throughput screening: theory and practice. *Drug Discovery Today, 4*(8), 350-362.

Pressman, B. C., & Fahim, M. (1982). Pharmacology and Toxicology of the Monovalent Carboxylic Ionophores. *Annual Review of Pharmacology and Toxicology, 22*(1), 465-490.

Priel, A., & Silberberg, S. D. (2004). Mechanism of Ivermectin Facilitation of Human P2X$_4$ Receptor Channels. *The Journal of General Physiology, 123*(3), 281-293.

Pronk, S., Páll, S., Schulz, R., Larsson, P., Bjelkmar, P., Apostolov, R., Shirts, M. R., Smith, J. C., Kasson, P. M., van der Spoel, D., Hess, B., & Lindahl, E. (2013). GROMACS 4.5: a high-throughput and highly parallel open source molecular simulation toolkit. *Bioinformatics, 29*(7), 845-854.

Qureshi, O. S., Paramasivam, A., Yu, J. C., & Murrell-Lagnado, R. D. (2007). Regulation of P2X$_4$ receptors by lysosomal targeting, glycan protection and exocytosis. *Journal of Cell Science, 120*(Pt 21), 3838-3849.

Ralevic, V., & Burnstock, G. (1998). Receptors for Purines and Pyrimidines. *Pharmacological Reviews, 50*(3), 413-492.

Raouf, R., Chabot-Doré, A.-J., Ase, A. R., Blais, D., & Séguéla, P. (2007). Differential regulation of microglial P2X$_4$ and P2X$_7$ ATP receptors following LPS-induced activation. *Neuropharmacology, 53*(4), 496-504.

Roberts, J. A., & Evans, R. J. (2004). ATP Binding at Human P2X1 Receptors: contribution of aromatic and basic amino acids revealed using mutagenesis and partial agonists. *Journal of Biological Chemistry, 279*(10), 9043-9055.

Robinson, L. E., & Murrell-Lagnado, R. D. (2013). The trafficking and targeting of P2X receptors. *Frontiers in Cellular Neuroscience, 7*, 233.

Royle, S. J., Bobanović, L. K., & Murrell-Lagnado, R. D. (2002). Identification of a Non-canonical Tyrosine-based Endocytic Motif in an Ionotropic Receptor. *Journal of Biological Chemistry, 277*(38), 35378-35385.

Royle, S. J., Qureshi, O. S., Bobanović, L. K., Evans, P. R., Owen, D. J., & Murrell-Lagnado, R. D. (2005). Non-canonical YXXGΦ endocytic motifs: recognition by AP2 and preferential utilization in P2X4 receptors. *Journal of Cell Science, 118*(14), 3073-3080.

Rubio, M. E., & Soto, F. (2001). Distinct Localization of P2X Receptors at Excitatory Postsynaptic Specializations. *The Journal of Neuroscience, 21*(2), 641-653.

Samways, D. S. K., Khakh, B. S., Dutertre, S., & Egan, T. M. (2011). Preferential use of unobstructed lateral portals as the access route to the pore of human ATP-gated ion channels (P2X receptors). *Proceedings of the National Academy of Sciences of the United States of America, 108*(33), 13800-13805.

Schachter, J. B., Sromek, S. M., Nicholas, R. A., & Harden, T. K. (1997). HEK293 human embryonic kidney cells endogenously express the P2Y1 and P2Y2 receptors. *Neuropharmacology, 36*(9), 1181-1187.

Schenk, U., Westendorf, A. M., Radaelli, E., Casati, A., Ferro, M., Fumagalli, M., Verderio, C., Buer, J., Scanziani, E., & Grassi, F. (2008). Purinergic Control of T Cell Activation by ATP Released Through Pannexin-1 Hemichannels. *Science Signaling, 1*(39), ra6-ra6.

Scholz, J., & Woolf, C. J. (2002). Can we conquer pain? *Nature Neuroscience, 5*(1062-1067).

Seye, C. I., Kong, Q., Erb, L., Garrad, R. C., Krugh, B., Wang, M., Turner, J. T., Sturek, M., González, F. A., & Weisman, G. A. (2002). Functional $P2Y_2$ Nucleotide Receptors Mediate Uridine 5′-Triphosphate–Induced Intimal Hyperplasia in Collared Rabbit Carotid Arteries. *Circulation, 106*(21), 2720-2726.

Shah, P., & Westwell, A. D. (2007). The role of fluorine in medicinal chemistry. *Journal of Enzyme Inhibition and Medicinal Chemistry, 22*(5), 527-540.

Sherman, W. R., & Robins, E. (1968). Fluorescence of substituted 7-hydroxycoumarins. *Analytical Chemistry, 40*(4), 803-805.

Silberberg, S. D., Li, M., & Swartz, K. J. (2007). Ivermectin Interaction with Transmembrane Helices Reveals Widespread Rearrangements during Opening of P2X Receptor Channels. *Neuron, 54*(2), 263-274.

Sim, J. A., Chaumont, S., Jo, J., Ulmann, L., Young, M. T., Cho, K., Buell, G., North, R. A., & Rassendren, F. (2006). Altered Hippocampal Synaptic Potentiation in $P2X_4$ Knock-Out Mice. *The Journal of Neuroscience, 26*(35), 9006-9009.

Simon, J., Jones, C. A., Chessell, I. P., Barnard, E. A., Michel, A. D., & Humphrey, P. P. A. (1999). Molecular cloning and characterisation of splice variants of the mouse P2X4 receptor. *British Journal of Pharmacology*, 127P.

Slack, S. E., Grist, J., Mac, Q., McMahon, S. B., & Pezet, S. (2005). TrkB expression and phospho-ERK activation by brain-derived neurotrophic factor in rat spinothalamic tract neurons. *The Journal of Comparative Neurology, 489*(1), 59-68.

Solini, A., Santini, E., Chimenti, D., Chiozzi, P., Pratesi, F., Cuccato, S., Falzoni, S., Lupi, R., Ferrannini, E., Pugliese, G., & Virgilio, F. D. (2007). Multiple P2X receptors are involved in the modulation of apoptosis in human mesangial cells: evidence for a role of P2X$_4$. *American Journal of Physiology - Renal Physiology, 292*(5), F1537-F1547.

Soto, F., Garcia-Guzman, M., Gomez-Hernandez, J. M., Hollmann, M., Karschin, C., & Stuhmer, W. (1996). P2X4: an ATP-activated ionotropic receptor cloned from rat brain. *Proceedings of the National Academy of Sciences of the United States of America, 93*(8), 3684-3688.

Stokes, L. (2013). Rab5 regulates internalisation of P2X$_4$ receptors and potentiation by ivermectin. *Purinergic Signalling, 9*(1), 113-121.

Stokes, L., Layhadi, J. A., Bibic, L., Dhuna, K., & Fountain, S. J. (2017). P2X$_4$ Receptor Function in the Nervous System and Current Breakthroughs in Pharmacology. *Frontier in Pharmacology, 8*, 291.

Stokes, L., Scurrah, K., Ellis, J. A., Cromer, B. A., Skarratt, K. K., Gu, B. J., Harrap, S. B., & Wiley, J. S. (2011). A Loss-of-Function Polymorphism in the Human P2X$_4$ Receptor Is Associated With Increased Pulse Pressure. *Hypertension, 58*(6), 1086-1092.

Sukkurwala, A. Q., Adjemian, S., Senovilla, L., Michaud, M., Spaggiari, S., Vacchelli, E., Baracco, E. E., Galluzzi, L., Zitvogel, L., Kepp, O., & Kroemer, G. (2014). Screening of novel immunogenic cell death inducers within the NCI Mechanistic Diversity Set. *OncoImmunology, 3*(4), e28473.

Surprenant, A. & North, R. A. (2009). Signaling at purinergic P2X receptors. *Annual Review of Physiology, 71*, 333-359.

Tian, M., Abdelrahman, A., Weinhausen, S., Hinz, S., Weyer, S., Dosa, S., El-Tayeb, A., & Müller, C. E. (2014). Carbamazepine derivatives with P2X$_4$ receptor-blocking activity. *Bioorganic & Medicinal Chemistry, 22*(3), 1077-1088.

Torres, G. E., Egan, T. M., & Voigt, M. M. (1999). Hetero-oligomeric Assembly of P2X Receptor Subunits: Specificities Exist with Regard to Possible Partners. *Journal of Biological Chemistry, 274*(10), 6653-6659.

Toulme, E., Garcia, A., Samways, D., Egan, T. M., Carson, M. J., & Khakh, B. S. (2010). P2X$_4$ receptors in activated C8-B4 cells of cerebellar microglial origin. *Journal of General Physiology, 135*(4), 333-353.

Toulmé, E., Soto, F., Garret, M., & Boué-Grabot, E. (2006). Functional Properties of Internalization-Deficient P2X$_4$ Receptors Reveal a Novel Mechanism of

Ligand-Gated Channel Facilitation by Ivermectin. *Molecular Pharmacology, 69*(2), 576-587.

Trang, T., Beggs, S., Wan, X., & Salter, M. W. (2009). P2X$_4$-Receptor-Mediated Synthesis and Release of Brain-Derived Neurotrophic Factor in Microglia Is Dependent on Calcium and p38-Mitogen-Activated Protein Kinase Activation. *Journal of Neuroscience, 29*(11), 3518-3528.

Trang, T., & Salter, M. W. (2012). P2X$_4$ purinoceptor signaling in chronic pain. *Purinergic Signalling, 8*(3), 621-628.

Tsien, R. Y. (1981). A non-disruptive technique for loading calcium buffers and indicators into cells. *Nature, 290*(5806), 527-528.

Tsien, R. Y., & Poenie, M. (1986). Fluorescence ratio imaging: a new window into intracellular ionic signaling. *Trends in Biochemical Sciences, 11*(11), 450-455.

Tsuda, M., Masuda, T., Kitano, J., Shimoyama, H., Tozaki-Saitoh, H., & Inoue, K. (2009). IFN-gamma receptor signaling mediates spinal microglia activation driving neuropathic pain. *Proceedings of the National Academy of Sciences of the United States of America, 106*(19), 8032-8037.

Tsuda, M., Mizokoshi, A., Shigemoto-Mogami, Y., Koizumi, S., & Inoue, K. (2004). Activation of p38 mitogen-activated protein kinase in spinal hyperactive microglia contributes to pain hypersensitivity following peripheral nerve injury. *Glia, 45*(1), 89-95.

Tsuda, M., Shigemoto-Mogami, Y., Koizumi, S., Mizokoshi, A., Kohsaka, S., Salter, M. W., & Inoue, K. (2003). P2X$_4$ receptors induced in spinal microglia gate tactile allodynia after nerve injury. *Nature, 424*(6950), 778-783.

Tsuda, M., Toyomitsu, E., Komatsu, T., Masuda, T., Kunifusa, E., Nasu-Tada, K., Koizumi, S., Yamamoto, K., Ando, J., & Inoue, K. (2008a). Fibronectin/integrin system is involved in P2X$_4$ receptor upregulation in the spinal cord and neuropathic pain after nerve injury. *Glia, 56*(5), 579-585.

Tsuda, M., Tozaki-Saitoh, H., Masuda, T., Toyomitsu, E., Tezuka, T., Yamamoto, T., & Inoue, K. (2008b). Lyn tyrosine kinase is required for P2X$_4$ receptor upregulation and neuropathic pain after peripheral nerve injury. *Glia, 56*(1), 50-58.

Ulmann, L., Hatcher, J. P., Hughes, J. P., Chaumont, S., Green, P. J., Conquet, F., Buell, G. N., Reeve, A. J., Chessell, I. P., & Rassendren, F. (2008). Up-Regulation of P2X(4) Receptors in Spinal Microglia after Peripheral Nerve Injury Mediates BDNF Release and Neuropathic Pain. *Journal of Neuroscience, 28*(44), 11263-11268.

Ulmann, L., Hirbec, H., & Rassendren, F. (2010). P2X$_4$ receptors mediate PGE2 release by tissue-resident macrophages and initiate inflammatory pain. *The EMBO Journal, 29*(14), 2290-2300.

Vavra, V., Bhattacharya, A., & Zemkova, H. (2011). Facilitation of glutamate and GABA release by P2X receptor activation in supraoptic neurons from freshly isolated rat brain slices. *Neuroscience, 188*(0), 1-12.

Viegas, A., Manso, J., Nobrega, F. L., & Cabrita, E. J. (2011). Saturation-Transfer Difference (STD) NMR: A Simple and Fast Method for Ligand Screening and Characterization of Protein Binding. *Journal of Chemical Education, 88*(7), 990-994.

Virginio, C., Robertson, G., Surprenant, A., & North, R. A. (1998). Trinitrophenyl-Substituted Nucleotides Are Potent Antagonists Selective for $P2X_1$, $P2X_3$, and Heteromeric $P2X_{2/3}$ Receptors. *Molecular Pharmacology, 53*(6), 969-973.

von Kügelgen, I., & Hoffmann, K. (2016). Pharmacology and structure of P2Y receptors. *Neuropharmacology, 104*(Supplement C), 50-61.

Walz, W., Ilschner, S., Ohlemeyer, C., Banati, R., & Kettenmann, H. (1993). Extracellular ATP activates a cation conductance and a K+ conductance in cultured microglial cells from mouse brain. *The Journal of Neuroscience, 13*(10), 4403-4411.

Wang, L., Jacobsen, S. E. W., Bengtsson, A., & Erlinge, D. (2004). P2 receptor mRNA expression profiles in human lymphocytes, monocytes and CD34+ stem and progenitor cells. *BMC Immunology, 5*, 16-16.

Webb, B., & Sali, A. (2014). Comparative Protein Structure Modeling Using MODELLER. *Current Protocols in Bioinformatics* (pp. 1-32): John Wiley & Sons, Inc.

Webb, T. E., Simon, J., Krishek, B. J., Bateson, A. N., Smart, T. G., King, B. F., Burnstock, G., & Barnard, E. A. (1993). Cloning and functional expression of a brain G-protein-coupled ATP receptor. *FEBS Letters, 324*(2), 219-225.

Wesselius, A., Bours, M. J., Jørgensen, N. R., Wiley, J., Gu, B., van Helden, S., van Rhijn, L., & Dagnelie, P. C. (2013). Non-synonymous polymorphisms in the P2RX 4 are related to bone mineral density and osteoporosis risk in a cohort of Dutch fracture patients. *Purinergic Signalling, 9*(1), 123-130.

Wildman, S. S., King, B. F., & Burnstock, G. (1999). Modulation of ATP-responses at recombinant rP2X4 receptors by extracellular pH and zinc. *British Journal of Pharmacology, 126*(3), 762-768.

Wilkinson, W. J., Jiang, L.-H., Surprenant, A., & North, R. A. (2006). Role of Ectodomain Lysines in the Subunits of the Heteromeric $P2X_{2/3}$ Receptor. *Molecular Pharmacology, 70*(4), 1159-1163.

Williams, A. C., & Barry, B. W. (2012). Penetration enhancers. *Advanced Drug Delivery Reviews, 64, Supplement*, 128-137.

Williams, D. A., Fogarty, K. E., Tsien, R. Y., & Fay, F. S. (1985). Calcium gradients in single smooth muscle cells revealed by the digital imaging microscope using Fura-2. *Nature, 318*(6046), 558-561.

Woehrle, T., Yip, L., Elkhal, A., Sumi, Y., Chen, Y., Yao, Y., Insel, P. A., & Junger, W. G. (2010). Pannexin-1 hemichannel–mediated ATP release together with P2X1 and P2X4 receptors regulate T-cell activation at the immune synapse. *Blood, 116*(18), 3475-3484.

Woolf, C. J., & Mannion, R. J. (1999). Neuropathic pain: aetiology, symptoms, mechanisms, and management. *The Lancet, 353*(9168), 1959-1964.

Wu, D., & Hurtubise, R. J. (1993). Fluorescence properties of 1-naphthol, 2-naphthol and 1,2,3,4-tetrahydronaphthol in aqueous alcohol solvents with and without beta-cyclodextrin. *Talanta, 40*(6), 901-907.

Wu, T., Dai, M., Shi, X. R., Jiang, Z. G., & Nuttall, A. L. (2011). Functional expression of $P2X_4$ receptor in capillary endothelial cells of the cochlear spiral ligament and its role in regulating the capillary diameter. *American Journal of Physiology-Heart and Circulatory Physiology, 301*(1), H69-78.

Xiaodi, Y., Shuangqiong, Z., Qianbo, C., Chengwen, C., & Hongbin, Y. (2010). $P2X_4$ receptor and brain-derived neurotrophic factor in neuropathic pain. *Journal of Medical Colleges of PLA, 25*(5), 275-284.

Xiong, K., Hu, X.-Q., Stewart, R. R., Weight, F. F., & Li, C. (2005). The mechanism by which ethanol inhibits rat $P2X_4$ receptors is altered by mutation of histidine 241. *British Journal of Pharmacology, 145*(5), 576-586.

Xiong, K., Li, C., & Weight, F. F. (2000). Inhibition by ethanol of rat $P2X_4$ receptors expressed in Xenopus oocytes. *British Journal of Pharmacology, 130*(6), 1394-1398.

Xu, J., Chai, H., Ehinger, K., Egan, T. M., Srinivasan, R., Frick, M., & Khakh, B. S. (2014). Imaging $P2X_4$ receptor subcellular distribution, trafficking, and regulation using P2X4-pHluorin. *Journal of General Physiology, 144*(1), 79-102.

Yale, H. L. (1959). The Trifluoromethyl Group in Medical Chemistry. *Journal of Medicinal and Pharmaceutical Chemistry, 1*(2), 121-133.

Yamamoto, K., Korenaga, R., Kamiya, A., Qi, Z., Sokabe, M., & Ando, J. (2000). P2X(4) receptors mediate ATP-induced calcium influx in human vascular endothelial cells. *American Journal of Physiology-Heart and Circulatory Physiology, 279*(1), H285-292.

Yamamoto, K., Sokabe, T., Matsumoto, T., Yoshimura, K., Shibata, M., Ohura, N., Fukuda, T., Sato, T., Sekine, K., Kato, S., Isshiki, M., Fujita, T., Kobayashi, M., Kawamura, K., Masuda, H., Kamiya, A., & Ando, J. (2006). Impaired

flow-dependent control of vascular tone and remodeling in P2X$_4$-deficient mice. *Nature Medicine, 12*(1), 133-137.

Yamashita, T., Yamamoto, S., Zhang, J., Kometani, M., Tomiyama, D., Kohno, K., Tozaki-Saitoh, H., Inoue, K., & Tsuda, M. (2016). Duloxetine Inhibits Microglial P2X$_4$ Receptor Function and Alleviates Neuropathic Pain after Peripheral Nerve Injury. *Plos One, 11*(10), e0165189.

Yang, T., Shen, J.-b., Yang, R., Redden, J., Dodge-Kafka, K., Grady, J., Jacobson, K. A., & Liang, B. T. (2014). A Novel Protective Role of Endogenous Cardiac Myocyte P2X$_4$ Receptors in Heart Failure. *Circulation: Heart Failure*.

Yardley, M. M., Wyatt, L., Khoja, S., Asatryan, L., Ramaker, M. J., Finn, D. A., Alkana, R. L., Huynh, N., Louie, S. G., Petasis, N. A., Bortolato, M., & Davies, D. L. (2012). Ivermectin reduces alcohol intake and preference in mice. *Neuropharmacology, 63*(2), 190-201.

Żamojć, K., Wiczk, W., Zaborowski, B., Jacewicz, D., & Chmurzyński, L. (2014). Analysis of Fluorescence Quenching of Coumarin Derivatives by 4-Hydroxy-TEMPO in Aqueous Solution. *Journal of Fluorescence, 24*(3), 713-718.

Zech, A., Wiesler, B., Ayata, C. K., Schlaich, T., Dürk, T., Hoßfeld, M., Ehrat, N., Cicko, S., & Idzko, M. (2016). P2rx4 deficiency in mice alleviates allergen-induced airway inflammation. *Oncotarget, 7*(49), 80288-80297.

Zemkova, H., Kucka, M., Li, S., Gonzalez-Iglesias, A. E., Tomic, M., & Stojilkovic, S. S. (2010). Characterization of purinergic P2X$_4$ receptor channels expressed in anterior pituitary cells. *American Journal of Physiology-Endocrinology and Metabolism, 298*(3), E644-651.

Zemkova, H., Tvrdonova, V., Bhattacharya, A., & Jindrichova, M. (2014). Allosteric modulation of ligand gated ion channels by ivermectin. *Physiological Research, 63 Suppl 1*, S215-224.

Zemkova, H., Yan, Z., Liang, Z., Jelinkova, I., Tomic, M., & Stojilkovic, S. S. (2007). Role of aromatic and charged ectodomain residues in the P2X$_4$ receptor functions. *Journal of Neurochemistry, 102*(4), 1139-1150.

Zhang, F. L., Luo, L., Gustafson, E., Palmer, K., Qiao, X., Fan, X., Yang, S., Laz, T. M., Bayne, M., & Monsma, F. (2002). P2Y$_{13}$: Identification and Characterization of a Novel Gαi-Coupled ADP Receptor from Human and Mouse. *Journal of Pharmacology and Experimental Therapeutics, 301*(2), 705-713.

Zhang, J., & De Koninck, Y. (2006). Spatial and temporal relationship between monocyte chemoattractant protein-1 expression and spinal glial activation following peripheral nerve injury. *Journal of Neurochemistry, 97*(3), 772-783.

Zhang, J., Shi, X. Q., Echeverry, S., Mogil, J. S., De Koninck, Y., & Rivest, S. (2007). Expression of CCR2 in both resident and bone marrow-derived microglia plays

a critical role in neuropathic pain. *Journal of Neuroscience, 27*(45), 12396-12406.